PhD Dissertation

Photophysiological responses of marine phytoplankton and ice algae to temperature, iron and light availability in subpolar and polar regions

(亜極域・極域に生息する海洋植物プランクトンおよび

海氷微細藻類の温度・鉄・光利用度への光合成生理応答)

A thesis submitted in partial fulfilment of the requirements for the degree of Doctor of Philosophy

Kazuhiro Yoshida

Course in Geochemistry
Division of Earth System Science
Graduate School of Environmental Science
Hokkaido University

CONTENTS

ACKNOWLEDGEMENTS

First, my sincere appreciation goes to my supervisor Prof. Koji Suzuki for his enormous support and helpful suggestions. I learnt the importance of quantitative analysis in microbiology and biogeochemistry. I absolutely could not complete my PhD projects for 5 years including my mater's work. I would also like to acknowledge that he gave me wonderful opportunities for international research experiences. I would like to express my cordial gratitude to Prof. Andrew McMinn, my supervisor in Institute for Marine and Antarctic Studies (IMAS), University of Tasmania, for his tremendous support in the aspects of ice algae research and daily life in the foreign country. Ice tank with him always excited me, and weekly discussion with him enlighted me every time. My journey to Hobart connected me to so many sea ice researchers and formed my research direction. I am so grateful to Prof. Yoshito Chikaraishi and Prof. Jun Nishioka for their insightful comments and helpful suggestions to my dissertation. I would like to express my gratitude to officers, crews and researchers of the R/V *Professor Multanovskiy*, R/V *Hakuho Maru and* TR/V *Misago Maru*. I deeply appreciate the kind support from Dr. Stanford B. Hooker (NASA) regarding the optical observations with their data. Also, I am grateful to Dr. Toru Hirawake and Dr. Hisatomo Waga (Faculty of Fisheries Sciences, Hokkaido University) for his helpful instructions on optical observations and samplings. I also express my deep thanks to Prof. Ondřej Prášil and Dr. Evelyn Lawrenz (Institute of Microbiology, Czech) for their collaborations with their FRRf and 77 K fluorometry. Their data added tremendous values to this thesis. In addition, I am grateful to Dr. Hisashi Endo for his numerous instructions, especially on the molecular biology experiments. I want to thank Dr. Yuya Tada for his numerous advice. I would like to thank Dr. Andrew Martin, Dr. Andreas Seger, Mr. Fraser Kennedy, and Ms. Aiko Hayashi for their enormouos help in Algal Lab throughout my stays in IMAS. I could not conduct the low-Fe ice tank incubation experiments without the help of Dr. Kristen Karsh, Dr. Robert Strzepek, Dr. Delphine Lannuzel, and Ms. Helene Aflenzer. Prof. Philip Boyd kindly permitted me to use his bench-top FRRf, taking me to the profound Chlorophyll *a* fluorescence world. I would appreciate many kindnesses from Ms. Akiko Kamimura, Ms. Natsuko Araki, Ms. Suzu Nakamura and Ms. Aiko Murayama for the field and laboratory experiments. For the stable isotopic

analyses, I thank Mr. Yuta Yoshino and members from the Sugimoto Laboratory. I also thank Prof. Yutaka W. Watanabe, Prof. Takafumi Hirata and Prof. Sohiko Kameyama for their kind suggestions for my work. Thanks are extended to all people in the Marine and Atmospheric Geochemistry (MAG) group and Algal Lab members. I truly thank Prof. Satoru Taguchi whom I would like to express my gratitude to my old friends and the family of Dewans for their continuous encouragement and warm friendship. Finally, I would like to express my deepest thanks to my parents for their unlimited support and encouragement.

ABSTRACT

Global warming increases sea temperatures and intensifies stratification of the water column, which directly and indirectly affects marine ecosystems and biogeochemistry (e.g., less nutrient supply due to the stratification). It has been suggested that the effects of climate change may emerge earlier in subpolar and polar regions, which are highly productive from spring to summer and ecologically important (e.g., phytoplankton blooms and ice algal production). In these regions, an increase in temperature may benefit some algal primary producers, but contracts extent of sea ice, which is an inhabitant of ice-associated biota. Light is also a crucial factor for all photosynthetic organisms, and its availability can change dramatically by sea ice melting. Iron (Fe) as a micro-nutrient plays a key role in algal metabolic processes including photosynthesis. This study thus aimed at clarifying the effects of temperature, light and Fe availability on the photophysiology of phytoplankton and ice algae in the changing subpolar and polar oceans.

Effects of temperature on a spring diatom bloom in the coastal Oyashio (COY) were investigated as a representative subpolar coastal spring bloom. The spring diatom blooms in COY waters are highly productive in spite of the low sea surface temperature (SST) (−1−2 ºC in early spring). This study thus focused on the photophysiology and community composition of phytoplankton in COY waters during the pre-bloom and bloom periods from March to April 2015. Next-generation sequencing targeting the 18S rRNA gene revealed that the diatom *Thalassiosira* generally dominated the phytoplankton community in COY waters on the shelf (shelf COY). Additionally, the relative contribution of *Thalassiosira* to the total diatom assemblages showed a positive correlation with maximum photosynthetic rates (P_{Bmax}) throughout this study, suggesting that the genus largely contributed to the bloom. We also conducted short-term on-deck incubation experiments to clarify the role of temperature in determining the photosynthetic functioning of phytoplankton. As a result, in the shelf COY, rising temperature led an increase in P_{Bmax} and transcription levels of the diatom-specific *rbcL* gene coding the large subunit of RuBisCO. It suggested that the rising temperature upregulated the diatom-specific *rbcL* gene and then triggered the higher P_{Bmax} as well as the spring diatom bloom in the shelf COY waters.

In summer, Fe availability is a crucial factor for the dynamics of spring diatom blooms in the western subarctic Pacific including the Oyashio region. The western subarctic Pacific is known as one of the largest High Nutrient Low Chlorophyll (HNLC) regions. At present, little is known about Fe deficiency in phytoplankton in neritic zones and its boundary region because of multiple Fe sources and strong vertical mixing along the Kuril Islands. This study also examined the effects of Fe on the community composition and photophysiology of phytoplankton in the western subarctic Pacific near the Kuril Islands and the eastern Kamchatka Peninsula during bloom and post-bloom phases from June to July 2014. An HNLC water was observed outside of the shelf slope. High Chl *a* concentrations were observed in the coastal region in early June, whereas spring diatom blooms seemed to be terminated in the coastal region near the Kamchatka Peninsula. Detailed scanning electron microscopy demonstrated a clear biogeographical difference in armoured plankton community composition between the coastal and offshore areas. The diatom *Chaetoceros* was abundant in the Fe-rich coastal waters, while the genera *Fragilariopsis* and *Pseudo-nitzschia* were dominant in the HNLC water outside of the shelf slope. Light availability was also important for primary productivity of phytoplankton, we thus conducted on-deck Fe enrichment bottle incubation experiments at stations with the second shallowest and the deepest surface mixed layer depths (MLD). Fe addition at the station with the second shallowest station did not affect biomass and photochemical efficiency at photosystem II (F_v/F_m), whereas Chl *a* biomass and F_v/F_m were increased at the deepest MLD station. These results suggest the Fe-light interaction at the station with the deepest MLD, also supported by the results of photophysiological parameters (E_k: light saturation index of photosynthesis versus irradiance curve). At the study area, it was indicated that light availability can significantly affect Fe deficiency in the phytoplankton assemblages (i.e., Fe-light co-limitations).

Sea-ice algae contribute 10–25% of the annual primary production of polar seas, and seed large-scale ice-edge blooms. Large fluctuations in temperature, salinity, light and Fe availability, associated with freezing and melting of sea ice, can significantly change the photophysiology of ice algae. Therefore, effects of multiple co-stressors (i.e., freezing temperature and high brine salinity in a freezing event; and sudden high light exposure during ice melting as well as Fe starvation) on the photophysiology of ice algae were investigated in a series of ice tank experiments with the polar diatom *Fragilariopsis*

cylindrus under different light intensities as well as different Fe availability. When algal cells were frozen into the ice, the maximum quantum yield of photosystem II (PSII) (F_v/F_m) decreased regardless of the treatments, possibly due to the damage of PSII reaction centers or high brine salinity stress suppressing the reduction capacity downstream of PSII. Gene expression of the *rbcL* gene was highly upregulated, suggesting a survival strategy for acclimating to the cold ice environment in the ice. The frozen algae within the ice showed almost the same levels of F_v/F_m regardless of the treatments. When the ice melted and the cells were exposed to high light (800 μmol photons m^{-2} s^{-1}), F_v/F_m sharply decreased, while non-photochemical quenching (NPQ) was upregulated to dissipate the excess light energy. Interestingly, the *psbA* gene encoding the D1 protein of PSII was upregulated under high Fe conditions and vice versa. These results suggested Fe repletion accelerated *de novo* synthesis of the D1 protein, whereas Fe starvation inhibited repair of the PSII damaged by the high light. Our results imply that Fe-starved cells cannot well regulate their photosynthetic plasticity to the environmental changes during ice melting, and would little contribute to ice-edge blooms.

LIST OF FIGURES

Figure 18. Maximum photochemical quantum yield of PSII (F_v/F_m) during the ice tank incubation experiments.

Figure 19. Functional absorption cross section of PSII (σ_{PSII}) during the ice tank incubation experiments.

Figure 20. Non-photochemical quenching based on the Stern-Volmer quenching kinetics (NPQ_{NSV}) during the ice tank incubation experiments.

Figure 21. Fraction of closed of PSII (1−qP) during the ice tank incubation experiments.

Figure 22. Light utilization efficiency under dim light (α) shown as initial slopes of the ETR_{RCII}-E curves during the ice tank incubation experiments.

Figure 23. Maximum electron transport rate (ETR_{max}) during the ice tank incubation experiments.

Figure 24. Light saturation index (E_k) during the ice tank incubation experiments.
Figure 25. Variable Chl *a* fluorescence parameters with different melting methods.

Figure 26. Concentrations of total Chl *a* [mg m^{-3}] (TChl *a*=Chl *a*+Chllide *a*+Chl *a*-epimer+Chl *a*-allomer) quantified with UHPLC (bar) and contributions of Chllide *a* to TChl *a* (open circle) during the ice tank incubations.

Figure 27. Size of DD and DT pool defined as DD-DT/Chl *a* (bars) and de-epoxidation state (DES) (open circle) during the ice tank incubations.

Figure 28. Ratio of photoprotective carotenoids (PPC) to photosynthetic carotenoids (PSC) during the ice tank incubations.

Figure 29. Gene expression of the *rbcL* gene calculated as ratio of cDNA to DNA copies of the gene during the ice tank incubation experiments.

Figure 30. Gene expression of the *psbA* gene calculated as ratio of cDNA to DNA copies of the gene during the ice tank incubation experiments.

LIST OF TABLES

LIST OF APPENDICES

Chapter 1

General introduction

1-1. Distribution and biogeochemical roles of microalgae in the ocean

Marine primary production accounts for ~45% of the global primary production (Field et al., 1997). Microalgae, including phytoplankton, are the most abundant primary producers in the ocean (Geider et al., 2014). They are ubiquitously distributed from the tropics to the poles and even occur in coral, in sea ice, and on snow. Microalgae are very diverse (500 reported genera and 4,000 reported species) (Sournia et al., 1991) with a wide size range covering three orders of magnitude (from <1 μm to 1 mm) (Lalli and Parsons, 1997). Aquatic photosynthesis by microalgae is controlled by light, temperature, and nutrients including micronutrients (e.g., Falkowski and Raven, 2007; de Baar et al., 1995) as well as biotic factors (e.g., cell size, and species interactions) (e.g., Paul et al., 2009; Yan et al., 2017). In addition, marine dissolved organic matter from microalgae as exudates fuels bacteria, and the bacteria are fed by protozoans and subsequently zooplankton through "microbial loops" (Azam, 1988; Ogawa et al., 2001; Jiao et al., 2010). For both cases, microalgae play a central role in marine ecosystems. However, their habitats are strictly limited in a thin sunlit layer called euphotic zone which is the zone from the surface of the ocean to the 1% light level depth to the surface irradiance (Morel, 1988; Kirk, 2011) where microalgal productivity and community respiration are almost in balance, locating above 180 m (Morel et al., 2007). Sarmiento and Gruber (2006) estimated the 1% light level depth was 38 m on average in the North Atlantic by using the formula suggested by Morel (1988), and the depth is only ~1% of mean ocean depth of ~3700 m. In addition, microalgae generally use photosynthetically available radiation (PAR) whose wavelength ranges from 400 nm to 700 nm， and PAR almost corresponds to ~45% of the sunlight energy (Kirk, 2011). Although the marine phytoplankton biomass is far less (1–2%) than that of terrestrial counterparts, their primary production values are comparable to each other (Falkowski, 1994; Falkowski et al., 2003). This indicates the high turnover rate of marine phytoplankton. It is known that the ocean is a major sink of anthropogenic carbon dioxide (CO_2), absorbing about one-third anthropogenic CO_2 (Sabine et al.,

2004). As mentioned above, since microalgae are the main primary producer in the ocean, the organisms play an important role in the conversion from inorganic carbon into organic compounds in the ocean. It is considered that the fixed carbon by microalgal photosynthesis is sequestrated by sinking as aggregates of microalgae, fecal pellets of zooplankton and carcass of marine organisms from the euphotic zones toward abysses of the oceans (e.g., Riebesell et al., 1993; Sarthou et al., 2005; Grossart et al., 2006; Tang and Elliott, 2013). The sinking carbon remains in deep waters and is sequestrated during a period of the ocean circulation, i.e. the order of thousands of years, which is so-called "biological pump" (Smetacek, 1985; 1999). Thus, the tiny algal cells have significant impacts on both the marine ecosystem and the ocean biogeochemical dynamics.

1.2. Primary producers in changing subpolar and polar regions

High-latitude oceans contribute significantly to global primary production, as revealed by *in situ* and satellite observations as well as model studies (e.g., Field et al., 1998; Arrigo et al., 2008; Hoegh-Guldberg and Bruno, 2010). The high primary production in subpolar and polar oceans is mainly due to considerable microalgal build-up in spring-summer, called spring blooms. In subpolar regions, the vernal phytoplankton blooms, often composed of diatoms, are induced by adequate light supply with increased SST and water-column stratification in spring-summer. At the climax, Chl *a* biomass often increases ~20 mg m^{-3} in the western subarctic Pacific and the Southern Ocean (e.g., Ryan-Keogh et al., 2017; Isada et al., 2018). After the blooms, a part of their production is exported downward and sequestrated (e.g. Gruber et al., 2002; Honda, 2003; see also Siegel et al., 2016), but the other remains in the surface layer as dissolved organic carbon (DOC). The remained DOC significantly stimulates bacterial growth after the diatom blooms (e.g. Tada et al., 2011, 2017; Gasol and Kirchman, 2018). In polar regions, open waters are a rather significant habitats for polar biota, sea ice is the largest biome, occupying from 4–5% up to 13% of the global ocean surface and largely covering the surface of both poles (Parkinson and Gloersen, 1993; Meier, 2017; Stammerjohn and Maksym, 2017). Microalgae proliferate even within and at the bottom of sea ice. The sea ice associate microalgae are called 'ice algae' or 'sympagic microalgae' (*sensu* Horner et al., 1992). Sea ice environments, however, can be challenging environments for photosynthesis due to low light availability by scattering of incident

light by sea ice as well as low temperature. Because of the low light availability, photosynthesis is severely restricted beneath the sea ice but ice algae, inhabiting microstructures within the ice and at the bottom of the sea ice, are able to actively photosynthesize by specifically acclimating to the shade environment (McMinn et al., 2003; Arrigo et al., 2010). Ice algae, mainly composed of diatoms, proliferate in brine channels or at the bottom of the sea ice (e.g., Horner, 1985; Hegseth, 1992; Garrison, 1991; Alou-Font et al., 2013). When sea ice is present, most primary production is carried out by sea ice algae, equivalent to 9–25% of the annual primary production in the Southern Ocean (Arrigo et al., 1997), 25–30% in Antarctic coastal regions (Legendre et al., 1992; Grose and McMinn, 2003), 15–20% in Arctic waters (Sakshaug 2004; Arrigo et al., 2008a), and 4% in Antarctic waters (Arrigo et al., 2008b), whereas contributing >50% of the total primary production in perennial ice-covered zones (Satoh et al., 1989; Legendre et al., 1992; Gosselin et al., 1997; McMinn et al., 2010; Fernandez-Mendez et al., 2015). Ice algal biomass inconceivably increases at the late season of frozen periods (160 and 975 mg Chl *a* m^{-3} on average in Arctic and Antarctic sea ice, respectively; see Arrigo, 2017). Ice algae are thus the main food source for polar zooplankton (Werner, 1997; Lizotte, 2001; Bluhm et al., 2010), krill (Kohlbach et al., 2017), fish larvae (Moteki et al., 2017), and benthic organisms (Boetius et al., 2015) during winter. In addition, within the ice, ice algae form aggregates within brine channels and at the base of the sea ice (Melnikov & Bondarchuk 1987; Assmy et al., 2013; Boetius et al., 2013; Katlein et al., 2014). They are released into the water column when ice melts in spring. Some released ice algae stay in the euphotic zone (Haecky et al. 1998, Mangoni et al. 2009) and seed extensive ice-edge blooms (Smith and Nelson, 1986; Arrigo et al., 2003). Released aggregates, however, sink rapidly to the seafloor (Taguchi et al., 1997; Ratkova & Wassmann 2005; Fernandez-Mendez et al., 2014; Katlein et al., 2014), indicating that the sinking aggregates potentially sequestrate much of the fixed carbon (Ambrose et al. 2005; Boetius et al., 2013; 2015; Arrigo, 2014), an efficient biological carbon pump (Smetacek, 1985).

These subpolar and polar oceans, however, are particularly sensitive to climate change (Sarmiento et al., 1998; Vaughan et al., 2003; Stroeve et al., 2007; Hoegh-Guldberg and Bruno, 2010). There have thus been many studies on effects of global climate change, including ocean acidification, on the physical and chemical properties of these high-latitude oceans, including changes in sea ice related

environments (e.g., Ohshima and Nihashi, 2005; Yamamoto-Kawai et al., 2009; Arrigo and van Oijken, 2015). The physical and chemical changes on photosynthesis due to the climate change seem to be amplified in subpolar and polar oceans because the limiting factors for microalgal photosynthesis in these oceans (i.e. light, temperature and the micronutrient iron) are tightly coupled with global warming and ocean acidification. However, changes in biological processes associated with the climate change under these co-stresses remain little understood in high-latitude oceans.

1.3. Photosynthesis mechanisms

1.3.1. Light reaction processes

Photosynthesis is a process of converting light energy into chemical energy and eventually organic compounds. The processes from light absorption to production of chemical energy are called the light reaction. This process starts from light absorption by light harvesting complexes (LHC), consisting of photosynthetic pigments and associated proteins. The absorbed light energy is transferred to a reaction centre of photosystem II (PSII, hereafter) (P_{680}). Charge separation occurs at this special pair of Chlorophyll (Chl *a*) molecules. Oxygen molecules are produced as a by-product via a reaction in the manganese cluster of PSII. An electron is emitted from a reaction centre when an excited reaction centre of PSII (P_{680}*) turns back to the ground state. The emitted electron travels along the electron transport chain of photosynthesis; quinones (i.e. Q_A and Q_B), the plastoquinone (PQ) pool and the cytochrome b_6/f complex. At another reaction centre at PSI, light energy, captured by the LHC, re-boosted the electron. The electron is then delivered to the ferredoxin protein. The electron transportation produces reduction power NADPH and chemical energy ATP as end-products. These compounds are further utilized for metabolic processes such as carbon fixation and nutrient assimilation.

1.3.2. Dark reaction processes

The NADPH and ATP produced in the light reaction play central roles in carbon fixation process, the dark reaction. NADPH and ATP are transferred to the stroma side of plastids. The dark reaction has 3 steps: carbon fixation, reduction, and regeneration of ribulose. The first step is carbon fixation

by the enzyme Ribulose-1,5-bisphosphate carboxylase/oxygenase (RuBisCO), consisting of its large and small subunits (RbcL and RbcS). The enzyme fixes CO_2 to produce a 6 carbon-containing compound by combining one CO_2 molecule to a 5-carbon ribulose-1, 5-bisphosphate (RuBP). The 6-carbon compound is subsequently broken down into two 3-carbon compounds, 3-phosphoglyceric acids (3PG), using 6 ATPs. The 3PGs are then reduced to glyceraldehyde 3-phosphates (G3P) using 6 NADPH. One trio carbons becomes an organic compound, while the other trio goes on the cycle further (i.e., recycled) for RuBP regeneration (see also Falkowski and Raven, 2013). In the Calvin cycle, the first step (i.e. carbon fixation by RuBisCO) is rate-limiting because of its slow carboxylation rate (Ellis, 2010). As its name suggests, the RuBisCO has two capabilities: carboxylation and oxygenation. The current oxic world is challenging for the enzyme because the concentration of CO_2 is much lower than the saturation level for RuBisCO whereas the oxygenation rate in the oxic condition is kinetically comparable (i.e. photorespiration) (Eckart, 2005). In addition, RuBisCO is highly temperature-sensitive that its enzymatic activity of carboxylation decreased exponentially with decreasing ambient temperature (Young et al., 2015) (also discussed in subsection 1.4.1). It can be a crucial issue for phytoplankton and ice algae in the cold environments in subpolar and polar regions. Microalgae thus acquired carbon-concentrating mechanism to optimize their intracellular CO_2 concentration by pumping into inorganic carbon species (e.g. Rost et al., 2003).

1.4. Environmental controls on aquatic photosynthesis in subpolar and polar regions

1.4.1. Temperature

In the cold and freezing subpolar and polar worlds, the low temperature is often or always a limiting factor of photosynthesis. It has long been documented that low temperatures inhibit the growth and photosynthesis of microalgae (e.g. Eppley, 1972; Verity, 1981; Geider et al., 1997). It is because that RuBisCO is a temperature-dependent enzyme as discussed above. Its activity is highly variable compared with other processes (Li et al., 1984; Descolas-Gros and De Billy, 1987; Raven and Geider, 1998) and even at 50 ºC the activity still increased for extracted RuBisCO (Crafts-Brandner and Salvucci, 2000). Young et al. (2015) demonstrated that carboxylation rate of RuBisCO critically slowed down by the low temperatures in the Southern Ocean, although the RuBisCO in psychrophilic

species adapted to the low temperature by mechanically modifying its structure. Therefore, temperature can be often a limiting factor for photosynthesis.

1.4.2. Iron

1.4.2.1. Fe in photosynthesis

Iron (Fe) is a crucial element for photosynthesis in microalgae, required for pigment and cytochrome synthesis, nitrate reduction as well as detoxification of reactive oxygen species (ROS) (Sunda and Huntsman, 1995; Twining and Baines, 2013; Behrenfeld and Milligan, 2014, and see review by Geider and LaRoche, 1994); these are required for light absorption, linear electron transfer, nitrogen metabolism and photoprotection, respectively. Fe affects both apparent growth rates and potential photosynthetic performance. It has long been known that Fe stimulates microalgal growth rates in the laboratory (Harvey, 1933; Timmermans et al., 2004). Moreover, microalgal cells reduce their cellular Fe requirement under Fe-limited conditions. Sunda and Huntsman (1995) reported that oceanic algae reduced their cell size and/or cellular Fe uptake to adapt to Fe-limited conditions. For instance, diatoms are more sensitive to Fe availability due to their large size (de Baar et al., 2005; Boyd et al., 2007; Hattori-Saito et al., 2010). Greene et al. (1991; 1992) attempted to investigate the underlying mechanisms of the physiological responses of microalgae to Fe availability with laboratory-based Fe-controlled incubations. They demonstrated that maximum photosynthesis rates, cellular Chl *a*, and the Chl *a*: carbon ratio were all lowered under Fe-limited conditions. In addition, cellular concentrations of all photosynthetic apparatus elements (PSII, cytochrome b_6/f, and PSI) also decreased (see also Geider and LaRoche, 1994) but PSII:PSI and cytochrome b_6/f:PSI ratios increased (Greene et al., 1992). This probably occurred to minimize the cellular Fe requirement because PSI needs 12 atoms of Fe whereas 2-3 atoms are required for PSI and 5 atoms for the cytochrome b_6/f complex.

1.4.2.2. Fe limitation

It has been an enigma of modern oceanography in some ocean provinces, occupying up to one third of the ocean; nutrients remained even after the growth of phytoplankton blooms in spring and summer. These regions have been called High Nutrient, Low Chlorophyll (HNLC) regions. Major

HNLC regions are located in subpolar and polar regions, i.e., in the Southern Ocean and the subarctic Pacific, as well as the eastern equatorial Pacific. Martin and Fitzwater (1988) first addressed this conundrum in the subarctic Pacific by using clean sampling techniques and showed that in fact Fe limited microalgal growth and photosynthesis *in situ*. Due to the low solubility of Fe(III) (the more abundant inorganic Fe species in seawater than Fe(II)), Fe concentration in seawater is very low (Kuma et al., 1996; Stumm and Morgan, 1996). After this revolutionary finding, many *in situ* Fe fertilization experiments were subsequently conducted and further demonstrated that Fe was the limiting micronutrient in HNLC regions (where TFe < 0.1 nM; e.g., Morel and Price, 2003) (e.g., Martin et al., 1990; 1994; Tsuda et al., 2003; 2007 and see review by Boyd et al.,2007), although responses of phytoplankton were slightly different among ocean provinces due to e.g., light availability and microzooplankton grazing (see Sarmiento and Gruber, 2006).

In subpolar and polar HNLC regions, sea ice plays a central role in Fe supply to seawater. Lannuzel (2007; 2008; 2015) reported higher Fe concentrations in sea ice than in seawater and suggested that sea ice is the major source of bioavailable Fe to seawater in the Southern Ocean. Wang et al. (2014) found support for this notion in their model simulation, demonstrating that sea ice is a major reservoir of Fe and fertilizes the Southern Ocean in spring/summer. Kanna et al. (2014; 2018) also found that sea ice was the major source of Fe. When sea ice melted, sea ice enriched Fe the seawater with Fe in spring, leading to phytoplankton growth in the Sea of Okhotsk. Sea ice also supplies Fe indirectly via brine rejection from sea ice in coastal polynyas that form dense shelf water (e.g., Honjo et al., 1988; Schauer,1995; Nakatsuka et al., 2002), this water then transports terrestrial Fe to the open ocean (Moore and Braucher, 2008; Nishioka et al., 2007; 2013; 2014; Nishioka and Obata, 2017). It is important to note that dissolved Fe is bound to organic compounds (>99%) which keep Fe dissolved by chelation (e.g., van den Berg, 1995). These ligands control Fe bioavailability and biogeochemistry (Gredhill and Buck, 2012; Shaked and Lis, 2012). The ligands are mainly from microbial extracellular substances (EPS) (Rue and Bruland, 1995): siderophores from bacteria (e.g., Kustka et al., 2015) and uronic acids and polysaccharides from microalgae (Nichols et al, 2005; Hasslaer and Schoemann, 2009; Hassler et al., 2015). The Fe-ligand complexation is thus a crucial controlling factor of Fe bioavailability and microalgal growth, the chemical structure and dynamics of these organic ligands,

however, remains to be uncovered (Misumi et al., 2014).

Kolber et al. (1994) and Suzuki et al. (2002) showed that Fe availability was related to photosynthetic activity (i.e., maximum quantum yield of PSII; F_v/F_m) determined with variable Chl *a* fluorescence measured with pulse amplitude modulation fluorometry (PAMf) and fast repetition rate fluorometry (FRRf). Functional absorption cross section of PSII (σ_{PSII}) increased under Fe-limited condition whereas F_v/F_m decreased. This was possibly due to the inactivation of reaction centres in PSII or Chlorolysis (Geider and LaRoche et al., 1994; Suggett et al., 2009b). As described above, ferredoxin delivers an electron from PSI to $NADP^+$ to produce a reductant, NADPH, but ferredoxin requires a substantial amount of Fe because it has a Fe-S cluster at its core. Ferredoxin is often replaced by flavodoxin, which does not require this cluster, under Fe-limited conditions although this response to Fe availability is species-specific (e.g., Pankowski et al., 2009). The physiological role of flavodoxin is the same as that of ferredoxin and their catalytic activity is almost equal (Smillie, 1965; Medina and Gómez-Moreno, 2004) but the molecular weight of flavodoxin is double that of ferredoxin. Ferredoxin/flavodoxin have been thus used to assess Fe limitation, both in the lab and in the field (e.g., LaRoche et al., 1995; McKay et al., 1999; Pankowski and McMinn, 2008a, 2008b, 2009; Hattori-Saito et al., 2010). From the insights of molecular biology, Cohen et al. (2017) investigated effects of Fe on gene expression using a metatranscriptomic approach and hypothesized that chronically Fe-limited oceanic diatoms upregulate carbon fixation and assimilation genes because cells are ATP-limited due to long-term Fe starvation. Mock et al. (2017) fully sequenced the genome of the polar diatom *Fragilariopsis cylindrus* and reported the gene expression of photosynthesis and metabolism using the expressed sequence tag (EST) analysis in combination with shotgun sequencing (Mock et al., 2015). The EST library showed that this polar diatom evolved genes and the genome to adapt to large environmental changes in polar regions, including Fe limitation, by diversifying and differentiating alleles. As described above, Fe limitation has negative effects on the growth and photosynthesis of microalgae, but it is expected that they have evolved strategies to overcome this environmental challenge.

1.4.2.3. Fe in sea ice

While most phytoplankton in the water column of HNLC regions suffer from Fe limitation, Pankowski and McMinn. (2008b) were the first reporting Fe limitation in ice algal assemblages in pack ice in the Southern Ocean (Pankowski and McMinn, 2009). Using an immunoassay for Fe-regulated proteins, Pankowski and McMinn (2008b) identified a large amount of flavodoxin at the bottom of sea ice but not in the middle or top of the ice. Because bottom ice algal communities are attached to the bottom of the sea ice, nutrients are percolated from the low Fe under-ice seawater. They found that ice algal photosynthesis could be Fe-limited (Pankowski and McMinn, 2008a; 2008b; McMinn, 2017), although brine communities within brine channels were relatively unaffected by Fe limitation due to the high concentration of Fe in brine (McMinn, 2017). Although these studies clearly demonstrated the possibility of Fe starvation in sea ice, photophysiological responses of ice algae to Fe availability has not been well documented. Light conditions in sea ice are very variable compared to those of the open ocean. Before the formation of sea ice, algal cells are planktonic, but once the cells are incorporated into the ice, the algal cells must acclimate to the low-light environment (Arrigo et al., 2010). When ice melts, they are subsequently exposed to sudden and intense light. The light exposure can cause serious photodamage (e.g., Melis, 1999). Dark acclimation at the bottom of sea ice requires Fe for photosynthetic pigment synthesis. Some studies have reported that ice algae at the bottom of sea ice were highly pigmented, although their photoacclimation strategy is still unknown under Fe-limited conditions. As described above, Fe is essential to synthesize photosynthetic components (e.g., photosystems), but it is also required to repair the damaged photosystems. Furthermore, physical and chemical stress associated with freezing and melting sea ice affects the physiology of ice algal photosynthesis (e.g., Ralph et al., 2007; Martin et al., 2012). How the dramatic changes in sea ice associated with sea ice formation and melting, co-stressors including Fe stress, on sea ice algae remains unknown (McMinn et al., 2017). With the exception of the pilot work by Pankowski and McMinn (2008a,b, 2009), the effects of Fe availability on sea ice algae are largely uninvestigated. However, several studies have been conducted on the distribution and chemical properties of Fe in sea ice (e.g., summarized in special issues on *Elementa*). Fast ice generally has higher Fe concentrations than pack ice (Lannuzel et al., 2016), probably due to the proximity to the land, and possibly supports the Fe starvation in pack ice found by Pankowski and McMinn (2008b).

Some studies have reported that the highest Fe concentrations (in the forms of dissolved and particulate; DFe and PFe, respectively) were found at the bottom of sea ice and these values were higher than those of seawater (e.g., Lannuzel et al., 2008; Tovar-Sanchez et al., 2010; van der Merwe et al., 2011). Some of the studies observed high Fe concentrations in upper parts of the sea ice, presumably due to rafting and flooding on ice surface (Sturm and Masson, 2010; Lannuzel et al., 2015). The highest Fe concentrations corresponded to the high concentrations of Chl *a* in sea ice (van der Merwe et al., 2011; Lannuzel et al., 2015). It is because bottom ice algae take up Fe from under-ice seawater (Grotti et al., 2005; Lannuzel et al., 2010). Their EPS may keep Fe in the sea ice (Lannuzel et al., 2015). In addition, Boyé et al. (2001) reported a >99% organic complexation of Fe in Antarctic sea ice as well as in seawater (described in 2-2). Significantly high concentrations of EPS (e.g., polysaccharides) were detected in the Chl *a*-rich bottom layer (Ugalde et al., 2014; Underwood et al., 2010; Krembs et al., 2011; Lannuzel et al., 2015). As described above, diatoms are abundant in ice algal assemblages, and diatom exudates are mainly composed of saccharides (e.g., Thornton, 2002). Algal-derived EPS such as polysaccharides loosely complexes Fe compared to bacterial EPS (e.g., Hassler et al., 2011; 2015; Kustka et al., 2015) and enhances Fe uptake and growth of ice algae because Fe chelated by algal EPS may be bioavailable to microalgae (e.g., Hutchins et al., 1999b; Norman et al., 2015). Lannuzel et al. (2015) clearly demonstrated that sea ice had higher concentrations of Fe and ligands at the bottom by performing adsorptive cathodic stripping voltammetry. The Fe-ligand complexation stability, on the other hand, showed vertical heterogeneity. In seawater, the importance of colloidal Fe was emphasized by Boyé et al. (2011), but no study has been conducted on colloidal Fe in sea ice for my best knowledge except for Boyé et al. (2010). The bottom layer is highly biologically active, bacterial abundance and production are also high (e.g., Martin et al., 2012; Ugalde et al., 2014, and see review by Bowman, 2015). As described above, bacteria also produce EPS, and their EPS tightly capture Fe (e.g., Maldonado and Price, 1999), the competition for Fe mediated by EPS can occur (Hutchins et al., 1999b) within the bottom of sea ice between ice algae and bacteria (Lannuzel et al., 2016).

1.4.3. Light

1.4.3.1. Light: essential but dangerous

As discussed in subsection 1.3.1, the light reaction is an essential process of photosynthesis, but this reaction is not static but highly dynamic. Light is requisite but also detrimental for photosynthesis because over-excitation of PSII reaction centre leads the production of reactive oxygen species (ROS). High light stress leads to excess charge separation events, reducing the capability of the photosynthetic electron transport (over-reduction) and causing triplet excited Chlorophylls and the special pair of Chl *a*; P680 reaction centre of PSII. The triplets finally reduce molecular oxygen to reactive singlet oxygen $^1O_2$ (Krieger-Liszkay et al., 2016), the major ROS in photosynthesis striking photosynthetic components (Triantaphylidès et al., 2008). The core protein of PSII, D1 protein is, however, highly fragile to light stress (Prášil et al., 1992; Aro et al., 1993). The turnover rate of the D1 protein is thus tuned high (Edelman and Mattoo, 2008), and antioxidant pigments (e.g., carotenes and xanthophylls) are produced to maintain PSII by capturing ROS to avoid additional damage on further components (e.g., PSI), costing highly energy to repair.

1.4.3.2. Light-Fe interactions

Light and Fe availability are tightly coupled because Fe is an essential trace metal for pigment synthesis. Microalgae are known to synthesize more Chlorophylls and carotenoids under low light conditions to maximize the efficiency of light utilization (e.g., Falkowski and Owen, 1980; Morel and Bricaud, 1981; Bricaud et al., 1995) causing the package effect (e.g., Berner et al., 1989). Because this *de novo* pigment synthesis further requires Fe, light limitation exacerbates Fe availability such as in a deeply mixed water column and at the bottom of sea ice. It is so-called Fe-light co-limitation (Sunda and Huntsman, 1997). This antagonistic Fe-light co-limitation has been observed both in the lab (Sunda and Huntsman, 1997; Timmermans et al., 2001) and in the field (Maldonado et al., 1999; Hopkinson and Babeau, 2008). Strzepek et al. (2012), however, first demonstrated that Fe-light co-limitation was not significant in Southern Ocean phytoplankton. In fact, some studies reported results that Fe-light co-limitation did not occur in Southern Ocean species (Moore et al., 2007). Traditionally, it had been thought that phytoplankton increases their photosynthetic apparatus (i.e., the number of photosynthetic components for electron transport chain) under low light conditions (e.g., Falkowski et

al., 1992), which requires Fe for the synthesis of photosynthetic apparatus such as for PSI in particular. Strzepek et al. (2012), however, proposed another acclimation strategy to overcome low Fe and low light availability: increasing the size of photosynthetic antennae relative to the number of reaction centres. This leads to an increase in σ_{PSII} to capture light efficiently for charge separation at reaction centres. This strategy does not require Fe. Strzepek et al. (2012) thus concluded that phytoplankton in the Southern Ocean did not get into Fe-light co-limitation by employing the strategy. Although phytoplankton can sustain photosynthesis in vertically well-mixed waters in the Southern Ocean, there is a concern about abrupt changes in light supply with shoaling of the mixed layer depth and/or sea ice treat in summer. Regardless of strategies to acclimate to low-Fe and low-light conditions, cellular Chlorophyll and accessory pigment contents are reduced under Fe-limited condition and the reduced package effect. These lead to photodamage and the production of ROS because the Fe-limited cells cannot deal with the absorbed photons exceeding the reduced electron transport capacity due to Fe limitation under high-light conditions (van Oijen et al., 2007). Behrenfeld et al. (2008) observed a decrease in PSII when microalgal photosynthesis is photoinhibited under high irradiance. However, little attention has been paid to the relationship between photoinhibitory and photoacclimation strategies and the fact that Fe availability is tightly coupled with photoinhibition under abrupt changes in light condition which occurs in the Southern Ocean in summer.

1.5. Photosynthesis versus irradiance (*P-E*) relationship

It is a central focus of biological oceanography to quantify the primary production in marine environments. Satellite remote sensing is a powerful tool to estimate Chl *a* biomass from space instantaneously with high spatial and temporal resolutions. However, biomass often mismatches primary productivity because photosynthetic physiology is the underlying mechanisms to drive primary production (see also Bannister, 1974). In addition, the responses of microalgae to environmental fluctuations, what this study is focusing on, cannot be assessed from biomass. The biomass is no more than an average production with multiple loss factors (i.e., sinking, grazing, and cell death). It is thus needed to understand the photophysiology of marine phytoplankton and ice algae to investigate their responses in the changing world. To assess the whole processes of phytoplankton

photosynthesis, we should consider from light absorption by photosynthetic pigments and following electron transportation to the production of organic carbon. It is thus necessary to understand the relationships between light and photosynthesis. One way to clarify this relationship is to measure primary productivity and surrounding incident light. To elucidate the physiological responses of phytoplankton photosynthesis to the light, Photosynthesis vs. Irradiance curves (*P-E* curve) have been used from the 1950s with the ^{14}C method in which carbon-based photosynthetic rates were estimated from uptake rates of the radioisotope ^{14}C (Steeman-Nielsen, 1952; Steeman-Niesen and Jørgensen, 1968; Jørgensen, 1968). The *P-E* curves are obtained by plotting photosynthetic rates under various irradiance levels and provide relationships between light and photosynthesis at a given time. The results obtained indicate their physiological states and light acclimation strategies. Photophysiological properties can thus represent how phytoplankton is affected by environmental factors. It enables us to understand the spatiotemporal variability of phytoplankton distribution and primary production, especially in the regions with high variability of primary production (Sakshaug et al., 1997; Furuya et al., 1998). In addition, many models of *P-E* relationships help quantification of physiological properties of phytoplankton and ice algal photosynthesis (Webb et al., 1974; Jassby and Platt, 1976; Platt et al., 1980). The resultant photosynthetic parameters after fittings provide powerful insights into photophysiological responses of phytoplankton to environmental variables (Harrison and Platt, 1985; Platt et al., 1992; Sakshaug et al., 1997; MacIntyre et al., 2002).

1.6. Active Chlorophyll *a* fluorescence

In 1931, Kautsky and Hilsch found a phenomenon of fluorescence induction and decay of Chlorophyll *a* when exposed to light, so-called the Kautsky effect (Kautsky and Hirsch, 1931; Govindjee, 1995). When the pigments absorb the light, not all photon energy is utilized for the photochemical reaction, i.e. primary charge separation. Basically, there are three pathways of the photon energy absorbed by photosynthetic organisms such as plants and algae: photochemistry, thermal dissipation, and fluorescence as the following equation:

$$k_T = k_F + k_P + k_D + k_Q \quad (1.1)$$

where k_T, k_F, k_P, k_D and k_Q are reaction rate constants of a total, fluorescence, photochemistry, thermal dissipation and another way such as transport between pigments, respectively. It is supposed that the sum of the 4 pathways is unity (Cosgrove and Borowitzka, 2011), suggesting that changes in utilization of the absorbed photon energy among the complementary pathways. It indicates that how much the absorbed light is used for each pathway. Based on this theory, there have been many attempts to estimate the quantum yield of photochemistry using pulse amplitude modulation (PAM) (Genty et al., 1989; Schreiber et al., 1995), pump-and-probe (P&P) (Kolber and Falkowski, 1993), or fast repetition rate (FRR) fluorometry (Kolber et al., 1998). Pump-and probe and FRR fluorometry measure the fluorescence of Chlorophyll *a* by applying the single-turnover flash protocol, whereas PAM fluorometry applies the multiple-turnover flash protocol to Chl *a*. The similarity in these methods is that all methods provide two lights; a very weak light and a very short intense flash to a plant cell not enough to induce the photochemical reaction but enough to emit the fluorescence to assess a potential maximum quantum yield of the photochemistry of PSII. The fundamental difference between single- and multiple-turnover flash protocols is a length of the short intense flashes, where the single-turnover protocol applies flash or flashlets in an order of tens to hundred microseconds for total, whereas multiple turnover flashes are for order of hundreds of milliseconds to one second (Cosgrove and Borowitzka, 2011). The shorter single-turnover flash oxidizes a reaction centre of PSII (i.e., charge separation) only once (Kolber and Falkowski, 1993; Falkowski and Raven, 2007), while the longer multiple turnover flashes are long enough to oxidize reaction centres of PSII repeatedly (i.e., multiple successive charge separation of reaction centres and subsequent reduction of quinones and the PQ pool) (Babin, 2008; Huot and Babin, 2011). The advantages and limitations of both protocols are discussed in the review by Kromkamp and Foster (2003): (a) inadequate amount of light of single-turnover flashes; too weak flashes to induce charge separation for all reaction centres in PSII, and (b) non-photochemical quenching build up (e.g., increases in the fraction of thermal dissipation) with multiple-turnover flashes; too long flashes over-inducing charge separation (Schreiber et al., 1995).

The fluorescence under the weak light (F_0) represents original and minimum fluorescence, which is emitted from Chlorophyll *a* acting as accessory pigments (Krause and Weis, 1984). The other fluorescence under an intense pulse cause a maximum fluorescence of Chlorophyll *a* (F_m) but with no

photochemical process because of the very short period for light exposure. Subtracting F_0 from F_m (F_m–F_0, so-called the variable Chlorophyll *a* fluorescence; F_v), it can be an indicator for the fraction of photochemistry. By dividing F_v by F_m, and assuming that the thermal dissipation is constant or its variation is negligible enough compared with others, this provides an F_v/F_m value which can represent a potential maximum quantum yield of the photochemistry of PSII using the reaction rate constants shown as follows:

$$\varphi_F = k_F / (k_F + k_P + k_D + k_Q) \quad (1.2)$$

where φ_F is a yield of fluorescence, and when a maximum value of photochemistry is observed i.e., at maximal P (P_{max}), a fraction of fluorescence k_F must be near to zero and the yield of photochemical reaction (φ_{Pmax}) can be expressed following equation (1.2):

$$\varphi_{Pmax} = k_{Pmax} / (k_F + k_{Pmax} + k_D + k_Q) \quad (1.3)$$

and then, that at F_m, a maximal value of F, we can ignore the fraction of photochemistry (P). With these assumptions, we can derive an F_v/F_m value:

$$\frac{F_v}{F_m} = \frac{F_m - F_0}{F_m} = \frac{\left(\frac{k_F}{k_F + k_D + k_T}\right) - \left(\frac{k_F}{k_F + k_{Pmax} + k_D + k_T}\right)}{\left(\frac{k_F}{k_F + k_D + k_T}\right)}$$

$$= 1 - \left(\frac{k_F + k_D + k_T}{k_F + k_{Pmax} + k_D + k_T}\right)$$

$$= \frac{k_{Pmax}}{k_F + k_{Pmax} + k_D + k_T}$$

$$= \varphi_{Pmax} \quad (1.4)$$

The resultant F_v/F_m value has the maximum value of ~0.65 and 0.6−0.8 with the single-turnover and multiple-turnover protocols, respectively (Kolber and Falkowski, 1993; Büchel and Wilhelm, 1993; Koblížek et al., 2001). The variable Chl *a* fluorescence, F_v/F_m, has been widely used as a proxy for the activity of light reaction because it can be measured instantaneously without any incubations and with non-destructive manner repeatedly. Furthermore, F_v/F_m has also been used for predicting physiological states of algal cells under certain environmental factors (Kolber et al., 1994; Suzuki et al., 2002). Chl *a* fluorescence can also generate a *P-E* curve, namely rapid light curve (RLC), by measurements of variable Chl *a* fluorescence under various actinic light intensity as F'_q/F'_m. Multiplication of F'_q/F'_m

and actinic light intensity provides a photosynthetic rate as an electron transport rate (ETR). Some fluorometers with a high sampling pitch (e.g., FRR fluorometer) quantify functional absorption cross section of PSII (σ_{PSII}) as an index of photosynthetic antennae size of PSII:

$$\sigma_{PSII} = \alpha / n \quad (1.5)$$

where α is a light utilization index calculated from a *P-E* relationship and n is the number of functional PSII. It indicates that σ_{PSII} shows how much absorbed light is transferred to one active reaction centre.

With these Chl *a* fluorescence parameters, some challenges have been attempted to estimate the primary productivity from the Chlorophyll *a* fluorescence (see a review by Suggett et al., 2011).

At room temperature, almost all Chl *a* fluorescence is from PSII, but PSI emits fluorescence at 77 K (i.e. −196.15 ºC) (e.g. Prášil et al., 2009; Hill et al., 2012). The 77 K fluorescence analysis enables quantification of PSII:PSI ratio and assessment of the state of photosynthetic antennae. Plant cells modify the ratio of PSII:PSI to increase PSI under high light stress to alleviate over-reduction of the electron transport chain (i.e., state transition). Suggett et al. (2009a) and D'Haene et al. (2015) suggested that the 77 K analysis identifies fluorescence emission from the core protein CP47. The CP47 protein is a bridge from light harvesting complexes (LHCs) to reaction centres of PSII, the emission is an indicator of (un)coupling of LHCs and PSII reaction centres.

1.7. Problems

1.7.1. Accessibility and missing pieces

The subpolar and polar oceans are still unexplored because it is difficult or impossible to conduct a field observation in wintertime due to the extreme and severe ocean condition. Although it is possible to head to subpolar seas using scientific ships, these subpolar regions are still lacking knowledge of photophysiology of phytoplankton. As discussed in section 1.1.2, the subpolar diatom blooms are a significant driver of carbon cycles. Although plausible conceptual models have been proposed (e.g. critical depth hypothesis, Riley, 1946; Sverdrup, 1953; dilution-recoupling model, Behrenfeld, 2010), it is still enigmatic how phytoplankton modifies their photosynthetic physiology to build up the extensive blooms in subpolar oceans. In addition, the subpolar regions have the two largest HNLC

regions (i.e., western subarctic and subantarctic waters). The Fe limitations in these regions have been well-documented by *in situ* Fe-fertilization experiments (see the review of Boyd et al., 2007), but these studies mainly focused on changes in biomass after the experiments. It has been argued that other factors more control biomass during the experiments (e.g. grazing, Banse, 1990, 1995; light limitation, Tranter, 1982). It is thus more direct and insightful to understand photophysiological responses of subpolar phytoplankton to Fe availability toward quantification how Fe controls phytoplankton photosynthesis and biomass.

In polar regions, sea ice sampling is, in particular, time-consuming, and spatiotemporal resolution should be sparse. It is the major obstacle to understand the life and fate of ice algae because no observation can be conducted to examine incorporation and release of ice algae. Moreover, it is problematic that an ice breaking ship is needed to conduct sea ice observation, and it is impossible to exclusively allocate ship time to one specific topic. Due to the difficulties in accessing to the polar regions, continuous or time-series sampling is also hard to be conducted, especially for pack ice where Pankowski and McMinn (2008b) detected Fe-limitation of sea ice algae.

1.7.2. Challenges for satellite and modelling

Satellite remote sensing has been used to estimate surface Chl *a* concentration and *PP* (Behrenfeld and Falkowski, 1997; Sathyendranath et al., 2007; Behrenfeld et al., 2017) as well as size distribution and class of phytoplankton (Claustre et al., 2005; Hirata et al., 2011; Hirata and Suzuki, 2017). This method is now a powerful tool for acquiring high resolution and frequent observation. However, estimation of phytoplankton *PP* has been highly underestimated using the most common VGPM model (Behrenfeld and Falkowski, 1997) in subpolar and polar regions because they assumed a seventh-order polynomial function between photosynthetic rate and temperature. Thus, this model cannot reproduce *PP* of cold-adapted phytoplankton in subpolar and polar waters, although other methods using phytoplankton absorption properties have been applied to reproduce realistically *PP* of subpolar and polar phytoplankton (e.g., Marra et al., 2007; Hirawake et al., 2011; 2012). In sea ice zone, satellite data are unavailable for ice algae due to strong scattering of sea ice (Miller et al., 2014), spatiotemporal resolution of sea ice data depends on frequency of *in situ* and manual observation. It is

still difficult to model ice algal *PP* due to the problems described above (Vancoppenole et al., 2013; Steiner et al., 2016; van Leeuwe et al., 2018), although Arrigo and Sullivan (1994) attempted to estimate ice algal *PP* with the use of numerical modelling. Steiner et al. (2016) and van Leeuwe et al. (2018) nicely summarized challenges and perspectives toward a better sea ice biogeochemical modelling. They suggested that it is an urgent issue to investigate the mechanisms of incorporation and release of sea ice biota.

1.8. Goals of this study

My PhD work tried to understand how subpolar spring diatom blooms and ice algal production will change with environmental variations in the changing climate. As discussed above, the climate change affects fundamental processes of photosynthesis. However, the problems discussed above in section 1.7 hindered understanding of subpolar diatom blooms and ice algal production in these productive oceans. This study thus focuses on the effects of temperature, light and Fe availability, crucial factors in subpolar and polar oceans, on photophysiology of phytoplankton and ice algae. In chapter 2, I tried to clarify how phytoplankton assemblages optimize their photophysiology when a spring diatom bloom occurs in the western subarctic Pacific during early spring, with a special focus on the effect of temperature on carbon fixation processes in the cold waters. Chapter 3 focused on the effects of light and Fe availability on the photophysiology of phytoplankton in HNLC and neritic waters in the western subarctic Pacific near the Kuril Islands. In this chapter, light-Fe interactions are one of the central interests. Chapter 4 focused on how freezing and melting events as well as prolonged frozen environments stress the photophysiology of ice algae. In this chapter, I used ice tank incubation techniques to incubate a model ice algae species *Fragilariopsis cylindrus* within artificial sea ice in the lab. Chapter 5 aimed to quantify the effects of Fe availability on ice algal photophysiology and its temporal changes associated with sea ice dynamics as well as light-Fe interactions at the bottom of the sea ice. I used a newly developed low-Fe ice tank to incubate *F. cylindrus* under different Fe concentrations as well as light availability. In addition, light exposure experiments were also conducted to provide insights into whether released ice algae can survive in open waters under high

light there and contribute to extensive ice-edge blooms. Finally, Chapter 6 overviewed the previous chapters and summarize them as general conclusions.

CHAPTER 2

Community composition and photophysiology of phytoplankton assemblages in coastal Oyashio waters of the western North Pacific during early spring

2.1. Introduction

Photosynthetic marine phytoplankton are responsible for about half of the global primary production (Field et al., 1998; Behrenfeld et al., 2001) and are one of the principal drivers for the global carbon cycle (e.g. Sarmiento and Siegenthaler, 1992; Falkowski, 1994; Smetacek, 1999). The western subarctic Pacific has one of the highest transport efficiencies of particulate organic carbon (POC) in the water column (Honda, 2003; Kawakami et al., 2004, 2015) and the largest biological effect on seasonal changes in surface pCO_2 drawdown in the world ocean (Takahashi et al., 2002). These remarkable biogeochemical features are partly caused by large to vast spring diatom blooms observed in Oyashio (OY) and coastal Oyashio (COY) waters (Chiba et al., 2004; Hattori-Saito et al., 2010; Yoshie et al., 2010; Suzuki et al., 2011), which are biologically highly productive during spring (Isoda and Kishi, 2003; Isada et al., 2010). The OY is the westernmost current of the Western Subarctic Gyre (WSG) and is influenced by both the Eastern Kamchatka current and the Okhotsk Mode water (Yasuda, 2003; Oguma et al., 2008). The COY, on the other hand, is also derived from sea ice meltwater within the Sea of Okhotsk (Sugiura, 1956; Ohtani, 1971; Ogasawara, 1990) flowing along the southeastern coast of Hokkaido in spring (Kono, 1997; Kono et al., 2004; Oguma et al., 2008; Kusaka et al., 2013). Consequently, COY waters can generally be distinguished from the OY by their lower salinity (<33) and lower temperature (– 1.8 to 2 °C) as the result of the sea ice meltwater in spring (Ohtani, 1971).

A number of studies have addressed the bloom dynamics in the OY region. For example, Suzuki et al. (2011) studied the community composition and bloom dynamics in OY waters and revealed that the annual spring bloom was often dominated by large, including chain-forming diatoms such as Thalassiosira, *Chaetoceros* and *Fragilariopsis* species. It was pointed out that development of steep density gradients in the water column (i.e., stratification) in spring can be associated with the initiation of the spring blooms in OY waters following the high nutrient supply into the surface mixed

layer by winter deep mixing (Yoshimori et al., 1995; Kasai et al., 1997). Yoshie et al. (2003) noted that the deep mixing can significantly affect the amplitude of the spring OY bloom not only by the supply of nutrients but also by the dilution of predators, which drastically reduces grazing pressure (see Behrenfeld, 2010). Indeed, macrozooplankton grazing has a great impact on phytoplankton abundance, influencing the dynamics of the spring blooms in OY waters (Kasai et al., 1997; Saito et al., 2002; Kono and Sato, 2010). Saito et al. (2002) and Saito and Tsuda (2003) also proposed that light and silicate limitations could control the bloom dynamics in the OY region, particularly the initiation and termination of the spring diatom blooms. The spring diatom blooms in the OY waters can effectively foster the high productivity of higher trophic levels in this region (Taniguchi, 1999; Sakurai, 2007; Ikeda et al., 2008).

In contrast, fewer studies have been conducted in COY waters (Yoshimori et al., 1995; Kasai et al., 1997), even though the spring diatom blooms in COY waters have generally greater magnitude than those in OY waters (Isada et al., 2010; Okamoto et al., 2010) and contributes considerably to fisheries and aquaculture in this region (Nishimura et al., 2002; Isoda and Kishi, 2003). Like in OY waters, water column stratification may be highly relevant to the initiation of the bloom in COY waters (Kasai et al., 1997). Yoshimori et al. (1995) noted that the blooms in COY waters can exist for a longer time than those in OY waters due to continuous nutrient supply with its weaker vertical stability. The phytoplankton bloom in COY waters would significantly affect primary production in surrounding waters including the OY by physical processes such as advection and eddy diffusion (Shinada et al., 1999; Okamoto et al., 2010). These pilot studies on the spring blooms in COY waters investigated relationships among physical and biological parameters for estimating the bloom dynamics, but no study has been conducted to investigate the photophysiology and community composition of phytoplankton in COY waters. Low temperatures observed in COY waters can decrease growth rates and the photosynthesis of phytoplankton (Eppley, 1972; Raven and Geider, 1988). In addition, low temperatures in COY waters could be far below the thermal optimum for the carbon fixing enzyme of the Calvin cycle, Ribulose 1, 5- bisphosphate carboxylase/oxygenase (RuBisCO) (Descolas-Gros and de Billy, 1987; Young et al., 2015). In spite of low temperatures, however, intense and extensive diatom blooms are observed in COY waters every

spring. Corresponding to the different origins of COY and OY waters, it can be expected that the composition of diatoms may also be distinct between these two water masses.

Regarding zooplankton community, significant differences in community composition were reported at the species level between these water masses (Yamaguchi et al., 2003; Abe et al., 2014), however, information about possible differences in phytoplankton community composition are still missing.

From the aforementioned results, we hypothesized that (i) phytoplankton community composition in COY waters is distinctly different from offshore regions, and (ii) low temperatures in COY waters inhibit phytoplankton photosynthesis, specifically carbon fixation processes. In regards to the latter, we expect the subsequent warming of the water column during spring enhances photosynthetic activity. In this study, phytoplankton community composition in COY waters during spring was assessed with both phytoplankton pigment signatures and DNA-based next-generation sequencing (NGS) technology. Pigment analysis using the Suzuki et al. (2015) method of ultra-high performance liquid chromatography (UHPLC) allowed us to estimate the community composition of phytoplankton assemblages at the class level, whereas the relative contributions of each diatom genus to the total biomass of diatoms were quantified with the NGS method. In addition, the photophysiology of phytoplankton in COY waters during the pre-bloom and bloom periods were investigated using the following: a) active Chlorophyll fluorescence techniques, e.g., pulse amplitude modulated (PAM) and fast repetition rate (FRR) fluorometry; b) the transcription activity of the diatom-specific *rbcL* gene, which encodes the large subunit of RuBisCO; c) carbon-based photosynthesis-irradiance (*P-E*) curve experiments; and d) 77 K emission spectroscopy. The active Chlorophyll fluorescence techniques enabled us to measure photosynthetic activities (i.e., the maximum quantum yield of photochemistry) in photosystem II (hereafter PSII). On the other hand, transcription levels of the diatom-specific *rbcL* gene determined by reverse transcribed quantitative PCR can be used as an indicator for the activity of the light independent reactions of photosynthesis because RuBisCO encoded by the *rbcL* gene is the rate-determining enzyme of the process (John et al., 2007). Moreover, carbon-based *P-E* curves provide powerful insights into photophysiological states such as photoacclimation and nutrient stress (Sakshaug et al., 1997; MacIntyre et al., 2002) through the whole photosynthetic processes from light absorption to carbon fixation. Emission

spectroscopy also provided semiquantitative information about the presence of major taxonomic groups and the physiological status of phytoplankton. The combination of these techniques provides us with holistic information on the photosynthetic processes of phytoplankton in COY waters. To elucidate the photophysiological responses of phytoplankton to temperature, we also performed, for the first time ever, temperature-controlled bottle incubation experiments in COY waters.

2.2. Materials and methods

2.2.1. Water sampling and optical observation

Surface (5 m) seawater samples were collected from the western subarctic Pacific off the southeastern Hokkaido (Japan) coast as part of the R/V *Hakuho Maru* KH-15-1 expedition during 6–26 March 2015 and the TR/V *Misago Maru* field study (hereafter AK15 expedition) during 16–17 April (Fig. 1). Prior to water sampling during the KH-15-1 expedition, vertical profiles of photosynthetically available radiation (PAR) spanning 400–700 nm, E_d(PAR) and spectral downward irradiance, $E_d(\lambda)$, were obtained with the Compact-Optical Profiling System (C-OPS) co-developed by Biospherical Instruments Inc. and NASA (Hooker et al., 2013). Vertical attenuation coefficients of downward PAR, K_d (PAR) were determined as the slopes of a least-squares regression of the natural-log transformed E_d(PAR) profiles using Processing of Radiometric Observation of Seawater using Information Technologies (PROSIT) software (Hooker, 2014). Based on the derived K_d (PAR) value, euphotic zone depth (Z_{eu}) was calculated as the depth with 1% of the surface PAR remaining (Kirk, 2010). The incident PAR above the sea surface (E_0) was measured on-deck continuously with an LI-190SB air quantum PAR sensor and recorded by a LI-1400 data logger (LI-COR, Inc.) every 5–10 min. Surface (~5 m depth) seawater samples were obtained using a CTD carousel multi-sampler system (CTD-CMS) with acid-cleaned Niskin bottles. Upon collection, seawater was poured into a 9 L polycarbonate (PC) carboy, four 300 mL PC bottles for the measurements of primary productivity, and two polystyrene tubes for nutrient analyses. Concentrations of nutrients (nitrate + nitrite, ammonia, phosphate, and silicate) were determined with a BRAN-LUEBEE autoanalyzer (QuAAtro). Mixed layer depths (MLD) at all stations were

calculated as the depth at which the potential density anomaly ($\Delta\sigma_\theta$) of the water column increased by 0.125 kg m^{-3} relative to the layer at 10 m (Monterey and Levitus, 1997).

2.2.2. Phytoplankton pigment composition

Seawater collected was dispensed into two 1 L PC bottles and these subsamples were filtered onto GF/F filters using a gentle vacuum (<0.013 MPa). Filters were then blotted dry between filter papers, placed into cryovials, and immediately frozen in liquid nitrogen. Frozen filters were stored at −80 °C until further analysis. Pigments were extracted with the *N*, *N*-dimethylformamide (DMF) sonication method of Suzuki et al. (2002). Pigment concentrations were then determined by high-performance liquid chromatography (HPLC) or UHPLC following Van Heukelem and Thomas (2001) with a few modifications and Suzuki et al. (2015), respectively. To estimate phytoplankton community composition at the class level, multiple linear regression analyses based on major diagnostic pigment signatures and Chlorophyll *a* (Chl *a*) were performed following Suzuki et al. (1997) and Obayashi et al. (2001), wherein fucoxanthin (Fuco) and peridinin (Peri) are representative algal marker pigment for diatoms and dinoflagellates, respectively. Although Fuco can also be observed in other phytoplankton taxa, e.g., chrysophytes, haptophytes and some dinoflagellates, we assumed Fuco was solely derived from diatoms in this study. This assumption can be justified with the results of Suzuki et al. (2011) who found a significant relationship between Fuco and diatom carbon during a spring bloom study in the study area. The following multiple linear regression of pigment markers was used:

$$[\text{Chl } a] = A[\text{Fuco}] + B[\text{Peri}] + C, \quad (2.1)$$

wherein [Chl *a*], [Fuco], and [Peri] are the concentrations of each pigment; *A* and *B* are partial regression coefficients for each concentration of the pigment markers; and *C* is a constant term of the multiple linear regression. The multiple linear regression analysis, and its validation with a *t*-test for each coefficient plus *F*-test, were performed with SigmaPlot software program ver. 11.0 (System Software). After this procedure, the contributions of each phytoplankton taxon to the total Chl *a* level were calculated by dividing a product of each concentration of pigment and its coefficient

value by [Chl *a*] for each station.

2.2.3. Size-fractioned Chl *a* concentration

Seawater samples were filtered onto a 47 mm nylon mesh (20 μm poresize), a 47 mm Nuclepore membrane (10 or 2 μm pore size) and a 25 mm Whatman GF/F filter (nominal pore size 0.7 μm) using a gentle vacuum (<0.013 MPa). After filtration, filters were placed in cryovials, immediately flash frozen in liquid nitrogen, and stored at −80 °C until further analysis. After thawing, the filters were transferred into glass cuvettes and soaked in 6 mL DMF at −20 °C for at least 24 h to extract phytoplankton pigments (Suzuki and Ishimaru, 1990). Chl *a* concentrations were determined with a Turner Designs 10-AU fluorometer using the non-acidification method of Welschmeyer (1994). The three size classes were defined as microphytoplankton (>20 μm), nanophytoplankton (2–20 μm), and picophytoplankton (0.7–2 μm).

2.2.4. Ion Torrent next-generation sequencing (NGS)

Seawater samples for DNA analysis were collected sequentially on 25 mm polycarbonate Isopore filters (Millipore, 2 μm pore size) with a gentle vacuum (<0.013 MPa) and then stored at −80 °C until further analysis. DNA samples were extracted using the method of Endo et al. (2013). Extracted DNA samples were purified using a NucleoSpin® gDNA Clean-up (Macherey-Nagel) following the manufacturer's protocols. The extracted DNA was sequenced with an Ion Torrent Personal Genome Machine (PGM) targeting the diatom-specific 18S rRNA gene V4 region. NGS libraries of DNA were constructed for each sample obtained from all stations and from the temperature-controlled incubation experiments. Gene fragments of the diatom-specific 18S rRNA V4 region sequences were amplified with the Takara Ex Taq Hot Start Version (Takara) and diatom-specific fusion primer pairs with 12 barcodes:

Forward primer: 5′-GATGATGARAAYATTAACTCW-3′

Reverse primer: 5′-TAWGAACCTTTWACTTCWCC-3′

The forward primer included the A-adapter sequence (5′-CCATCTCATCCCTGCGTGTCTCCGAC-3′), the key sequence (5′-TCAG-3′), the barcode sequences set by the manufacturer (Thermo Fisher

Scientific) and a barcode adapter sequence (5′-GAT-3′) upstream of the forward primer. The reverse primer included the truncated Pi-adapter (trP1: 5′-CCTCTCTATGGGCAGTCGGTGAT-3′) sequence upstream of the reverse primer. PCR mixtures consisted of 1 × Ex Taq Buffer, 0.2 mM dNTP, 0.4 μM of the fusion primers, 0.625 unit of Taq polymerase, and 2 μL DNA template for a 25 μL total volume. PCR cycles within a thermal cycler were performed using the following conditions: 94 °C for 60 s, 30 cycles under 98 °C for 10 s, 56 °C for 30 s, and 72 °C for 60 s. After the final cycle, the temperature was held at 72 °C for 10 min to complete the PCR reactions. PCR products were purified with an Agencourt AMPure XP Kit (Beckman Coulter) and 70% ethanol following the manufacturer's protocols. The concentration of the purified amplicons was determined with an Agilent 2100 Bioanalyzer (Agilent Technologies) using an Agilent 1000 Assay Kit according to the manufacturer's protocol. Based on the results of the Bioanalyzer, the purified amplicons were diluted to a concentration of 13 pM. Once NGS libraries were constructed, emulsion PCR was conducted with an Ion One Touch 2 system and an Ion PGM Template OT2 400 kit (Thermo Fisher Scientific). The resultant emulsion PCR products were then enriched with Ion One Touch ES (Thermo Fisher Scientific) according to the manufacturer's protocols. The enriched templates were loaded onto an Ion 318 v2 chip (Thermo Fisher Scientific) and amplicon libraries were sequenced with an Ion Torrent PGM system using the Ion PGM sequencing 400 kit v2 (Thermo Fisher Scientific) following the manufacturer's protocols.

To remove sequences with low quality and polyclonal sequences which did not match the A-adapter, quality filtering was initially performed with the Torrent Suite™ Software (Thermo Fisher Scientific). Additionally, inapplicable sequencing reads which unmatched the trP1 adapter sequence and the reverse primer sequence were removed with the FASTX-Toolkit (http://hannonlab.cshl.edu/fastx_toolkit/). After removal of forward and reverse primers, reads between 18 and 270 bp were extracted as 18S rRNA V4 regions. In addition, reads with a quality score of less than 23 were also excluded from the analysis. The obtained sequences were exported as FASTQ files and then converted to FASTA files with the mothur v. 1.25.0 (SChloss et al., 2009) software.

Using the FASTA files obtained for taxonomic classification based on the diatom-specific 18S

rRNA V4 region, representative 10,000 reads were deposited to the SILVAngs web interface (https://www.arb-silva.de). The reads were classified with >93% classification similarity to SILVA SSU Ref dataset 123.1. Data which did not match diatoms were excluded from the classification results. For full details of the sequencing methods, see Endo et al. (2016).

2.2.5. Variable Chl *a* fluorescence by PAM and FRR fluoremetry

Seawater was dispensed in a 30 mL amber bottle and stored in the dark at ambient temperature for 30 min for dark acclimation to ensure fully open PSII reaction centers. After acclimation, samples were transferred to a quartz cuvette (15 mm pathlength) in a dark environment and placed inside a pulse amplitude modulation (PAM) fluorometer (Walz, Germany) and a fast repetition rate (FRR) fluorometer (Chelsea Technologies Group, West Mosley, UK) to determine the maximum quantum yield of photochemistry in PSII defined as F_v/F_{mPAM} and F_v/F_{mFRRf} for measurements made with the PAM and FRR fluorometers, respectively. In addition to F_v/F_{mFRRf}, the FRRf also provided measurements of the effective absorption cross sections of PSII, σ_{PSII}, and the concentration of functional PSII reaction centers, [RCII]. PAM and FRR fluorometry measurements were conducted on multiple subsamples from each sample (i.e., pseudo-replication) following Liu et al. (2009) for PAM fluorometry, and Kolber et al. (1998) and Oxborough et al. (2012) for FRRf fluorometry.

2.2.6. Light absorption coefficient of phytoplankton

Seawater was filtered onto Whatman GF/F filters using a gentle vacuum (<0.013 MPa). After filtration, filters were carefully wrapped in aluminum foil to avoid any creases and then stored at −80 °C until further analysis. Following Kishino et al. (1985), the optical density of particles and detritus on the filters (OD_{fp} and OD_{fd}, respectively) was measured with a multipurpose scanning spectrophotometer (MPS-2450, Shimadzu) equipped with an end-on type photomultiplier tube in 1 nm steps from 350 to 800 nm before and after soaking filters in methanol for 15 min to remove phytoplankton pigments. Measurements before methanol extraction corresponded to the total absorption, those after methanol extraction to OD_{fd} and the difference between the two to OD_{fp}. All spectra were scatter corrected by subtracting the average value from 730 nm to 750 nm across the

visible range (Babin and Stramski, 2002). Both OD_{fp} and OD_{fd} were converted to absorption coefficients, $a_p(\lambda)$ and $a_d(\lambda)$, respectively, using an appropriate path length amplification factor (Cleveland and Weidemann, 1993). The resultant $a_p(\lambda)$ values were then averaged from 400 to 700 nm and weighted to the spectral irradiance of the incubator lamp, $E_{PARinc}(\lambda)$ used for photosynthesis versus irradiance measurements to give mean absorption coefficients of phytoplankton ($\bar{a}_{ph}$) and mean Chl *a*-specific absorption coefficient of phytoplankton, $\bar{a}^*_{ph}$ following Isada et al. (2013).

2.2.7. Photosynthesis vs. irradiance (*P-E*) curve and photosynthetic parameters

For each curve, surface seawater samples and incubation experiment samples (see section 2.2.9) were dispensed into twelve 275 mL polystyrene bottles and inoculated with ca. 0.1 mg of $NaH^{13}CO_3$ (99 atom% ^{13}C purity, Cambridge Isotope Laboratories, Inc.). Two bottles at time zero remained without any isotope. Samples were then incubated in a temperature-controlled incubator under 10 different light intensitiesbetween 1.44 and 1800 μmol photons m^{-2} s^{-1} for 2 h under both, ambient or an altered temperature (see details below under point 2.9). After incubation, samples were filtered onto pre-combusted 25 mm GF/F glass fiber filters (Whatman), which were stored at −80 °C until further analysis. Photosynthetic rates were calculated from ^{13}C uptake rates measured with an on-line element analyzer (FlashEA1112, Thermo Finnigan)/isotope ratio mass spectrometer (Delta-V, Thermo Finnigan) (EA/IRMS) following Hama et al. (1983), normalized to Chl *a* and plotted versus irradiance. The resultant P^B-*E* curves were fitted to the model of Platt et al. (1980). Detailed descriptions of *P-E* curve parameters were shown in Table 4.

2.2.8. Primary productivity

Seawater was dispensed into four acid-cleaned 300 mL PC bottles, inoculated with ∼0.1 mg of $NaH^{13}CO_3$ and incubated for 24 h in an on-deck incubator at ambient temperature, either at ambient irradiance (3 replicate samples) or in darkness (1 sample). After incubation, samples were filtered onto pre-combusted 25 mm GF/F glass fiber filters (Whatman) and stored at −80 °C until further analysis as described above. Primary productivity, *PP*in the units of mg C m^{-3} day^{-1} for each sample

was then calculated following Hama et al. (1983).

2.2.9. Temperature-controlled incubation experiments

To assess the effects of temperature on phytoplankton assemblages in COY waters, on-deck temperature-controlled bottle incubation experiments were conducted using surface seawater collected from ca. 5 m depth, and dispensed into three 9 L PC carboys at stations Bio-6, Bio-7, Bio-10, and Bio-13 (Fig. 1). One of the three carboys was used for time zero samples, the remaining two were used to test for the effect of temperature, with ambient temperature being the control and +7 °C being the high temperature treatment. The +7 °C-increased temperatures were almost comparable to those at the peak of blooms in studied area (e.g., Isada et al., 2018) and after the warm-core eddy instrusions which frequently occur in the area (Okamoto et al., 2010). To avoid any interference from possible light effects, bottles were covered with black foil during the entire 24 h incubation. After incubation subsamples were collected to determine diatom community composition by NGS (Section 2.4) and to measure photosynthetic physiology by variable fluorescence and *P-E* experiments (Sections 2.2.5 and 2.2.7) combined with analyses of the transcription level of the diatom-specific *rbcL* gene by qRT-PCR(see following).

2.2.10. Transcriptional level of diatom-specific *rbcL* with qRT-PCR method

Sampling and extraction of DNA were performed as described above (Section 2.2.4). Seawater for RNA samples was filtered onto 25 mm polycarbonate Isopore filters (Millipore, 2 μm pore size) with a gentle vacuum (<0.013 MPa). Filters for RNA analysis were placed in cryotubes containing 0.2 g of pre-combusted 0.1 mm glass beads and 600 μL RLT buffer (Qiagen), to which 10 μL β-mercaptoethanol (Sigma-Aldrich) were added. After filtration, RNA samples were immediately frozen in liquid nitrogen and stored at −80 °C until further analysis. RNA retained on the filters were extracted following Endo et al. (2015). The extracted RNA was then reverse transcribed into cDNA with the PrimeScriptTM RT Master Mix (RR036, Takara) according to the manufacturer's specifications. Copy numbers of the diatom-specific *rbcL* gene in extracted DNA and transcribed cDNA samples were quantified by quantitative PCR (qPCR) with standards of the diatom-

specific *rbcL* gene, which were produced from the diatom *Thalassiosira weissflogii* (CCMP1336) in accordance with Endo et al. (2015).

2.2.11. Low temperature (77 K) emission spectra

The emission spectra at 77 K were measured on board using a custom-built portable emission spectrometer (Prášil et al., 2009) and measuring procedures described in Hill et al. (2012) with the following exceptions: the volume of seawater filtered on the 25 mm Whatman GF/F filters was 1.2 L. For each sample, six emission spectra were collected, using LEDs with different excitation wavelengths (390, 455, 470, 505, 530 and 590 nm). From each spectrum, a blank spectrum (measured using filter soaked in distilled water) was subtracted.

2.2.12. Statistical analyses

Statistical analyses were conducted using the SigmaPlot software program ver. 11.0 (SystStat Software, Inc.) except for the cluster analysis evaluating diatom community composition, which was carried out in the statistical software R (http://www.r-project.org). Spearman's correlation analysis was used to assess relationships between variables. Multiple linear regression analysis was conducted to determine the contributions of each diatom group to total Chl *a*. Cluster analysis was performed to investigate differences in community composition of diatoms using Bray-Curtis dissimilarity and an average clustering method. Statistically significant differences between clusters were assessed with a multivariate analysis of variance (MANOVA) test and the Wilks' lambda discriminant analysis.

2.3. Results

2.3.1. Hydrographic conditions

Sea surface temperatures (SST) observed during the KH-15-1 expedition were generally low ranging from 0.0 to 1.6 °C whereas higher SST between 2.4 and 3.8 °C were observed during the AK15 cruise (Table 1). Values of sea surface salinity (SSS) were lower than 33 throughout both expeditions with the lowest SSS value of 32.1 being observed at Station AK15-1 (Table 1). Nutrients in surface waters

were generally abundant during the KH-15-1 expedition. The deepest mixed layer depth (MLD) of 28.6 m was found at Station Bio-10 whereas the shallowest MLD of 15.8 m was found at Station Bio-6 (Table 1 and Fig. 1). During the KH-15-1 expedition, the depth (z) of the euphotic zone (Z_{eu}) was generally shallower than the MLD with Station Bio-6 being an exception (Table 1). Stations on the shelf ($z \leq 100$ m) were classified as shelf COY, whereas those in rather oceanic regions ($z > 100$ m) were defined as offshore COY (Fig. 1 and Table 1). Warm water masses with a relatively high temperature of ~4 °C intruded into offshore COY waters from the western part of the coast between the isopycnal surfaces ($\sigma_\theta = 26.7–26.8$; Appendix A). Thus, we refer to these stations as "Tokachi" to distinguish them from the other offshore and shelf sites (stations Bio-4 and Bio-13).

2.3.2. Phytoplankton pigments

Concentrations of Chl *a* were generally <1 mg m^{-3} except at stations Bio-14, AK15-1 and AK15-2 (hereafter bloom stations) (Fig. 2a). Chl *a* concentrations were positively correlated with SST, but negatively with SSS (Table 2). Fuco, Peri, and diadinoxanthin (DD) were the predominant carotenoids (Appendix B) and were used in the following multiple regression to derive total Chl *a* according to:

$$[\text{Chl } a] = 2.00\,[\text{Fuco}] + 1.78\,[\text{Peri}] + 0.107, \quad (2.2)$$

wherein $n = 21$, $r^2 = 0.994$, t-value for Fuco = 56.0 ($p < 0.001$), t-value for Peri = 2.85 ($p < 0.05$), t-value for the constant = 2.12 ($p < 0.05$), and $F = 367$ ($p < 0.001$). Diatoms were predominant at all sampling stations contributing between 54 and 96% of total Chl *a* and >90% at the bloom stations (Fig. 3a).

2.3.3. Size-fractioned Chl *a* concentration

Nanophytoplankton dominated the phytoplankton community during the KH-15-1 expedition with the exception of the bloom stations and Station Bio-7, where microphytoplankton (>20 μm) dominated the phytoplankton assemblages. The lowest contribution (8.36% of total Chl *a*) of microphytoplankton was found at the farthest offshore Station Bio-10 (Fig. 3b).

2.3.4. Diatom community composition

The genera *Thalassiosira*, *Minidiscus*, *Skeletonema*, *Fragilariopsis*, and *Pseudo-nitzschia* dominated the diatom assemblages (Fig. 4) with minor contributions of diatoms belonging to the subdivision of Coscinodiscophytina. The genus *Thalassiosira* contributed >40% to the total Chl *a* at the bloom stations (Bio-14, AK15-1 and AK15-2) and stations Bio-6 and Bio-7 (Fig. 4). Thus, the composition of the diatom community at these shelf COY stations was significantly different from that at other stations ($p < 0.01$, One-way MANOVA, Wilk's lambda; Fig. 5). At the offshore COY and Tokachi stations, diatom communities were characterized by the dominance of *Thalassiosira*, *Minidiscus* and *Fragilariopsis*.

2.3.5. Variable Chl *a* fluorescence

$F_v/F_{m\ PAM}$ values determined with the PAM fluorometer varied between 0.17 and 0.55 (Fig. 2b), giving an average of 0.35 ± 0.11 across all sites. The highest and lowest $F_v/F_{m\ PAM}$ values were observed at Stations AK15-1 and Bio-10, respectively. Also, $F_v/F_{m\ PAM}$ was significantly correlated with Chl *a*, P^B_{max}, Φ_{Cmax}, and *PP*, ($p < 0.01$, $<0.01 < 0.05$, and <0.001, respectively; Spearman-Rank correlation, Table 3). During the KH-15-1 expedition, F_v/F_m measured by FRR fluorometry ($F_v/F_{m\ FRRf}$) (Appendix C) showed a similar spatiotemporal variations as $F_v/F_{m\ PAM}$ ($\rho = 0.483$, $n = 20$, $p < 0.05$, Spearman-Rank correlation), although a large difference between $F_v/F_{m\ FRRf}$ and $F_v/F_{m\ PAM}$ was observed at Station Bio-1. Values of the functional absorption cross-section for PSII (σ_{PSII}) varied between 2.43 and 3.78 $nm^2\ PSII^{-1}$. The lowest and highest values were observed at Stations Bio-14 and Bio-2, respectively, which deviated from values at the other stations. A much larger variability, however, was observed in the concentration of functional PS II centers [RCII], which varied between 0.49×10^{-9} and 5.57×10^{-9} mol m^{-3} at Station Bio-1 and Bio-14, respectively (Appendix C). The latter was also the site with the highest Chl *a* concentration.

2.3.6. Light absorption coefficient of phytoplankton

The Chl *a*-normalized light absorption coefficient for phytoplankton ($\bar{a}^*_{ph}$) at the bloom stations as

well as at Station Bio-6 were relatively low compared to the other sites of this study (Fig. 2c). In particular, values of $\bar{a}^*_{ph}$ obtained during the AK15 cruise were one order of magnitude smaller than those during the KH-15-1 expedition.

2.3.7. Low temperature (77 K) emission spectra

We have observed significant variability among the 77 K emission spectracollected at each station. The variability can be linked to species composition and the physiological state of phytoplankton. An example of emission spectra in the 660–700 nm region is given in Appendix D, panels A and B. The phytoplankton emission in this spectral region is composed of several overlapping bands: the major band peaks at 685 nm and originates from PSII reaction centers, the band at 695 nm originates from active PSII containing CP47 (Suggett et al., 2009a; D'Haene et al., 2015) and in some cases less intense bands at 675 and 680 nm were observed. In eukaryotic phytoplankton, the 680 nm band originates from loosely coupled antenna pigments with less efficient energy transfer to the PSII reaction center. The 675 nm band (Appendix D, panel B) is specific for emission from Peri containing peripheral peridinin-Chlorophyll *a*-protein (PCP) antenna proteins in dinoflagellates and is excited only by the 500–600 nm wavelengths absorbed by PCP (Hill et al., 2012). Using simple analysis of the emission spectra based on the measured emission intensities at given wavelength, we have observed correlation ($r^2 = 0.598$) between the relative content of Peri (determined by UHPLC) and the increase of emission at 675 nm (Appendix D, panel C) or between the functional cross-section of PSII measured by FRR fluorometry and the intensity of the emission in the 675–680 nm region ($r^2 = 0.732$, see Appendix D, panel D). The increased emission band around 695 nm, indicating phytoplankton with active PSII (Suggett et al., 2009a), was observed only at station Bio-14 (Appendix D, panel B).

2.3.8. *P-E* curves and their photosynthetic parameters *in situ*

Values of α^B varied between 0.00949 and 0.0383 (mg C mg Chl a^{-1} h^{-1}) (μmol photons m^{-2} $s^{-1})^{-1}$ (Fig. 2d), and the β^B values ranged between 0.000628 and 0.00912 (mg C mg Chl a^{-1} h^{-1}) (μmol photons m^{-2} $s^{-1})^{-1}$(Fig. 2e). P^B_{max} values, however, were relatively constant and ranged between 1 and 2 mg C mg Chl a^{-1} h^{-1} except at the bloom stations (Fig. 2f). The E_k values varied from 83.2 to

235.0 μmol photons m^{-2} s^{-1} giving an average value with standard deviation of 131.8 ± 53.2 μmol photons $m^{-2}s^{-1}$ (Fig. 2g). Values of Φ_{Cmax} were rather constant (0.0068–0.0275) except at the bloom stations (Fig. 2h). The P^B_{max} and E_k showed negative correlations with respect to SSS (Table 2).

2.3.9. Primary productivity

Primary productivity (*PP*) at all sampling stations ranged between 3.56 and 255.40 mg C m^{-3} d^{-1} (Fig. 2i) being highest at the bloom stations. Lowest *PP* was observed at Station Bio-1, which also had the lowest SST values (Fig. 2i, Table 1). Also note that *PP* was significantly correlated with SST and Chl *a* ($p < 0.05$ and < 0.001, respectively, Spearman-Rank correlation, Table 2, Table 3).

2.3.10. On-deck temperature-controlled bottle incubation experiments

Phytoplankton pigment signatures revealed that algal community composition calculated from Eq. (2.2) changed relatively little (<5%) during our incubations, except at Station Bio-6 where the contribution of dinoflagellates increased from 39.7% to 47.7% in the 7 °C treatment (Fig. 6). Similarly, little changes in the composition of diatoms occurred throughout all experiments except at Station Bio-13 (Tokachi waters) where growth of *Minidiscus* was stimulated in the 7 °C treatment (Fig. 7).

At the end of the incubation, the *P-E* curve parameters varied differently between incubations at different stations (Fig. 8). Values of α^B increased by ca. three-fold in the 7 °C treatment during the Bio-7 experiment, while changes at the other sites were much less pronounced (Fig. 8a). The P^B_{max}values increased in both treatments at most sites. The exception was Station Bio-10, where P^B_{max} showed a slight decrease in both the control and 7 °C treatment (Fig. 8c). Changes in E_k were variable increasing after incubation at 7 °C during experiments at stations Bio-6 and Bio10, but decreasing at Station Bio-7 (Fig. 8d). Φ_{Cmax} was highest in the +7 °C treatment at Stations Bio-7 and Bio-13 (Fig. 8f). At the shelf COY (Bio-6 and Bio-7) and Tokachi (Bio-13) stations where the water was <100 m deep, values of the diatom-specific *rbcL* gene expression for the +7 °C treatments were higher than those of the controls (Fig. 8g). Values of $\bar{a}^*_{ph}$and F_v/F_{mPAM} varied little among treatments at all stations (Fig. 8e, h).

2.4. Discussion

2.4.1. Hydrography

Cold, low-salinity waters extended completely across our sampling sites throughout the observation period i.e., early spring (Table 1). Following the water mass definitions in this study area proposed by Ohtani (1971), OY waters were not detected. The results were similar to observations of Kasai et al. (1997) who demonstrated that COY waters extended from the coast off Hokkaido to the offshore station at 42° 40′ N, 144° 55′ E in March 1990, 1991, and 1992.

2.4.2. Abundance and community composition of spring phytoplankton in the COY

The temporal variation in Chl *a* concentration suggests that the sampling period covered both, the pre-bloom and bloom phase (Fig. 2a), with the former being characterized by low Chl *a* concentrations (<1 mg m^{-3}). The subsequent increase in Chl *a* concentration during the AK15 expedition represented the spring bloom at the shelf COY stations (Fig. 2a), which matches the observations of Kasai et al. (1997) who also reported peaks in Chl *a* in COY waters in April. Kasai et al. (1997) also proposed that shoaling of the MLD due to water-column stratification may be an important factor for bloom initiation. In this study, however, there was no significant relationship between any of the photosynthetic parameters (including Chl *a*) and MLD (Table 2).

The substantial increases in Chl *a* and Fuco at the bloom stations indicated that the blooms on the COY shelf were dominated by diatoms (Fig. 3a and Appendix B). The large increase in the relative contribution of microphytoplankton to the total phytoplankton also supports this notion (Fig. 3b). Interestingly, our DNA sequencing analysis showed that the composition of the diatom assemblages in most of the shelf COY stations differed from those of other water masses (Fig. 4, Fig. 5). Because the shelf COY stations were located in relatively shallow waters, resuspensionof benthic diatoms from shelf sediments might affect either or both community composition and bloom formation (e.g. McQuoid and Godhe, 2004), although no information on the composition of the benthic algal community is available for our study area. The discrimination between the shelf COY and other waters masses was based mainly on the presence and dominance of *Thalassiosira* (Fig. 4). Shinada et

al. (1999) observed *Thalassiosira* blooms in Funka Bay when COY waters intruded into the bay in early spring. In this study, the genus *Thalassiosira* was the bloom-forming species in the shelf COY waters indicated by the contribution of *Thalassiosira* becoming high at the bloom stations (Fig. 4). The genera *Fragilariopsis* and *Minidiscus* were relatively abundant in offshore COY and Tokachi waters (Fig. 4). Suzuki et al. (2011) reported that the genus *Fragilariopsis* was abundant in OY waters. The substantial abundance of *Minidiscus*, however, has not been reported in both COY and OY waters likely because the genus *Minidiscus* can be overlooked with conventional light microscopy due to its small size, i.e., nanophytoplankton (Hasle and Syvertsen, 1996). Although blooms of the genus *Chaetoceros* are commonly and annually observed during the bloom period (Mochizuki et al., 2002; Hattori-Saito et al., 2010; Suzuki et al., 2011), the contributions of *Chaetoceros* to the diatom assemblages (as determined with the next-generation sequencing method) were generally low and negligible (<4%) (Fig. 4). Hattori-Saito et al. (2010) also observed the predominance of *Thalassiosira* at the pre-bloom station at COY and OY regions, whereas *Cheatoceros* outcompeted other taxa at the OY bloom station. Both pigment analysis (presence of peridinin, Appendix B) and 77 K emission spectroscopy (Appendix D, panel C) indicated increased presence of dinoflagellates at near-coast stations Bio-6, 7 and 4.

2.4.3. Photosynthetic physiology of spring phytoplankton in the COY

At the bloom stations with high Chl *a* concentrations (i.e., stations Bio-14, AK15-1, and AK15-2), we also observed high P^{B}_{max}, Φ_{Cmax}, and *PP* values (Fig. 2a, f, h, and i), suggesting that the photophysiological states of phytoplankton had improved from the pre-bloom period. In addition, P^{B}_{max} showed a significant correlation with other photosynthetic parameters, i.e. F_v/F_{mPAM}, $\Phi_{Cmax,}$ and *PP* (Table 3). In turn, it should be noted that the F_v/F_{mPAM} values correlated with *PP* and Chl *a* concentration as well (Table 3). Consequently, light reaction processes in PSII are important for the underlying mechanisms such as coupling of antenna pigments to PSII reaction centers (discussed below) to control *PP*and phytoplankton biomass during the observation period. Indeed, the increase in [RCII] (i.e., the concentration of PSII reaction centers) at Station Bio-14 indicated the significance of light reaction processes in the bloom development (Appendix C). We also observed, for the first time,

correlations between the effective absorption cross-section of PSII (σ_{PSII}) and the relative intensity of the emission band at 680 nm that forms a low-wavelength shoulder of the main emission band assigned to PSII (see Appendix D, panels A and D). We assign this band to emission from antenna Chlorophylls that are not tightly coupled to PSII reaction centers. We note that phytoplankton with high σ_{PSII} also shows a higher proportion of loosely coupled antenna pigments. Interestingly, at the high-Chlorophyll station Bio-14 we detected both, low values of σ_{PSII}, a low proportion of uncoupled antenna and a significant increase in active PSII (see emission at 695 nm, Appendix D, panels A and B). This enhanced coupling of antenna pigments at Station Bio-14 could lead the high F_v/F_m, P^B_{max} and *PP* values (Fig. 2b, f, and i), which might be associated with bloom development in COY waters. Interestingly, the SSS showed significant negative correlations with the photosynthetic parameters including P^B_{max}values and Chl *a* concentration (Table 2), which implies the surface phytoplankton assemblages in low saline shelf COY waters had relatively higher carbon fixation rates. Co-variations of the P^B_{max} and α^B values were not found in this study (Table 3), indicating E_k-dependent variability (Behrenfeld et al., 2004) in photosynthesis. According to Behrenfeld et al. (2004), the physiological mechanisms responsible for E_k-dependent variability generally involve acclimation strategies aimed at maximizing growth under variable light conditions. On the other hand, in the OY region, E_k-independent variability, which is the result of co-variation in P^B_{max} and α^B, was observed from March to May by Isada et al. (2009) and in the post-bloom phase by Yoshie et al. (2010). Additionally, Yoshie et al. (2010) pointed out that water temperature and ammonium levels significantly affected the E_k-independent variability. In this study, water temperatures of COY remained relatively low (<4 °C; Table 1) and ammonia did not influence any photosynthetic parameters (Table 2). The SST values, however, showed significant positive correlations with Chl *a* and *PP*, suggesting that temperature was a significant driver for biomass and primary production. The contribution of microphytoplankton to total Chl *a* correlated positively with the photosynthetic parameters including Chl *a*, F_v/F_{mPAM}, P^B_{max}, and *PP* (Table 2), indicating that microphytoplankton contributed considerably to bloom formation in this area. The contributions of diatoms to Chl *a* concentrations, however, did not show any significant correlation with these photosynthetic parameters (Table 2). The results imply that some specific diatoms had different

photosynthetic strategies and formed the bloom in April. In fact, the contributions of *Thalassiosira* to the total diatoms showed a positive relationship with P^{B}_{max} among the diatom groups (Table 2), which suggests the genus *Thalassiosira* bloomed in COY waters.

2.4.4. Physiological response of phytoplankton to temperature in COY waters

In the temperature-controlled experiments, the phytoplankton assemblages showed different responses among stations. Changes in the P^{B}_{max} values with the increase in temperature were prominent for the phytoplankton assemblages in the shelf COY (Stations Bio-6 and -7) and the Tokachi (Station Bio-13) waters, whereas no increase in P^{B}_{max} was observed for those in the offshore COY at Station Bio-10 (Fig. 8c). Similarly, the diatom-specific *rbcL* cDNA copies normalized by their DNA copies for the shelf COY and Tokachi assemblages also notably increased after the temperature change (Fig. 8g), suggesting that the transcriptional levels of the diatom-specific *rbcL* gene could be upregulated by the increase in temperature at these stations. Interestingly, the offshore COY assemblages showed little change in the transcription level of diatom-specific *rbcL* as well as P^{B}max (Fig. 8c, g). These concomitant increases indicate that the enhancement of the P^{B}_{max} for the shelf COY and Tokachi assemblages could be caused by the increases in the transcription level of the large subunit of RuBisCO with temperature. This hypothesis is supported by the fact that P^{B}_{max} values are controlled by the activity of RuBisCO (Li et al., 1984; Descolas-Gros and de Billy, 1987; Raven and Geider, 1988). In general, the optimal temperature of RuBisCO (40–50 °C) (Descolas-Gros and de Billy, 1987; Young et al., 2015) was far above the *in situ* SST (0–4 °C) observed in this study, and, thus, its activity would increase exponentially with temperature up to a certain point (Descolas-Gros and de Billy, 1987; Crafts-Brandner and Salvucci, 2000). The temperature increase, therefore, enhanced both the expression of the *rbcL* gene and the catalytic efficiency of RuBisCO, which eventually led to high carbon fixation rates. The genus *Thalassiosira* became the bloom-forming group in the shelf COY (Fig. 4), so the genus *Thalassiosira* might be capable of responding rapidly to environmental changes such as an increase in temperature. Their rapid growth, however, was not observed in the short-term incubation experiments. On the other hand, relative contributions of the genus *Minidiscus* to the diatom

assemblages increased at the Tokachi station (Bio-13) after the temperature increase (Fig. 7). Because the physiological and phylogenic information on *Minidiscus* were limited, further studies on this group are needed to understand their rapid increase.

Among the other photosynthetic parameters from *P-E* curve analyses, $\alpha^B$was considered to have little variation with temperature because α^B is an index for the capability of carbon fixation in light-limited environments and, thus, reflects mainly the light-dependent reactions of photosynthesis (Platt and Jassby, 1976; Kiefer and Reynolds, 1992; Kolber and Falkowski, 1993). In the incubation experiments at Stations Bio-7 and Bio-13, however, increases in α^B values were observed with temperature (Fig. 8a). Although similar results were also observed in the previous studies (e.g. Verity, 1981; Palmisano et al., 1987), the mechanisms are still unclear. As estimated from the small variations in F_v/F_{mPAM} (Fig. 8h), temperature negligibly affected the maximum quantum yield of PSII for the phytoplankton assemblages at all stations in this study, but the light-harvesting property of PSII could be affected by temperature. Because α^Bvalues relate to σ_{PSII} and the number of photosynthetic antennae (n) with varying non-photochemical quenching (e.g., Sakshaug et al., 1997), temperature might affect the light harvesting property of PSII i.e., n and σ_{PSII} (e.g., Mock and Hoch, 2005; Ralph et al., 2005).

2.5. Conclusions

This study demonstrated how phytoplankton assemblages changed their photophysiological properties in the COY regions in the early spring 2015 by combining the results of *in situ* measurements and on deck temperature-controlled incubation experiments. The SST and SSS were relatively low at the surface throughout the observation (< 4 ºC and < 33, respectively) and Chl *a* concentrations were generally near or far less than 1 mg m^{-3}, but the high Chl *a* concentrations exceeding 1 mg m^{-3} were observed at end of the KH-15-1 expedition and during the AK15 observation in the shelf COY water. It indicated that this study successfully captured development of the spring blooms in the shelf COY waters. The outstanding increase in the microphytoplankton and concentratios of fucoxanthin demonstrated that diatoms formed the bloom in the COY water. The NGS sequencing clarified that the

genus *Thalassiosira* mainly formed the blooms, and the community composition of diatoms in shelf COY waters was substantially different from other waters. The significant positive correlation between *Thalassiosira* abundance P^{B}_{max} as well as F_v/F_m supported the *Thalassiosira* bloom. Among physicochemical parameters, SST significantly correlated with the Chl *a* concentration and *PP*, suggesting temperature controlled phytoplankton biomass and carbon fixation. The temperature-controlled experiments showed that increases in temperature enhanced P^{B}_{max} of phytoplankton assemblages in shelf COY and Tokachi waters, whereas it was not the case for the offshore COY assemblage. Transcription levels of the diatom-specific *rbcL* gene showed the similar trend with P^{B}_{max} for the shelf COY and the Tokachi assemblages with upregulations under the increased temperatures. This study, therefore, clarified that phytoplankton assemblages in the shelf COY and Tokachi waters enhanced the transcription activity of large subunits of RuBisCO (i.e., potential synthetic rates of RuBisCO) with the increase in temperature. A temperature increase itself enhances the enzymatic activity of RuBisCO. The increase in SST has dual positive effect enhancing carbon fixation processes. Moreover, the 77K analysis clearly demonstrated that more photosynthetic antennae were coupled during the bloom than pre-bloom with a concomitant decrease in σ_{PSII}. This study applied multiple methods (i.e., active and 77K Chlorophyll *a* fluorescence, the qRT-PCR and the NGS sequencing) to quantify the activity of each photosynthetic process individually and comprehensively. This holistic approach successfully provided the temperature control on carbon fixation of phytoplankton and photosynthetic optimization when subpolar diatom blooms occur.

Chapter 3

Effects of iron and light availability on the photophysiology and community composition of phytoplankton in the western subarctic Pacific near the Kuril Islands

3.1. Introduction

Iron (Fe) is a crucial micronutrient for algal photosynthetic processes such as pigment synthesis, linear electron transfer, nitrate reduction, and detoxification of reactive oxygen (Sunda and Huntsman, 1995; Twining and Baines, 2013; Behrenfeld and Milligan, 2013). Indeed, a number of *in situ* mesoscale Fe fertilization experiments have revealed that Fe input enhances phytoplankton biomass and primary productivity in High Nutrient, Low Chlorophyll (HNLC) waters (e.g., Boyd et al., 2007). The western subarctic Pacific is a known HNLC region in summer (e.g., Tsuda et al., 2003; Suzuki et al., 2009; Hattori-Saito et al., 2010; Fujiki et al., 2014). This region is, on the other hand, the largest CO_2 sink by biological activity (Takahashi et al., 2002) and has high transport efficiency of particulate organic carbon in spring (Honda, 2003; Kawakami et al., 2004; 2015). These distinctive characteristics can be attributed to the active photosynthesis during the spring diatom bloom in the Oyashio region off the Kuril Islands (Isada et al., 2010; Yoshie et al., 2010; Suzuki et al., 2011). Fe deficiency for large (> 20 μm) diatoms, on the other hand, occurrs in the Oyashio region during the bloom phase (Hattori-Saito et al., 2010) and in the straits between the Kuril Islands (Yoshimura et al., 2010; Sugie et al., 2013; Suzuki et al., 2014).

Nishioka et al. (2007; 2013; 2014) and Nishioka and Obata (2017) suggested that the North Pacific Intermediate Water (NPIW) supplies terrestrial Fe from the Amur River via the Sea of Okhotsk and the Kuril straits to the Pacific. Nishioka et al. (2011) also pointed out that the Fe supply by upward flux was much larger than that of aeolian dust, and the temporal variation of Fe concentration in seawater reflected the vertical flux of Fe rather than that of dust.

As described above, distribution and dynamics of Fe in the western subarctic Pacific, in particular near the Kuril Islands, are highly heterogeneous and complex, it is thus crucial to unravel Fe-related biogeochemical processes such as phytoplankton photosynthesis in the western subarctic Pacific. At present, little is known about Fe deficiency in phytoplankton in the neritic zone and its boundary

regions. There are two obstructions to address the Fe availability for phytoplankton in the western subarctic Pacific near the Kuril Islands: a) little attention to physiological response of phytoplankton to Fe availability to date; and b) sparse available information on the upstream of the Oyashio around the eastern Kamchatka Peninsula regarding the biological, physical, and chemical properties.

This study, therefore, aims to reveal the effects of Fe on the photophysiology of phytoplankton in the western subarctic Pacific near the Kuril Islands and the eastern Kamchatka Peninsula. Effects of Fe availability on phytoplankton were assessed from *in situ* observations and on-deck bottle incubation experiments. The photophysiology of phytoplankton was estimated by photosynthesis-irradiance (*P-E*) curves, providing powerful insights into physiological states of phytoplankton such as light-dark adaptation and nutrient availability (Sakshaug et al., 1997; MacIntyre et al., 2002). Spatial patterns of photophysiology were also investigated with physicochemical parameters. Furthermore, phytoplankton community composition was investigated with scanning electron microscopy (SEM), enabling the identification and quantification of armored cells such as diatoms and dinoflagellates (e.g., Sugie and Suzuki, 2017).

3.2. Materials and methods

3.2.1. Water samplings and optical observations

Seawater sampling was conducted in the western subarctic Pacific along the Kuril Islands and off the eastern Kamchatka Peninsula on board the R/V *Professor Multanovskiy* from 2 June to 8 July 2014 (Fig. 9). Optical observations were conducted to acquire *in situ* vertical profiles of photosynthetically available radiation (PAR, 400-700 nm), E_d(PAR), and the spectra of downward irradiance, $E_d(\lambda)$ with a Compact-Optical Profiling System (C-OPS, Biospherical Instruments Inc., Hooker et al., 2013). Diffuse attenuation coefficients of PAR (K_d(PAR)) were calculated with the software PROSIT (NASA) with the reference of the incident PAR (E_0(PAR)) above the sea surface. Additionally, a LI-190SB air quantum sensor and a LI-1400 data logger (LI-COR, Inc.) were used for the continuous measurement of E_0(PAR). Based on the results of K_d(PAR), euphotic zone depth (Z_{eu}) was calculated as a 1% light depth compared to the surface PAR (Kirk, 2010). Surface seawater samples were

obtained from ca. 5 m layer around noon using a CTD carousel multisampler system (CTD-CMS) with acid-cleaned Niskin bottles washed with trace-metal-clean techniques (Obata et al., 1993; Takeda and Obata, 1995; Nishioka et al., 2001). At each station, seawater was collected into a 9 L polycarbonate (PC) bottle which was also acid-cleaned and trace-metal-free. In addition, seawater was dispensed into four 300 mL PC bottles and two polystyrene tubes as primary productivity and nutrient samples, respectively. Concentrations of major nutrients (nitrate + nitrite, ammonium, phosphate, and silicate) were determined with a BRAN-LUEBEE autoanalyser (QuAAtro). Mixed layer depths (MLD) were calculated as the depth at which the potential density anomaly ($\Delta\sigma_\theta$) of the water column increased by 0.125 kg m^{-3} relative to the sea surface at 10 m (Monterey and Levitus, 1997).

3.2.2. Fe analysis

Dissolved Fe (DFe) samples were collected from each station, and pre-filtered with 0.22 μm Millipore Durapore filters (Millipak-100), followed by the addition of ultrapure HCl following Nishioka et al. (2001). Seawater for total dissolvable Fe (TFe) samples were collected during the bottle incubation experiments described below and dispensed into an acid-cleaned 125 mL LDPE bottle. Samples were then acidified with 20% ultrapure HCl (Tamapure AA-10, Tamapure Co., Ltd.) to solubilize all labile Fe in seawater (Obata et al., 1997). Samples were buffered with 10 M formic acid and 2.4 M ammonium formate buffer to adjust pH to 3.2 just before measurements on board the ship or on land. Concentrations of TFe and DFe were determined with an automatic Fe (III) flow injection analytical system (Kimoto Electric, Ltd.) that uses pre-concentration with a chelating resin following the chemiluminescence method (Obata et al., 1993; 1997).

3.2.3. Size-fractioned Chlorophyll *a* concentration

See section 2.2.3.

3.2.4. Microscopy

Seawater was fixed with a buffered neutral formaldehyde solution (final concentration 2%). Fixed samples were stored at 4 °C until analysis. A subsample of the fixed sample was filtered onto a 25

mm, 0.4 μm Nuclepore membrane filter set on a glass funnel under gentle vacuum (< 0.013 MPa). The filter was rinsed with deionized water to desalt and then naturally dried. The dried filter was secured with conductive carbon tape on a microscope stage, and the surface of the filter on the stage was coated with Pt-Pb alloy by vapor deposition using a MSP-1S magnetron spatter device (Vacuum device Inc.). Armored phytoplankton cells were counted with a scanning electron microscope (VE-8800, Keyence Co., Ltd.) with a magnification of >1000× according to Nosaka et al. (2014; 2017). Species identification was based on Tomas (1997), Round et al. (2007), Konno et al. (2007), and Medvedeva and Nikulina et al. (2014). For identification of *Chaetoceros* species, the number of plastids in a cell was enumerated under a bright field microscopy (Keyence BZ-9000). The redundancy analysis (RDA) was performed to evaluate relationships between physicochemical properties and community composition of diatoms at the level of genus following Endo et al. (2018) (see also section 3.2.10). Size of diatoms (i.e., apical length or valve diameter of diatoms) was measured if >20 cells of a given diatom could be observed using the software ImageJ (National Institutes of Health).

3.2.5. Variable Chlorophyll *a* fluorescence

To assess the photochemical efficiency of photosystem II (PSII), variable Chl *a* fluorescence was measured with Pulse Amplitude Modulation (PAM) fluorometry and Fluorescence Induction and Relaxation (FIRe) fluorometry for the samples at 5 m and 5% optical depths at each station and the bottle incubation experiments (section 3.2.9). Seawater was dispensed into a 30 mL shading polyethylene bottle and stored in an incubator at *in situ* temperature for 30 minutes for dark acclimation to open the reaction centers of algal PSII. After incubation, maximum quantum yields of PSII photochemistry (F_v/F_m) for phytoplankton were measured with a Water-PAM (Walz) following Liu et al. (2009). The use of a FIRe fluorometer (Satlantic Inc.) allowed measurements of functional absorption cross-section of PSII (σ_{PSII}; Å quanta^{-1}) for phytoplankton. A single turnover excitation protocol was applied to the dark-acclimated cells with a blue light emitting diode (LED) equipped with a FIRe fluorometer. The single turnover flash was illuminated for 80 μs and iterated 10 times with 1000 ms intervals between each flash. The obtained induction curves were averaged and fitted to

the model proposed by Kolber et al. (1998) using the MATLAB-based program fireworx developed by Audrey Barnett (Dalhousie University). The difference in σ_{PSII} values between samples from the surface and the depth of the 5% light level was defined as $\Delta\sigma_{PSII}$. F_v/F_m data from PAM fluorometry were used for further discussion as representative values in this study.

3.2.6. Light absorption coefficient of phytoplankton

See section 2.2.6.

3.2.7. Photosynthesis vs. Irradiance (*P-E*) curve experiment and photosynthetic parameters

See section 2.2.7.

3.2.8. Primary productivity

See section 2.2.8.

3.2.9. Fe-enrichment bottle incubation experiments

Seawater was collected at stations C5 and A5 (Fig. 9) into 9 L bottles for Fe-enrichment experiments. At both stations, seawater was dispensed into six 9 L bottles previously washed with clean washing techniques (Obata et al., 1993; Takeda and Obata, 1995; Nishioka et al., 2001). Two out of the six bottles were Fe-enriched by adding $FeCl_3$ solution (final Fe concentration of 10 nM; hereafter +Fe treatments). For the other two bottles, the Fe chelator deferoxamine B was amended (final concentration to be 1 μM, hereafter +DFB treatments) to reduce Fe availability for phytoplankton (e.g., Wells, 1999; Hutchins et al., 1999a; Kondo et al., 2013). The other two bottles were set up as a control treatment without any addition (Control, hereafter). These six bottles were incubated in a temperature-controlled on-deck incubator under *in situ* temperature and natural light environment (100% surface light) for 3 to 5 days at both stations.

3.2.10. Statistical analyses

Statistical analyses were performed using the SigmaPlot software program ver. 11.0 (SysStat

Software, Inc.). Spearman's correlation analysis was used to investigate relationship between variables by assuming heteroscedasticity. For Fe-enrichment incubation experiments, one-way ANOVA in combination with Tukey test was adopted to assess responses of biological parameters to Fe and DFB addition. To assess the validity of RDA analysis, it was beforehand confirmed that the lengths of gradients of the physicochemical parameters were sufficiently small (<3 standard deviations) assessed using the detrended correspondence analysis (DCA). The Hellinger transformation (Legendre and Gallagher, 2001) was performed for the normalization of diatom community composition data. Ordinations of physicochemical parameters and diatom genera were plotted onto the RDA coordinate plane.

3.3. Results

3.3.1. Hydrography

Sea surface temperature and salinity (SST and SSS, respectively) were generally low ranged between 2.7–9.2 ºC and 32.3–32.9, respectively (Table 5). Relatively low temperatures were observed near the Kuril straits (e.g., stations A2 and OP3). At all sampling stations, the MLD were shallower than Z_{eu}. The deepest MLD was observed at station C5, while the shallowest was found at PS5. Stations with relatively shallow Z_{eu} were observed near the Bussol' Strait (i.e. stations D9 and A2) and the Kamchatka Peninsula (i.e., stations PS1, and PS5) (Table 5). Nutrients were low at stations PS1 and PS5 near the Kamchatka Peninsula. Relatively low nitrate concentrations (< 5 µM) were observed at some coastal stations (i.e., stations D9, B5, and B6).

3.3.2. Dissolved Fe (DFe) distribution

High values of DFe were observed around straits and the Kamchatka Peninsula (Table 5). The highest DFe value (0.71 nM) was observed at station D9 in the Sea of Okhotsk. Low values (< 0.1 nM) were found in offshore regions. Stations A2 and OP3, however, had a relatively low value (0.13 nM) in the Bussol' Strait even being close to the islands (Table 5).

3.3.3. Size-fractioned Chl *a* concentration

Nanophytoplankton and picophytoplankton were dominant at sampling stations except at stations PS1, PS5, and B5 (Fig. 10) wherein the phytoplankton assemblages were dominated by microphytoplankton (ca. 60%). Total Chl *a* concentration, obtained by summing all fractions, were was generally low (~1 mg m^{-3}), except higher values were observed at the three exceptional stations D9, A2, and B5 (Fig. 11).

3.3.4. Microscopy

Under SEM, 52 centric diatoms, 17 pennate diatoms, 4 coccolithophores, 10 parmales, and 13 flagellates including dinoflagellates were identified (Tables 6a and 6b, plus Appendices A and B). Among them, the centric diatom *Chaetoceros* species were dominant, in particular *Ch. debilis*, *Ch. diadema*, *Ch. furcellatus*. For pennate diatoms, *Fragilariopsis* spp., *Neodenticula seminae*, *Nitzschia* spp., and *Pseudo-nitzschia* spp. were often abundant (Table 6a). Generally, *Chaetoceros* species were abundant at coastal stations (e.g., D9, A2, PS5, B5, and B6 in Fig. 9 and Table 6a), whereas, at offshore stations (e.g., stations C3 and A6), *Fragilariopsis* and *Pseudo-nitzschia* species were abundant, although the small *Thalassiosira oceanica* was also predominant at station B3. At station C5, parmales were highly abundant and diverse, although they were not observed much at the other stations. Coccolithophores were only abundant at station C5 (Table 6a). It was difficult to conduct species identification for the sample obtained at station PS1, but it was filled with intertwined and coagulated setae of *Corethron pennatum* and *Chaetoceros* species including *Ch. atlanticus*. Resting spores of *Chaeroceros* spp. were also detected at the sampling stations except for stations C5 and A6. The RDA showed that the first component was explained by the predominance of *Chaetoceros* and *Fragilariopsis.* The two environmental variables, DFe and NH_4, had negative vectors for the first component. The contribution of *Fragilariopsis* had almost an opposite vector to that of DFe. The vector of *Cylindrotheca* was in almost the same direction as that of NH_4. Only two environmental variables (i.e., DFe and MLD) were positive for the second component, while the predominance of *Neodenticula* and *Nitzschia* also had positive scores (Fig. 12).

3.3.5. Variable Chlorophyll *a* fluorescence by PAM flurometry

Average F_v/F_m value at the surface was 0.37 ± 0.11 throughout the expedition, ranging from 0.15 to 0.51 (Fig. 13a). High F_v/F_m values were found at coastal stations (e.g., A2 and B6), whereas some offshore stations had relatively low F_v/F_m (e.g., at C3, B3, and A5). A clear gradient of F_v/F_m was observed from offshore to the coastal region in the B stations transect, whereas relatively high values were sometimes found in the offshore regions (e.g. station A6).

3.3.6. *P-E* curves and photosynthetic parameters

Values of the initial slope α^B were generally low (~0.02 [(mg C mg Chl a^{-1} h^{-1}) (µmol photons m^{-2} s^{-1})$^{-1}$]) except at stations PS1, PS5, and OP3 (Fig. 13b). On the other hand, β^B values at stations PS1 and PS5 were relatively high, and the value at station A6 was conspicuously high (Fig. 13c). The maximum photosynthetic rate P^B_{max} values were relatively high at stations PS1 and PS5 (10.3 and 6.66 mg C mg Chl a^{-1} h^{-1}, respectively) compared to other stations. The average value of the other stations was 2.18 mg C mg Chl a^{-1} h^{-1} ranging from 1.20 to 3.70 mg C mg Chl a^{-1} h^{-1} (Fig. 13d). The average value of light saturation indices, E_k, was 112 µmol photons m^{-2} s^{-1} with the highest at station A5 and the distinctly low value at station OP3 located in the strait (Fig. 13e). The $\bar{a}^*_{ph}$ values were highly variable, but relatively high values were observed offshore stations at B3 and A6 as well as station OP3 in the strait (Fig. 13f). Maximum quantum yields of carbon fixation, Φ_{Cmax}, showed high values near the Kamchatka Peninsula except at stations D9, A2, and C3 (Fig. 13g). The α^B and β^B were positively correlated with F_v/F_m (p<0.01, Table 7). Except for these significant correlations, no other distinct and strong correlation between photosynthetic parameters was found, but the parameters were correlated with some physicochemical parameters (Table 8). A significant negative correlation was observed between α^B and MLD (p<0.05, Table 8). A positive correlation was observed between P^B_{max} and SST (p<0.01, Table 8). E_k had significant positive relationships with NH_4 and Z_{eu} (p<0.05, 0.01, respectively, Table 8). Nutrients were all negatively correlated with Φ_{Cmax} (p<0.05, Table 8), and Φ_{Cmax} was negatively correlated with SST and SSS as well as with Z_{eu} (p<0.05, Table 8).

3.3.7. Primary productivity

Values of *PP* were also highly variable. Station D9, only located in the Sea of Okhotsk, had a

remarkably high *PP* value (326 mg C m^{-3} d^{-1}) (Fig. 13h). In the Pacific Ocean, station B5 showed the highest *PP* followed by stations A2, PS5, and PS1 (88.5−211 mg C m^{-3} d^{-1}). Other stations, however, had relatively low values of ~20 mg C m^{-3} d^{-1}, although station A5 showed a relatively high value among these stations (Fig. 13h). Significant relationships were found with other photosynthetic parameters: positive relationships with Chl *a*, $\bar{a}^*_{ph}$, and Φ_{Cmax} (p<0.05, Table 7); a negative relationship with E_k (p<0.05, Table 7). Physico-chemical parameters were also correlated with *PP*: negative correlations with Z_{eu} and nutrients except for NO_2 and SiO_2 (p<0.05, Table 8).

3.3.8. Fe-enrichment bottle incubation experiments

During the Fe-enrichment bottle incubations at the two stations C5 and A5, incident PAR intensities for all treatments were almost stable, varying <5 % (data not shown). Changes over time in TFe concentrations showed a similar pattern at the two stations; the largest was derived from the Fe-added bottles, followed by the initial (i.e., time-zero) and control treatments (Appendix H). Unfortunately, one of the +DFB bottles were contaminated with external Fe due to immersion of waters into bottles (see below), the results were thus excluded from further discussion. At station C5, a significant increase in Chl *a* after Fe addition was observed compared to the control treatment (p<0.01, Fig. 14). The +DFB bottles had the lowest value at station C5, although no significant difference was found as compared the initial and control bottles (p>0.05, Fig. 14). At station A5, concentrations of Chl *a* in the control and +Fe bottles were comparable (p>0.05, Fig. 14). Concentration of Chl *a* in the DFB bottle was placed in the second lowest following the initial value (Fig. 14). For the C5 incubations, abundance of coccolithophores and parmales decreased in the course of incubations. *Chaetoceros* species, on the other hand, maintained their dominance both in the control and +Fe bottles, although the highest abundance was observed for the control treatment (Table 6b). *Pseudo-nitzschia* spp. was the only species showing a great increase after +Fe addition. Under +DFB treatment, *Cheatoceros* species were, however, replaced by large and robust diatoms (e.g., *Corethron pennatum*, *Neodenticula seminae*, and *Thalassionema nitzschioides*) with an increase in *Fragilariopsis* species and armored ciliates (Appendix F). For station A5, abundance of originally dominant *Chaetoceros* species was also the highest in the control bottles followed by +Fe bottles as at station C5. *Pseudo-nitzschia* spp. also

increased both in the control and +Fe bottles, and *Cylindrotheca closterium* greatly increased under +Fe condition. As well as at station C5, large and robust species outcompeted in +DFB bottles, replacing *Chaetoceros* species with two exceptional *Chaeroceros* species (i.e., increases in abundance of large and robust *Ch. concavcornis* and *Ch. convolutus*) (Table 6b). Length of chains of *Neodenticula seminae* were often long (>5 up to 23 cells in chain) in the +DFB bottles at both stations although solitary cells or short chains of the species were normally observed at the other stations and in the other bottles (Fig. 15). The F_v/F_m values behaved differently after the Fe amendment between stations C5 and A5 (Fig. 16). After Fe addition at station C5, the F_v/F_m values increased significantly as compared with the control treatment ($p<0.01$, Fig. 16). No significant increase in F_v/F_m, was, on the other hand, observed between control and +Fe treatments at station A5 ($p>0.05$, Fig. 16). The F_v/F_m values for +DFB treatments at both stations were almost same or lower than the initial values except for the contaminated +DFB bottle showing high F_v/F_m (0.57±0.01) (described above). FIRe fluorometry provided σ_{PSII} values at the surface and 5% light depths at both stations. Little variation was found at station C5 between samples collected from the surface and 5% light depth (i.e., $\Delta\sigma_{PSII}$=~0), whereas the $\Delta\sigma_{PSII}$ at station A5 was large: 71% higher value at 5% depth than that from the surface (Appendix I).

3.4. Discussion

3.4.1. Abundance and community composition of diatoms along the Kuril Islands and the eastern Kamchatka Peninsula

HNLC water extended to oceanic stations as shown in Fig. 9 (HNLC stations, hereafter; denoted as blue closed circles) as estimated from DFe<0.1 nM, NO_3>2 μM, and Chl *a*<1 mg m^{-3} (Table 5 and Fig. 11). Other stations, not in the HNLC water, were restricted in the coastal area along the Kuril Islands. At the HNLC stations, nanophytoplankton and picophytoplankton were predominant (Fig. 10). The predominance of smaller phytoplankton in the HNLC water was probably due to the allometry of cells that smaller species have advantages in nutrient uptake because they have a higher surface-to-volume ratio than large cells (Taguchi, 1976; de Baar et al., 1995; Sunda and Huntsman, 1997). The]. Stations not belonging to the HNLC water were defined as northern and southern coastal

waters (denoted as green and red closed circles in Fig. 9, respectively). These stations were on the shelf slope, whereas the HNLC stations discussed above were outside the slope (Fig. 9). Some of the northern coastal stations (i.e., stations PS1, PS5, and B5) near the Kamchatka Peninsula, on the other hand, had high contributions of microphytoplankton (Fig. 10). Although the most offshore station showed a high nitrate concentration possibly due to the diffusive supply from outside of the shelf slope, the northern coastal stations had relatively low nitrate and low Chl *a* concentrations (Table 5; Fig. 11), suggesting that the spring phytoplankton blooms were terminated due to nutrient depletion (Table 5) and grazing effects by zooplankton (also discussed in section 4.2). On the contrary to the northern coastal stations, the southern stations near the Bussol' Strait during the first half (i.e., stations D9 and A2) had relatively high Chl *a* biomass (6−8 mg m^{-3}) and moderate to high DFe concentration (>0.1 nM) (Table 5; Fig. 11), indicating bloom development in early June (Table 5 and Fig. 11). It, therefore, appears that the field sampling described herein was conducted between the bloom and post-bloom phases. The other southern coastal stations (i.e., stations OP3 and A5) showed the HNLC-like properties (i.e., relatively low DFe and Chl *a* with excessive NO_3; Table 5 and Fig. 11) in the last half of the expedition, suggesting that the blooms around the Bussol' Strait might be potentially limited by Fe unless this trace element was supplied from the Sea of Okhotsk, although grazing by zooplankton might be also significant (discussed below). During the field campaign, diatoms accounted for more than half of the phytoplankton assemblages in terms of Chl *a* biomass as estimated from pigment signatures (K. Suzuki, personal communication). With SEM observation, *Chaetoceros* and *Fragilariopsis* species were the most abundant diatom species (Table 6a). Interestingly, *Chaetoceros* spp. was abundant at the coastal stations, whereas *Fragilariopsis* spp. was abundant in the HNLC water (Table 6a), suggesting that the biogeography of these species was probably determined by DFe concentration. This biogeographical species shift regarding Fe availability was well supported by the results of RDA (Fig. 12), showing the clear ecological compartmentalization with the opposite vectors for the first component of the RDA plane between these genera. Timmermans et al. (2001) indicated that *Chaetoceros* has the capability to outcompete other diatom genera under Fe-replete conditions. This notion was also supported by other field studies (Hutchins et al., 1998; Tsuda et al., 2003; Marchetti et al., 2006). *Fragilariopsis*, on the other hand, is

often observed in Fe-limited waters in the Southern Ocean (de Salas et al., 2011; Eriksen et al., 2018) and has the ability to survive in Fe-limited waters (Mock et al., 2017), although the ability may change among species (Wright et al., 2010). The good agreement between the vectors of *Cylindrotheca* and NH_4 (Fig. 12) was likely because of the growth of *Cylindrotheca* which can be enhanced with high availability of ammonium (Grant et al., 1967; Underwood and Provot, 2000). The RDA possibly suggested a coupling between DFe and *Neodenticula seminae* (Fig. 12), indicating that Fe addition could enhance growth of the heavily silicified species, followed by considerable sinking flux of this species in the western subarctic Pacific (e.g., Katsuki and Takahashi, 2005; Onodera et al., 2005), although the physiology of this species has not been well documented thus far. The large dinoflagellates (e.g., *Ceratium longipes* and *Gonyalux* spp.) found at station PS5 might be mixotrophy (e.g., Stoecker, 1999) as well as ciliates and choanoflagellates (Table 6a). The dominance of microphytoplankton in the northern coastal stations (Fig. 10) might be caused by preferential grazing on small phytoplankton cells by these small grazers. The considerable number of resting spores of *Chaeroceros* spp. at stations PS5 and C3 (Table 6a) might also indicate the termination of the bloom (i.e., post-bloom). It was also the case for the HNLC-like station OP3. *Sugie and Kuma* [2008] reported that *Thalassiosira nordenskioeldii* forms resting spores under Fe-limited condition.

3.4.2. Photophysiological state of phytoplankton

Photosynthetic parameters did not show a significant relationship with DFe concentrations (Table 5). It is difficult to simply discuss the relationship between Fe availability and photosynthesis, because of the algal assimilations of, for example, organically-complexed Fe and particulate Fe (Hutchins et al., 1999b; Maldonado and Price, 1999; Sugie et al., 2013). At the northern coastal stations where the bloom seemed to be terminated, α^B, and P^B_{max} were overwhelmingly high at stations PS1 and PS5 (Figs. 5b; d), and a slightly high P^B_{max} was also observed at station B5 with relatively high F_v/F_m (Figs. 5a, d). It suggested that the vegetative cells during the bloom and post-bloom period showed the high activity of photosynthesis around PSII. Stations PS1 and PS5, however, showed lower Chl *a* concentrations in spite of high P^Bmax, implying the significant grazing and/or sinking effects on the

biomass. The photosynthetic parameters showed a parallel change between P^{B}_{max} and α^{B} (i.e., the positive and significant relationship between these parameters; Table 7), so-called E_k-independent variability (Behrenfeld et al., 2004). Although E_k-dependent variability was well studied both in the field and in the lab and noted as a light-shade adaptation (e.g., Falkowski and Owens, 1980; Sakshaug et al., 1997; MacIntyre et al., 2002), Behrenfeld et al. (2004; 2008) pointed out that E_k-independent variability was driven by downstream photochemical electron transport such as the utilization ratio of NADPH and ATP. Diatoms possess capabilities of exchange ATP between plastids and mitochondria and of changing the NADPH/ATP ratio (Bailleul et al., 2015). The diatom blooms and diatom-dominated community sometimes showed E_k-independent variability (e.g., Platt et al., 1992; Yoshie et al., 2010; Isada et al., 2013; Morán and Scharek, 2015). Other studies also pointed out a relationship between E_k-independent variability and phytoplankton community structure in the field (Forbes et al., 1986; Morán, 2007; Morán and Scharek, 2015) as well as a few laboratory studies with unialgal cultures (Prézelin, 1992; Bruyant et al., 2005). SST was significantly positively correlated with P^{B}_{max} (Table 8), so temperature could be an important driver of photosynthesis during the expedition because temperature controls the activity of the carbon fixation enzyme, ribulose-1,5-bisphosphate carboxylase/oxygenase (RuBisCO) (e.g., Li et al., 1984; Raven and Geider, 1988; Young et al., 2015; Yoshida et al., 2018). Interestingly, E_k was significantly and positively correlated with Z_{eu} (Table 8), suggesting that phytoplankton well-acclimated to the light environment (i.e., light-shade acclimation). The negative relationship between α^{B} and MLD (Table 8) supported the light-shade acclimation because a smaller ratio of Z_{eu}/MLD (i.e., shallower light penetration) led a lower E_k and a higher α^{B}, indicating low-light acclimation and vice versa. Light environments in the water-columns thus influenced the photophysiology as well as *PP* during the expedition (Table 8).

3.4.3. Community and physiological responses of phytoplankton in the Fe enrichment experiments

The initial community structure of both assemblages at stations C5 and A5 were relatively similar comparing to those of the other stations (Fig. 10), although their responses were different from each other. The significant increase in Chl *a* compared to that of the control treatment at station C5 after

the addition of Fe (Fig. 14) suggested that Fe limitation occurred at the station. The significant increase in F_v/F_m values after Fe addition (Fig. 16) supported the Fe limitation at the station. The Fe addition to the algal assemblages at station A5 did not show any significant variation in Chl *a* (Fig. 14) between the control and +Fe bottles. The F_v/F_m values with Fe addition was invariant compared with the value of the control bottle (Fig. 16), indicating that Fe in the control bottle was replete for the phytoplankton assemblages at station A5. These results can be contradictive that station A5 was not Fe-limited in spite of the relatively low DFe concentration (DFe=0.05 nM). It was possibly due to presence of alternative forms of bioavailable Fe such as particulate Fe (e.g. Sugie et al., 2013) as discussed in section 3.4.2. It was possible that phytoplankton at station A5 had an access to more particulate Fe because strong vertical mixing in the Bussol' Strait might enhance the upward supply of suspended particulate Fe from the Fe-rich intermediate waters (e.g., Nishioka et al., 2007) via strong intense vertical mixing in the strait (Yagi and Yasuda, 2012) as suggested by Sugie et al. (2013). One of the major differences in physical and biological properties between the stations were MLD and E_k. Station C5 had the deepest MLD and the second smallest E_k (Table 5 and Fig. 13e), whereas station A5 had the second shallowest MLD and the highest E_k. As discussed in section 3.4.2, phytoplankton in the study area well-acclimated to light environments, that is, the phytoplankton assemblage at station C5 could be low light-acclimated, whereas that at station A5 could be high light-acclimated. Inherent photophysiological status of the phytoplankton assemblages (e.g., pigmentation and cellular Fe requirement) might be different between the two stations. The difference in degree of light acclimation between phytoplankton at stations C5 and A5 was supported by the results from FIRe fluorometry (Appendix G). The small $\Delta\sigma_{PSII}$ value at station C5 suggested the water-column was well mixed, and phytoplankton experienced lower average light intensity in the water-column, and then acclimated to lower light conditions (i.e., the low E_k) and vice versa (Fig. 13e and Appendix I). The large $\Delta\sigma_{PSII}$ value at station A5 suggested phytoplankton were well acclimated to the light intensity at each depth specifically due to the shallow MLD (Table 5 and Appendix I). The phytoplankton assemblages at station C5 were thus dark-adapted, and Fe-light co-limitation likely occurred as suggested by Suzuki et al. (2014) in the well mixed water-columns in the western subarctic Pacific near the Kuril Islands. The phytoplankton assemblages at station A5 could employ other strategies to

overcome Fe limitation. Greene et al. (1992), Geider and LaRoche (1994), and McKay et al. (1997) discussed that phytoplankton decrease the ratio of more Fe-requiring PSI/cytochrome b_6/f complex to less Fe-requiring PSII. In addition, Strzepek et al. (2012) demonstrated that phytoplankton increase photosynthetic antenna size rather than the number of antennae although their work was conducted for Southern Ocean species. These strategies might not change in Chl *a* concentration, but could effectively cope with the Fe-limited condition. At both stations, DFB inhibited the growth of phytoplankton (Fig. 14), which suggested that Fe controlled the responses of algal biomass during incubation. Incidentally, Chl *a* in the DFB-added bottles at station A5 also significantly increased than the initial condition (Fig. 14) in spite of the Fe chelation. Maldonado and Price (1999) clarified that Fe bound to DFB could be utilized via Fe reduction by large phytoplankton (> 3 μm) such as diatoms. From the microscopic observations, shifts in community composition at the genus level were little observed after Fe addition at both stations (Table 6b). The genus *Chaetoceros* was dominated in each bottle and might have capability to outcompete under Fe-replete conditions as observed in other on board Fe-enrichment incubations (Timmermans et al., 2001) and *in situ* Fe fertilization experiments (Tsuda et al., 2003). This study demonstrated, at the species level, that the species which were most stimulated by Fe addition (e.g., *Pseudo-nitzschia* spp. and *Cylindrotheca closterium* at stations C5 and A5, respectively) were different from the originally dominated species (i.e.., *Chaetoceros* spp.) (Table 6b). Their smaller cell size could benefit the efficiency of their nutrient uptake than *Chaetoceros* species, because of allometry of the cells described above. The *Chaetoceros* spp., except the larger *Ch. concavicornis*, were not abundant in the +DFB bottles and were replaced by much larger diatoms such as *Thalassionema nitzschioides*, *Neodenticula seminae*, *Corethron pennatum*, and *Asteromphalus* spp. (Table 6b). The larger cells could store surplus Fe in their larger vacuoles which can play an important intracellular Fe source and support their growth for a while even under Fe-deficient conditions (Sugie et al., 2011). Larger diatoms could thus outcompete in the +DFB bottles and sustain their growth under short-term Fe depletion. This study first reported the elongation of *Neodenticula seminae* chains with +DFB treatment (Fig. 15). In the western subarctic Pacific, considerable amount of scales of the species were often observed in sediment traps (Katsuki et al., 2003; Katsuki and Takahashi, 2005; Onodera et al., 2005). The species *Neodenticula seminae* might

have a strategy to sink rapidly under Fe-limited conditions by their chain elongation. These community shifts in the +DFB bottles might be an explanation for high biological pump efficiency in the western subarctic Pacific because the post-bloom Fe depletion can alter the algal community to larger diatom-dominated assemblages.

3.5. Conclusions

This study conducted in the western subarctic Pacific in summer covered bloom and post-bloom periods dominated by diatoms. The SEM demonstrated that a clear biogeography of diatom community composition with Fe availability between coastal and offshore waters near the Kuril Islands and Kamchatka Peninsula in the western subarctic Pacific. In the Fe-replete coastal waters, the genus *Chaetoceros* was dominant, whereas *Fragilariopsis* was abundant in the HNLC waters (Table 6a), as supported by the RDA results (Fig. 12). The active Chl *a* fluorescence results (i.e., F_v/F_m) somewhat supported the biogeographical difference that costal phytoplankton tended to have higher photochemical efficiency of PSII than those of phytoplankton at the HNLC stations. Photophysiological properties of phytoplankton assessed with *P*-*E* relationships clarified that light availability associated with Z_{eu} and MLD evidently controlled photosynthetic light-shade acclimation. The on board Fe enrichment incubation experiments indicated that Fe limitation occurred for the dark-acclimated phytoplankton assemblages with the low E_k at station C5 with the deep MLD (Table 5 and Figs. 13e and 14), suggesting the light-Fe interaction was significant (i.e., Fe-light co-limitation) proposed by Suzuki et al. (2014) in the studied area. The SEM found that Fe addition stimulated the growth of *Chaetoceros*, but addition of the Fe inhibitor DFB led the shift in the diatom communities to heavily-silicified species (Table 6b). Tréguer et al. (2017) suggested that large and heavily-silicified species have more potentials contributing to carbon sink via the biological carbon pump. Their work indicated that (i) the high contributions of *Chaetoceros* in the coastal waters can lead high carbon sinking and carbon sequestration ability from the shelf to open ocean regions (e.g., Tsunogai et al., 1999), and (ii) Fe depletion, which can occur in a post-bloom period, leads heavily-silicified species and then high carbon sinking flux. This can be a possible explanation for the high particulate carbon flux (Honda, 2003; Kawakami et al., 2004, 2015) and significant pCO_2 drawdown associated

with biological activity in the western subarctic Pacific (Takahashi et al., 2002).

CHAPTER 4

Freezing and melting stress on the photophysiology of ice algae: *Ex situ* incubation of ice algae using an ice tank

4.1. Introduction

Sea ice algae are a significant primary producer in sea ice zones. They contribute 10−25% of the total primary production (*PP*) in seasonally ice-covered regions (Lizotte, 2001; Legendre et al., 2002; Michel et al., 2006; Loose et al., 2011; Arrigo, 2017) and ~50% of the annual *PP* in perennial ice-covered regions (Satoh et al., 1989; McMinn et al., 2010; Fernandez-Mendez et al., 2015). Ice algae are a main, sometimes exclusive, energy source for sea ice biota such as zooplankton, krill, fish larvae and benthos (Lizotte, 2001; Boetius et al., 2013, 2015; Kohlbach et al., 2017; Moteki et al., 2017; Bernard et al., 2018). In addition to their ecological importance, they also seed ice-edge phytoplankton blooms in marginal sea ice zones during the spring-summer ice melt period (e.g., Smith and Nelson, 1986; Syvertsen, 1991; Arrigo, 2003, 2014). The primary production in the marginal sea ice zone, which is associated with ice-edge blooms, contributes ~50% of the total *PP* of perennially ice-covered regions of the Southern Ocean (Smith and Nelson, 1986; Sakshaug et al., 1991), although it is still controversial which, ice algae or phytoplankton actually contributes to the blooms (see review of van Leeuwe et al., 2018). When ice algae, which form aggregates within microstructures within the sea ice (Melnikov and Bondarchuk 1987; Assmy et al., 2013; Boetius et al., 2013; Katlein et al., 2014; Fernandez-Mendez et al., 2014; Boetius et al., 2015), are released from the sea ice during melting, they rapidly sink and transport carbon down to the abyss. This process can contribute to an efficient biological carbon pump (Riebesell et al., 1991; Taguchi et al., 1997; Boetius et al., 2013; Katlein et al., 2014). Sea ice environments are subject to large fluctuations in temperature (~−20ºC to −1.8ºC; Petrich and Eicken, 2017), salinity (~25 to 170; Arrigo et al., 2010) and light availability (~0 to 1000 μmol photons m^{-2} s^{-1}; Galindo et al., 2017). Within sea ice, these environmental factors affect the photosynthesis of the algae in a complex way, that is not independent (i.e. multiple co-stressors; McMinn et al., 2017). Although a few studies have addressed the multiple co-stressors on photophysiology of microalgae with incubation experiments on melted sea ice algae

samples (Ralph et al., 2005, 2007; Ryan et al., 2011; Martin et al., 2011; McMinn et al., 2014; see review of McMinn, 2017 and references therein), little is known how multiple co-stressors, associated with forming and melting sea ice, affect ice algal photosynthesis and production (McMinn, 2017). It is has been found to be difficult to directly obtain the photophysiological properties of the underlying mechanisms that drive primary production in sea ice despite their significant ecological and biogeochemical importance Kennedy et al. (2012) were the first to undertake ice tank incubation techniques,which enabled short-term incubation of ice algae within artificial sea ice in the laboratory. The biggest advantage of this technique is that ice algae can be incubated in an environment similar to *in situ* pack ice environments. Although many studies have addressed ice algal photosynthesis and production using isolates from sea ice resuspended in a water, it is very difficult to incubate them in the laboratory (e.g. in a culturing flask) in realistic environmental conditions, such as sea ice temperatures (<−1.8ºC) (McMinn et al., 2017). Using an ice tank, Kennedy (2012), were the first to report that a freezing event suppresses the photochemical efficiency of PSII. Although their first attempt was successful and revealed the effects of freezing on the photophysiology of ice algae, their short-term incubation experiments did not address the mechanism of freezing stress. Understanding how ice algae maintain photosynthesis and survive within sea ice is and how high light exposure affects the photosynthesis of released ice algal cells when the ice melts, however, is of considerable importance.. For the experiments reported here, a novel large volume (i.e. 70 L) ice tank, made of titanium, was designed and constructed for incubation of ice algae for extended time periods to investigate the effects of multiple co-stressors on ice algal photophysiology: (1) freezing stress with low temperature and high brine salinity; (2) chronic low light availability under the low temperature and high salinity; (3) melting stress with exposure to less saline meltwaters and sudden high light (e.g., 1000 μmol photons m^{-2} s^{-1} at the surface of ice-edge waters; Galindo et al., 2017). With the new ice tank a 20-day *ex situ* incubation of the ice algal diatom *Fragilariopsis cylindrus* was conducted using high light exposure experiment on melted ice samples to reproduce the environment that released ice algae from sea ice experience during melting. This study aims to investigate effects of multiple co-stressors on ice algal photophysiology in sea ice environments from ice formation, during frozen, to ice melt using the purpose designed ice tank. It provides insights into whether ice algae are

able to tolerate the environmental fluctuations that contribute to the massive ice-edge blooms.. In this study, active Chlorophyll *a* fluorescence measurements with fast repetition rate fluorometry (FRRf) and pigment analysis was undertaken together with a combination of molecular approaches. The FRR technique enables the detailed monitoring of algal photophysiology, whereas pigment signatures reveal the photoacclimative and photoprotective responses of algae. To look into apparent physiological responses of algae, transcriptional activities of the photosynthesis-related *psbA* and *rbcL* genes were also monitored.

4.2. Materials and Methods

4.2.1. Ice tank incubation

The polar pennate diatom *Fragilariopsis cylindrus*, isolated from Antarctic pack ice in 2015 (Davis station, East Antarctica) was incubated in a purpose designed ice tank (Island Research, Tasmania). The ice tank, which was constructed of titanium to minimize Fe contamination, was placed into a freezer (–20ºC), and the ice thickness and temperature gradient controlled by interactions between a basal heater and the adjustable ambient freezer temperature (see Kennedy et al., 2012). This enabled an ice thickness of approximately 5.5 cm to be maintained during the experiment. *F. cylindrus* was incubated in Aquil media (Price et al. 1989), buffered with ethylenediaminetetraacetic acid (EDTA) (final concetration 5.00 μM) at 150 μmol photons m^{-2} s^{-1} (PAR), a salinity of 35, and a Fe concentration of 400 nM, where the concentration of total inorganic forms of Fe (Fe') was 1.54 nM, this being continuously supplied to the medium and the exact value calculated using the software Visual MINTEQ, ver. 3.1 (https://vminteq.lwr.kth.se). Before a freezing cycle started, the seawater temperature was maintained at 2.5ºC and a sample was obtained to assess the original physiological state of the algae (Day−5, hereafter). After obtaining the sample, the temperature was set at −1.8ºC to initiate ice formation in the ice tank. Once ice had formed on day two, the under-ice water was partially replaced with ultrapure water to reduce the salinity down to 35; because the salinity had increased (to approximately 38) as a result of brine rejection from the ice. After a 2-day acclimation to the new salinity, ice samples were obtained every 5 days for 20 days (i.e., Days 0, 5, 10, 15, and 20). To minimize the heterogeneity among ice cores, ice samples were randomly collected from the tank

chamber with a trace metal-free hand drill (2 cm in diameter) from randomly annotated grids on the ice surface, following normal random sampling numbers generated by the software R (https://www.r-project.org/). To assess the effects of melting and high light exposure, the ice was melted at 2.5ºC for 2 days. After the ice had completely melted (Melt samples, hereafter), intense light was exposed to the melted samples (Light samples, hereafter), which was adjusted to represent the likely summer light intensity at the ice surface in ice-edge regions (800 μmol photons m^{-2} s^{-1}; MODIS/Aqua), Water samples were obtained both after the melting and light exposure events.

4.2.2. Fast repetition rate (FRR) fluorometry

To monitor the photophysiology of *F. cylindrus* during the freezing and melting processes, variable Chlorophyll *a* fluorescence (ChlF) measurements were conducted using a bench-top Fast Repetition Rate fluorometer (FRRf) (FastOcean Act2Run Systems, Chelsea Technologies) with Act2Run software (Chelsea Technologies). Ice samples were directly thawed at 2ºC in the dark for 30 min, and the slushily melted ice samples were placed in a quartz tube and their fluorescence (ChlF) was measured. A single turnover protocol was applied for the ChlF measurements; 100 flashlets with 1 μs duration at a wavelength 450 nm and 2 μs intervals for excitation of reaction centres of PSII and 20 flahlets with 1 μs duration and 100 μs intervals for relaxation. Eighteen light steps were applied to generate a rapid light curve (RLC) from 0 to 1800 μmol photons m^{-2} s^{-1}, taking <5 min to complete one RLC. At each light step (~15 s), at least five induction and relaxation curves were averaged to obtain ChlF yields, described in Table 9, after calibrating the ChlF yields with filtered s (5) er. According to the models proposed by Kolber et al. (1998), photosynthetic parameters of Chlorophyll *a* (Chl *a*) induction curves were calculated based on the ChlF yields as shown in Table 9. Electron transport rate through the reaction centres of PSII (RCII) (ETR_{RCII}) was calculated as follows:

$$\mathrm{ETR_{RCII}} = E \times \sigma_{PSII} \times \frac{F'_\mathrm{q}/F'_\mathrm{m}}{F_\mathrm{v}/F_\mathrm{m}} \times \Phi_\mathrm{RCII} \times 6.022 \times 10^{-1}$$

following Suggett et al. (2011) and Schuback et al. (2016), an alternative approach to calculating absolute ETR_{RCII} of Kolber et al. (1998), wherein Φ_{RCII} is the quantum yield of RCII assumed as 1, and the following number is a conversion factor to mol quanta mol $RCII^{-1}$ s^{-1}. The calculated ETR_{RCII}

at each light step were fitted to the model of Platt et al. (1980) to obtain photosynthesis−irradiance (ETR_{RCII}−E) parameters (Table 9). To assess the heat dissipation of algal cells, non-photochemical quenching based on the Stern-Volmer (S-V) kinetic equation (NPQ_{NSV}) was also calculated following McKew et al. (2013):

$$\mathrm{NPQ_{NSV}} = F_o'/F_v' \qquad (6)$$

where F_o' is minimum ChlF yield after a relaxation sequence calculated following Oxborough and Baker (1997), based on the S-V approach (Table 9). Quantum yield of NPQ_{NSV}, Φ_{NPQ}, was further calculated following Kramer et al. (2004), assuming the lake model (e.g. Joliot and Joliot, 1964, 2013) (Table 9).

4.2.3. Validation of the ChlF measurement method for ice samples: direct versus buffered melting and fast versus slow melting

Chlorophyll *a* fluorescence measurements have been widely used for seawater samples (e.g., Suggett et al., 2011), while ChlF has not been broadly applied to ice algae research (Miller et al., 2014), because ice samples need to be melted, which may greatly change the photophysiology of the algal cells (e.g., Garrison and Buck, 1986; Arrigo et al., 2015). Here, multiple comparisons were conducted on melt methods of two ice samples from the ice tank. Measurements of ChlF were performed on three treatments of ice samples; (1) intact crushed ice, (2) slushily and directly melted ice without filtered seawater, (3) slowly (24 h) and directly melted samples. The calibration for F_o measurement was conducted with filtered seawater as described in section 4.2.2, however, an empty quartz tube was used for the calibration because it was impossible to prepare a blank ice sample. It was thus assumed that the ice samples for the treatment had a high enough biomass without F_o calibration. All samples were stored or melted in the dark for 30 min for the treatments 1 and 2, whereas the other samples (i.e. the treatment 3) were placed directly into a Chlorophyll *a* fluorometer after the overnight melting. The FRRf was used for the ice samples from the ice tank as described above (section 4.2.2).

4.2.4. Cell abundance of ice algae

Cell abundance of ice algal and planktonic *F. cylindrus* was determined with an inverted microscope (Axiovert 25, Zeiss) and a Sedwick-Rafter counting chamber (Pyser-SGI Lmd.). At least 500 cells were enumerated to determine cell abundance (LeGresley and McDermott, 2010). Growth rate was calculated following Wood et al. (2005): (7)

$$\mu = \frac{\ln(N_t/N_0)}{t - t_o}$$

4.2.5. Pigment composition

Pigment concentrations were determined to quantified Chlorophyll, photoprotective carotenoids, and Chlorophyll derivatives with an Ultra High Performance Liquid Chromatography (UHPLC) (Suzuki et al., 2015). Fast and directly melted ice samples and seawater samples were filtered onto a 25 mm GF/F filter (Whatman) with gentle vacuum (<0.013MPa) passing through a 25 mm polypropylene in-line filter holder (Swinnex, Merck). Rintala et al. (2014) confirmed that fast and direct melting was a reliable method for pigment analysis. The filter was flash frozen in liquid nitrogen and stored in a deep freezer (−80ºC). After thawing the filter was blotted dry with filter paper, and the pigments were extracted using the *N, N*-dimethylformamide (DMF) bead-beating method (Suzuki et al., 2015). The extracted pigments were suspended in DMF and then injected into an UHPLC and measured. The ratio of diadinoxanthin (DD) and diatoxanthin (DT) was calculated to assess the xanthophyll epoxidation-de-epoxidation cycle and photoprotective strategies of algae upon intense light exposure likely occurring during melting (Katayama et al., 2017), assessed as a de-epoxidation state (DES; DT/(DD+DT)). Total Chl *a* (TChl *a*: sum of Chl *a*, Chlorophyllide *a*, Chl *a*-allomer, and Chl *a*-epimer) concentrations were calculated as an indicator of algal biomass. Contributions of Chlorophyllide (Chllide *a*) *a* to TChl *a* were also calculated as an index of the breakdown of Chl *a*. Ratio of photoprotective carotenoids (PPC) in diatoms (DD, DT, and β,β-carotene) to photosynthetic carotenoids (PSC: only fucoxanthin here) and xanthophyll pool ((DD+DT)/TChl *a*) were calculated for quantifying photoprotective potentials of the diatom *F. cylindrus*.

4.2.6. Gene expression of photosynthesis-related genes, *psbA* and *rbcL*

To investigate the mechanisms of freezing and melting stress on cells of *F.cylindrus* in water and in the ice, gene expression of the photosynthesis-related genes, *psbA* and *rbcL* was measured. To stabilize the RNA, RNAlater (Sigma) was immediately added to the ice core after collection. Melted ice and seawater samples were filtered onto two 25 mm, 2 μm polycarbonate Isopore membrane filters (Millipore) with gentle vacuum (<0.013MPa) passing through a 25 mm polypropylene in-line filter holder (Swinnex, Merck) for DNA and RNA samples. The DNA samples were placed in a cryotube and flash frozen in liquid nitrogen and stored in a deep freezer (−80ºC). RNA samples were suspended in 600 μL RLT buffer (Qiagen) in a cryotube, to which 10 μL of β-mercaptoethanol (Sigma-Aldrich) was added. The RNA sample then was flash frozen in liquid nitrogen, and then stored in a deep freezer (−80ºC) until further analysis. DNA and RNA were extracted following Endo et al. (2013) and Endo et al. (2015), respectively. The extracted RNA was reverse-transcribed to complementary DNA (cDNA) with the PrimeScriptTM RT Master Mix (RR036, Takara) reagent according to the manufacturer's specification. DNA and cDNA copy numbers of the *psbA*, *psaA*, and *rbcL* genes were quantified by quantitative PCR (qPCR) and quantitative reverse-transcribed PCR (qRT-PCR), respectively. The primer sets and PCR conditions are shown in Appendix J.

4.3. Results

Note: This chapter only focuses on left panels (a and b panels in Figs. 18−24 and 26−30)

4.3.1. Ice physics and ice algal growth

Throughout the incubation experiments, ice thickness was stable at 5.5 cm on average with little basal ice melting and sublimation of ice from the ice surface. During the experiments, temperature within the ice increased from the ice surface (−22.5 ºC) to the ice-water interface (−2.2 ºC) (Fig. 17), and seawater temperature beneath was maintained at ca. −1.8ºC throughout the incubations with ice. Brine salinity and brine fraction were estimated following Cox and Weeks (1983) and Eicken (2009). Brine salinity decreased with depth from 293.7±0.0 to 39.4±0.5. Assuming no gas bubbles were in the ice, the brine fraction ranged from 3.7±0.0% to 34±0%, increasing with depth. Nutrient

concentrations were not depleted during the incubations (data not shown). Cells of *F. cylilndrus* were certainly incorporated into the ice, and cells showed slow but constant positive growth in all treatments within the ice environments (Table 10); there was no significant difference in growth rate between the treatments (p>0.05).

4.3.2. Variable Chl *a* fluorescence

4.3.2.1. Dark values (F_v/F_m and σ_{PSII})

At the beginning of the incubations on day −05, planktonic *F.cylindrus* showed comparable and relatively high F_v/F_m values at both light conditions (HL: 0.47±0.05; LL: 0.45±0.6) (p<0.05) (Fig. 18). Once algal cells were frozen into the ice on day 00, F_v/F_m sharply dropped down to ~0.2−0.3 regardless of the light environment (p<0.01) (Fig. 18), while σ_{PSII} changed little in the freezing events (p>0.05) (Fig. 19). During the frozen periods (i.e., algal cells were within the ice), F_v/F_m values were relatively stable until day 20 and showed almost identical values regardless of the light availability. The lowest F_v/F_m was found in the middle of the incubations on days 5 or 15 (Fig. 18). The σ_{PSII} at both light levels was relatively stable throughout the incubations with slight decreases with time (Fig. 19). Once the ice had melted, F_v/F_m values recovered towards the original values on day−05. These, however, were not exactly the same with the F_v/F_m values of the HL treatments 39% lower and those of the LL treatment 15% higher than their initial values on day−05 (Fig. 18). The responses of σ_{PSII} were different from those of F_v/F_m being significantly different from the initial values on day −05 but similar to σ_{PSII} values on day 20 regardless of the light availability (Fig. 19). Soon after the light exposure to the melted sample at 800 μmol photons m^{-2} s^{-1}, F_v/F_m values significantly dropped in both light treatments (decreased 39% and 29% for HL and LL treatments, respectively). In spite of the significant and large decreases in F_v/F_m, σ_{PSII} showed little variation although that in the HL slightly decreased (a 16% decrease) after the light exposure (Figs. 18 and 19).

4.3.2.2. Quenching parameters (NPQ_{NSV} and 1-qP)

Non-photochemical quenching (NPQ_{NSV}) of each treatment was at the same level as at the initial stage on day −05 (p<0.05) (Fig. 20). Closed fractions of PSII were ~70% on day −05 for both light

treatments (Fig. 21). The freezing event greatly enhanced NPQ_{NSV} in both treatments. NPQ_{NSV} in the HL tank had maximum values in the early stages of the incubations (i.e., day 00), while those in the LL showed a gradual increase and reached its maximum on day 05 (Fig. 20). The closed fractions of PSII increased slightly but not significantly, with higher 1-qP values, at or after the freezing event, although the timing of the increments in 1-qP was not consistent between the treatments (Fig. 21). After ice melt, NPQ_{NSV} decreased to identical level as those on day −05 in the LL tank, whereas the HL treatment showed a significant increase in NPQ_{NSV}. The 1-qP values did not show any consistent behaviour upon melting: the HL tank showed a higher value compared to the initial value, while the counterpart with LL showed a decreased value. The light exposure after the melting event significantly enhanced NPQ_{NSV} (almost doubled), whereas the 1-qP upon light exposure showed little variation and a significant increase for the HL and LL treatments, respectively (Figs. 20 and 21).

4.3.3.3. Photosynthesis-irradiance (ETR_{RCII}-E) curve

Initial values of all treatments were the same as at the beginning of the incubation experiments (Figs. 22, 23, and 24). The initial slopes of ETR_{RCII}-E curves; α, regarded as light utilization efficiency, dropped significantly when the algae were frozen into the ice ($p<0.05$) (Fig. 22). During frozen, α values were stable in both treatments, although a slight increase was observed in the LL tank at the end of the incubation ($p<0.05$). After the ice melted, α values did not show any apparent change but had slightly lower α values than the initial values; the α value in the LL tank returned to the initial value. After the light exposure, little variation in α were observed in either light treatment (Fig. 22). In the case of maximum electron transport rates (ETR_{max}) (Fig. 23), both treatments showed significant decreases in ETR_{max} during frozen ($p<0.05$), although the HL treatment showed a gradual decrease while it's LL counterpart showed a sudden decrease. When the ice melted, ETR_{max} values in the LL treatment recovered to the initial values whereas the HL treatment showed identical values to those during frozen (Fig. 23). Light saturation indices, E_k, gradually decreased in the course of the incubation experiments without any conspicuous variation during frozen (Fig. 24). The HL tank showed higher E_k throughout the incubation. During melting, however, E_k values increased to the

initial levels before freezing on day −05. When algal cells were exposed to light, E_k significantly decreased in both treatments (p<0.05) (Fig. 24).

4.3.3. Validation of sample melt methods

Active Chlorophyll *a* fluorescence parameters varied between the different melt methods of the two ice samples (Fig. 25). When crushed ice samples were packed directly into a quartz tube, F_v/F_m values were lower, followed by those of slushily melted samples for both ice cores. These values were almost the same and did not show any significant difference (p>0.05), whereas the slow-direct melt samples showed significantly higher values compared to their counterparts (p<0.05). Unlike F_v/F_m values, σ_{PSII} little varied regardless of the melt methods and did not show any significant enhancement or suppression (p>0.05) (Fig. 25).

4.3.4. Pigment composition

Initial TChl *a* concentrations differed slightly between incubations with higher TChl *a* in the HL ice tank (Fig. 26). After the *F. cylindrus* cells were incorporated into the ice, they maintained a stable TChl *a* biomass in both ice tanks until the ice melted. Contributions of Chllide *a* to TChl *a* were higher in the HL treatment than in the LL tank throughout the incubations (Fig. 26). Although there were slight decreases in the Chllide *a* contributions once the ice had melted, the relative contribution of Chllide *a* again increased with light exposure. The cellular DD-DT pool size in both the HL and LL treatments at the beginning of the incubations was comparable, whereas during the frozen period the cellular pool size grew faster in in the HL ice tank than those in the LL tank. DES concentrations were also high in the HL ice tank (Fig. 27). Although the melted ice samples showed decreases in DES in both treatments, light exposure enhanced the to DES until light exposure; higher PPC/PSC were present in the HL ice tank and there was a decreased contribution of PPCs after ice melt (Fig. 28).

4.3.5. Gene expression of photosynthesis-related genes

4.3.5.1. *rbcL*

Gene expressions of the *rbcL* gene at the initial stage of both incubations were at a relatively similar

level (Fig. 29). Regardless of the light availability, transcriptional activity of the gene was highly upregulated when algae were frozen into the ice (Fig. 29). During the freezing process, gene expression levels dropped sharply to a lower level than that of the values from the seawater prior to freezing (Fig. 29). The low level was sustained until day 20, when slightly higher gene expressions were observed in both treatments. Comparing the results of Melt and Light periods, the *rbcL* gene expression did not show any conspicuous change in either treatment.

4.3.5.2. *psbA*

Unlike the *rbcL* gene, gene expression of the *psbA* gene behaved differently with the different light availability (Fig. 30). At first, their initial values were different between the HL and LL treatments; ~2-fold higher under in HL than in LL. In HL, transcription of the *psbA* was highly upregulated during frozen; similar to the response of the *rbcL* gene. In LL, such upregulation of the gene was not evident. Cells in the HL tank showed similar patterns to those observed in the *rbcL* gene; a sharp decrease in the gene expression, followed by a large upregulation and then recovery to their initial values when ice melted (Fig. 30). Cells under LL, however, showed constant gene expressions throughout the incubation. It became clear that upregulations of the gene was most evident after light exposure (i.e., Δ*psbA* were positive) in both light treatments (Fig. 30).

4.4. Discussion

4.4.1. Freezing event

The freezing events in the ice tank experiments reported herein suppressed photochemical quantum efficiency of PSII (Fig. 18). Kennedy et al. (2012) also reported F_v/F_m drawdown when cells were frozen into artificial ice during their ice tank incubation experiments. This is also supported by previous studies showing that ice algae had lower F_v/F_m than under-ice phytoplankton in the field (McMinn et al., 2008; Yamamoto et al., 2014) as well as in higher plants (Lundmark et al., 1998). The high amount of Chllide *a* produced during frozen was observed throughout the incubations (Fig. 26). The large concentration of Chl *a* break-down products has also reported in ice algae of both landfast and pack ice in the Arctic and Antarctic (Horner, 1985; Arrigo, 2014). The Chllide *a* concentration

was not negligible and might imply inactivation of PSII reaction centres. The amount of Chllide *a*, however, was maintained at identical levels to the initial concentration of both treatments, indicating the existence of Chllide *a* had only a little effect on the activity of PSII reaction centres. Suggett et al. (2009b) demonstrated that chronic stress decreases F_v/F_m with concomitant enhancement of σ_{PSII} because the light energy absorbed by light harvesting complexes is transferred to fewer active PSII reaction centres (i.e., an apparent increase in σ_{PSII}) if some reaction centres are damaged or inactive (Falkowski and Raven, 2007; Suggett et al., 2009b, 2011). During frozen, little variation in σ_{PSII} was observed (Fig. 19). Although the possibility of photoinactivation cannot be excluded, it has been suggested that other mechanisms might decrease F_v/F_m when cells are frozen into ice. Freezing stress, with low temperatures and high brine salinity, could be the main cause of the reduction in the photochemistry of PSII (Ralph et al., 2007; Ensminger et al., 2006). The imposition of multiple co-stressors does not impact RCII directly, but might affect other components downstream of RCII. Low temperatures have little affect on light absorption and charge separation in RCII and the following electron transportation can be affected by temperature and salinity due to excitation pressure imbalance (Ensminger et al., 2006). At the same time, high brine salinity might suppress the reduction capability of electron donors around PSII. Ralph et al. (2007), using picosecond fluorescence techniques, demonstrated that salinity stress lowered the reduction capacity of Q_A and the PQ pool, although Q_B was stable because the redox state of Q_B was balanced by the redox states of the electron donor and acceptor (i.e. Q_A and the PQ pool) (Huner et al., 1998). Although they suggested low-salinity stress on ice algae was more evident, the high brine salinity in this study was also high enough to suppress the downstream components of PSII. Urao et al. (2010) found that osmotic stress stimulates the production of osmolytes to protect cells from dynamic osmotic stress in higher plants. This stress leads to lower plasmamembrane fluidity, which affects photochemical reactions in the electron transport chain. Low temperature also reduces membrane viscosity in psychrophilic microalgae, including diatoms (Morgan-Kiss et al., 2006) as well as higher plants (Huner et al., 1998, 2003). The combined stress has been found to stagnate electron transportation down to ferredoxin and cause "electron clogging" (e.g., Lazár et al., 2005). The resulting' electron clogging', lowered F_v/F_m (e.g., Schwarz et al., 2017). This 'electron clogging' might lead overreduction of the PQ pool

(Maxwell et al., 1995; Allen and Nilson, 1997; Pfannschmidt et al., 2003), as the redox state of the PQ pool is the most critical factor imbalancing the photochemical electron transport chain, 'photostasis' (Öquist and Huner, 2003). NPQ_{NSV} was thus possibly enhanced for alleviating excess excitation pressure under a high transmembrane pH difference (ΔpH) (e.g. Caron et al., 1987; Ting and Owens, 1993; Goss and Jakob, 2010), although of 1−qP values did not support this over-reduction because of its scattered values (Fig. 21). The pigment analysis showed enlargement of the DD-DT pool and the contribution of PPC to PSC in the HL treatment during freezing but this was not evident in the LL ice tank (Figs. 27 and 28). These responses in the HL treatment were consistent with the results of Kropuenske et al. (2009, 2010), Schuback et al. (2016), and Galindo et al. (2017), demonstrating that increased light in bottom ice algae increased the contributions of PPCs, possibly for up-front protection to mitigate the production of reactive oxygen species under high light (McMinn and Hegseth, 2004; Katayama and Taguchi, 2013; Kuczynska et al., 2015). After the light exposure, DES was also enhanced (Fig. 27), (Goss and Lepetit, 2015) consistent with the activity of the DD-DT xanthophyll cycle, which is the major pathway for energy dissipation (Kropuenske et al. 2009, 2010). The lower PPC/PSC and DES in the LL ice tank supports the relationship between light availability and photoprotective activity (Figs. 27 and 28) (Lavaud et al., 2002; Domingues et al., 2012). Photosynthetic performance, assessed with ETR_{RCII}−*E* curves, showed rapid photoacclimation responses during freezing; a greater decrease in ETR_{max} than that of α led to apparent dark acclimation with a lower E_k after freezing (Figs. 22, 23, and 24). The decrease in ETR_{max} could be consistent with the suppressed F_v/F_m values (Fig. 18), although the concomitant decrease in α is at variance with a classical interpretation of photoacclimative strategies (e.g. MacIntyre et al., 2002). Lacour et al. (2018) also reported another type of photoacclimation, different from the classic concept of photacclimation above, that NPQ mainly modified *α* rather than pigmentation. Values of α are represented as a product of σ_{PSII} and n_{PSII}, the active fraction of PSII to Chl *a* (e.g. Falkowski and Raven, 2007). As noted above, σ_{PSII} values were almost identical before and after the freezing event It is thus suggested that photoinactivation of cells occurred when they were frozen into the ice. The freezing event, therefore, suppressed RCII photochemistry, both directly and indirectly. The strong upregulation of expression of the *psbA* gene in the HL treatment accelerated repair of damaged PSII

under overexcitation pressure at HL and vice versa (Fig. 30) (Petrou et al., 2010; Galindo et al., 2017). The dark reactions were also affected by freezing stress with gene expression of the *rbcL* gene highly upregulated in both treatments (Fig. 29). This could be a cold acclimation strategy to increase cellular RuBisCO to compensate for the low catalytic activity of the temperature-sensitive enzyme by increasing its concentration (Devos et al., 1998; Lyon and Mock, 2014; Young et al., 2015), although Mock and Hoch (2008) reported downregulation of *rbcL* transcription under low temperature compared to a moderate temperature in *F. cylindrus*.

4.4.2. During the frozen periods

ChlF parameters were relatively stable during frozen. Although several significant variations were observed, F_v/F_m, σ_{PSII}, and NPQ_{NSV} values were stable within the ice (Figs. 18, 19, and 20). These results are consistent with previous studies that show sea ice is a stable platform for algal photosynthesis (Macchario et al., 2015; Arrigo, 2017). The comparable levels of F_v/F_m, σ_{PSII} between the HL and LL treatments show that the *F. cylindrus* cells sustained or optimized their photosynthesis within the ice regardless of light availability. This physiological acclimation to ice environments may play a central role for the proliferation of ice algae within and at the bottom of sea ice (Kropuenske et al., 2010; Lacour et al., 2018). McMinn and Hegseth (2004) suggested that ice algal cells can grow in sea ice if F_v/F_m is >0.125, which suggests that the ice algal cells in the ice tank should actively grow in the ice. However, the stable light utilization index α, which was also observed, increased and could be a dark acclimation strategy, in concordance with the classical concept of photoacclimation (MacIntyre et al., 2002). As noted above, σ_{PSII} was stable in the LL tank. Cells under LL might have increased the proportion of active RCII relative to Chl *a* to enhance light utilization capability for capturing light energy more efficiently, coinciding with the decreasing E_k.Thus, algal cells in the HL ice tank did not need to improve their light capturing ability because light supply seemed to have been sufficient (Figs. 19 and 24). The E_k values in the HL treatment were thus higher than those of the LL, especially at the end of the incubations on days 15 and 20 (Fig. 24). The different photosynthetic performance was also reflected in pigment signatures. Only algae in the LL ice tank showed a gradual increase in TChl *a* concentrations, in spite of the same algal growth rate in both ice tanks (Fig. 26);

this could be further evidence of dark acclimation (e.g., Falkowski and Owens, 1980). The smaller contribution of PSC in the LL ice tank also supports this suggestion because the cells might preferentially synthesize photosynthetic Chlorophylls and carotenoids rather than PPC (Fig. 28). However, *cells* in the HL ice tank, strengthened their photoprotective capability, reflected in higher values of PPC/PSC and DES compared to cells in LL (Figs. 27 and 28) (Kropuenske et al., 2009, 2010). Cells under both light levels increased their DD-DT pool and DES, suggesting again the highly reduced PQ pool. Interestingly, NPQ_{NSV} levels were comparable between the light treatments but NPQ_{NSV} in the LL ice tank were mostly higher than those of the HL ice tank regardless of the difference in DES. Nymark et al. (2013) suggested that low-light acclimated cells have more Lhcx proteins, which enlarges their NPQ capacity (Bailleul et al., 2010). Non-photochemical quenching via the DD-DT cycle might work as the primary safety valve against sudden excitation stress (Petrou et al., 2016; Lacour et al., 2018). Interestingly, transcriptional activity of the *rbcL* gene greatly decreased after the sharp increase on day 00, suggesting that cells had used the high abundance of RuBisCO that was synthesized during frozen. The constant but lower expression of *psbA* could keep the repair of PSII to a 'business as usual' senario, whereas the downregulation of the gene after the significant upregulation in the HL treatment might be caused to alleviate photochemical imbalance in the electron transport chain due to the over upregulation when shocked by freezing stress (e.g. changes in PSII to PSI ratio).

4.4.3. Light exposure after ice melt event

The light exposure decreased F_v/F_m values due to the high excitation pressure, although the melted samples showed improved photochemical activity. Improvement of F_v/F_m after melting was consistently evidently with the results of the validation experiments reported in Fig. 25. The degree of drawdown in F_v/F_m was comparable regardless of the incubation light intensity prior to the light exposure. NPQ_{NSV} was downregulated when the ice melted but was enhanced after light exposure. This reverse response to light exposure between F_v/F_m and NPQ_{NSV} might be evidence for fast activation of photoprotection, especially in the HL treatment, with the higher values of DES. Damage to PSII, however, was likely because of the considerable increase in the ratio of Chllide *a* to TChl *a*

after light exposure in both ice tanks (Fig. 26). Jeffery and Hallegraeff (1987) observed significant increases in the amount of Chllide *a* per cell when purified water was added for pigment extraction. This was thought to have been caused by the activation of Chlorophyllase. One might suspect that the melting process prior to sample filtration caused significant breakdown of Chl *a*, but a stable level of Chllide *a* to TChl *a* was observed throughout the incubation period, including after freezing (i.e., melted into water samples) and there was a considerable increase in Chllide *a* in the seawater when light was exposed to the melted samples (Fig. 26). It was thus unlikely that the melting process was responsible for high Chllide *a* and other degraded pigments production by osmotic stress. However, the excessive light energy might also break down the Chl *a* because *F.cylindrus* has a naturally high qI (non-photochemical quenching by photoinactivation) (Kropuenske et al., 2010) and a high qI could lead to NPQ accumulation (Petrou et al., 2010, 2011; Petrou and Ralph, 2011; van de Poll et al., 2011). After the ice melted, the contribution of PSC increased concomitantly with improvements in F_v/F_m, indicating a re-optimization of photosynthetic performance to a water environment after release from freezing stress. Light exposure, however, activated the DD-DT xanthophyll cycle (i.e., de-epoxidation), although the size of the DD-DT pool was little changed (Fig. 27). Activation of the DD-DT cycle is the fastest photoprotective strategy and occurs at a scale of seconds to minutes (Goss and Jakob, 2010), whereas the size of the pool actually changes much slower (i.e. minutes to hours). Interestingly, NPQ_{NSV}' in the HL treatment was much higher than that of the LL treatment, with differences in their DD-DT pool size suggesting that pigmentation and light history were largely responsible for their potential photoprotective ability (Szechyńska- Hebda et al. 2010; Galindo et al. 2017). It seems unusual that E_k values significantly decreased (i.e. dark acclimation) upon light exposure, contrary to the expected response from high-light acclimation (Fig. 24). Transcriptional activity of the *psbA* gene was upregulated in both treatments after light exposure (Fig. 30). It is suggested that over-repair or an imbalance between the reaction centres and their downstream components under the extreme light environment occurred. The dark reactions might be independent or slow to respond to the light exposure event because the gene expression of the *rbcL* gene was invariant before and after light exposure (Fig. 29).

4.5. Conclusions

This study demonstrates how the combined effects of ice formation and melting together with light exposure affect the photophysiology of *F.cylindrus*. This study is also the first attempt to quantify the effects of multiple co-stressors in sea ice and to provide insights into the fate of ice algae by conducting *ex situ* incubation of the ice algal *F. cylindrus* in artificial sea ice. A freezing event, where algal cells were incorporated into the ice, suppressed the photochemical process of RCII, even though they had been maintained in an optimal light rnvironment prior to the event (Fig. 18). It was presumably that damage to RCII directly reduced the capacity of electron delivery (i.e. reduction capacity) of quinones and the PQ pools by the stress of the high salinity of brine. As previous studies have observed, a significant amount of the breasdown products of Chl *a*, i.e. Chllide *a*, was observed (Fig. 26) and a part of the Chllide *a* could have been caused by the melting process for sample filtration. However, Chllide *a* had little effect on ChlF because σ_{PSII} was stable throughout the incubations with only a slight, gradual decrease. Sea ice should be a stable platform for ice algal photosynthesis. Ice algal cells rapidly optimize their photophysiology to the dark environment within the ice with decreases in E_k (Figs. 18 and 24). NPQ_{NSV} and PPC were sustained at high levels in the HL ice tank (Figs. 20 and 28). Ice algae in the LL ice tank showed dark acclimation to a greater extent than those in the HL, possibly by increasing active RCII. Although the ice melt event improved algal photosynthesis, subsequent light exposure for 2 h caused a decrease of F_v/F_m (Fig. 18). The significant accumulation of Chllide *a* and NPQ_{NSV} enhancement after light exposure suggests photoinhibition (Figs. 20 and 26), but photoprotection was rapidly activated with high regardless of the amount of PPC and their prior light history (Fig. 27). The diatom *F. cylindrus* was able to cope with the light stress better than other algal species reported in the literature; this supports the ecological success of the diatom both in sea ice and the water-column when ice-edge blooms occur.

CHAPTER 5

Effects of iron and light availability on the photophysiology of ice algae: *Ex situ* incubation of ice algae using a low-Fe ice tank

5.1. Introduction

Iron (Fe) is a crucial element for photosynthesis in microalgae, as summarized in section 1.4.2. In extreme sea ice conditions, light and nutrient availability are the most significant controls on photosynthesis in ice algae, although the of salinity stress can also be important. Pankowski and McMinn (2008a, b, 2009) first reported Fe starvation in Antarctic pack ice and suggested that because the open waters in the Southern Ocean are known to be deficient in Fe, areas known as High Nutrient Low Chlorophyl (HNLC) regions.,that bottom ice algal communities in pack ice would experience low-Fe conditions, Light and Fe availability are tightly coupled because Fe is an essential trace metal for pigment synthesis. Microalgae are known to synthesize more Chlorophyll and carotenoids under low light conditions to maximize the efficiency of light utilization (e.g., Falkowski and Owens, 1980; Morel and Bricaud, 1981; Bricaud et al., 1995) causing the package effect (e.g., Berner et al., 1989). Because this *de novo* pigment synthesis further requires Fe, light limitation causes less Fe availability in subsurface waters, i.e. the so-called the Fe-light co-limitation (*sensu* Sunda and Huntsman, 1997). This antagonistic Fe-light co-limitation can be observed in extremely low-light acclimated ice algae. Cellular Chlorophyll and accessory pigment content are reduced under Fe-limited conditions and the reduced cellular pigment concentrations may lead to photodamage and the production of reactive oxygen species (ROS), because the Fe-limited cells cannot cope with the absorbed photons that exceed the reduced electron transport capacity due to Fe limitation under high-light conditions (van Oijen et al., 2007). In particular, it is a serious problem when Fe-limited ice algal cells suddenly experience high light exposure when ice melts and they are relased from the bottom of sea ice to open waters (i.e., the environment where ice-edge blooms occur). It is thus ecologically and biogeochemically important to investigate how Fe and light control the photosynthetic performance of ice algae to further understand sea ice and marginal ice ecosystems. It has been reported that ocean acidification (OA), associated with the increasing anthropogenic CO_2 input, modifies Fe availability

(Millero et al., 2009). OA can suppress Fe availability by stabilizing Fe-ligand complexation (Sunda and Huntsman, 2003; Shi et al., 2010) but also extends the oxidation rate of Fe(II), which is believed to be the most highly bioavailable source of Fe (Millero, et al., 1987, 2009; Breitbarth et al.,2009). Polar ecosystems are more sensitive to OA than those in temperate and tropical regions (Gibson and Trull, 1999; Orr et al., 2005; Yamamoto-Kawai et al., 2009; McNeil et al., 2010) and furthermore sea ice has greater fluctuations in pH than those in pelagic oceans (Matson et al., 2014; McMinn et al., 2014). Future predictions of sea ice algal biomass and photosynthesis in the changing polar oceans are absent from sea ice biogeochemical models thus far (Vancoppenolle et al., 2013; Constable et al., 2014; Steiner et al., 2016; van Leeuwe et al., 2018). However, there are considerable limitations to the investigation of ice algal photosynthesis: almost all studies so far have worked on ice algal photosynthesis in the laboratory, during which ice algae were rinsed out from ice samples and resuspended in a water medium. This melting process hinders realistic photophysiological information because water media cannot reproduce the temperature in sea ice (<−1.8ºC). Kennedy et al. (2012) and Kameyama et al. (submitted) successfully incubated ice algae in artificial sea ice produced in their lab-based ice tanks. Ice tank techniques enable *ex situ* incubation of ice algae within the ice and manipulation of the ice environment by maintaining ice thickness stable. Here, we use a newly-developed low-Fe ice tank, made of titanium, to control Fe concentration in the ice. This study, therefore, aimed to investigate the effects of Fe and light availability on the photophysiology of ice algae using the low-Fe ice tank. In this study, the polar diatom *Fragilariopsis cylilndrus*, as a representative ice algal species with a fully sequenced genome, was used (Mock et al., 2017), enabling the application of molecular techniques to understand the underlying mechanisms driving photophysiology. Photophysiological responses of *F. cylindrus* were monitored with variable Chl *a* fluorescence and their pigment composition.

5.2. Materials and methods

5.2.1. Ice tank incubation and preparation of low-Fe medium

The polar pennate diatom *Fragilariopsis cylindrus*, isolated from Antarctic pack ice in 2015 (Davis

station, East Antarctica) was incubated in a purpose-designed ice tank (Island Research, Tasmania). The low-Fe ice tank, which was constructed of titanium to minimize Fe contamination, was placed into a freezer (–20ºC), and the ice thickness and temperature gradient controlled by interactions between a basal heater and the adjustable ambient freezer temperature (see Kennedy et al., 2012). This enabled an ice thickness of approximately 5.5 cm to be maintained during the experiment. Incubations were conducted in Aquil media (Price et al. 1989) buffered with ethylenediaminetetraacetic acid (EDTA) (final concentration 20 μM) at 150 μmol photons m^{-2} s^{-1} (PAR) and a salinity of 35. Total Fe concentrations were set at 400 nM and 20 nM, where the concentrations of total inorganic forms of Fe (Fe') were 1.54 nM and 15.5 pM, respectively. It is considered that the EDTA-buffered Fe was maintained in the medium and the exact value was calculated using the software Visual MINTEQ, ver. 3.1 (https://vminteq.lwr.kth.se). For the ice tank incubation setup, see section 4.2.1. To check whether contamination by external Fe (e.g. aerosol deposition on the ice during ice sampling) occurred, concentrations of Fe in under-ice seawater were monitored. Fe concentrations in ice were difficult to determine because ice thickness was too thin to obtain a brine sample. In addition, the Fe source for the ice algae in the artificial sea ice should have been restricted to from the under-ice water. Fe concentrations in the water samples were thus determined by the Ferrozine colorimetric method (Stookey, 1970). Fe samples were placed into a 60 mL low density polyethylene (LDPE), previously cleaned, bottle (Thermo Scientific) following the GEOTRACES protocol (Cutter et al., 2010). Briefly, a 50 mL ferrozine cocktail was prepared with 10 mM Ferrozine (Sigma) and 1.44 M hydroxylamine hydroChloride (ultratrace analysis glade, Wako) dissolved in ultrapure water acidified with ultrapure hydroChloric acid (HCl) (Wako). The 0.4 mL of ferrozine cocktail was added to a 20 mL sample acidified with suprapure HCl (Merck) at least 2 months before the measurements (Farid et al., 2018). The sample was heated at 70 ºC for 15 min to accelerate reduction Fe(III) to Fe(II) and for detaching Fe (II) from the Fe-EDTA complex. After cooling, 0.4 mL of an ammonium acetate (Fe analysis glade, Wako) buffer solution, prepared with a trace metal grade ammonia solution (Wako), was added to the sample. The buffered sample was incubated at room temperature for 24 h to fully recover Fe in the sample (Farid et al., 2018). Fe concentrations were determined with a spectrophotometer at the absorbance of Fe(II)-ferrozine

complexes at a wavelength of 562 nm (UV-2450, Shimadzu) with a 50 mm path length glass tube. A Fe standard curve was drawn with a series of known Fe concentrations by diluting a Fe standard solution (Wako) (r>0.999, n=7). The detection limit of the measurement was 10 nM, which was consistent with previous studies (Farid et al., 2018). The quantification limit, defined as 3 SD of a standard, was 15 nM.

5.2.2. Fast repetition rate (FRR) fluorometry

See section 4.2.2.

2.3. Cell abundance of ice algae

See section 4.2.4.

5.2.4. Pigment composition

See section 4.2.5.

5.2.5. Gene expression of photosynthesis-related genes, *psbA* and *rbcL*

See section 4.2.6.

5.3. Results

5.3.1. Ice physics and ice algal growth

Throughout the incubation experiments, ice thickness was stable at 5.5 cm on average with little basal ice melting or sublimation of ice from the ice surface. During the experiments, temperature within the ice increased from the ice surface (−22.5 ºC) to the ice-water interface (−2.2 ºC) (Fig. 17), and seawater temperature beneath was maintained at ~ −1.8ºC throughout the incubations. when ice was present. Brine salinity and its fraction were estimated following Cox and Weeks (1983) and Eicken (2009), respectively. Brine salinity decreased with depth from 293.7±0.0 to 39.4±0.5. Assuming no gas bubbles were in the ice, the brine fraction ranged from 3.7±0.0% to 34±0%,

increasing with depth. Macronutrients were not depleted throughout the incubations (data not shown). During the LFe incubations, a trace amount of Fe was inevitably introduced but this contamination was considered to be negligible. Fe concentrations ranged from 11 nM to 43 nM in the LFe treatments, which were equivalent to 2.2 pM and 8.7 pM of Fe', respectively. Initial Fe concentrations were 23 nM and 20 nM (4.5 pM and 4.0 pM as Fe' concentrations) for HL and LL ice tanks, respectively. Final Fe concentrations in the LFe ice tanks were, 27 nM and 25 nM (5.4 pM and 5.1 pM) for HL and LL ice tanks, respectively. Concentrations of Fe were stable throughout the incubations (Appendix K and see detailed discussion in the table caption therein). No significant variation in Fe concentration during the incubations was observed in either ice tank incubation (One-way ANOVA, $p<0.05$). Algal cells of *F. cylilndrus* were certainly incorporated into the ice, and ice algal cells showed slow but constant positive growth in all treatments within the ice environments (Table 10), showing no significant difference in growth rate between the treatments ($p>0.05$).

5.3.2. Variable Chl *a* fluorescence

5.3.2.1. Dark values (F_v/F_m and σ_{PSII})

At the beginning of the incubations on day −05, planktonic *F.cylindrus* showed relatively high F_v/F_m values (HFe+HL: 0.47±0.05; HFe+LL: 0.45±0.6) for HFe treatments and lower values (LFe+HL: 0.32±0.03; LFe+LL: 0.31±0.01) for LFe treatments (Fig. 18). Once algal cells were frozen into the ice on day 00, F_v/F_m sharply dropped down to ~0.2−0.3 regardless of Fe and light environments ($p<0.01$), except for the LFe+LL treatment (Fig. 18), while σ_{PSII} was little changed in the freezing events ($p>0.05$) (Fig. 19). During the frozen period (i.e, ice algal cells were within the ice), F_v/F_m values were relatively stable until day 20 and showed almost identical values regardless of the Fe or light availability. The lowest F_v/F_m was found in the middle of the incubations on days 5 or 15 (Fig. 18). The σ_{PSII} under the LFe availability, however, gradually increased toward the end of the incubation within the ice, although those of the HFe counterparts showed stable values with slight and gradual decreases throughout the incubations in the ice (Fig. 19). Once the ice was melted, F_v/F_m values recovered to the original values on day −05, although this was not the case for the HFe treatments: 39% lower and 15% higher values than those on day −05 for HFe+HL and HFe+LL, respectively

(Fig. 18). The responses of σ_{PSII} were different from those of F_v/F_m. The σ_{PSII} values were significantly different from the initial value on day −05 but similar to σ_{PSII} values on day 20 regardless of the Fe and light availability (Fig. 19). Soon after the light exposure to the melted samples at 800 μmol photons m^{-2} s^{-1}, F_v/F_m values significantly dropped in all treatments (decreased 18%−31%) (Fig. 18). In spite of the significant and large decreases in F_v/F_m, σ_{PSII} showed little variation although that in the HFe+HL decreased significantly (a 16% decrease) after the light exposure (Fig. 19).

5.3.2.2. Quenching parameters (NPQ_{NSV} and 1-qP)

Non-photochemical quenching (NPQ_{NSV}) in the HFe treatments was smaller than those of the LFe treatments at the initial stage on day −05 (Fig. 20). Closed fractions of PSII were ~50% on day −05 with slightly higher values in the HFe+LL treatment (70%) (Fig. 21). The freezing event greatly enhanced NPQ_{NSV} of the HFe treatments, while the LFe algal cells showed only moderate increases. NPQ_{NSV} in the HFe incubations were at a maximum in the early stages of the incubations (i.e., days 00 or 05), those in the LFe reached their maxima when the incubations were near their end (i.e., days 15 or 20). During frozen, NPQ_{NSV} was significantly upregulated in both light treatments (p<0.05), although the LFe+LL treatment did not also show a significant variation in NPQ_{NSV}. The closed fraction of PSII slightly increased but not significantly, with higher 1-qP values, at or after freezing, although the timing of the increments in 1-qP was not consistent among the treatments. NPQ_{NSV} values were stable in the middle of the incubations in the HFe treatments, while those in the LFe treatments showed gradual increases in NPQ_{NSV} during the frozen periods (Figs. 20 and 21). Although the behaviour of 1−qP was variable during the frozen periods, higher 1−qP values were found in the HL treatments. After the ice melt, NPQ_{NSV} decreased to the identical levels obseved on day −05, whereas 1-qP did not show any consistent behaviour upon melting. The light exposure after the melting event significantly enhanced NPQ_{NSV}, but the increments in NPQ_{NSV} in the LFe tank (HL: 20.9%; LL: 57.8% increases, respectively) were smaller than the HFe counterparts (HL: 98.3%; LL: 89.5%) (Fig. 20). All tank except for the HFe+LL tank showed slight decreases in 1-qP upon the light exposure.

5.3.3.3. Photosynthesis-irradiance (ETR_{RCII}-*E*) curve

The initial slopes of ETR_{RCII}-*E* curves; α, regarded as light utilization efficiency, dropped significantly when algae with HFe were frozen into the ice, while algal cells under LFe did not show any change in α values (Fig. 22). During the frozen periods, α values were stable in the HFe treatments, although a slight increase was observed at the end of the incubation of HFe+LL. The LFe treatments, on the other hand, showed gradual increases in α values under both HL and LL conditions. After the ice melted, α values decreased in all treatments, but the HFe cells showed slightly lower α than the initial values, while α of the LFe cells returned to their initial levels. After the light exposure, little variations in α were observed except in the HFe+HL incubation (Fig. 22). Maximum electron transport rates (ETR_{max}) showed significant decreases in all treatments during the frozen period (Fig. 23). The ice algal cells under LFe showed higher ETR_{max} values throughout the incubations. It seemed that ETR_{max} values under HL gradually decreases while those of the LFe incubations dropped more sharply and maintained their ETR_{max} values at lower levels. When the ice melted, ETR_{max} values recovered to their initial values or were slightly higher before freezing, except for the HFe+HL treatment (Fig. 23). Values of the light saturation index, E_k, gradually decreased over the course of the incubation experiments without any conspicuous variation during the frozen period (Fig. 24). Melting, however, increased the E_k values to the initial levels before freezing on day −05. When the algal cells were exposed to light, the E_k decreased in all treatments, although their extent of the decreases was different among the treatments (Fig. 24).

5.3.3. Pigment composition

Initial TChl *a* concentrations were comparable regardless of light and Fe availability, although that of the HFe+LL treatment had a lower value (as discussed in chapter 5). The contribution of Chllide *a* to TChl *a* gradually increased during the course of the LFe+HL incubation as well as increasing at the beginning of the LFe+LL incubation (Fig. 26). Both LFe incubations showed increases in TChl *a* biomass when *F. cylindrus* cells were trapped in the ice and higher Chl *a* biomass was observed in the

LL ice tank as the HFe+LL ice tank showed higher biomass than the HFe+HL incubation. When cells were exposed to light after the ice had melted, there were substantial increases in the Chllide *a* to TChl *a* ratio in both ice tanks (Fig. 26). The DD-DT pool size in the HL treatment was slightly higher than that in the LL treatment at the initial stage on day −05 and also showed a larger pool size during the frozen period. Values of DES increased slightly later than the algal cells that had been frozen into the ice and remained stable in the HL treatment. Whereas the LL treatments showed lower values with an exceptional peak on day 15. DES levels decreased when the ice melted and continued to decrease after light exposure, unlike in the HFe incubations (Fig. 27). The HL treatment showed a gradual but strong increase in PPC/PSC, whereas only a slight increase was observed in the LL ice tank. When the ice melted, there was a decrease in the PPC contributions to PSC, down to the level prior to the start of the frozen period or at the beginning of the incubations on day −05. The short light exposure of 2 h little affected the PPC/PSC ratio (Fig. 28).

5.3.4. Gene expression of photosynthesis-related genes

5.3.4.1. *rbcL*

Gene expressions of the *rbcL* gene at the initial incubation stage were similar, but showed a slightly higher value in the LFe+HL treatment (Fig. 29). Regardless of the Fe and light availability, transcriptional activity of the gene was highly upregulated when the algal cells were frozen into the ice (Fig. 29). During the frozen periods, however, gene expression levels dropped sharply to a lower level than that of the values from the seawater prior to the initiation of freezing (Fig. 29). The low level was sustained until day 20, when slightly higher gene expressions were observed in both treatments. Comparing the results of Melt and Light conditions, the *rbcL* gene expression did not show any conspicuous changes in either treatments.

5.3.4.2. *psbA*

Unlike the *rbcL* gene, gene expression of the *psbA* gene behaved differently with differences in light availability (Fig. 30). Initial values of the HFe and LFe treatments were different, between; under HFe conditions they were ~2-fold higher than the than those in the LFe counterparts. In the HL conditions,

transcription of the *psbA* gene was highly activated during the frozen period, similar to the response of the *rbcL* gene. In the LL conditions, such upregulations of the gene were not evident under either HFe or LFe availability. The algal cells in the HFe tanks showed similar patterns to those observed in the *rbcL* gene; a sharp decreases in the gene expression after the initial upregulation and then a recovery to their initial values when the ice melted (Fig. 30). The algal cells under the LFe conditions, however, showed constant gene expressions throughout the incubation. It was evident that upregulation of the gene was found after light exposure (i.e. Δ*psbA* became positive), whereas downregulations were observed in the LFe treatments upon the light exposure (i.e. Δ*psbA* showed negative) (Fig. 30).

5.4. Discussion

5.4.1. Freezing event

The initial F_v/F_m values in the LFe incubations were significantly lower than those in the HFe treatments (Fig. 18). Kolber et al. (1994) and Suzuki et al. (2002) demonstrated that Fe availability affects photochemical reaction at RCII because PSII has 2 Fe atoms and a high turnover rate (Greene et al., 1992; Geider and LaRoche, 1994; Govindjee, 2010). (Fig. 18). σ_{PSII} was stable during the frozen period of the HFe treatments, suggesting that the stress associated with the high brine salinity might have played a central role in the suppression of photochemical processes around PSII, especially reduction capacities of quinones and the PQ pool in the HL treatment (Fig. 19). NPQ_{NSV}' in the HL treatment increased, whereas that of the LL counterpart did not show any significant change in the NPQ_{NSV}', which was a clear reversal of the response of F_v/F_m to the freezing stress (Figs. 18 and 20). Unlike in the HFe incubations, the light utilization index, α, did not respond to the freezing event, whereas ETR_{max}, interestingly, maintained the higher values compared to the HFe treatments (Figs. 22 and 23). Schuback et al. (2015) also reported relatively high ETR_{max} values in Fe-limited waters in the Southern Ocean. They hypothesized the existance of alternative pathways for electrons to dissipate the excess energy, rather than NPQ, were upregulated; these included pseudo-cyclic and cyclic electron flow (Prasil et al., 1996; Feikema et al., 2006; Cardol et al., 2011), which would have reduced the high transmembrane ΔpH as well as active PTOX (McDonald et al., 2011) under Fe

limitation. The resultant E_k value eventually showed the dark-acclimated state (Fig. 24). The contribution of Chllide *a* to TChl *a* was stable when cells were frozen into the ice, indicating a smaller effect of the melting process on pigment breakdown and the production of Chllide *a* (Fig. 26). The size of DD-DT pool was also stable and xanthophyll cycle had not been activated (Fig. 27), suggesting that other non-photochemical quenching pathways were responsible for the NPQ_{NSV} during the frozen period (Fig. 20). Gene expressions of the *rbcL* gene were upregulated in both light treatments as well as that in the HFe treatments (Fig. 29), emphasizing the cold acclimation strategy. The contrasting response of the *psbA* gene, i.e. upregulation in the HL treatment while constant in the LL treatment, was also evident in both HFe and LFe treatments (Fig. 30). The upregulation of the *psbA* in the HL treatment could be a strategy to overcome over-excitation associate with HL and possibly the freezing stress causing electron clogging.

5.4.2. During the frozen period

Sea ice provides a stable platform for photosynthesis of ice algae, which might optimize their photophysiology in spite of the low Fe availability. F_v/F_m values in the LFe during the frozen period treatments were comparable to those in the HFe treatments, regardless of light availability, suggesting that Fe and light availability might not be crucial for ice algal photosynthesis and growth in the sea ice environment. Pankowski and McMinn (2008a) reported similar growth rates of *F. cylindrus* both in Fe-replete and Fe-starved culturing media. Although F_v/F_m values were stable, σ_{PSII} showed gradual increases during the course of the incubation (Fig. 19). Interestingly, during the HFe ice incubation the other index of light absorption efficiency, α, increased synchronously with σ_{PSII} (Figs. 19 and 22), suggesting that the increase in α was due to increasing photosynthetic antennae size (i.e. increase in σ_{PSII}; 'σ_{PSII} strategy', hereafter) but not increasing the number of photosynthetic units (n_{PSII} strategy). Strzepek et al. (2012) demonstrated that Southern Ocean phytoplankton in Fe-limited waters employed the σ_{PSII} strategy by conducting culture incubation experiments using representative Southern Ocean species. They proposed that the σ_{PSII} strategy is used to overcome Fe-light co-limitation in the Southern Ocean; this study (i.e. herein) is the first to demonstrate that ice algae in the Antarctic also employ this strategy. As in the HFe incubations, NPQ_{NSV} in the LFe incubations was

enhanced when cells were trapped in the ice. Interestingly, NPQ_{NSV} seemed to synchronize with DES, whereas this was not evident in the HFe incubations (Fig. 20 and 27). That was feasible because DD and DT do not possess Fe, although there are some effects of Fe availability on the genetic translations of the pigments, such as operon regions (e.g., Laudenbach et al., 1988; Geider and LaRoche, 1994; Lommer et al., 2012; Georg et al., 2017). The DD-DT xanthophyll cycle was thus responsible for photoprotection in the LFe conditions. The pool size of DD plus DT in the HL incubation was larger than that of the LL counterpart (Fig. 27), again suggesting more photoprotective capability under HL. The higher PPC/PSC ratio in the HL incubation was also supportive evidence of the large range of photoprotective capability (Fig. 28). NPQ_{NSV} capability (maximum values of NPQ_{NSV}) was, however, comparable between the HL and LL treatments (Fig. 20). This was possibly due to the effective xanthophyll cycles rather than other factors such as the active proton back transport by the PTOX, the cyclic electron flow via ferredoxin or flavodoxin (discussed in chapter 4). Ferredoxin and flavodoxin are interchangeable, but Fe availability affects the electron sink potential of these two proteins (Geider and LaRoche, 1994; LaRoche, 1996) because their molecular weight are considerably different. The transmembrane ΔpH was thus alleviated via this electron pathway under the HFe condition, whereas cells under the LFe had to exclusively rely on the DD-DT xanthophyll cycle because other electron sinks might not be active. This notion, however, is inconsistent with the proposed mechanisms under Fe limitation by Schuback et al. (2015). As noted above, under both light intensities α gradually increased during the course of the incubations, whereas ETR_{max} remained constant at relatively high values, leading to the gradual decrease in E_k and dark acclimation in the ice (Fig. 22 and 23). It is of interest that the cells in the LFe incubations altered their photophysiology for dark acclimation by maintaining a high ETR_{max} and increasing α values, this differs from the behaviour in the HFe ice incubation and might maximize their photosynthetic potentials under Fe starvation to maintain their photosynthesis. Gene expression of the photosynthesis-related genes behaved similarly in the HFe treatments between light treatments. Transcriptional activity of the *rbcL* gene was sharply downregulated and maintained at a low level (Fig. 29), suggesting that algal cells acclimated to their ice environment and optimized the balance between photochemical reactions and energy allocation to the dark reaction processes such as carbon fixation by RuBisCO. The constant

gene expression of the *psbA* gene in the LL ice tank seems reasonable as the constant freezing stress in the ice could have damaged the fragile D1 protein in PSII by over-reduction (Fig. 30). Downregulation in the transcriptional activity of the gene in HFe, however, was enigmatic because light stress was more evident in the HL treatment. The relationship between the *psbA* gene and the transcript D1 protein is not directly infered by the considerable post-transcriptional regulation (e.g., mRNA splicing and RNA editing) (Kettunen et al., 1997). The significant upregulation of the *psbA* gene, associated with the sudden freezing stress, might thus provide excess mRNA to maintain synthesis of the D1 proteins.

5.4.3. Light exposure after the ice melt event

The light exposure significantly decreased F_v/F_m values due to both the excess excitation pressure in the reaction centres of PSII (Fig. 18) and also photoinhibition (Melis, 1999). NPQ_{NSV}' also responded to light exposure to dissipate excess energy (Fig. 20). The NPQ_{NSV}' enhancement in the LFe treatments, which were less efficient than those of their HFe counterparts (shown in Fig. 20) indicate that Fe starvation suppressed NPQ ability. Moreover, xanthophyll activity, shown as DES, was downregulated in spite of the high light stress, whereas cells under the HFe conditions upregulated the xanthophyll cycle (Fig. 27). The lower DES in the LFe treatments after the light exposure were plausible to explain the less enhancement of NPQ_{NSV}' following the light exposure event. The xanthophyll pool and PPC/PSC ratio were, however, relatively stable, because pigment synthesis is slower than photoprotective processes (i.e., xanthophyll cycles and D1 protein repair) (Kuczynska et al., 2015). At the same time, the significant accumulation of Chllide *a* after light exposure reflected the the high level of absorbed energy that subsequently broke down intact Chl *a* possibly due to the presence of ROS (Fig. 26). The stable contribution of Chllide *a* again implied that production of Chllide *a* was not due to ice melt events. High contributions of Chllide *a* were, however, observed at the surface of the Southern Ocean during ice retreat in spring (Bidigare et al., 1986; Wright et al., 2010). Light exposure after ice algae are released from ice is more likely the reason for the high Chllide *a* contributions. Interestingly, repair of damaged PSII, as indicated from gene expression of the *psbA* gene, was inactivated after light exposure, whereas Fe-replete cells upregulated *psbA* gene

expression (Fig. 30). In addition, the slower repair of damaged PSII at low temperature (Kropuenske et al., 2009; van de Poll et al., 2011; Lacour et al., 2018) could exacerbate the photoinhibition. The chronic Fe starvation thus led to the increased vulnerability of photosynthesis to high light stress in ice algal cells released from the ice. The contribution of ice algae to ice-edge blooms may thus be smaller in changing polar sea ice environments.

5.5. Conclusions

Under the low Fe conditions, initial F_v/F_m values were lower than those of their HFe counterparts . Although the frozen period negatively affected the photochemistry of PSII (i.e. $F_v/F_{m)}$, it was not evident in the LFe+LL treatment. NPQ_{NSV}'activity declined in both light treatments, which supports the suggestion that ice algal cells immediately regulated NPQ to protect themselves. During the frozen period, F_v/F_m values were stable regardless of the light availability as well as the Fe availability, when comparing all four treatments. The stable and comparable F_v/F_m within the ice supports the notion that sea ice is a stable platform for ice algal photosynthesis, as discussed in chapter 4. When the ice melted and intense light was exposed to the melted samples, too much light commonly suppressed PSII photochemistry due to the over-excitation of PSII; this also occurred in the HFe treatments. In spite of the stable F_v/F_m values during the frozen period, light history affected potential photosynthetic capability, in particular, NPQ capacity. Indeed, NPQ capacity after light exposure in the LL treatments was lower than those in the HFe treatments. The lower upregulation of NPQ_{NSV}' and *psbA* gene expression in the LL treatments indicates that the released ice algae in Fe-starved conditions became vulnerable to high light stress because they were unable to adequately self-protect and slow down the repair of damaged PSII (i.e., D1 protein synthesis). Ice algae maintained and optimized their photosynthesis in sea ice during the frozen period,but chronic Fe starvation as well as their light history under LL led to less flexibility of photoacclimation. It further suggests that ice algal production may be reduced when sea ice decreases, which will remove platforms for ice algal production and ice algae will be less able to contribute to ice-edge blooms.

CHAPTER 6

General conclusions and perspectives

6.1. Subpolar diatom blooms in changing subpolar regions

Subpolar phytoplankton bloom events can be affected by (a) increasing temperature, (b) intensification of surface stratification, and (c) ocean acidification (e.g., Boyd et al., 2014). Intensification of stratification enhances light availability to surface phytoplankton but reduces nutrient supply to the euphotic zone. In the study area, coastal Oyashio and Oyashio regions, Ono et al. (2002) demonstrated that the MLD has gradually shallowed with a decrease in nutrient supply. They also suggested that the Chl *a* inventory is decreasing at the rate of -2.35 ± 1.22 mg m^{-2} $year^{-1}$ in Oyashio waters. Chapter 2 demonstrated that temperature was a controlling factor of the spring diatom bloom in coastal Oyashio waters on the shelf (i.e., shelf COY). In particular, the combined analyses of conventional *P-E* curve experiments and gene expression measurements on the *rbcL* gene revealed that an increase in temperature dually benefited carbon fixation processes and finally led to high P^{B}_{max}. In the shelf COY waters, the genus *Thalassiosira* formed a spring bloom. Although the temperature increase might have benefited the *Thalassiosira* blooms in the shelf regions, temperature in COY cannot be easily changed because COY originates from sea ice meltwater from the Sea of Okhotsk (Sugiura, 1956; Ogasawara 1990). It is thus expected that the increase in temperature associated with global warming brings forward the timing of the sea ice melt and reduces sea ice production in the Sea of Okhotsk. This leads to the earlier onset and reduced spreading of the *Thalassiosira* blooms in the shelf COY waters. In addition to the findings above, ocean acidification affects nutrient and CO_2 availabilities, which benefit or disadvantage specific phytoplankton groups. Using diagnostic pigment analysis, Endo et al. (2016) revealed that compared to present and pre-industrial CO_2 levels in Oyashio waters diatoms responded negatively to ocean acidification (OA). (e.g. Bacillariaceae and Thalassiosiraceae, respectively). Future perspectives regarding Chapter 2; transgenus studies on the effects of temperature on gene expression of the *rbcL* gene are needed because it is important to clarify whether the genetic response of the *rbcL* gene to temperature is universal or restricted to specific diatoms during bloom. This study, however, reported sufficient

insights on spring diatom blooms because *Thalassiosira* blooms have a global distribution, including subpolar and polar regions such as in the Arctic and Antarctic as well as the Atlantic and the North Pacific.

Chapter 3 focused on the blooms in the western subarctic Pacific, including Oyashio waters, near the Kuril Islands and the eastern kamtchatka Peninsula. This chapter demonstrated that a clear gradient of diatom biogeography occurred along the Kuril Islands and the eastern Kamchatka Peninsula. The HNLC water was dominated by *Fragilariopsis*, which spread to offshore regions, whereas Fe-replete waters were dominated by *Chaetoceros*, which were restricted in coastal areas. The shoaling MLD reduced upward Fe supply from the intermediate water (Nishioka and Obata, 2017), while the MLD shoaling relieved Fe-light co-limitation in the deeply mixed waters. Upward Fe supply to coastal areas along the Kuril Islands is mainly driven by diapycnal mixing with the dFe-containing intermediate water (i.e., NPIW). This water originates from DSW, which is formed by sea ice brine rejection (Nakatsuska et al., 2002). Although it might be suspected that the Fe supply would decrease with reduced sea ice production in the Polynya at the estuary of the Amur River, it is not clear how a decrease in the NPIW affects surface phytoplankton production because the pathways of DSW to NPIW are complex (e.g., water trapping at the Kuril Basin) (Wakatsuchi and Martin, 1991). The alleviation from the Fe-light co-limitation might shift the diatom community from *Fragilariopsis* to *Cheatoceros* domination. In addition, during the post-bloom phase, the Fe-replete *Cheatoceros* community shifted to a community with robust and long-chained diatoms (e.g. *Neodenticula seminae*). The shoaling MLD might have had a negative effect on the primary production of the phytoplankton by reduced Fe supply to the coastal areas by reduced Fe-replete NPIW production, whereas the enhanced light supply would alleviate Fe-light co-limitation. The Fe-light co-limitation could be an overlooked process to aid the understanding of primary productivity in the Oyashio regions. If the Fe-light co-limitation could be alleviated by a shoaling MLD, it could lead to higher a biological pump capacity along the slopes of the Kuril Islands (i.e., via continental shelf pump; *sensu* Tsunogai et al., 1999). For Chapter 3, SEM provided many insights into diatom community shifts with Fe availability. It is evident that the western subarctic Pacific is the largest biological CO_2 sink (Takahashi et al., 2002) and contributes to a high carbon flux down to deep oceans (Honda, 2003;

Kawakami et al., 2004, 2017). The fact that a great quatity of *N. seminae* scales has frequently been observed in sediment traps (Katsuki et al., 2005; Katsuki and Takahashi, 2005; Onondera et al., 2005), although they are rarely found in surface water has long been unexplained. This study, for the first time, reported elongation of *N. seminae* in the Fe-limited bottle with DFB during on board bottle incubations. Studies that determine their growth and elongation can disentangle this *Neodenticula* paradox.

6.2. Ice algae in changing polar regions: Sea ice bottom blooms and ice-edge blooms

Primary production of sea ice algae has not been well adequately incorporated into biogeochemical models of polar regions in spite of many reports of Chl *a* biomass in sea ice cores (>4000-core data; Steiner et al., 2016; Arrigo, 2017; van Leeuwe et al., 2018; Meiners et al., in press). This is possibly because only biomass data are available for biogeochemical modellers whereas 'rate' data (i.e. photosynthetic rate, grazing rate, and loss rate from sea ice) have not been documented. In addition, some might not accept data measured with conventional incubation methods, because sea ice samples are needed to be melted for incubation (Stefel et al., 2012; Roukaerts et al. in press). This study was the first attempt to apply FRRf to sea ice algae, enabling non-invasive and instantaneous measurements of photosynthetic rates. The non-invasive FRRf apporoach is totally different from the conventional *PP* measurements with the invasive ^{13}C or ^{14}C methods and can minimize the effects of melting processes: the overnight melting greatly modifies photophysiology of ice algae as discussed in section 4.2.3. Although the FRRf method can only measure the photochemical efficiency of PSII, strenuous efforts have been made for coverting photochemical electron transport at PSII to carbon fixation (Lawrenz et al., 2014; Schuback et al., 2015, 2016; Ryan-Keogh et al., 2017), which might enble us to quantify of *PP* from FRRf data near future. The validation experiments on different melting methods seemed to successfulyl identify the best methods for ice samples for FRRf (i.e. fast direct melt even with slush ice). Although FRRf can only assess the activity of PSII and its downstream components, this study was the first step toward quantification of primary productivity of ice algae. Chapter 4 focused on how freezing and melt events affect the photophysiology of ice algae.

Lower F_v/F_m values were documented in sea ice algae than those of under-ice phytoplankton (McMinn et al., 2010). The FRRf and pigment analysis demonstrated that multiple co-stressors could affect the activity of downstream of PSII. Ice algae, however, immediately acclimated to this ice environment and optimized their photosynthesis by regulating NPQ ability. The flexible photoprotection to excess excitation pressure can be a key for the active production of ice algae. (Lacour et al., 2018). NPQ plasticity is, however, affected by their light history. Thus when ice algae are released from the ice into the sea they experience intense light; NPQ upregulation in the LL treatment was lower upon light exposure. This suggests that thinning of sea ice in a warming world, especially in the Arctic sea ice zone, will benefit ice algae primary production by enhancing light supply (e.g., Galindo et al., 2017), because ice algal cells can modify their potential photosynthetic ability with their light history. Global sea ice extent, however, has been contracting, indicating that the platforms for ice algal production are being lost. Consequently, more active primary production but in more limited areas can be expected. This retraction also implies there will be a reduction in habitat for other key sea ice biota such as juvenile krill and fish larvae, which live the ice algae (Moteki et al., 2017; Bernard et al., 2018). Chapter 5 demonstrated the effects of Fe availability on the photophysiology of ice algae. The freezing stress equally suppressed photochemical processes as the in the LFe and HFe incubations, although the decrease in the LFe+LL treatment was not significantly different. Interestingly, Fe and light availability did not affect photosynthetic activity at PSII during the frozen period, supporting the concept that sea ice is a stable environment with a stable light regime and continuous upward nutrient diffusion into the ice from the under-ice water. However, their potential photosynthetic capability, changed; σ_{PSII} showed dynamic increases in both light treatments possibly to alleviate the Fe-light co-limitation within the ice (Strzepek et al., 2012). The Fe-light interaction enlarged photosynthetic antennae rather than photosynthetic units such as reaction centres and this might be one explanation of why Fe-starved cells became vulnerable to high light stress as they absorbed more energy which went to fewer reaction centres. The reduced enhancement of NPQ exacerbated the photoinhibition. Indeed, DES was lowered upon light exposure, which supported the lowered NPQ ability. However, the DD-DT cycle seemed not to relate to Fe availability. It was likely that if ATP was in short supply for the synthesis of xanthophylls, the DD-DT pool size in the LFe

treatments would be comparable to those in the HFe counterparts. However, It is unclear what the ecological relevance is if NPQ is downregulated with lower DES under Fe limitation. It was also unexpected that *psbA* gene expression would be suppressed under the Fe-limited conditions because additional synthesis of the D1 protein is required for more damaged PSII. It is not certain but *psbA* gene expression might have been regulated by factors such as uncovered relationships between operon transcriptional regulation and e.g. Fe availability for transcription of the gene as observed around the *rbcL* gene. These results indicated that ice algae became vulnerable to high light stress after chronic Fe starvation in sea ice. It suggested and re-emphasized that ice algae can maintain and optimize their photosynthesis even under Fe starvation. However, because of ice loss, they would, contribute less to ice-edge blooms. As Lannuzel et al. (2008; 2015; 2016) have found, sea ice is a major Fe fertilizer of the ice-edge. However, ice algae might stop actively photosynthesising before they take up the surface bioavailable Fe because previous reports have observed that photosynthesis ceased when ice algal ice cells were dark-acclimated at the bottom of the sea ice within a few hours, even they were not Fe-limited, (Galindo et al., 2017). As noted above, Fe-starved cells are more vulnerable, with large photosynthetic antennae and fewer reaction centres,. than smaller cells Consequently, sea ice reduction and chronic Fe starvation in sea ice may change the biodiversity and biomass of sea ice biota by causing a mismatching between trophic interactions with reduced availability of ice algae for them (Constable et al., 2014; Deppler and Davidson, 2017). This study has demonsrated that is worth appling ice tank incubation techniques to other ice algal species, such as the haptophyte *Phaeocystis antarctica*, which is abundant in the Southern Ocean, especially before the diatom bloom (Kropuenske et al., 2009; Alderkamp et al., 2012), or to mixed ice algal assemblages to reproduce more realistic environments in the ice tank.

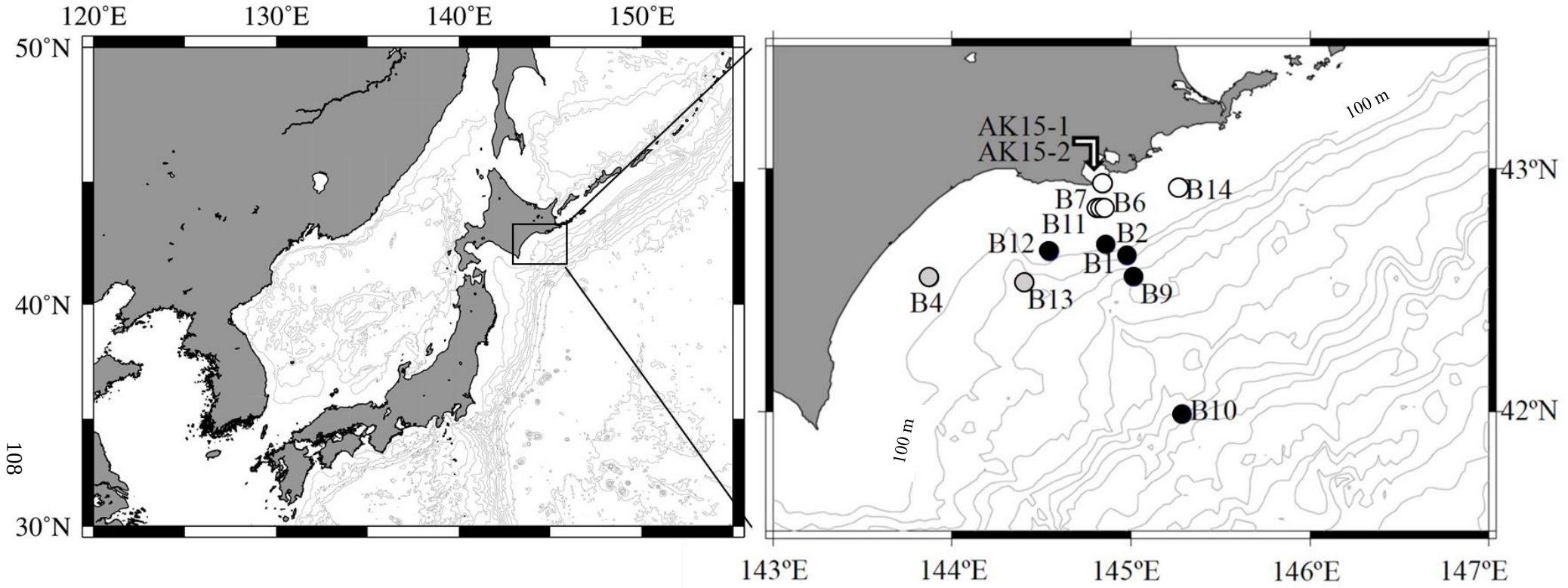

Figure 1. Seawater sampling stations during the KH-15-1 and AK15 expeditions off the coast of Hokkaido, Japan.
Stations for the KH-15-1 expedition are denoted as B plus station numbers.
Stations Bio-6, Bio-7, and Bio-11 overlap as well as stations AK15-1 and AK15-2. Open circles denote shelf COY stations, black closed circles denote offshore COY stations, and grey closed circles denote Tokachi stations.

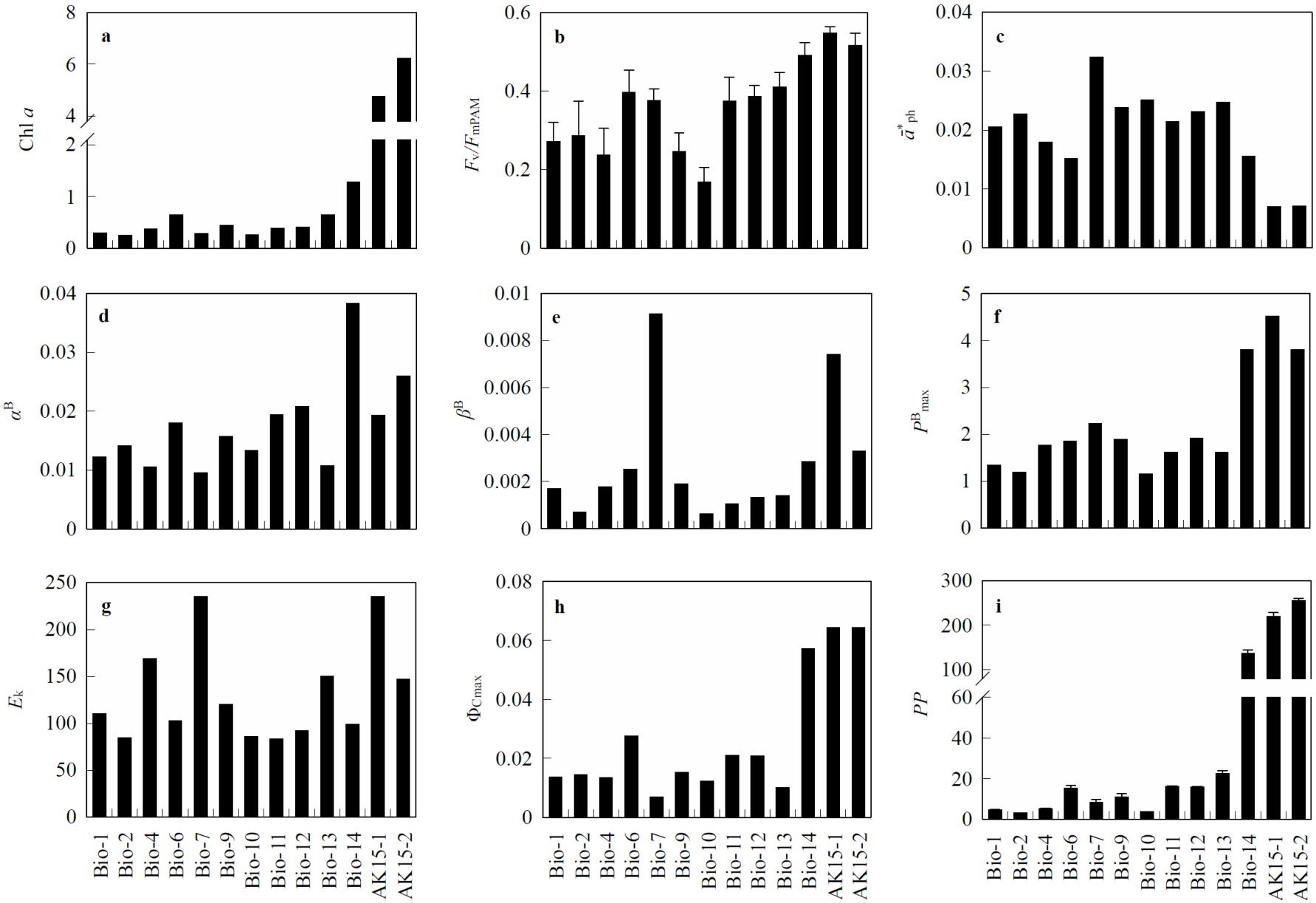

Figure 2. Photosynthetic parameters obtained from *P-E* curve experiments at *in situ* sampling stations.
Chl *a*: Chl *a* concentration [mg m^{-3}]; F_v/F_{mPAM}: Maximum quantum yield of PSII obtained by PAM fluorometry; $\bar{a}^*_{ph}$: Chl *a*-normalized light absorption coefficient of phytoplankton [m^2 mg Chl *a*]; α^B: Initial slope of *P-E* curve [mg C mg Chl a^{-1} h^{-1} (µmol photons m^{-2} s^{-1}) $^{-1}$]; β^B: Photoinhibition index [mg C mg Chl a^{-1} h^{-1} (µmol photons m^{-2} s^{-1}) $^{-1}$]; P^B_{max}: Maximum photosynthetic rate [mgC mgChl a^{-1} h^{-1}]; E_k: Light saturation index [µmol photons m^{-2} s^{-1}]; Φ_{Cmax}: Maximum quantum yield for carbon fixation [mol C mol photons^{-1}]; *PP*: Primary productivity [mg C m^{-3} day^{-1}]. Error bars are standard deviations, $n \geq 3$.

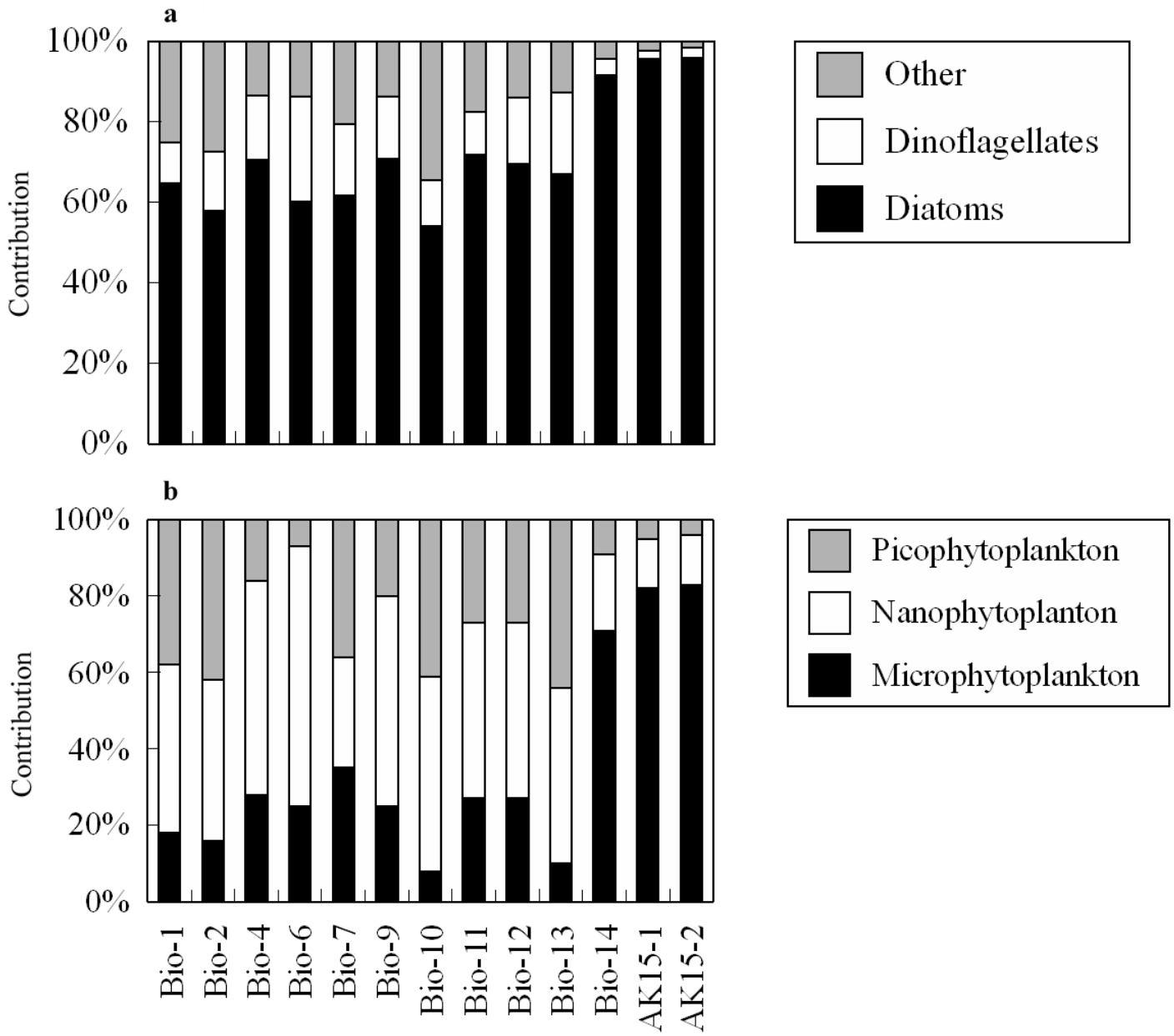

Figure 3. Relative contribution of phytoplankton groups to Chl *a* (a) at the class level class at the different sampling stations determined by multiple regression analysis based on diagnostic pigment signatures and (b) at the level of size class of phytoplankton determined by size-fractioned Chl *a* measurement.

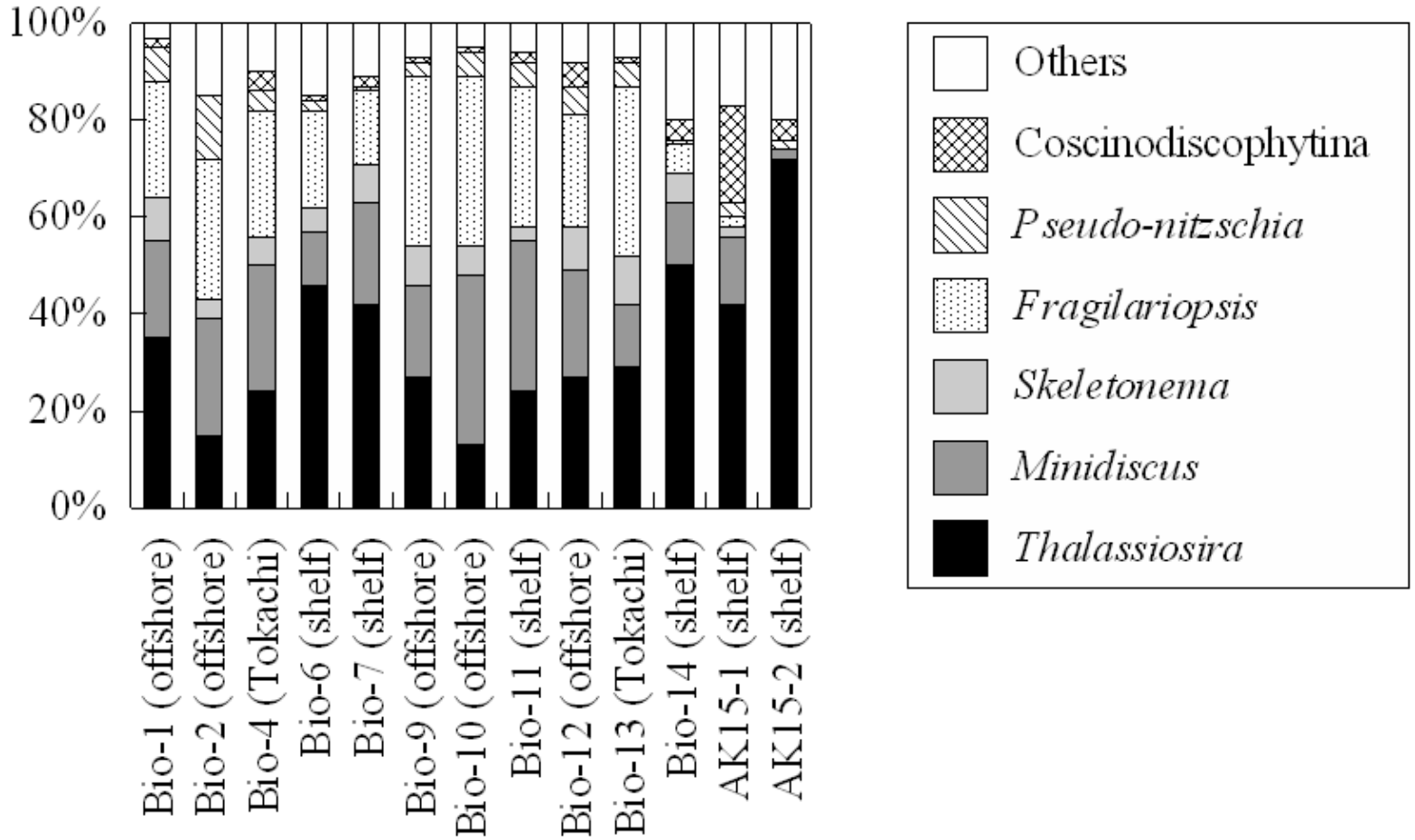

Figure 4. Relative contribution of diatom community composition to total number of sequences determined by the next-generation sequencing method at *in situ* sampling stations.

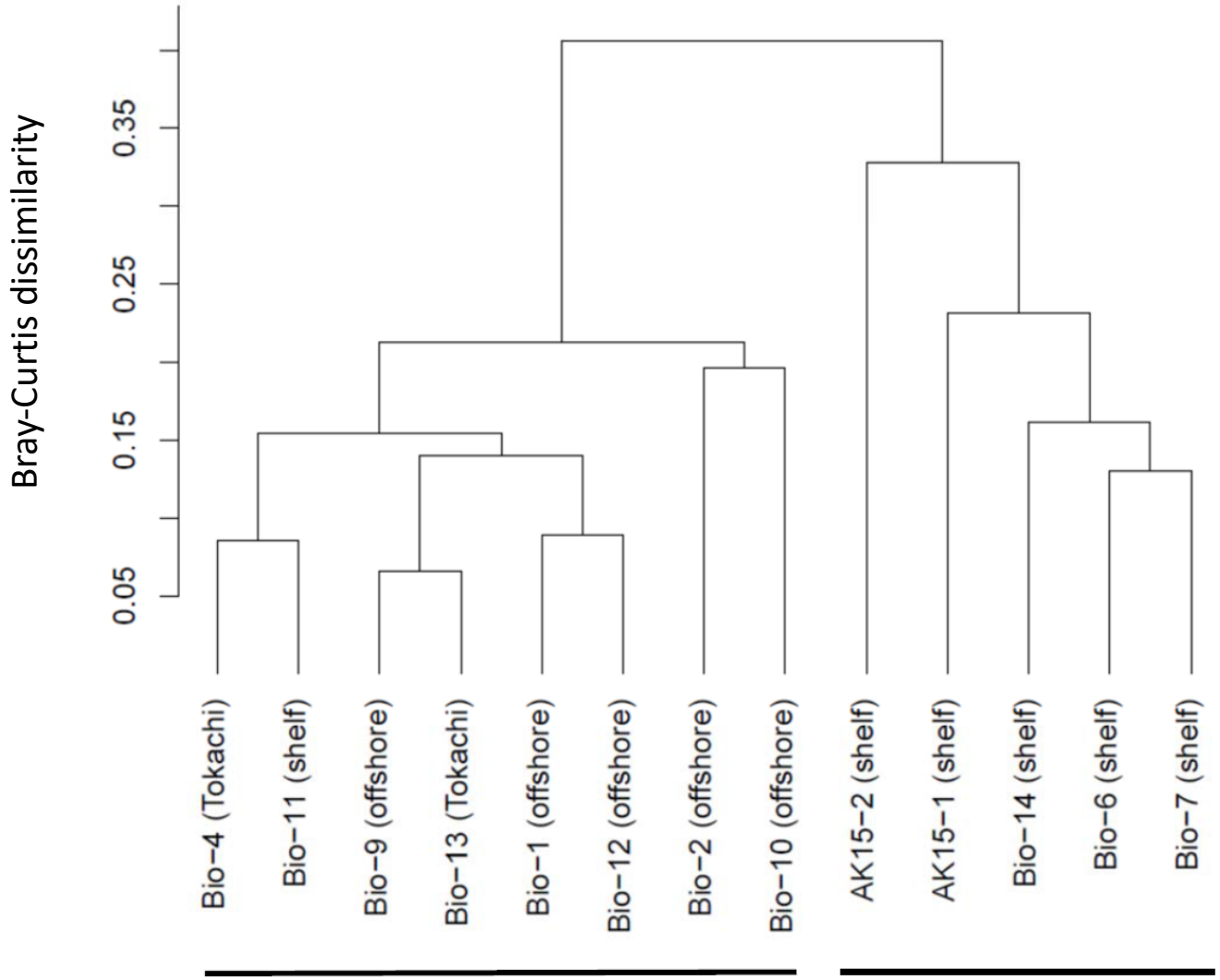

Figure 5. Dendrogram of the cluster analysis of diatom community composition determined with the next-generation sequencing method. Clustering is based on Bray-Curtis dissimilarity and the group average method. The cluster on the right-hand side includes samples from shelf COY water, which had a community composition significantly different from the other sites (One- way MANOVA, Wilk's lambda, $p < 0.01$).

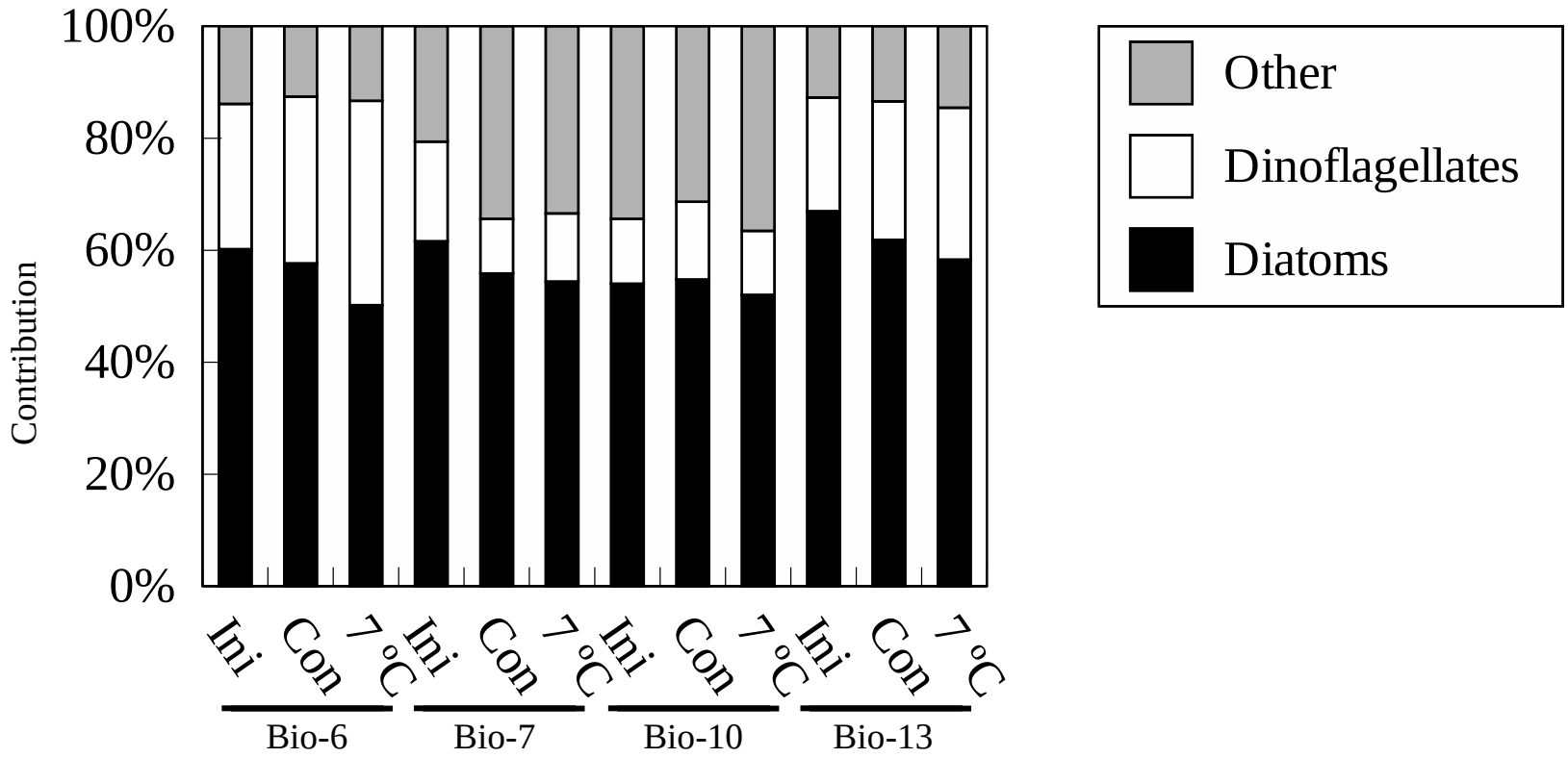

Figure 6. Relative contribution of phytoplankton groups to Chl *a* at the class level during the temperature-controlled incubation experiments determined by the multiple regression analysis based on diagnostic pigments.

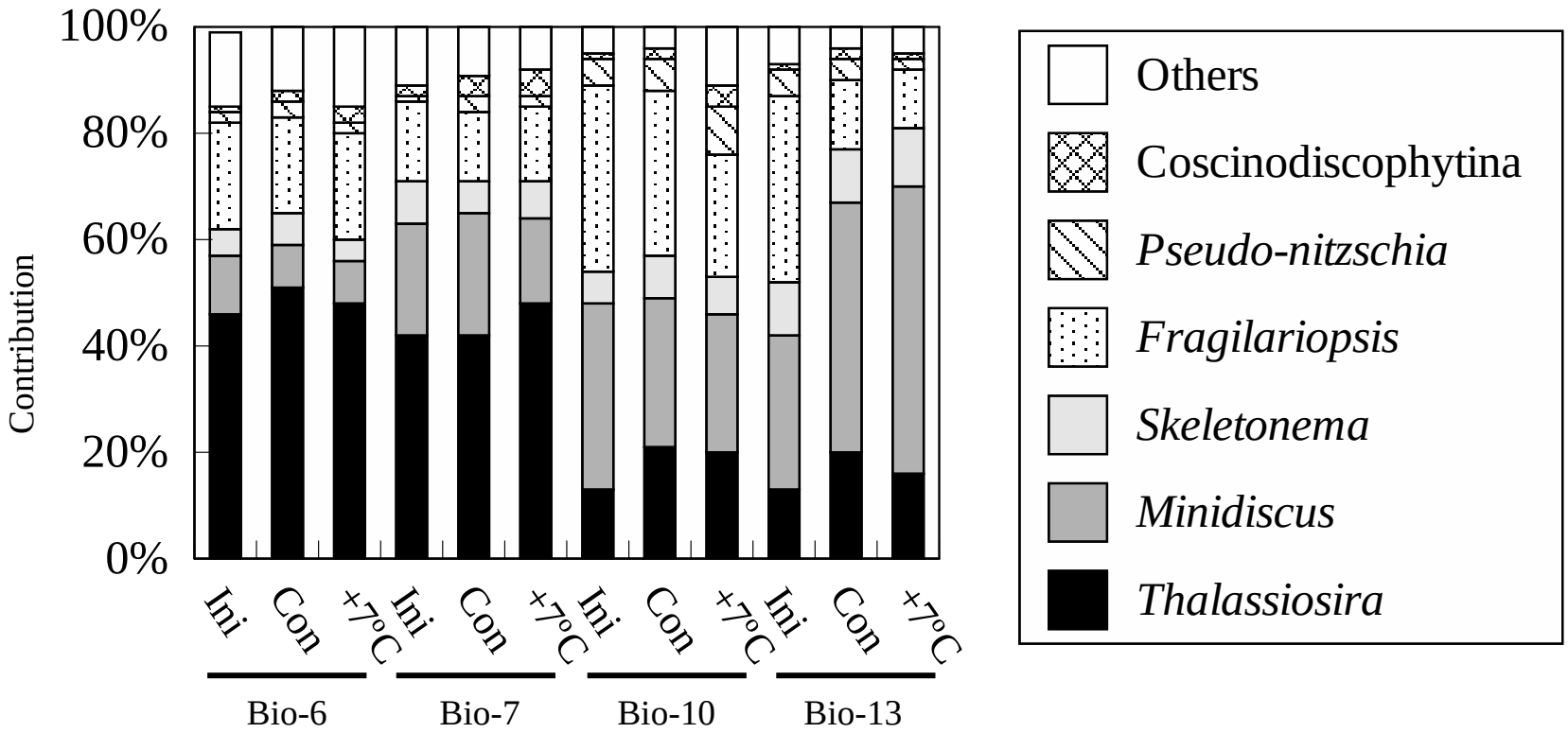

Figure 7. Relative contribution of diatom community composition to total number of sequences during the temperature-controlled incubation experiments determined with the next-generation sequencing method.

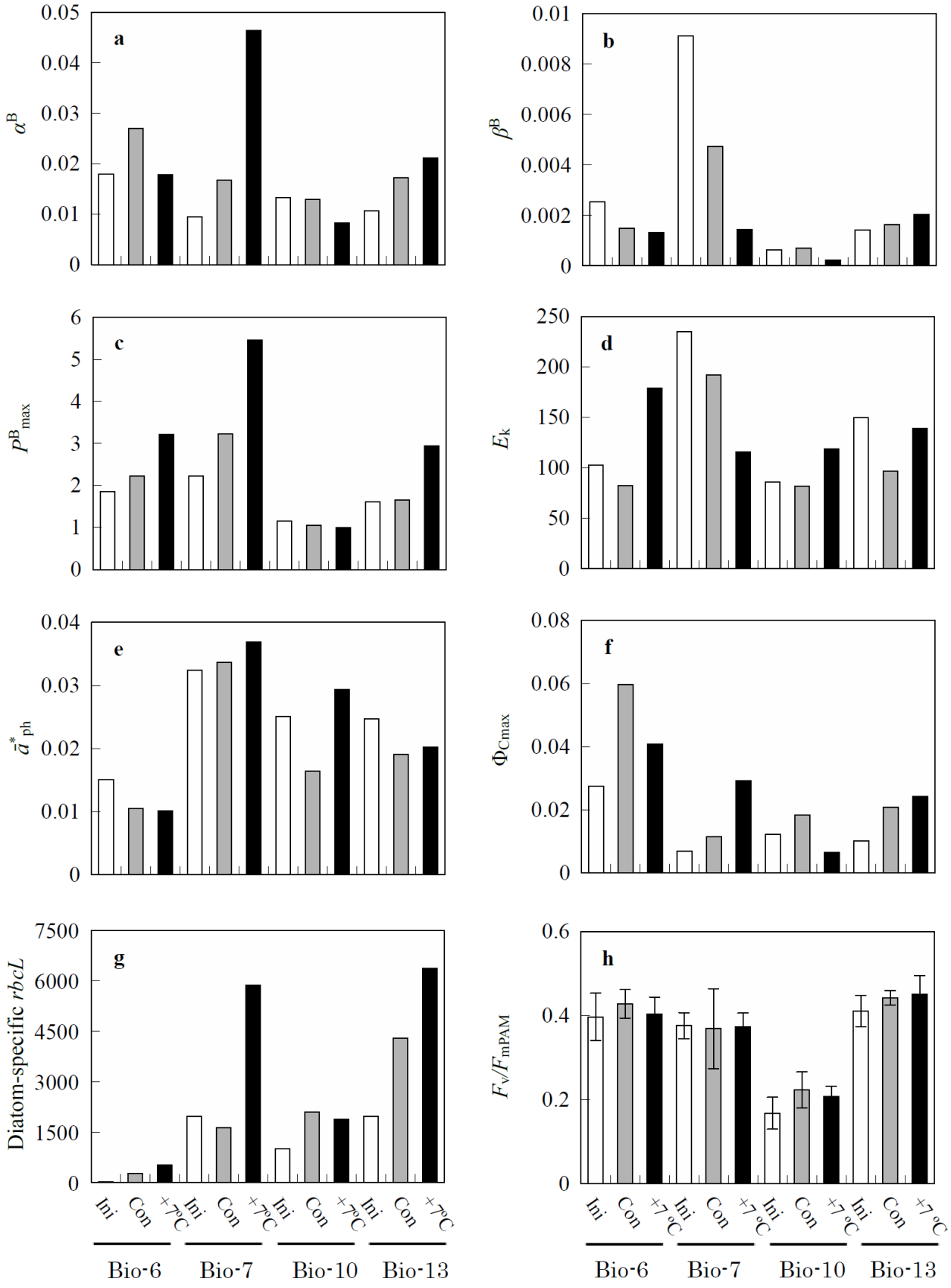

Figure 8. Photosynthetic parameters during the temperature-controlled incubation experiments. The open bars indicate values of initial bottles, shaded bars indicate values of control treatments, and closed bars show values of the +7 ºC treatment.

(a) α^B: Initial slope of *P-E* curve [mg C mg Chl a^{-1} h^{-1} (µmol photons m^{-2} s^{-1}) $^{-1}$]; (b) β^B: Photoinhibition index [mg C mg Chl a^{-1} h^{-1} (µmol photons m^{-2} s^{-1}) $^{-1}$]; (c) P^B_{max}: Maximum photosynthetic rate [mgC mgChl a^{-1} h^{-1}]; (d) E_k: Light saturation index [µmol photons m^{-2} s^{-1}];

(e) $\bar{a}^*_{ph}$: Chl *a*-normalized light absorption coefficient of phytoplankton [m^2 mg Chl *a*]; (f) Φ_{Cmax}: Maximum quantum yield for carbon fixation [mol C mol photons^{-1}]; (g) Diatom-specific *rbcL*: Transcription level of the diatom-specific *rbcL* gene (cDNA copies/DNA copies); (h) F_v/F_{mPAM}: Maximum quantum yield of PSII obtained by PAM fluorometry. Error bars are standard deviations, $n \geq 3$

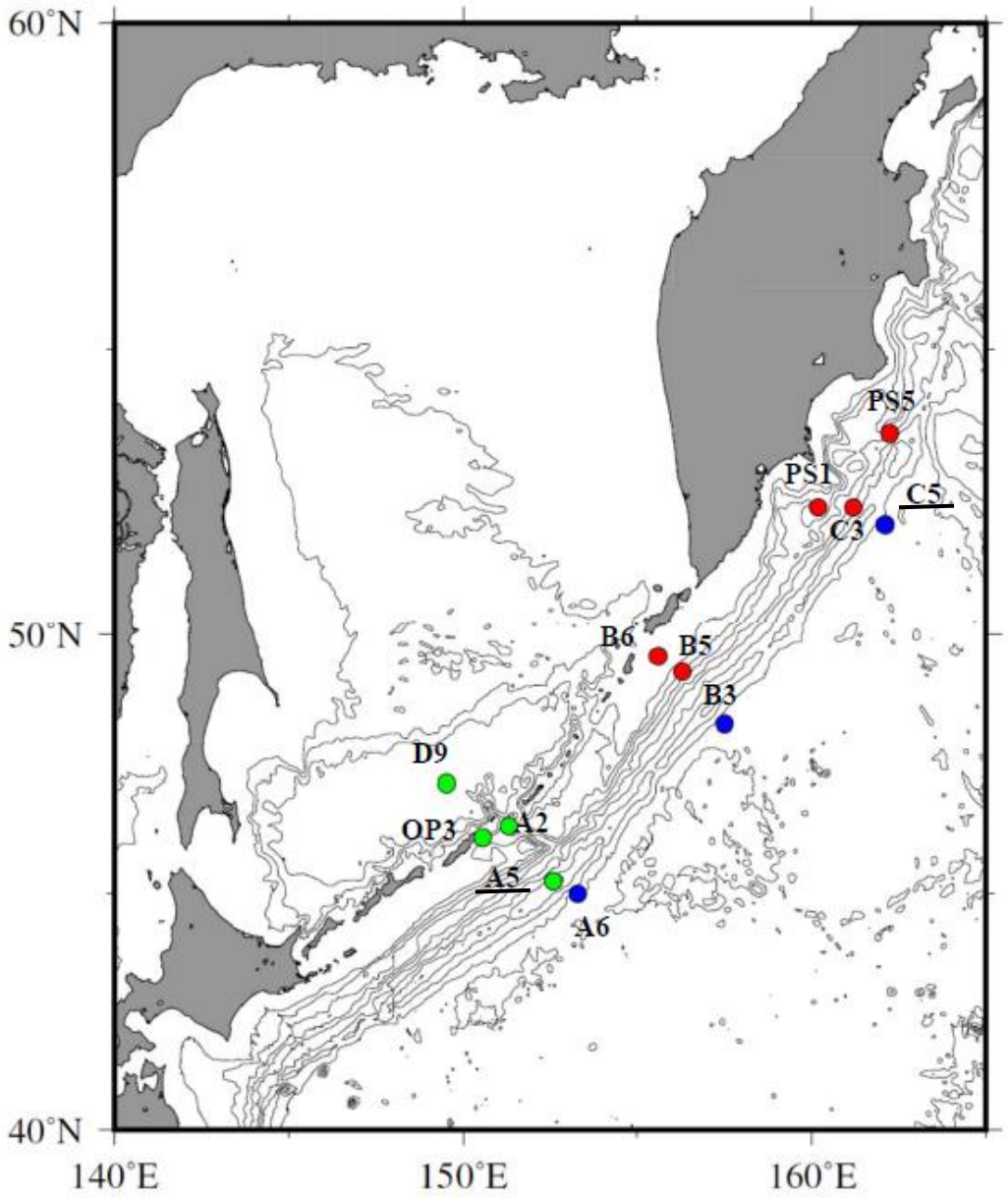

Figure 9. Seawater sampling stations during the Mu14 expedition along the Kuril Islands and off the eastern Kamchatka Peninsula.
The blue, red, and green closed circles in the map denote HNLC, northern coastal, and southern coastal stations, respectively. The stations for the Fe enrichment incubation experiments (i.e., stations C5 and A5) were underlined on their name labels.

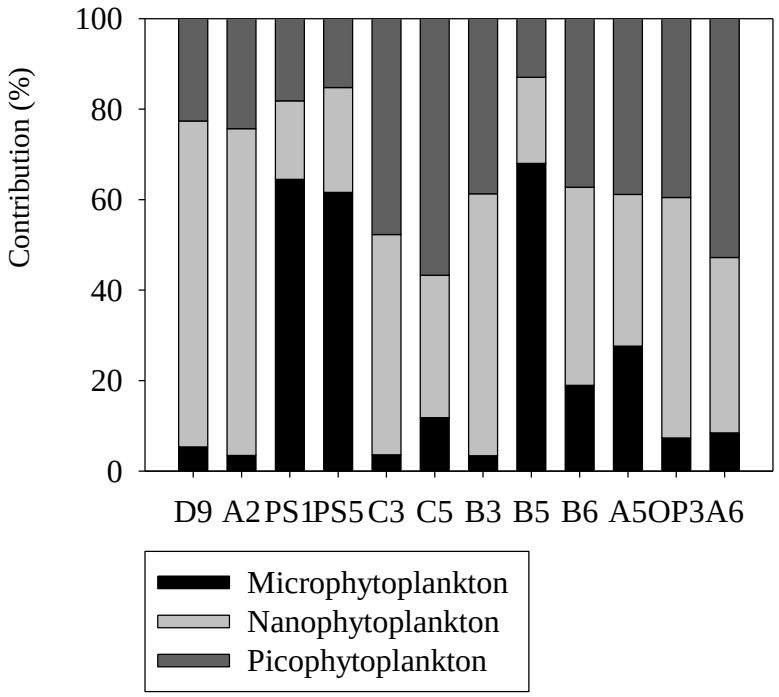

Figure 10. Relative contribution of phytoplankton groups to total Chl *a* at the level of size class of phytoplankton determined by size-fractioned Chl *a* measurement with the non-acidification fluorometric method of Welshmeyer (1994) at *in situ* sampling stations.

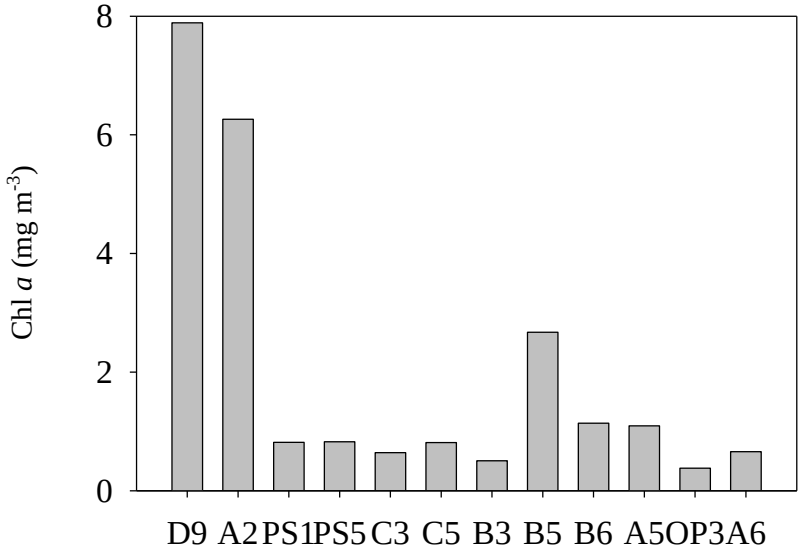

Figure 11. Concentrations of Chl *a* determined with non-acidification fluorometric analysis based on Welshmeyer (1994) at *in situ* sampling stations.

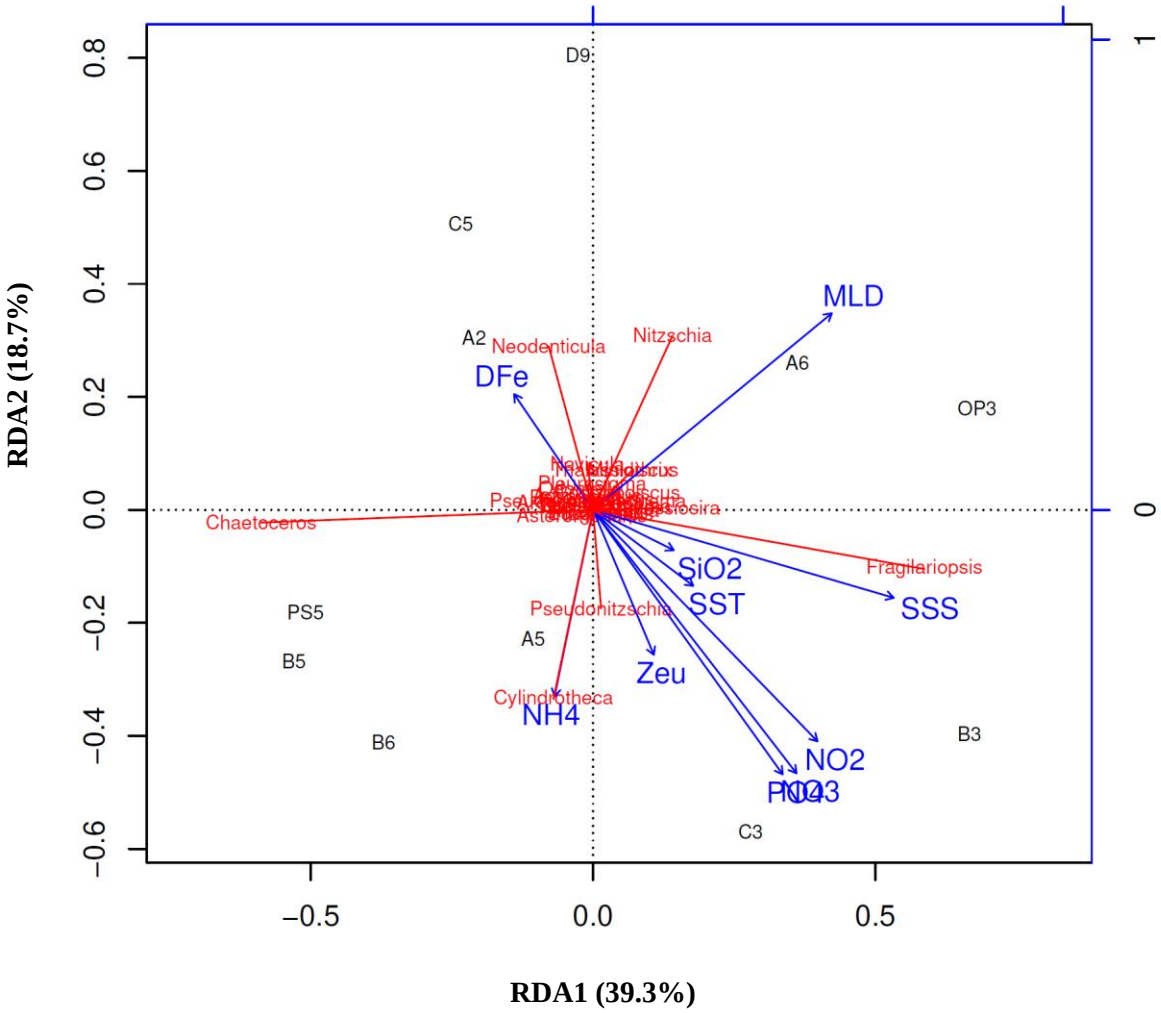

Figure 12. The coordinate plane of the redundancy analysis (RDA) on the diatom community composition determined with scanning microscopy.
The validity of the RDA analysis was previously checked with the detrended corresponding analysis (DCA) that the lengths of gradients of environmental parameters were sufficiently small for the RDA analysis (<3SD) The proportions shown in percent indicate contributions of each RDA axis to the total variance (i.e., proportions explaining the total variance).

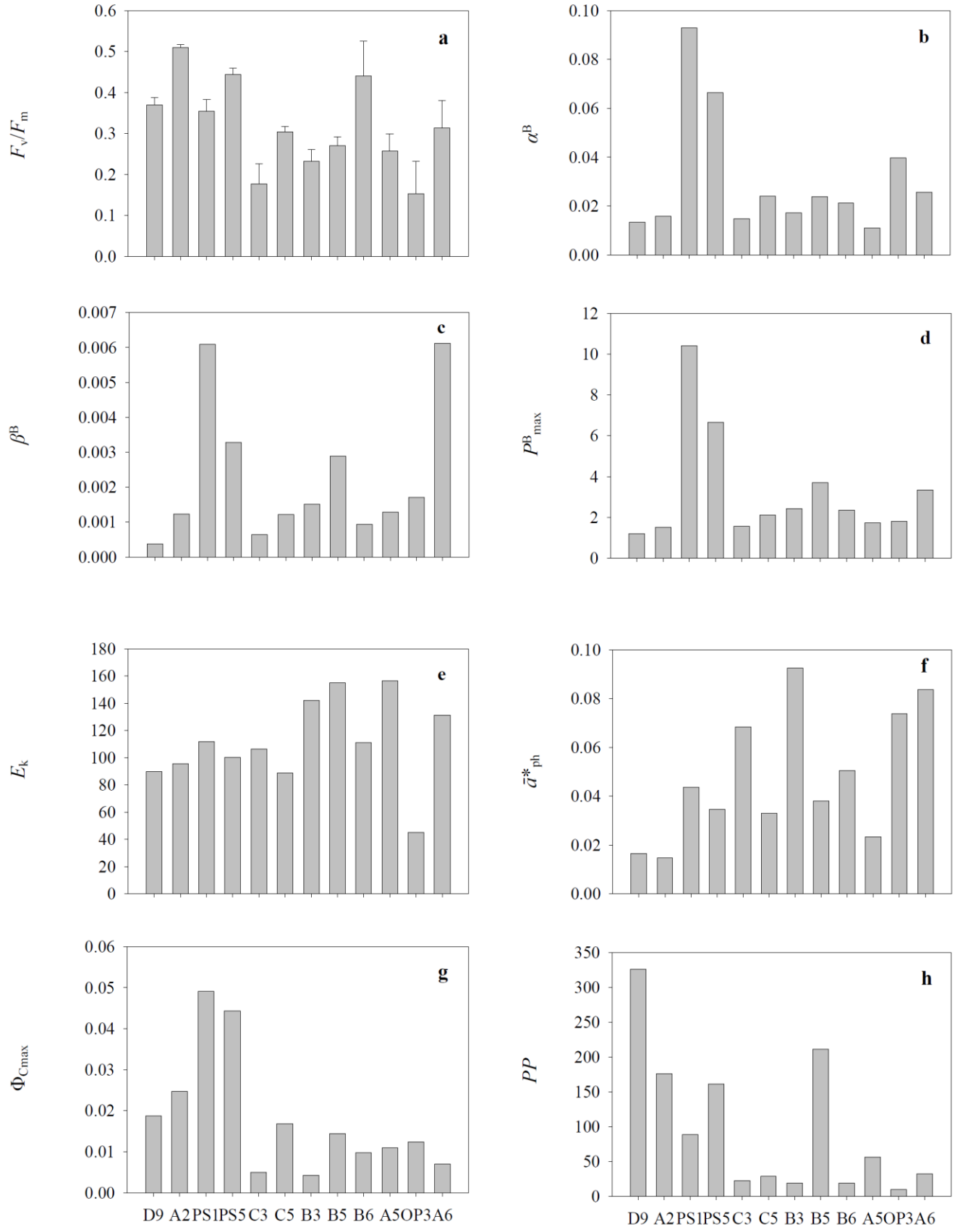

Figure 13. Photosynthetic parameters obtained from the *P-E* curve experiments at *in situ* sampling stations. (a) F_v/F_m: Maximum quantum yield of PSII determined with PAM fluorometry; (b) α^B: Initial slope of a *P-E* curve [mg C mg Chl a^{-1} h^{-1} (µmol photons m^{-2} s^{-1})$^{-1}$]; (c) β^B: Photoinhibition index [mg C mg Chl a^{-1} h^{-1} (µmol photons m^{-2} s^{-1})$^{-1}$]; (d) P^B_{max}: Maximum photosynthetic rate [mgC mgChl a^{-1} h^{-1}]; (e) E_k: Light saturation index [µmol photons m^{-2} s^{-1}]; (f) $\bar{a}^*_{ph}$: Chl *a*-normalized light absorption coefficient of phytoplankton [m^2 mg Chl a^{-1}]; (g) Φ_{Cmax}: Maximum quantum yield for carbon fixation [mol C mol photons^{-1}]; (h) *PP*: Primary productivity [mg C m^{-3} day^{-1}]. Error bars indicate standard deviations, $n \geq 3$

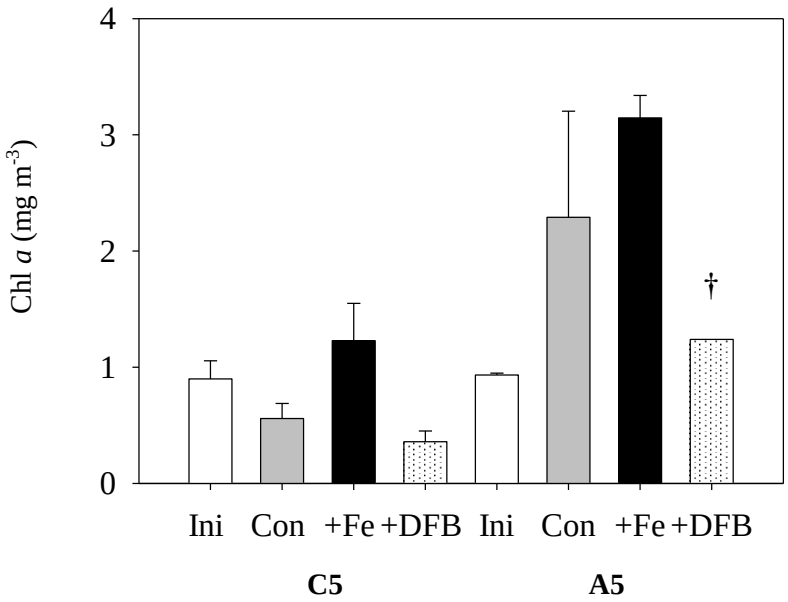

Figure 14. Chl *a* concentrations [mg m^{-3}] determined with the non-acidification method of Welshmeyer (1994) of each treatment of the Fe enrichment incubation experiments.

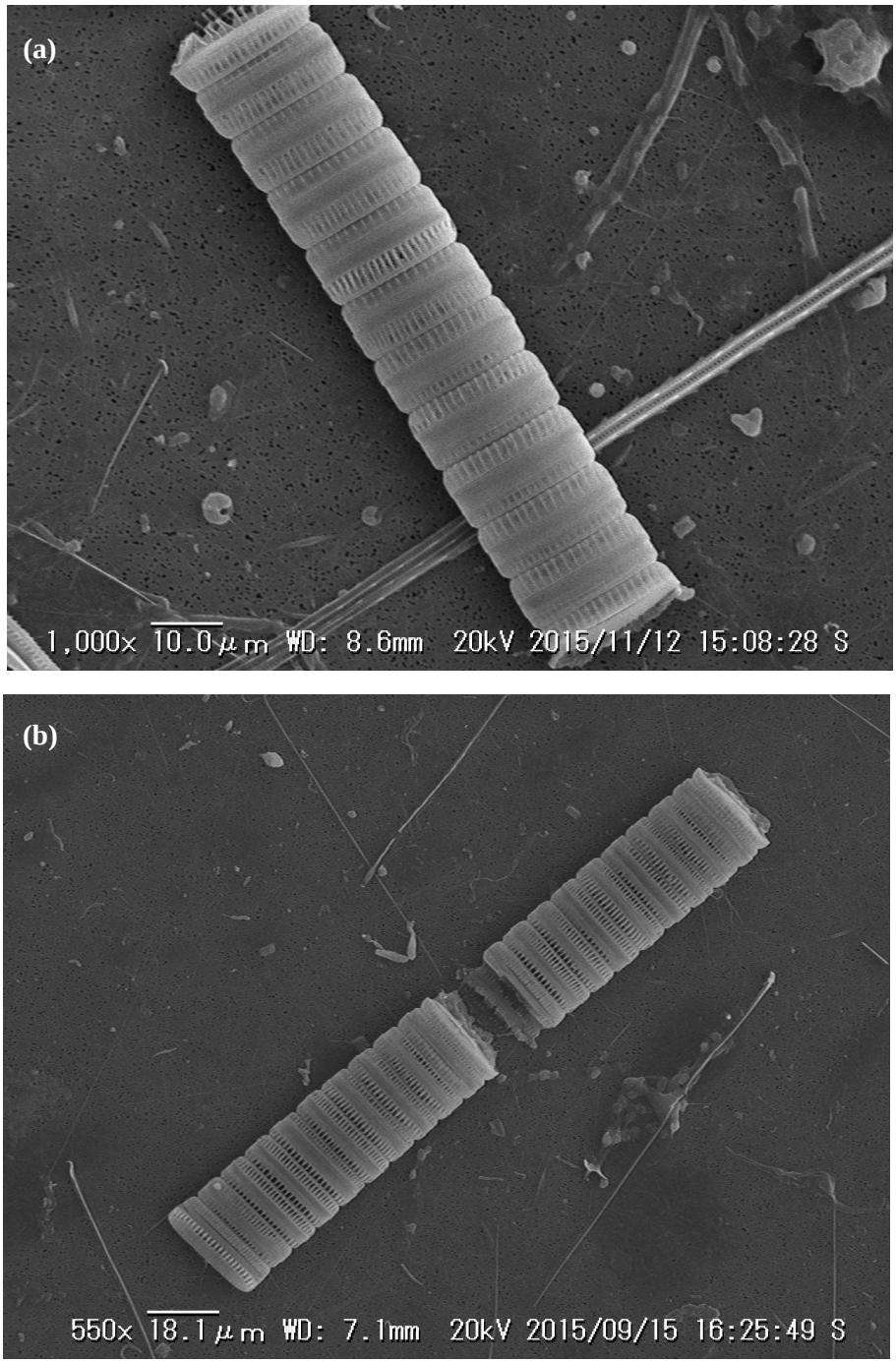

Figure 15. Electron micrographs of the diatom *Neodenticula seminae* in elongated chains from the +DFB bottles (a) at station C5 and (b) station A5.

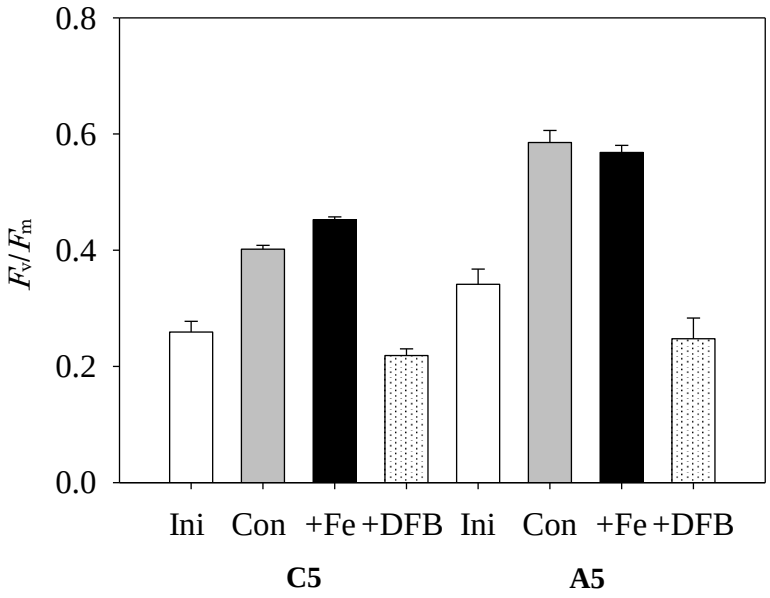

Figure 16. Maximum quantum yields of PSII (F_v/F_m) determined with PAM fluotometry of each treatment of the Fe enrichment incubation experiments.
Open, shaded, closed, and dotted bars indicate initial, control, +Fe, and +DFB values, respectively. Error bars indicate standard deviations, $n \geq 3$, although the symbol † indicates single data without replication because of the considerable Fe contamination discussed in the text.

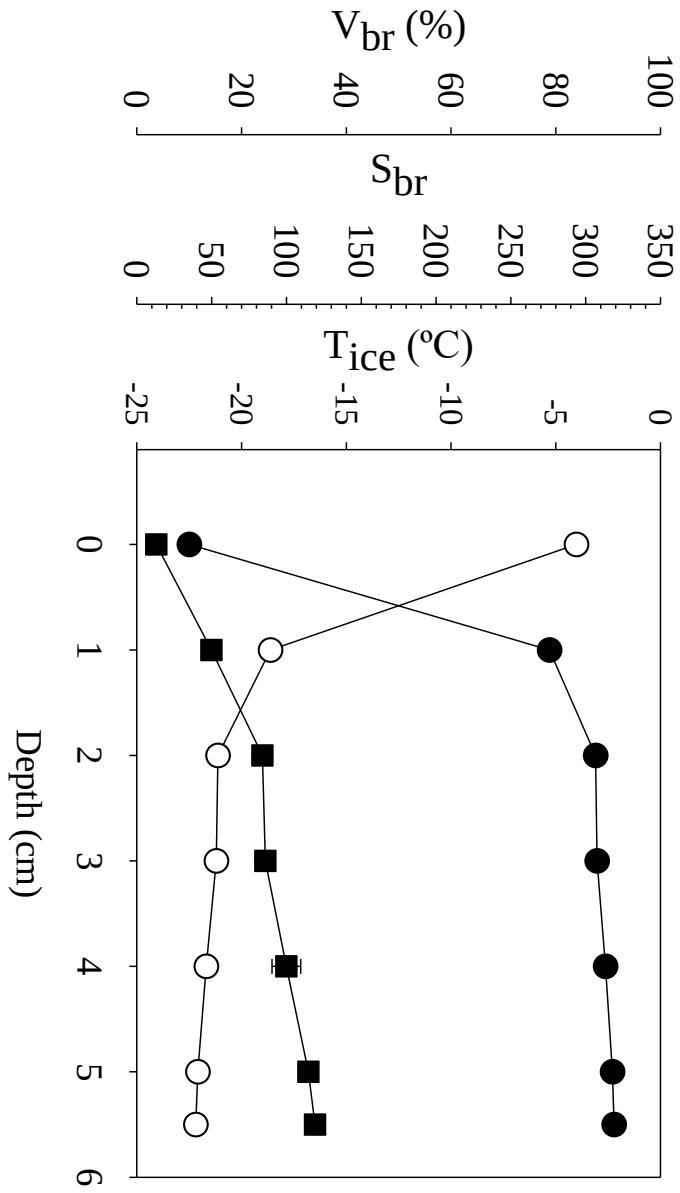

Figure 17. Vertical profiles of ice temperature (T_{ice}; closed circle), brine salinity (S_{br}; open cicle), and fraction of brine volume (V_{br}; square) in artificial sea ice in the ice tank.
T_{ice} was determined directly with a thermometer, and then S_{br} and V_{br} were estimated with the empirical equations suggested by Cox and Weeks (1983) and Eicken (2009).
Error bars indicate 1 standard deviation (*n*=3).

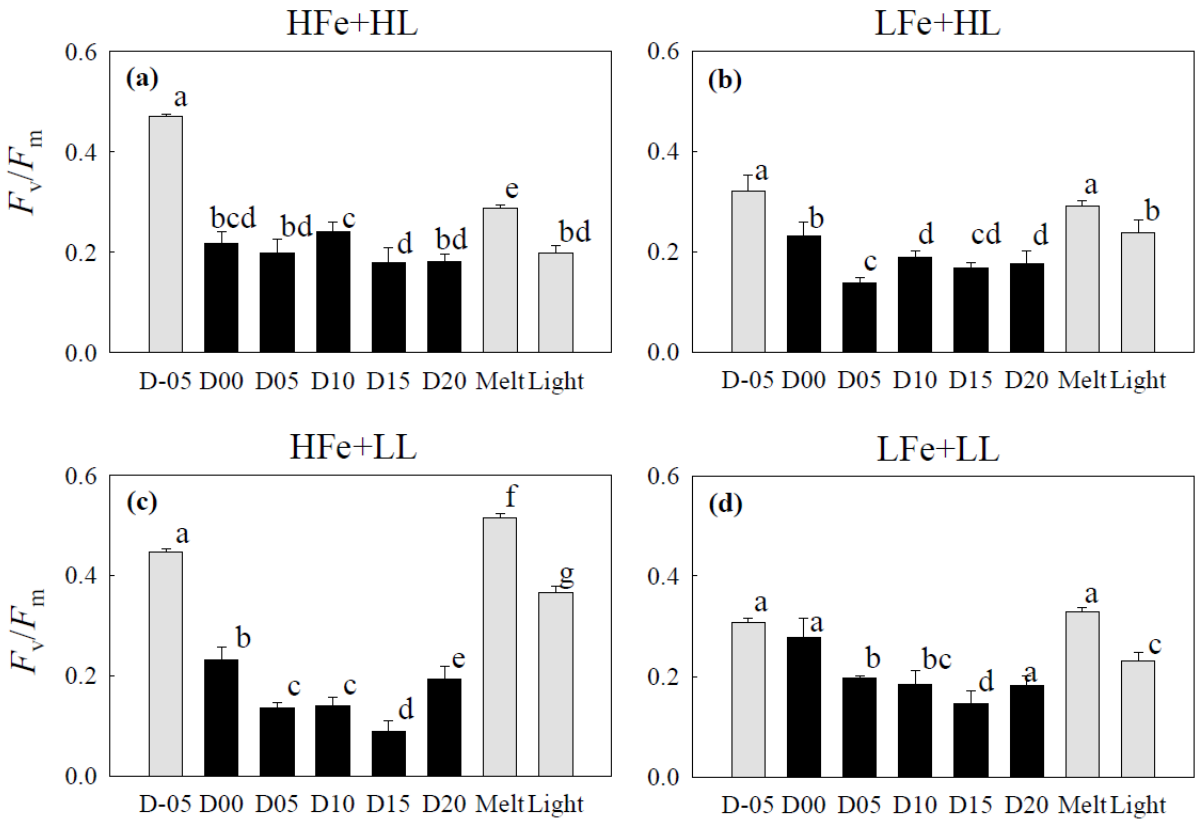

Figure 18. Maximum photochemical quantum yield of PSII (F_v/F_m) during the ice tank incubation experiments.
Left and right panels show data from the HFe and LFe treatments, respectively, while upper and bottom panels indicate data from the HL and LL treatment, respectively. Shaded and closed bars indicate values of seawater samples before plus after freezing and ice samples, respectively. Alphabets above bars show (in)significant difference with One-way ANOVA with a combination of the Tukey test. The D stands 'day', while Melt and Light indicate values after melting and light exposure event, respectively. Error bars show 1 standard deviation ($n \geq 6$).

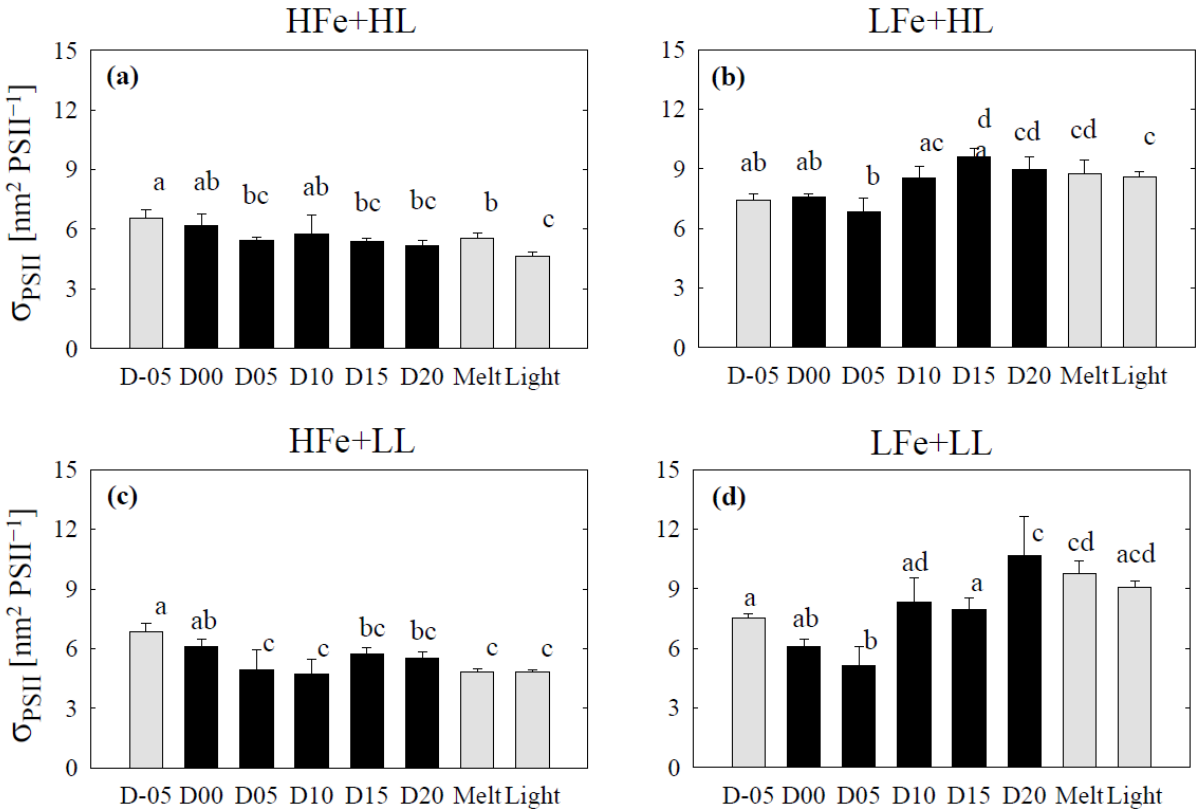

Figure 19. Functional absorption cross section of PSII (σ_{PSII}) during the ice tank incubation experiments.
See the caption of Fig. 3.2 for bar purport, statistical methods, and abbreviations.

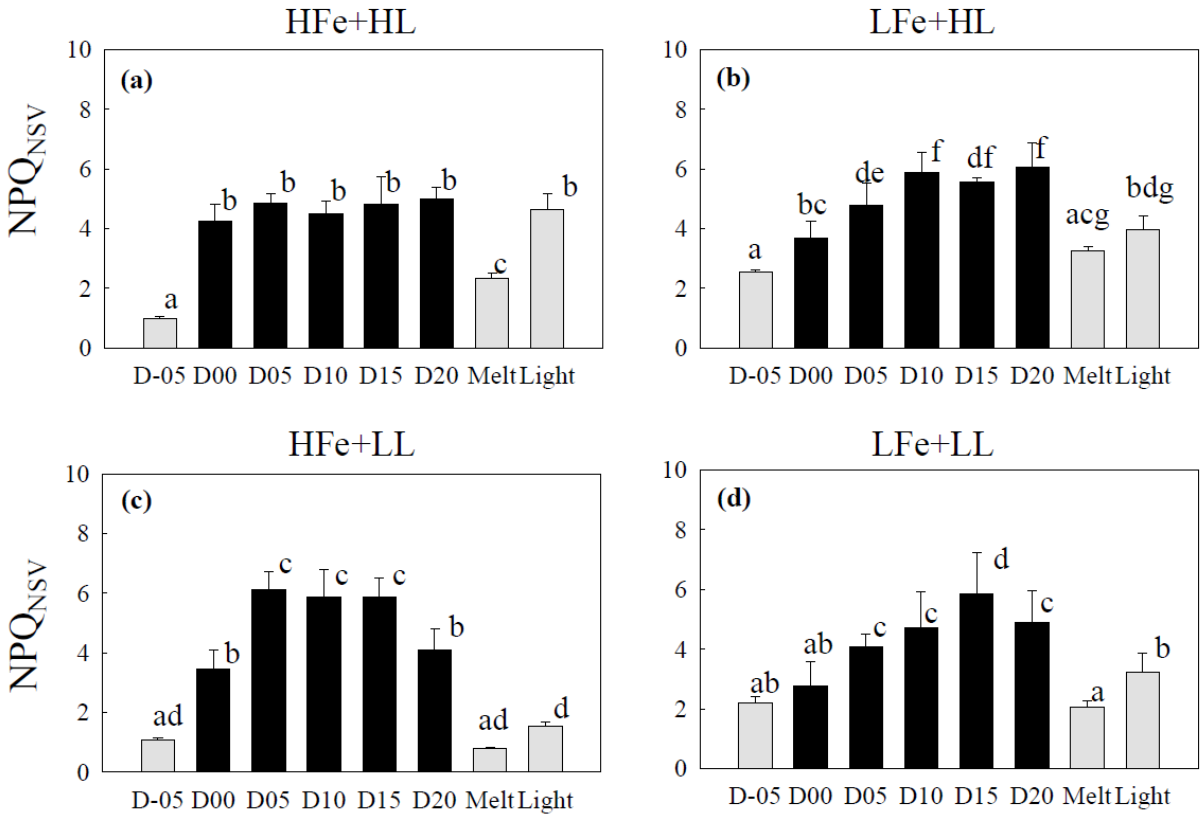

Figure 20. Non-photochemical quenching based on the Stern-Volmer quenching kinetics (NPQ_{NSV}) during the ice tank incubation experiments. See the caption of Fig. 3.2 for panel and bar purport, statistical methods, and abbreviations.

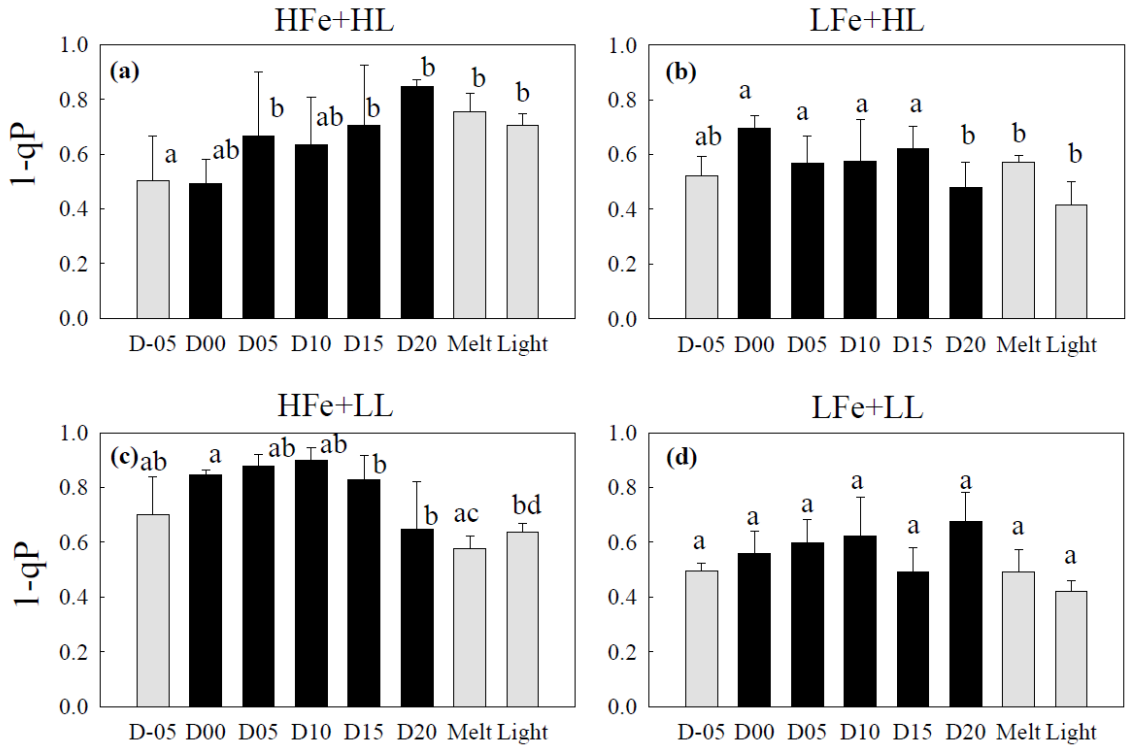

Figure 21. Fraction of closed of PSII (1−qP) during the ice tank incubation experiments.
See the caption of Fig. 3.2 for bar purport, statistical methods, and abbreviations.

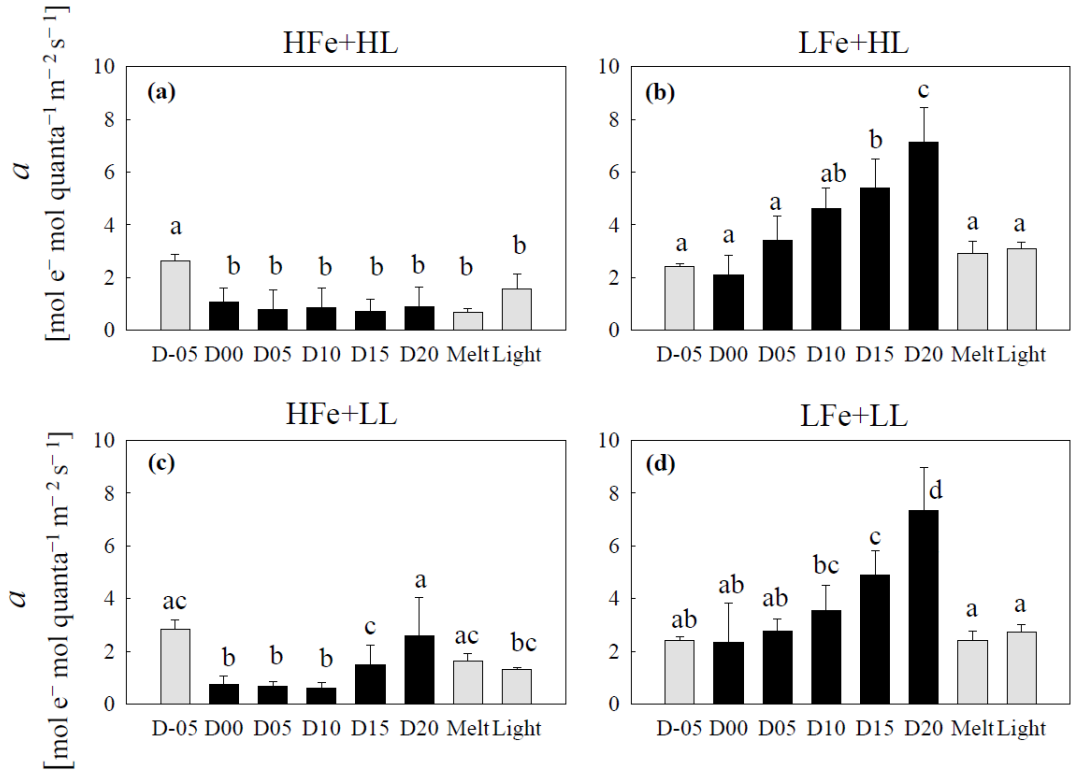

Figure 22. Light utilization efficiency under dim light (α) shown as initial slopes of the ETR_{RCII}-*E* curves during the ice tank incubation experiments. See the caption of Fig. 3.2 for bar purport, statistical methods, and abbreviations.

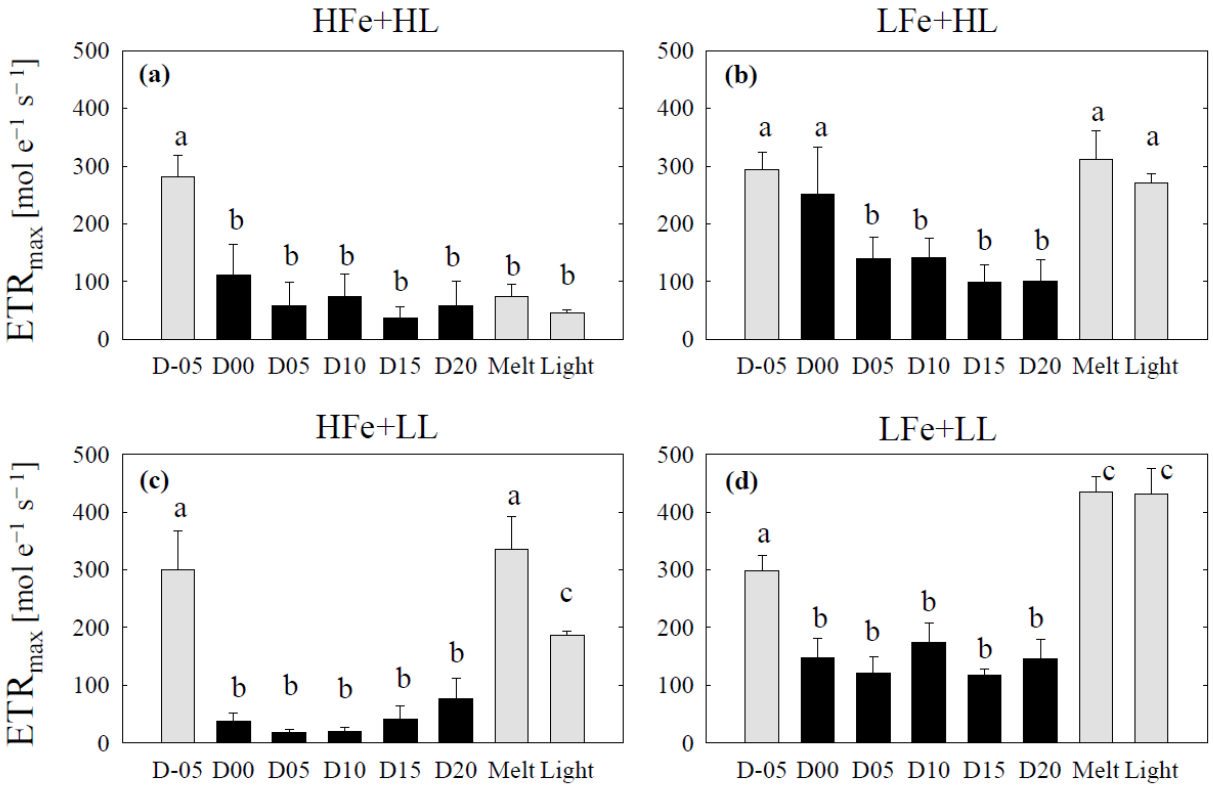

Figure 23. Maximum electron transport rate (ETR_{max}) during the ice tank incubation experiments.
See the caption of Fig. 3.2 for bar purport, statistical methods, and abbreviations.

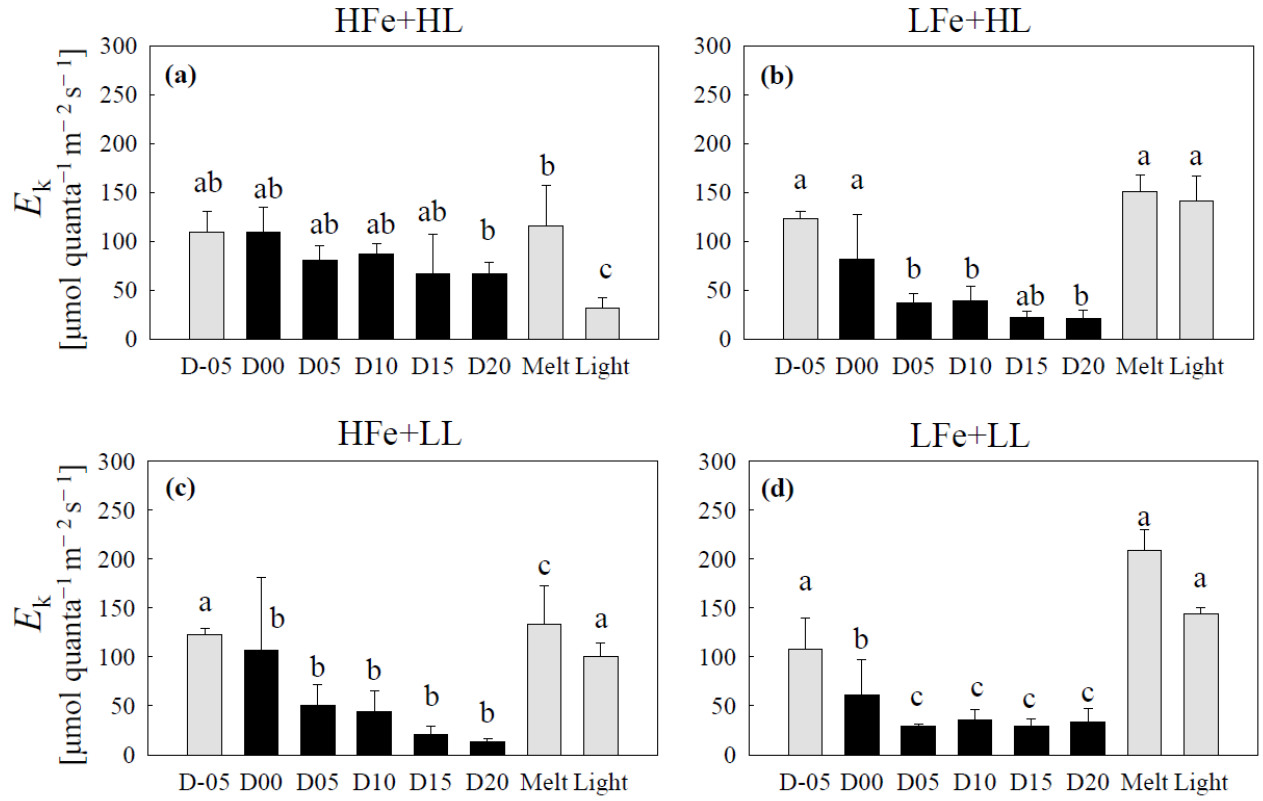

Figure 24. Light saturation index (E_k) during the ice tank incubation experiments.
See the caption of Fig. 3.2 for bar purport, statistical methods, and abbreviations.

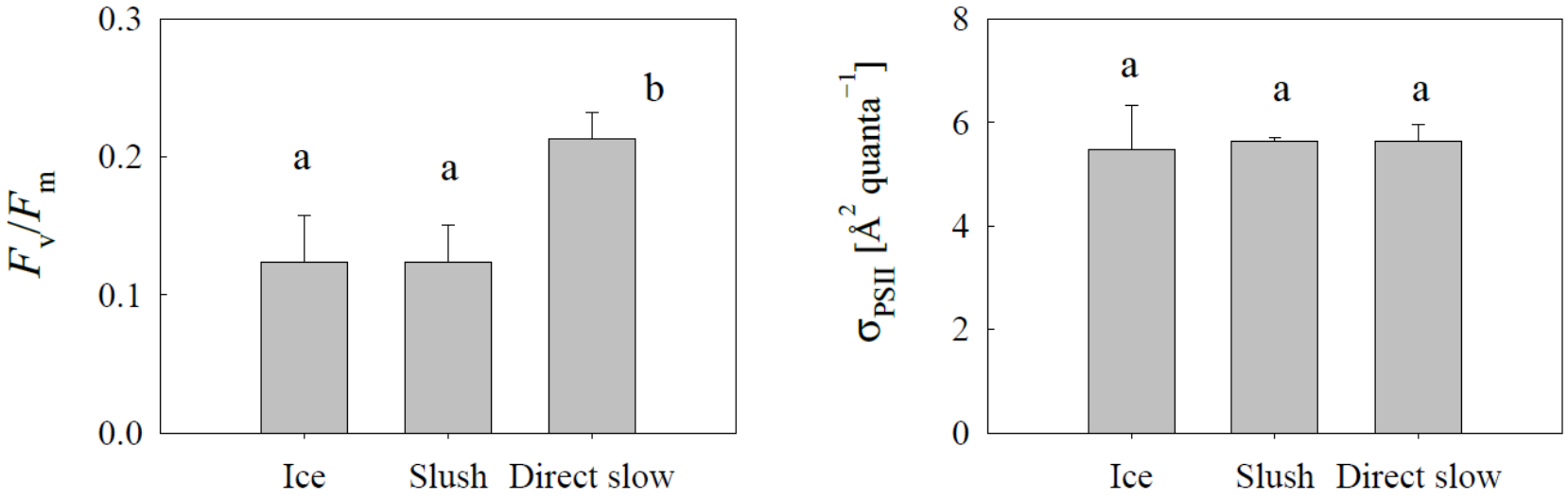

Figure 25. Variable Chl *a* fluorescence parameters with different melting methods.
(a): Maximum quantum yield of PSII photochemistry,F_v/F_m; (b): functional absorption cross section, σ_{PSII}, determined with FRR fluorometry.
Ice: intact ice placed into the cuvette for ChlF measurement; slush; ice sample partially melted in filtered seawater; Direct slow: melted ice sample under the room temperature. Diffrerent alphabets indicate significant differences between given values. Error bars indicate 1 standard deviation. *n*=6.

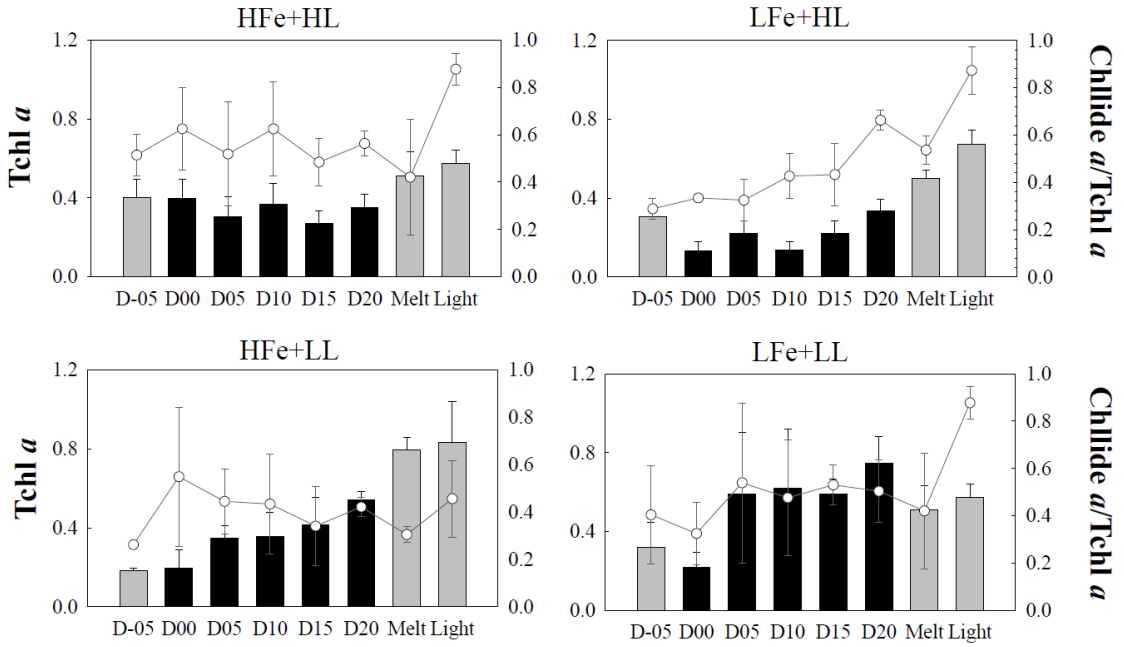

Figure 26. Concentrations of total Chl *a* [mg m^{-3}] (TChl *a*=Chl *a*+Chllide *a*+Chl *a*-epimer+Chl *a*-allomer) quantified with UHPLC (Suzuki et al., 2015) (bar) and contributions of Chllide *a* to TChl *a* (open circle) during the ice tank incubations.
See the caption of Fig. 3.2 for bar purport, statistical methods, and abbreviations.

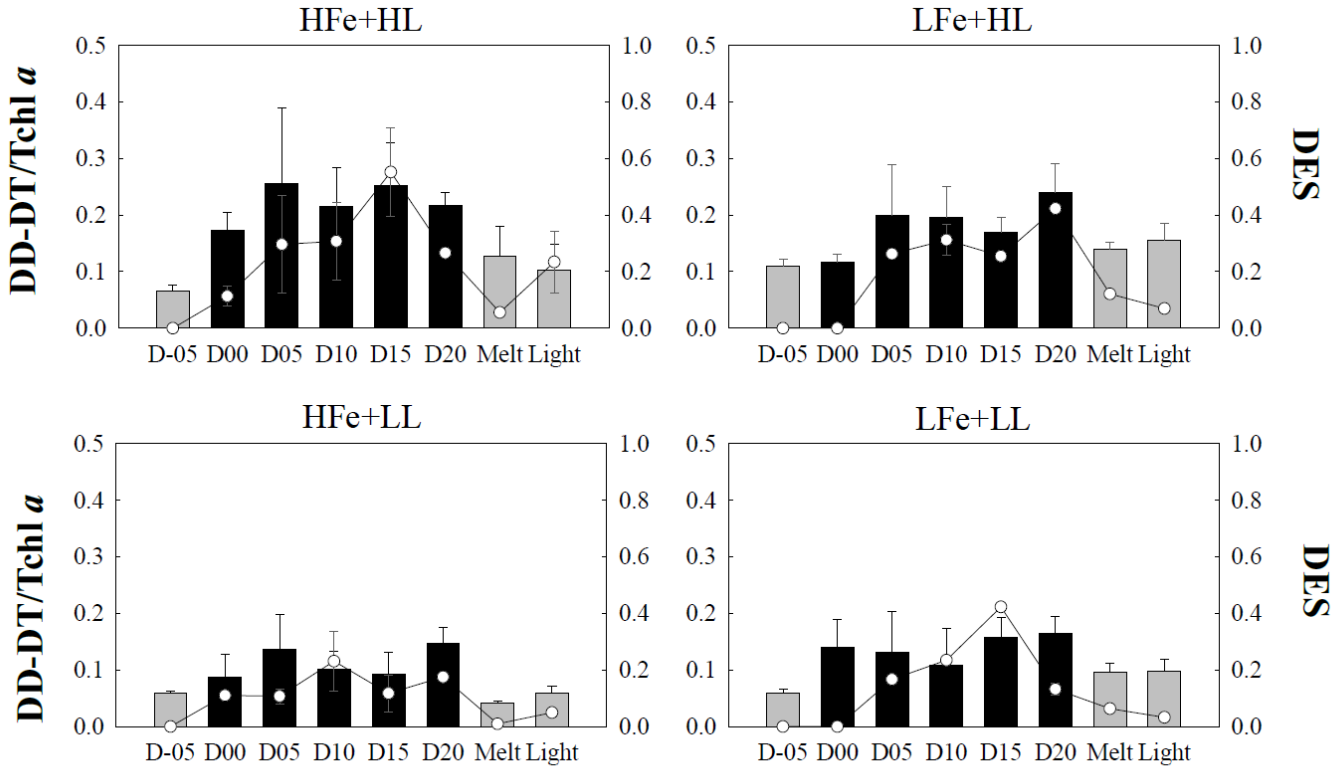

Figure 27. Size of DD and DT pool defined as DD-DT/Chl *a* (bars) and de-epoxidation state (DES) (open circle) during the ice tank incubations. See the caption of Fig. 3.2 for bar purport, statistical methods, and abbreviations.

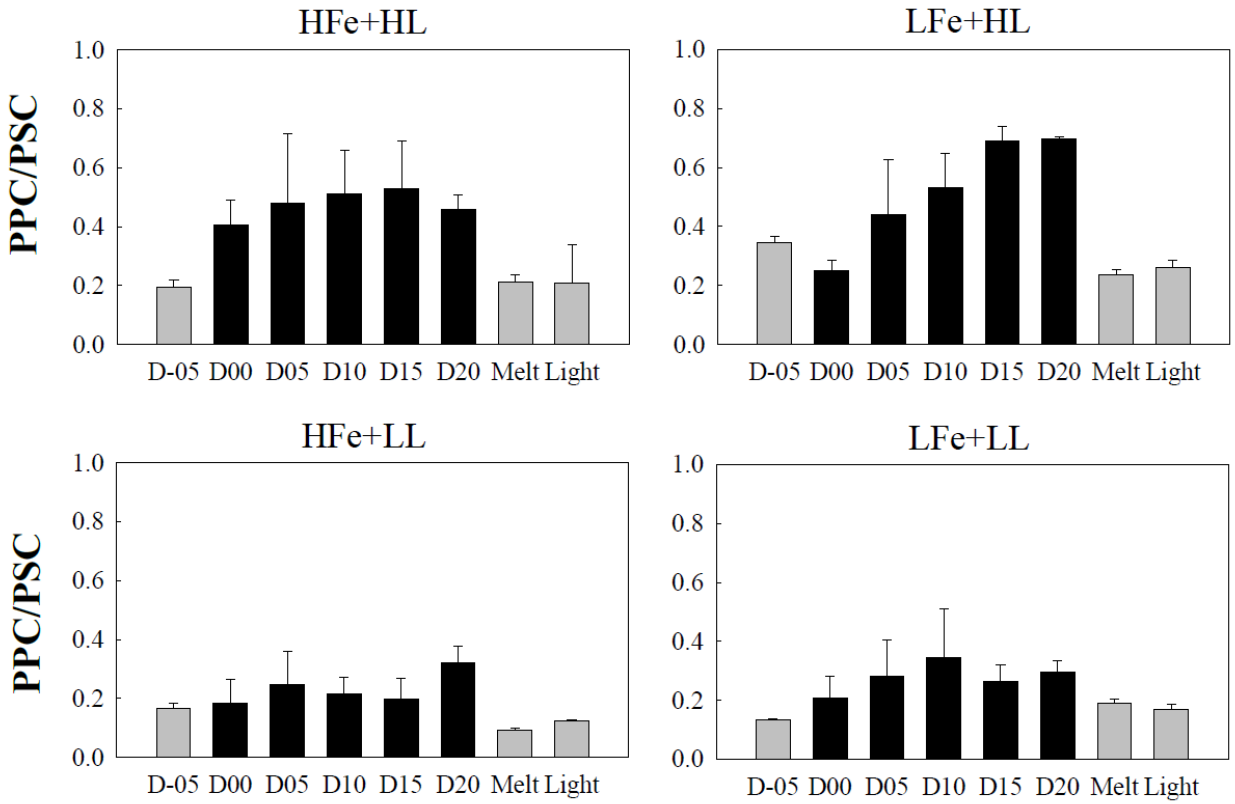

Figure 28. Ratio of photoprotective carotenoids (PPC) to photosynthetic carotenoids (PSC) during the ice tank incubations. See the caption of Fig. 3.2 for bar purport, statistical methods, and abbreviations.

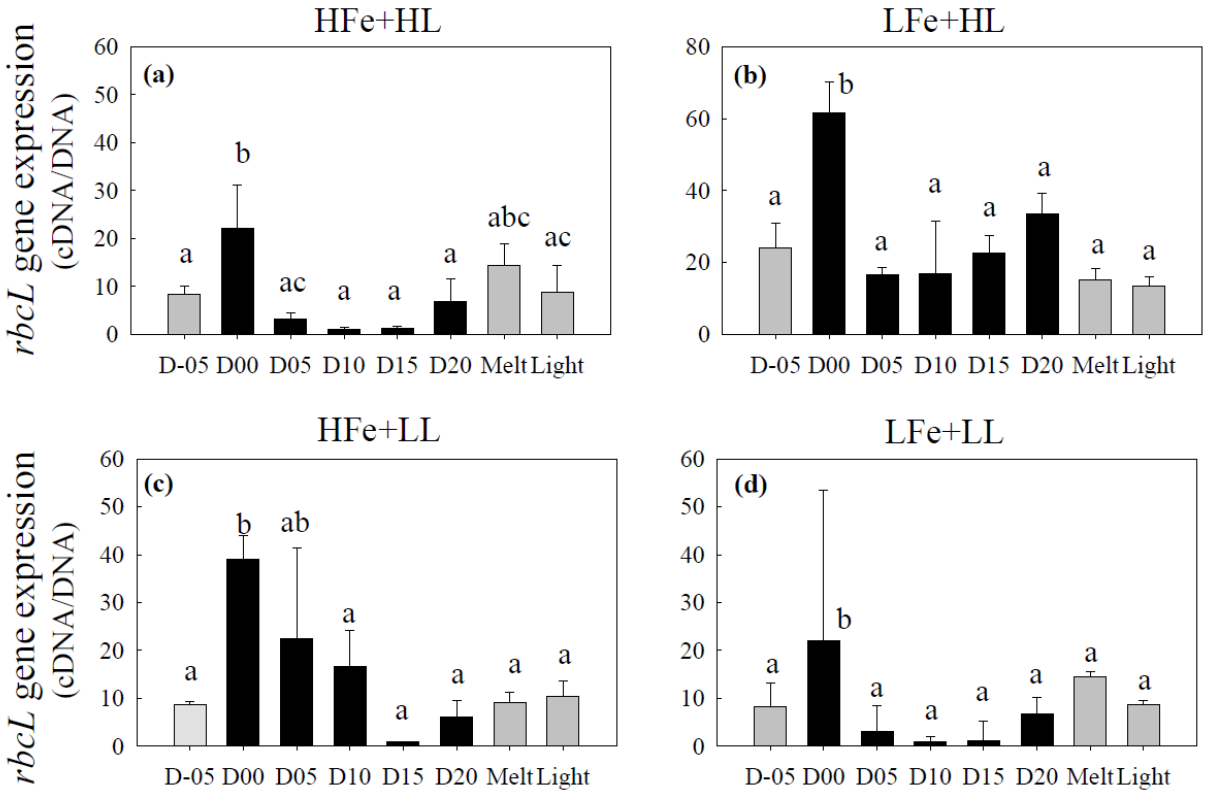

Figure 29. Gene expression of the *rbcL* gene calculated as ration of cDNA to DNA copies of the gene during the ice tank incubation experiments. The gene *rbcL* encodes the large subunit of the carbon fixation enzyme RuBisCO. See the caption of Fig. 3.2 for bar purport, statistical methods, and abbreviations.

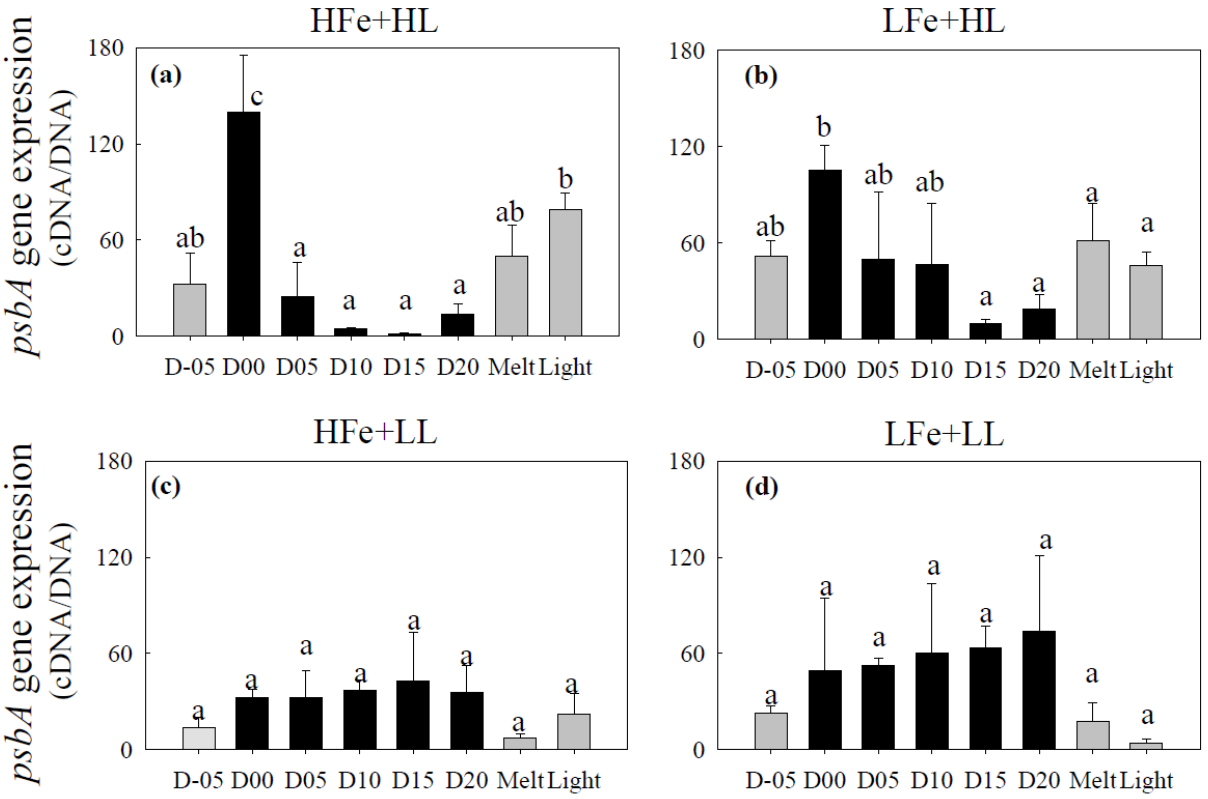

Figure 30. Gene expression of the *psbA* gene calculated as ration of cDNA to DNA copies of the gene during the ice tank incubation experiments. The gene *psbA* encodes the D1 protein of PSI to repair damaged PSII. See the caption of Fig. 3.2 for bar purport, statistical methods, and abbreviations.

Table 1. Sampling conditions and hydrographic and optical data during the KH-15-1 and AK15 expeditions.

Sampling date	Station	Water mass	Bottom depth (m)	SST (°C)	SSS	NO_3 (μM)	NO_2 (μM)	NH_4 (μM)	PO_4 (μM)	SiO_2 (μM)	K_d(PAR) (m^{-1})	Z_{eu} (m)	MLD (m)
2015.03.08	Bio-1	Offshore	852	0.03	32.58	21.29	0.18	0.69	1.81	35.50	0.105	44.1	26.6
2015.03.09	Bio-2	Offshore	564	0.39	32.71	22.20	0.11	0.44	1.93	35.38	0.12	38.5	29.9
2015.03.13	Bio-4	Tokachi	103	0.42	32.36	18.43	0.23	0.71	1.71	33.73	0.291	15.8	27.3
2015.03.14	Bio-6	Shelf	100	0.93	32.17	19.77	0.18	1.43	1.54	39.24	0.363	12.7	15.8
2015.03.15	Bio-7	Shelf	97	0.67	32.55	20.64	0.18	1.02	1.85	36.25	0.145	31.7	20.2
2015.03.17	Bio-9	Offshore	1477	0.64	32.38	18.13	0.23	0.54	1.76	32.19	0.159	28.9	19.5
2015.03.18	Bio-10	Offshore	4100	1.60	32.78	24.70	0.17	UD	2.21	43.22	0.087	52.6	28.6
2015.03.20	Bio-12	Offshore	529	0.63	32.62	27.21	0.21	0.35	2.45	48.93	0.137	33.9	23.6
2015.03.21	Bio-13	Tokachi	1084	1.47	32.62	24.53	0.27	0.29	2.30	46.03	0.131	35.0	18.9
2015.03.22	Bio-14	Shelf	100	0.56	32.52	31.43	0.33	0.27	2.94	59.28	0.143	32.1	19.5
2015.04.16	AK15-1	Shelf	33	3.84	32.06	0.83	0.05	UD	0.34	4.12	ND	ND	27.8
2015.04.17	AK15-2	Shelf	32	2.41	32.22	2.01	0.08	UD	0.48	1.78	ND	ND	21.4

SST: Sea surface temperature; SSS: Sea surface salinity; NO_3, NO_2, NH_4, PO_4, and SiO_2: Concentration of nitrate, nitrite, ammonium, phosphate, and silicate; K_d(PAR): Vertical attenuation coefficient of downward photosynthetically available radiation (PAR); Z_{eu}: Euphotic layer depth; MLD: Mixed layer depth

Table 2. Spearman-rank correlation coefficients between photosynthetic, environmental and community composition data.

	Chl *a*	$F_v/F_{m\,PAM}$	α^B	β^B	P^B_{MAX}	E_k	$\bar{a}^*_{ph}$	Φ_{cm}	PP
SST	**0.57***	0.52	0.22	0.27	0.35	0.26	–0.14	0.28	**0.57***
SSS	**–0.66***	–0.50	–0.20	**–0.83*****	**–0.76****	**–0.65***	**0.70****	–0.55	–0.50
NO_3	–0.29	–0.13	0.12	**–0.57***	–0.48	**–0.60***	0.45	–0.20	–0.17
NO_2	0.08	–0.10	–0.14	–0.03	–0.08	0.07	0.28	–0.32	–0.04
NH_4	–0.36	–0.33	–0.51	0.15	–0.15	0.20	0.19	–0.41	–0.45
PO_4	–0.26	–0.13	0.08	–0.52	–0.33	–0.51	**0.56***	–0.34	–0.12
SiO_2	–0.12	0.00	0.11	–0.30	–0.25	–0.43	0.39	–0.23	–0.03
MLD	–0.49	–0.32	–0.15	–0.31	–0.24	–0.12	–0.02	–0.09	–0.44
rbcL	0.41	0.29	0.19	0.15	0.33	0.27	0.00	0.20	0.47
%Micro	**0.57***	**0.61***	0.46	**0.77****	**0.91*****	0.44	**–0.59***	**0.59***	**0.66***
%Nano	–0.31	–0.63*	–0.33	–0.44	–0.53	–0.23	0.28	–0.35	–0.47
%Pico	**–0.69***	**–0.49**	**–0.58***	**–0.60***	**–0.77****	–0.27	**0.80****	**–0.80****	**–0.61***
%Diatom	**0.61***	0.40	0.53	0.34	0.54	0.17	**–0.57***	**0.61***	0.64*
%Dino	–0.35	–0.22	–0.52	–0.19	–0.35	0.04	0.52	–0.59*	–0.30
%*Thalassiosira*	**0.70***	**0.76****	0.34	**0.84*****	**0.74****	0.48	–0.51	0.47	**0.65***
%*Minidiscus*	–0.80	**–0.75****	–0.37	**–0.67***	**–0.59***	–0.39	0.52	–0.51	**–0.66***
%*Skeletonema*	–0.21	–0.29	–0.45	–0.17	–0.25	0.17	0.60*	**–0.64***	–0.27
%*Fragilariopsis*	–0.45	**–0.65***	–0.45	**–0.73****	**–0.77****	–0.32	**0.65***	**–0.61***	–0.49
%*Pseudo-Nitzschia*	–0.45	–0.41	–0.18	**–0.83*****	**–0.72****	–0.50	0.25	–0.29	–0.47
%Coscinodiscophytina	0.52	0.53	0.53	0.42	**0.69****	0.21	**–0.59***	**0.58***	**0.62***

Bold values indicate significant relationships with asterisks denoting different significance levels: * = 0.05, ** = 0.01, *** = 0.001, n = 13
SST: Sea surface temperature; SSS: Sea surface salinity; NO_3, NO_2, NH_4, PO_4, and SiO_2: Concentration of nitrate, nitrite, ammonium, phosphate, and silicate; MLD: Mixed layer depth; *rbcL*: Diatom-specific *rbcL* gene expression, Micro: microphytoplankton, Nano: nanophytoplankton, Pico: Picophytoplankton, Dino: dinoflagellates, Other: other functional groups than diatoms and dinoflagellates. The % denotes relative contribution of given phytoplankton groups.

Table 3. Spearman-rank correlation coefficients between *P-E* curve parameters.

	Chl *a*	$\bar{a}^*_{ph}$	F_v/F_{mPAM}	α^B	β^B	P^B_{max}	E_k	Φ_{Cmax}
F_v/F_{mPAM}	**0.80****	–						
$\bar{a}^*_{ph}$	**–0.62***	–0.53	–					
α^B	0.60*	0.54	–0.55	–				
β^B	**0.56***	**0.58***	–0.40	0.09	–			
P^B_{max}	**0.72****	**0.72****	–0.48	0.50	**0.84*****	–		
E_k	0.33	0.28	–0.09	–0.42	**0.75****	0.51	–	
Φ_{Cmax}	**0.69***	**0.62****	**–0.83*****	**0.87*****	0.34	**0.61***	–0.15	–
PP	**0.92*****	**0.88*****	–0.53	**0.64***	0.52	**0.75****	0.25	**0.68****

Bold numbers indicate significant relationship between given parameters. Significance levels are denoted by numbers of asterisks: * = 0.05, ** = 0.01, *** = 0.001, n = 13.

α^B: Initial slope of *P-E* curve [mg C mg Chl a^{-1} h^{-1} (μmol photons m^{-2} s^{-1}) $^{-1}$]; β^B: Photoinhibition index [mg C mg Chl a^{-1} h^{-1} (μmol photons m^{-2} s^{-1}) $^{-1}$]; P^B_{max}: Maximum photosynthetic rate [mgC mgChl a^{-1} h^{-1}]; E_k: Light saturation index [μmol photons m^{-2} s^{-1}]; Chl *a*: Chl *a* concentration [mg m^{-3}]; $\bar{a}^*_{ph}$: Chl *a*-normalized light absorption coefficient of phytoplankton [m^2 mg Chl *a*]; Φ_{Cmax}: Maximum quantum yield for carbon fixation [mol C mol photons^{-1}]; *PP*: Primary productivity [mg C m^{-3} day^{-1}].

Table 4. Summary of terms and abbreviation of photosynthetic parameters used for *P-E* curves

Symbol	Definition	Unit
α^{B}	Chl *a*-normalized initial slope of *P-E* curve	(mg C mg Chl a^{-1} h^{-1}) (μmol photons m^{-2} s^{-1})$^{-1}$
β^{B}	Chl *a*-normalized photoinhibition index of *P-E* curve	(mg C mg Chl a^{-1} h^{-1}) (μmol photons m^{-2} s^{-1})$^{-1}$
P^{B}_{max}	Chl *a*-normalized maximum photosynthetic rate	mg C mg Chl a^{-1} h^{-1}
E_k	Light saturation index	μmol photons m^{-2} s^{-1}

Table 5. Sampling conditions and hydrographic and optical data during the Mu14 expedition.

Station	Date	SST (°C)	SSS	NO_3 (μM)	NO_2 (μM)	NH_4 (μM)	PO_4 (μM)	SiO_4 (μM)	DFe (nM)	$E_0(PAR)_{max}$ (μmol photons m^{-2} s^{-1})	$K_d(PAR)$ (m^{-1})	Z_{eu} (m)	MLD (m)
D9	2014.06.08	6.33	32.36	2.03	0.11	0.13	0.35	20.78	0.71	1458	0.160	29.8	24.1
A2	2014.06.09	2.67	32.67	9.57	0.17	0.29	0.96	28.32	0.13	1097	0.182	26.7	19.5
PS1	2014.06.14	5.60	32.40	0.31	0.06	UD	0.19	0.61	0.21	1755	0.159	29.5	17.2
PS5	2014.06.15	5.50	32.28	1.68	0.08	0.25	0.29	2.32	0.21	796	0.154	29.8	10.0
C3	2014.06.16	6.40	32.87	20.7	0.25	0.50	1.83	34.43	0.22	1185	0.104	44.6	20.9
C5	2014.06.18	6.05	32.77	9.93	0.16	0.39	1.09	12.91	0.05	1111	0.115	40.3	28.5
B3	2014.06.20	6.80	32.82	18.87	0.24	0.66	1.76	30.9	0.04	666	0.097	47.6	23.8
B5	2014.06.21	7.20	32.68	3.75	0.11	0.33	0.69	3.53	0.07	864	0.102	45.5	14.0
B6	2014.06.22	6.80	32.36	4.89	0.11	0.71	0.79	3.19	0.69	785	0.103	45.4	17.2
A5	2014.06.28	6.80	32.81	16.64	0.27	0.30	1.53	14.88	0.06	632	0.127	36.2	12.8
OP3	2014.06.29	3.60	32.39	12.14	0.18	0.85	1.35	28.32	0.14	1162	0.101	46.2	18.2
A6	2014.06.30	9.20	32.77	17.45	0.24	0.35	1.66	18.5	0.03	757	0.111	41.4	14.7

SST: Sea surface temperature; SSS: Sea surface salinity; NO_3, NO_2, NH_4, PO_4, and SiO_2: Concentration of nitrate, nitrite, ammonium, phosphate, and silicate, respectively; DFe: Dissolved iron concentration; $E_0(PAR)_{max}$: Maximum photosynthetically available radiation within a day; $K_d(PAR)$: Vertical attenuation coefficient of downward photosynthetically available radiation (PAR); Z_{eu}: Euphotic layer depth; MLD: Mixed layer depth

Table 6. Contributions of armored plankton to the total plankton (a) collected at *in situ* sampling station and (b) from the bottles for the Fe enrichment incubation experiments enumerated under scanning electron microscopy.

(a)		D9	A2	PS5	C3	C5	B3	B5	B6	OP3	A5	A6
Unidentified		7.26%	46.4%	6.87%	20.2%	0.65%	5.35%	3.61%	12.3%	21.3%	9.74%	39.9%
Coccolithophores						3.67%		0.06%				
Parmales		0.38%	0.17%		0.31%	**44.4%**	0.11%	0.39%	2.24%	1.36%	0.29%	
Silicoflagellates		0.08%	0.09%		0.50%	0.55%				**17.7%**	0.19%	
Dinoflagellates				0.42%	0.19%		0.46%		0.21%	0.45%	2.98%	2.25%
Flagellates				0.10%	0.57%		1.77%	0.58%	3.31%	1.36%	0.77%	1.12%
Diatoms		**99.5%**	**99.7%**	**99.5%**	**98.4%**	**51.4%**	**97.7%**	**99.0%**	**94.2%**	**79.1%**	**95.8%**	**96.6%**
Diatoms	Size (µm)											
Centric diatoms												
Asteromphalus spp.	25−180[v]*			+	+						+	
***Chaetoceros* spp.**		++++	++++	++++	+++	++++	+	++++	++++	+++	++++	+
- *Ch. concavicornis*	29.3±8.3[a]	*				*	*	*	*		*	****
- *Ch. convolutus*	31.1±4.8[a]	*		*							*	
- *Ch. debilis*	11.0±1.7[a]		*	***	**	***		*			**	***
- *Ch. diadema*	23.7±3.2[a]	*	*	**	**	***	*	*	*	*	***	
- *Ch. furcellatus*	10.3±1.8[a]		*	***	*	**		*			*	
- Resting spores	-	*	*	**	***			*	*	****	*	
- Other *Chaetoceros*	-	****	****	*	**	*	****	****	*****	**	***	
Corethron pennatum	135.7±44.9[a]	+			+	+	+	+	+		+	+
Minidiscus spp.	> 5[v]*	+			+	+	+			+	+	
Thalassiosira spp.	4.7±1.3[v]*	+	+	+	++	+	+	+	+	+	++	+++
Pennate diatoms												
Cylindrotheca closterium	~17[a]**			+	+		+	+	+		+	+
***Fragilariopsis* spp.**	**12.5±7.8[a]**	++	+	+	+++	++	++++	+	+	++++	++	++
Neodenticula seminae	**21.4±3.7[a]**	+	+	+		+	+	+	+	+	+	++
Nitzschia spp.	**34.6±9.4[a]**	+	+	+		+	+	+	+	+	+	++
***Pseudo-nitzschia* spp.**	**9.8±2.5[a]**	+	+	+	+++	+	+	+			+	
Thalassionema spp.	10−200a*			+	+	+		+		+	+	+
Other diatoms	-	+	++		+	+	+	+	+	+	+	++

(b)		C5-Ini	C5-Con	C5-Fe	C5-DFB	A5-Ini	A5-Con	A5-Fe	A5-DFB
Unidentified		0.65%	1.82%	3.76%	11.4%	9.74%	4.47%	17.7%	20.2%
Coccolithophores		3.67%	0.74%	0.42%					
Parmales		**44.4%**	6.19%	6.75%	0.24%	0.29%	2.22%	0.04%	0.42%
Silicoflagellates		0.55%	0.33%	0.31%	0.60%	0.19%	0.05%	0.09%	0.31%
Dinoflagellates			0.14%		2.74%	2.98%	0.24%	0.85%	3.98%
Flagellates			0.59%	0.75%	**10.4%**	0.77%	0.14%		1.36%
Diatoms		**51.4%**	**92.8%**	**92.2%**	**86.0%**	**95.8%**	**97.4%**	**99.0%**	**93.9%**
Diatoms	Size (μm)								
Centric diatoms									
Asteromphalus spp.	25−180[v]*		+		+	+	+		+
***Chaetoceros* spp.**		++++	++++	++++	+	++++	++++	++++	++
- *Ch. Concavicornis*	29.3±8.3[a]	*	*	*	*	*	*	*	**
- *Ch. Convolutes*	31.1±4.8[a]					*	*	*	**
- *Ch. Debilis*	11.0±1.7[a]	***	**	**		**	**	*	*
- *Ch. Diadema*	23.7±3.2[a]	***	***	**		***	**	**	*
- *Ch. Furcellatus*	10.3±1.8[a]	**	**	**		*	**	*	*
- Resting spores	-		*	*	***	*		*	*
- Other *Chaetoceros*	-	*	**	***	***	***	***	****	****
Corethron pennatum	135.7±44.9[a]	+	+	+	+	+	+	+	+
Minidiscus spp.	> 5[v]*	+	+	+	+	+	+	+	
Thalassiosira spp.	4.7±1.3[v]*	+	+	+	++	+	+	+	+
Pennate diatoms									
Cylindrotheca closterium	~17[a]***		+	+	+	+	+	++	++
***Fragilariopsis* spp.**	**12.5±7.8[a]**	++	+	+	++	++	+	+	+
Neodenticula seminae	**21.4±3.7[a]**	+	+	+	++	+	+	+	++
Nitzschia spp.	**34.6±9.4[a]**	+	+	+	+	+	+	+	+
***Pseudo-nitzschia* spp.**	**9.8±2.5[a]**	+	+	++	+	+	++	++	++
Thalassionema spp.	10−200a*	+	+	+	++	+	+	+	++
Other diatoms	-	+	+	+	++	+	+	+	+

Unidentified materials shown in the first row were excluded from the analysis. Contributions of diatoms were indicated with number of plus (+) symbols: +: >0−10%, ++: >10−25%, +++: >25%−50%, ++++: >50%. Contribution of each *Chaetoceros* species were indicated with number of asterisks (*) with the same criteria as those of diatoms described above. The contributions of diatoms were independently calculated within diatoms (i.e., excluding other planktonic species; coccolithores, parmales, silicoflagellates, dinoflagellates, and flagellates). For more details, see Appendices A and B. Size of major diatoms were shown in the second column. The superscripts a and v indicate apical length and valve diameter to measure the size of a given species, respectively. The * indicates that information of the size was obtained from Tomas (1997) because the cells, often weakly-silicified, were not well preserved or broken, whereas the ** indicates the approximate apical length of the diatom *Cylindrotheca closterium* that it was difficult to precisely measure due to their weak silicification and twisted or bended body on the filter for SEM.

Table 7. Spearman-rank correlation coefficients (ρ) between photosynthetic parameters.

	F_v/F_m	α^B	β^B	P^B_{max}	E_k	$\bar{a}^*_{ph}$	Φ_{Cmax}	PP
Chl *a*	−0.37	−0.30	−0.23	0.07	**−0.80*****	0.71	0.50	**0.82*****
F_v/F_m		**0.73****	**0.78****	−0.20	0.36	0.12	0.39	−0.14
α^B			**0.80*****	0.36	0.37	0.00	0.18	0.04
β^B				0.41	0.42	0.09	0.17	−0.03
P^B_{max}					0.23	−0.15	−0.37	0.09
E_k						−0.55	**−0.67***	**−0.73***
$\bar{a}^*_{ph}$							**0.62***	**0.59***
Φ_{Cmax}								**0.66***

Bold numbers indicate significant relationship between given parameters. Significance levels are denoted by numbers of asterisks: * = 0.05, ** = 0.01, *** = 0.001, n = 12.
Chl *a*: Chl *a* concentration [mg m^{-3}]; F_v/F_m: Maximum quantum yield of PSII measured with PAM fluorometry: α^B: Initial slope of a *P-E* curve [mg C mg Chl a^{-1} h^{-1} (µmol photons m^{-2} $s^{-1})^{-1}$]; β^B: Photoinhibition index [mg C mg Chl a^{-1} h^{-1} (µmol photons m^{-2} $s^{-1})^{-1}$]; P^B_{max}: Maximum photosynthetic rate [mgC mgChl a^{-1} h^{-1}]; E_k: Light saturation index [µmol photons m^{-2} s^{-1}]; $\bar{a}^*_{ph}$: Chl *a*-normalized light absorption coefficient of phytoplankton [m^2 mg Chl a^{-1}]; Φ_{Cmax}: Maximum quantum yield for carbon fixation [mol C mol photons^{-1}]; *PP*: Primary productivity [mg C m^{-3} day^{-1}]

Table 8. Spearman-rank correlation coefficients (ρ) between photosynthetic and environmental parameters data.

	Chl *a*	F_v/F_m	α^B	β^B	P^B_{max}	E_k	$\bar{a}^*_{ph}$	Φ_{Cmax}	*PP*
SST	–0.01	–0.25	0.11	0.23	**0.75****	0.40	–0.27	**–0.66***	–0.07
SSS	–0.44	–0.40	–0.07	–0.16	0.45	0.31	**–0.63***	**–0.65***	–0.32
NO_3	**–0.61***	–0.41	–0.18	–0.36	0.18	0.50	**–0.66***	**–0.87*****	**–0.63***
NO_2	–0.42	**–0.59***	–0.22	–0.52	0.21	0.23	**–0.64***	**–0.72****	–0.41
NH_4	**–0.60***	–0.04	–0.19	–0.12	–0.10	**0.64***	**–0.58***	**–0.76****	**–0.87*****
PO_4	**–0.61***	–0.41	–0.18	–0.36	0.18	0.50	**–0.66***	**–0.87*****	**–0.63***
SiO_2	–0.36	–0.55	–0.41	**–0.68***	–0.18	0.24	–0.50	**–0.58***	–0.34
MLD	–0.14	–0.31	**–0.66***	–0.55	–0.54	–0.01	–0.16	–0.17	–0.24
Z_{eu}	–0.54	–0.03	–0.02	0.09	0.19	**0.73****	**–0.71****	**–0.77****	**–0.66***
DFe	0.43	–0.10	–0.47	–0.26	–0.38	–0.31	0.37	0.35	0.27

Bold values indicate significant relationships with asterisks denoting different significance levels: *= 0.05, ** = 0.01, *** = 0.001, n = 12. SST: Sea surface temperature; SSS: Sea surface salinity; NO_3, NO_2, NH_4, PO_4, and SiO_2: Concentration of nitrate, nitrite, ammonium, phosphate, and silicate; MLD: Mixed layer depth; Z_{eu}: Euphotic layer depth; DFe: Dissolved iron concentration. Photophysiological parameters and their units were the same as shown in the caption of Table 4

Table 9. Terminology and Definition of Chlorophyll a fluorescence yields obtained from FRRf and FIRe fluorometers

Yield and parameter		Unit	Derivation or reference
Fluorescence yield			
F	Fluorescence yield	Unitless	
F_o	Minimum fluorescence yield of dark regulated cells	Unitless	
F_m	Maximum fluorescence yield of dark regulated cells	Unitless	
F_v	Maximum variable fluorescence yield	Unitless	$F_m - F_o$
F'	Fluorescence yield under actinic light	Unitless	
F_o'	Minimum fluorescence yield of actinic light-acclimated cells	Unitless	Oxborough and Baker (1997)
F_m'	Maximum fluorescence yield of actinic light-acclimated cells	Unitless	
F_v'	Variable fluorescence yield under actinic light	Unitless	$F_m' - F_o'$
F_q'	Difference in fluorescence yields between F' and Fm'	Unitless	$F_m' - F'$
Fluorescence parameters in the dark			
σ_{PSII}	Functional absorption cross scetion of PSII in the dark	nm^2 $RCII^{-1}$	Kolber et al. (1998)
F_v/F_m	Maximum quantum yield of photochemistry of PSII	Unitless	$(F_m - F_o)/F_m$
τ	Reoxidation rate of PSII	µs	Kolber et al. (1998)
Fluorescence parameters under actinic light			
$F_q'/F_{m'}$	Effective photochemical efficiency of PSII under actinic light	Unitless	$(F_m' - F')/F_m'$
NPQ_{NSV}	Non-photochemical quenching based on the Stern-Volmer kinetic equation	Unitless	McKew et al. (2013)
Φ_{NPQ}	Quantum yield of NPQNSV under actinic light	Unitless	Kramer et al. (2004)
Φ_{NO}	Quantum yield of other non-photochemical losses	Unitless	Kramer et al. (2004)
***ETR*$_{RCII}$-*E* curve parameters**			
ETR_{RCII}	Absolute electron transport rate through RCII	mol quanta mol $RCII^{-1}$ s^{-1}	Schuback et al. (2016)
E	Actinic light irradiace	mol quanta m^{-2} s^{-1}	
α	Light utilazation index under dim light	(mol quanta mol $RCII^{-1}$ s^{-1}) (mol quanta m^{-2} s^{-1})$^{-1}$	Platt et al. (1980)
β	Light inhibition index under strong light	(mol quanta mol $RCII^{-1}$ s^{-1}) (mol quanta m^{-2} s^{-1})$^{-2}$	Platt et al. (1980)
$ETR_{RCIImax}$	Maximum electron transport rate though RCII	mol quanta mol $RCII^{-1}$ s^{-1}	Platt et al. (1980)
E_k	Light saturation index	mol quanta m^{-2} s^{-1}	Platt et al. (1980)

Table 10. Growth rate of ice algae during frozen periods

	Growth rate		
HFe+HL	0.020	±	0.001
HFe+LL	0.020	±	0.002
LFe+HL	0.022	±	0.006
LFe+LL	0.019	±	0.009

No siginificant difference in their growth rates was not observed between treatments assessed with one-way ANOVA test (p<0.05).

Appendix A. Potential temperature (θ) between the isopycnal surfaces σ_θ = 26.7 and 26.8 at all sampling stations.

Station	θ between σ_θ = 26.7-26.8
Bio-1	0.6
Bio-2	0.6
Bio-4	3.5
Bio-6	2.3
Bio-7	1.1
Bio-9	1.3
Bio-10	1.0
Bio-11	0.9
Bio-12	1.3
Bio-13	4.0
Bio-14	0.5
AK15-1	ND
AK15-2	ND

Appendix B. Pigment composition determined with the UHPLC analysis method (Suzuki et al., 2015) at all stations.

Station	Chl c_3	Chl c_2	Chlide *a*	Peri	19'-BF	Fuco	Neo	Prasino	Viola	19'-HF	DD	Allo	DT	Zea	Lut	Chl *b*	Chl *a*	α, β-caro
Bio-1	0.0324	0.0467	0.0240	0.0248	0.0286	0.138	0.0060	0.0114	0.0104	0.0210	0.0536	0.0015	0.0037	0.0041	0.0016	0.0393	0.286	0.0144
Bio-2	0.0321	0.0522	0.0213	0.0327	0.0337	0.113	0.0061	0.0094	0.0104	0.0314	0.0473	UD	0.0034	0.0042	0.0010	0.0365	0.248	0.0169
Bio-4	0.0336	0.0907	0.0411	0.0725	0.0208	0.281	0.0103	0.0155	0.0131	0.0163	0.0755	UD	0.0059	0.0090	0.0026	0.0600	0.371	0.0310
Bio-6	0.0231	0.0900	0.0428	0.113	0.0156	0.232	0.0086	0.0112	0.0124	0.0093	0.0820	UD	0.0104	0.0091	0.0016	0.0470	0.639	0.0321
Bio-7	0.0199	0.0555	0.0185	0.0522	0.0132	0.160	0.0056	0.0098	0.0089	0.0086	0.0593	UD	0.0094	0.0047	0.0016	0.0459	0.280	0.0240
Bio-9	0.0323	0.0951	0.0500	0.0687	0.0238	0.277	0.0099	0.0175	0.0186	0.0167	0.0822	0.0018	0.0071	0.0076	0.0032	0.0667	0.438	0.0285
Bio-10	0.0257	0.0354	0.0251	0.0202	0.0254	0.0839	0.0038	0.0087	0.0038	0.0300	0.0379	UD	0.0116	0.0072	0.0023	0.0306	0.256	0.0112
Bio-11	0.0360	0.0828	0.0380	0.0371	0.0344	0.219	0.0077	0.0128	0.0157	0.0386	0.0624	0.0006	0.0052	0.0061	0.0031	0.0559	0.386	0.0273
Bio-12	0.0408	0.0985	0.0499	0.0706	0.0388	0.265	0.0095	0.0182	0.0216	0.0288	0.0902	0.0016	0.0089	0.0087	0.0032	0.0753	0.404	0.0314
Bio-13	0.0743	0.1506	0.0686	0.0964	0.0841	0.282	0.0104	0.0169	0.0238	0.0784	0.127	UD	0.0098	0.0077	0.0058	0.0761	0.647	0.0421
Bio-14	0.0537	0.2949	0.1635	0.0556	0.0389	1.13	0.0148	0.0202	0.0210	0.0249	0.162	0.0018	0.0153	0.0097	0.0043	0.100	1.28	0.0679
AK15-1	0.0233	0.0064	UD	0.0469	UD	2.11	0.0060	UD	UD	0.0106	0.219	0.110	0.0108	0.0083	UD	0.0631	4.76	0.0794
AK15-2	0.0195	0.0068	UD	0.0880	UD	3.08	0.0101	UD	UD	UD	0.218	0.0661	0.0222	UD	UD	0.0634	6.22	0.0920
Bio-6_Ini	0.0231	0.0900	0.0428	0.113	0.0156	0.232	0.0086	0.0112	0.0124	0.0093	0.0820	UD	0.0104	0.0091	0.0016	0.0470	0.639	0.0321
Bio-6_Con	0.0113	0.0113	UD	0.143	0.0139	0.245	UD	0.0124	UD	0.0132	0.0627	0.0506	UD	UD	UD	0.0361	0.801	0.0194
Bio-6_+7ºC	UD	UD	UD	0.164	0.0130	0.201	0.0042	0.0111	UD	0.0123	0.0534	0.0481	UD	UD	UD	0.0308	0.740	0.0180
Bio-7_Ini	0.0199	0.0555	0.0185	0.0522	0.0132	0.160	0.0056	0.0098	0.0089	0.0086	0.0593	UD	0.0094	0.0047	0.0016	0.0459	0.280	0.0240
Bio-7_Con	0.0103	0.0146	UD	0.0170	0.0053	0.0867	0.0024	0.0047	UD	0.0047	0.0138	0.0101	UD	UD	UD	0.0136	0.222	0.0054
Bio-7_+7ºC	UD	UD	UD	0.0219	0.0056	0.0870	0.0029	0.0050	UD	0.0049	0.0133	0.0094	UD	UD	UD	0.0152	0.229	0.0053
Bio-10_Ini	0.0257	0.0354	0.0251	0.0202	0.0254	0.0839	0.0038	0.0087	0.0038	0.0300	0.0379	UD	0.0116	0.0072	0.0023	0.0306	0.256	0.0112
Bio-10_Con	UD	UD	UD	0.0267	0.0274	0.0933	0.0033	0.0048	0.0055	0.0300	0.0289	0.0124	UD	UD	UD	0.0272	0.353	0.0073
Bio-10_+7ºC	0.0210	0.0227	UD	0.0189	0.0214	0.0761	UD	0.0075	UD	0.0225	0.0157	0.0076	UD	UD	UD	0.0369	0.324	0.0101
Bio-13_Ini	0.0743	0.151	0.0686	0.0964	0.0841	0.2818	0.0104	0.0169	0.0238	0.0784	0.127	UD	0.0098	0.0077	0.0058	0.0761	0.647	0.0421
Bio-13_Con	0.0930	0.0827	UD	0.111	0.0695	0.2465	0.0068	0.0164	0.0148	0.0632	0.0658	0.0598	UD	UD	UD	0.0544	0.857	0.0241
Bio-13_+7ºC	UD	0.0440	UD	0.112	0.0638	0.2145	0.0062	0.0147	0.0127	0.0569	0.0538	0.0541	UD	UD	UD	0.0524	0.774	0.0197

Chl: Chlorophyll, Chlide: Chlorophilide, Peri: peridinin, 19'-BF: 19'-butanoyloxyfucoxanthin, Fuco: fucoxanthin, Neo: neoxanthin, Prasino: prasinoxanthin, Viola: violaxanthin, 19'-HF: 19'- hexanoyloxyfucxanthin, DD: diadinoxanthin, Allo: alloxanthin, DT: diatoxanthin, Zea: zeaxanthin, Lut: lutein, Caro: carotene

Appendix C. FRRf parameters obtained at all sampling stations ± standard deviations, $n = 2$.

Station	$F_v/F_{m\,FRRf}$	σ_{PSII}	[RCII]
	–	× nm^2 $PSII^{-1}$	× 10^{-9} mol m^{-3}
Bio-1	0.582	2.69	0.49
Bio-2	0.322 ± 0.064	3.78 ± 0.64	1.54 ± 0.84
Bio-4	0.421 ± 0.024	2.79 ± 0.16	1.04 ± 0.20
Bio-6	0.467 ± 0.068	2.56 ± 0.19	1.50 ± 0.31
Bio-7	0.515 ± 0.064	2.85 ± 0.15	0.76 ± 0.33
Bio-9	0.394 ± 0.026	2.91 ± 0.16	1.23 ± 0.25
Bio-10	0.377 ± 0.050	3.06 ± 0.30	0.62 ± 0.11
Bio-11	0.504 ± 0.033	2.78 ± 0.14	1.24 ± 0.12
Bio-12	0.475 ± 0.049	3.01 ± 0.08	1.15 ± 0.27
Bio-13	0.432 ± 0.020	3.13 ± 0.19	1.94 ± 0.16
Bio-14	0.477 ± 0.005	2.43 ± 0.15	5.57 ± 0.22
AK15-1	ND	ND	ND
AK15-2	ND	ND	ND

F_v/F_{mFRRf}: Maximum quantum yield of PSII obtained by FRR fluorometer. σ_{PSII}: Functional absorption cross-section for PSII; [RCII]: Concentration of functional PSII reaction center

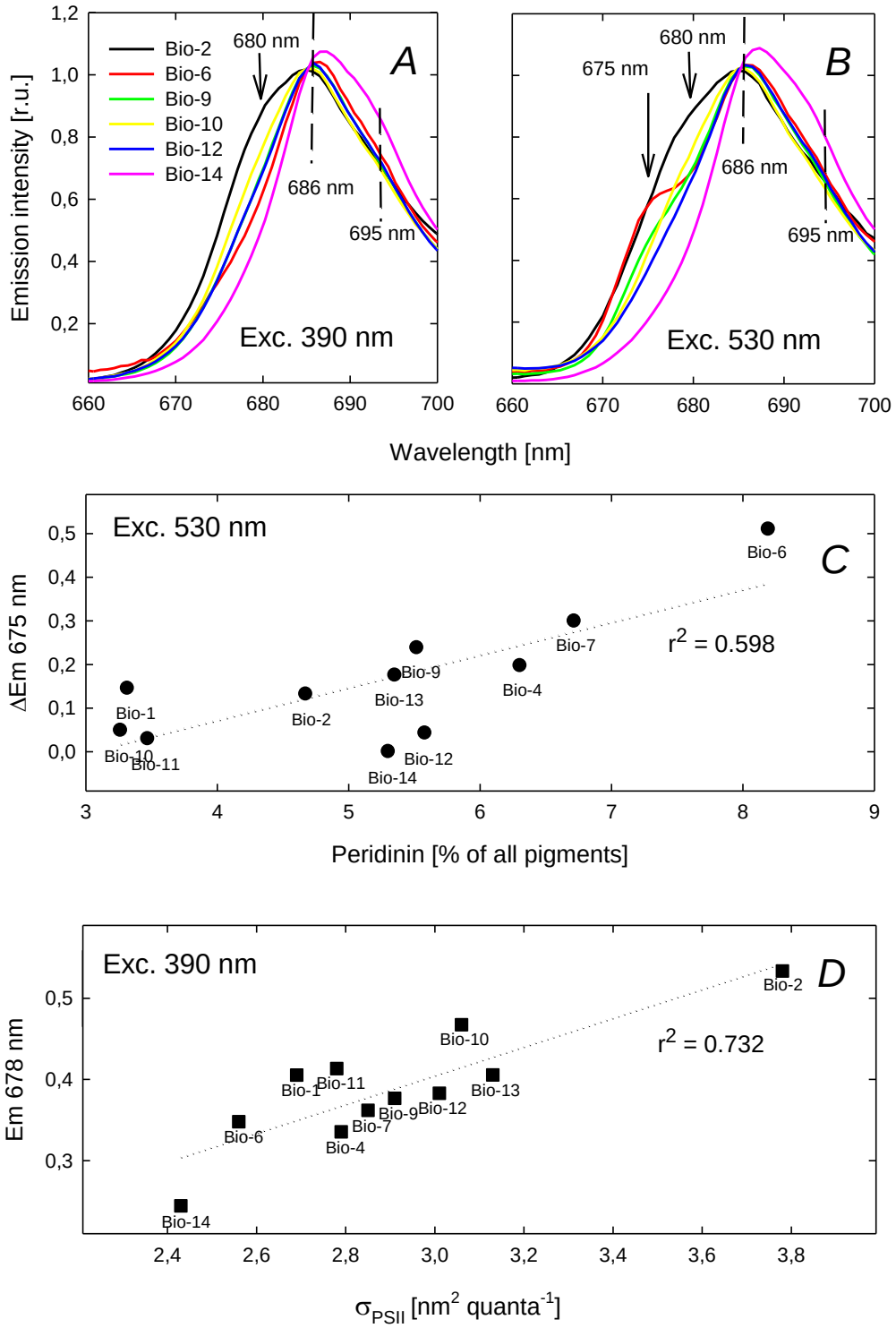

Appendix D. Low temperature (77K) emission spectra.
Panels A and B show part of the emission in the range 660-700nm of selected samples from different stations. (A) shows spectra excited by 390 nm, (B) shows spectra excited at 530 nm. The arrows and lines indicate the positions of individual emission bands (675, 680, 685, 695 nm). (C) shows relationship between the relative content of peridinin (% of all pigments) and the increase of the 675 nm emission when excited at 530 nm (calculated as difference between emission at 675 nm when excited at 530 and 390 nm). (D) shows the relationship between PSII effective cross-section (σ_{PSII}) and the emission band intensity at 678nm when excited at 390 nm.

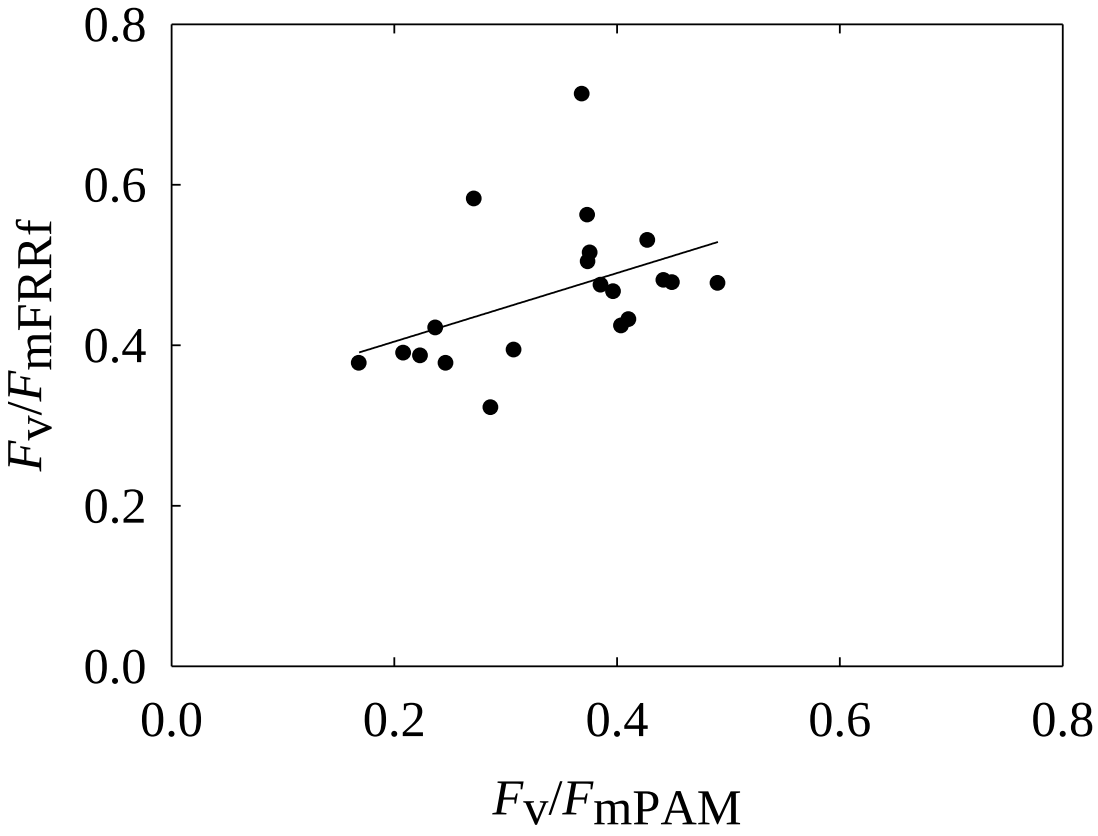

Appendix E. A relationship between F_v/F_{mPAM} and F_v/F_{mFRRf}.

The parameters were significantly correlated each other (ρ=0.483, n=20, p<0.05, Spearman's Rank correlation)

F_v/F_{mPAM}: Maximum quantum yield of PSII obtained by PAM fluorometry.

F_v/F_{mFRRf}: Maximum quantum yield of PSII obtained by FRR fluorometer.

Appendix F. Contributions of each armoured plankton species enumerated with SEM at *in situ* sampling stations.

	D9	A2	PS1	PS5	C3	C5	B3	B5	B6	OP3	A5	A6
Coccolithophores												
Emiliania huxleyi **type B**						2.97%		0.1%				
Calciopappus caudatus						0.52%						
Coccolithus pelagicus **ssp.** *Pelagicus* **HOL**						0.10%						
Pleurochrysis carterae						0.05%						
Centric diatoms												
Actinocyclus **spp.**						0.05%						
Asteromphalus elegans												
Asteromphalus hookeri				0.29%							0.32%	
Asteromphalus hyalinus				0.10%								
Asteromphalus **spp.**					0.05%							
Arcocellulus mamifer						0.04%						
Arcocellulus cornucevis		8.33%			0.25%	0.05%	0.3%	0.1%	0.9%			
Baceriostrum **sp.**						0.21%						
Chaetoceros affinis		4.35%									0.54%	
Chaetoceros atlanticus		0.05%		0.10%		0.27%	0.4%	0.1%	0.9%		3.20%	
Chaetoceros **cf.** *borealis*								0.1%				
Chaetoceros **cf.** *compressus*				0.68%							0.15%	
Chaetoceros concavicornis	0.35%					0.17%	0.2%	0.1%	0.1%		1.85%	2.70%
Chaetoceros convolutus	0.21%			0.48%							0.65%	
Chaetoceros debilis		2.71%		24.30%	2.96%	14.50%		2.9%			5.85%	2.03%
Chaetoceros **cf.** *decipiens*												
Chaetoceros diadema	4.02%	2.29%		12.58%	4.57%	18.28%	0.1%	5.0%	2.7%	0.34%	18.55%	
Chaetoceros didymus												
Chaetoceros furcellatus		2.62%		27.98%	0.40%	4.68%		1.4%			3.78%	
Chaetoceros radicans				0.19%							0.35%	
Chaetoceros socialis	9.51%	2.99%			0.30%			0.7%				
Chaetoceros tenuissima		2.62%			0.15%	2.11%		0.1%			0.17%	
Chaetocerous **spp.**	46.51%	13.99%		6.97%	4.22%	0.45%	2.8%	75.1%	56.0%	2.36%	9.16%	
Chaetoceros **spp. Resting spores**	4.02%	0.70%		12.49%	8.03%			2.9%	9.2%	12.16%	1.00%	
Coscinodiscus centralis												
Coscinodiscus granii												
Coscinodiscus marginatus											0.08%	
Coscinodiscus radiatus											0.08%	
Coscinodiscus wallesii												
Coscinodiscus **spp.**	0.07%	0.05%					0.1%	0.2%			0.82%	4.73%
Corethron criophilum	0.14%				0.10%	0.18%	0.1%	0.1%	0.2%		4.21%	2.03%
Eucampia antarctica											0.09%	
Minidiscus **spp.**	0.92%				0.60%	0.38%	0.8%			0.34%	0.35%	
Odontella aurita		0.28%				0.01%						
Proboscia alata												
Rhizosolenia **cf.** *borealis*											1.65%	
Rhizosolenia hebetata f. semispina												
Rhizosolenia setigera												
Rhizosolenia **spp.**									0.2%		0.63%	2.03%
Skeletonema **sp.**												
Shionodiscus oestrupii	0.14%				0.20%							
Thalassiosira anguste-lineata		0.89%			0.25%	0.15%					0.09%	
Thalassiosira bulbosa						0.07%		0.1%		0.34%	0.15%	2.70%
Thalassiosira confusa											0.16%	
Thalassiosira eccentrica							0.1%				0.08%	
Thalassiosira gravida									0.1%		0.30%	
Thalassiosira nordenskioeldii				0.39%		0.10%		0.8%				
Thalassiosira minima											0.52%	
Thalassiosira oceanica	3.31%			0.58%	6.63%	0.72%	1.2%	0.6%	1.9%	0.34%	8.78%	16.89%
Thalassiosira pacifica						0.01%					0.09%	
Thalassiosira proschkinae												0.68%
Thalassiosira **spp.**		2.53%		0.19%	1.26%	0.07%	0.1%	0.2%	0.7%	1.35%	0.82%	1.35%
Pennate diatoms												
Cylindrotheca closterium				0.19%	3.06%		2.4%	2.4%	5.2%		3.98%	0.68%
Entomoneis **spp.**											0.09%	
Fragilariopsis cylindrus	2.61%	1.17%		0.87%							1.23%	
Fragilariopsis cylindformis						0.10%					1.08%	
Fragilariopsis oceanica		0.09%					0.2%				0.58%	
Fragilariopsis pseudonana												
Fragilariopsis **spp.**	8.25%	4.02%		0.68%	24.35%	5.93%	81.0%	0.7%	4.1%	35.47%	6.02%	8.78%
Cf. *Pleurosigma* **spp.**	0.21%											
Navicula **spp.**	0.49%					0.01%						
Neodenticula seminae	2.89%	2.29%			0.25%	1.83%	0.1%	0.4%	0.2%	1.69%	4.24%	0.68%
Nitzschia **spp.**	7.75%	0.09%		0.19%		0.24%	1.1%	0.2%	0.2%	3.72%	0.08%	6.76%
Plagiotropis **sp.**							0.1%				0.30%	
Pseudogomophonema kamchatkatium		0.09%										
Pseudo-nitzschia **spp.**	0.21%	0.33%		2.81%	20.68%	0.09%	1.6%	0.9%			1.82%	
Thalassionema nitzschioides				0.48%		0.29%		0.1%		0.34%	0.89%	1.35%
Thalassionema **spp.**				0.10%	0.20%			0.1%				
Thalassiothrix longissima		0.94%				0.01%				0.34%	1.69%	4.73%
Parmales										4.39%		
Tetraparma catinifera									0.1%			
Tetraparma gracilis						0.15%	0.1%					
Tetraparma pelagica						11.72%			0.7%	0.68%	0.09%	
Tetraparma **spp.**	0.21%				0.10%	0.76%		0.1%	0.1%			
Triparma columacea f. convexa						9.50%					0.09%	
Triparma columacea f. fimbriata						5.59%						
Triparma laevis f. longispina												
Triparma strigata	0.14%	0.09%				10.76%	0.1%	0.1%	0.7%	0.34%		
Triparma verrucosa						1.79%			0.3%			
Triparma **spp.**					0.15%	3.77%		0.2%	0.1%		0.09%	
Silicoflagellate												
Dictyocha octonaria												
Dictyocha speculum	0.07%	0.05%			0.40%	0.55%				13.18%	0.17%	
Dinoflagellates												
Phalacroma rapa					0.10%						0.30%	
Phalacroma rotundatum											0.15%	
Ceratium longipes				0.19%								
Gymnodinium **spp.**				0.10%							0.09%	
Gonyalax polygramma				0.10%								
Gonyalax **spp.**											0.23%	
Prorocentrum **spp.**					0.05%		0.4%		0.2%	0.34%	1.85%	0.68%
Protoperidinium **spp.**											0.08%	0.68%
Pyrophacus horoligium												
Flagellates												
Ciliates				0.10%	0.40%		0.6%	0.3%	2.2%	1.01%	0.45%	0.68%
Choanoflagellates					0.05%		1.1%	0.2%	0.7%		0.24%	
Unidentified	7.26%	46.42%		6.87%	20.23%	0.65%	5.3%	3.6%	12.3%	21.28%	9.74%	39.86%

Appendix G. Averaged contributions of each armoured plankton species enumerated with SEMfrom each bottle of the Fe enrichment incubation experiments.

	C5-Ini	C5-Con	C5-Fe	C5-DFB	A5-Ini	A5-Con	A5-Fe	A5-DFB
Coccolithophores								
Emiliania huxleyi type B	2.97%	0.03%						
Calciopappus caudatus	0.52%		0.08%					
Coccolithus pelagicus ssp. *Pelagicus* HOL	0.10%	0.69%	0.32%					
Pleurochrysis carterae	0.05%							
Centric diatoms								
Actinocyclus spp.	0.05%							
Asteromphalus elegans				0.42%		0.05%		0.42%
Asteromphalus hookeri		0.03%		1.80%	0.32%			0.17%
Asteromphalus hyalinus								0.17%
Asteromphalus spp.				0.74%				
Arcocellulus mamifer	0.04%	0.15%				0.05%		
Arcocellulus cornucevis	0.05%	0.54%	2.96%			0.36%	0.10%	
Baceriostrum sp.	0.21%		0.03%					
Chaetoceros affinis		1.53%	4.46%		0.54%	2.66%	0.45%	0.42%
Chaetoceros atlanticus	0.27%	0.13%			3.20%	0.45%	0.91%	1.51%
Chaetoceros cf. *borealis*						0.09%		
Chaetoceros cf. *compressus*		0.71%	0.62%		0.15%	0.95%	0.56%	
Chaetoceros concavicornis	0.17%	1.24%	0.90%	0.42%	1.85%	0.77%	0.07%	2.51%
Chaetoceros convolutus					0.65%	0.86%	0.38%	2.59%
Chaetoceros debilis	14.50%	14.89%	10.39%		5.85%	13.49%	1.61%	0.08%
Chaetoceros cf. *decipiens*		0.31%						
Chaetoceros diadema	18.28%	25.24%	10.80%		18.55%	19.62%	9.55%	0.42%
Chaetoceros didymus			0.10%			0.63%		
Chaetoceros furcellatus	4.68%	16.18%	11.74%		3.78%	13.22%	2.59%	0.17%
Chaetoceros radicans					0.35%		0.42%	0.84%
Chaetoceros socialis		1.69%	2.68%			1.71%	0.66%	
Chaetoceros tenuissima	2.11%	1.48%	2.29%		0.17%	0.63%		
Chaetocerous spp.	0.45%	5.91%	7.62%	2.22%	9.16%	14.16%	29.81%	4.68%
Chaetoceros spp. Resting spores		0.17%	0.24%	1.90%	1.00%		0.14%	0.17%
Coscinodiscus centralis				1.37%				0.08%
Coscinodiscus granii				0.21%				
Coscinodiscus marginatus				0.84%	0.08%			0.08%
Coscinodiscus radiatus				1.16%	0.08%			
Coscinodiscus wallesii				0.21%				
Coscinodiscus spp.		0.03%	0.53%	3.60%	0.82%		0.14%	0.50%
Corethron criophilum	0.18%	0.18%	0.07%	5.61%	4.21%	0.54%	0.52%	3.18%
Eucampia antarctica				0.21%	0.09%			
Minidiscus spp.	0.38%	0.89%	1.73%	0.21%	0.35%	0.14%	0.07%	
Odontella aurita	0.01%							
Proboscia alata			0.77%				0.31%	0.08%
Rhizosolenia cf. *borealis*					1.65%			
Rhizosolenia hebetata f. semispina				0.63%				
Rhizosolenia setigera			0.24%	2.12%		0.41%	0.84%	
Rhizosolenia spp.					0.63%			0.25%
Skeletonema sp.								
Shionodiscus oestrupii		0.20%	0.16%	0.64%		0.09%	0.03%	0.75%
Thalassiosira anguste-lineata	0.15%				0.09%			
Thalassiosira bulbosa	0.07%	0.26%	0.33%	3.38%	0.15%	0.14%	0.10%	
Thalassiosira confusa					0.16%			
Thalassiosira eccentrica		0.19%		0.11%	0.08%			
Thalassiosira gravida					0.30%			
Thalassiosira nordenskioeldii	0.10%	0.38%	0.26%	0.53%		0.09%		0.25%
Thalassiosira minima					0.52%			0.17%
Thalassiosira oceanica	0.72%	2.69%	2.77%	0.21%	8.78%	1.80%	0.77%	0.42%
Thalassiosira pacifica	0.01%			0.32%	0.09%			
Thalassiosira proschkinae				0.11%				
Thalassiosira spp.	0.07%	0.35%	0.15%	3.70%	0.82%	0.05%	0.07%	0.67%
Pennate diatoms								
Cylindrotheca closterium		0.98%	1.44%	1.79%	3.98%	0.27%	12.60%	17.73%
Entomoneis spp.					0.09%			
Fragilariopsis cylindrus					1.23%	0.09%		
Fragilariopsis cylindformis	0.10%	0.98%	0.18%	6.87%	1.08%	0.18%		
Fragilariopsis oceanica			0.07%	0.42%	0.58%	0.05%	0.03%	0.17%
Fragilariopsis pseudonana			0.03%	0.42%		0.36%		
Fragilariopsis spp.	5.93%	7.44%	6.26%	10.26%	6.02%	4.15%	1.19%	1.09%
Cf. *Pleurosigma* spp.			0.07%	0.21%		0.05%		
Navicula spp.	0.01%					0.05%		
Neodenticula seminae	1.83%	0.40%	1.23%	10.56%	4.24%	1.22%	0.14%	10.20%
Nitzschia spp.	0.24%	0.55%	0.55%	2.43%	0.08%	0.32%	0.14%	0.08%
Plagiotropis sp.		0.16%	0.07%		0.30%	0.27%	0.28%	0.25%
Pseudogomophonema kamchatkatium							0.03%	
Pseudo-nitzschia spp.	0.09%	4.23%	15.71%	0.21%	1.82%	12.67%	15.19%	13.96%
Thalassionema nitzschioides	0.29%	0.19%	0.34%	5.39%	0.89%	0.18%	0.59%	3.85%
Thalassionema spp.		0.10%		4.87%			0.98%	5.52%
Thalassiothrix longissima	0.01%		0.10%	0.11%	1.69%	0.23%	0.14%	1.59%
Parmales			0.45%					
Tetraparma catinifera		0.46%	0.47%			0.41%		
Tetraparma gracilis	0.15%		0.24%			0.09%		
Tetraparma pelagica	11.72%	1.37%	0.95%		0.09%	0.23%		
Tetraparma spp.	0.76%	0.26%	0.07%					
Triparma columnacea f. convexa	9.50%	1.11%	1.10%		0.09%	0.41%	0.03%	0.17%
Triparma columnacea f. fimbriata	5.59%	0.69%	0.92%			0.72%		
Triparma laevis f. longispina			0.03%			0.05%		
Triparma strigata	10.76%	1.63%	1.46%			0.14%		
Triparma verrucosa	1.79%		0.74%					
Triparma spp.	3.77%	0.51%	0.46%	0.21%	0.09%	0.09%		0.17%
Silicoflagellate								
Dictyocha octonaria			0.08%					
Dictyocha speculum	0.55%	0.32%	0.22%	0.53%	0.17%	0.05%	0.07%	0.25%
Dinoflagellates								
Phalacroma rapa					0.30%			
Phalacroma rotundatum					0.15%	0.05%		0.08%
Ceratium longipes								0.08%
Gymnodinium spp.				0.95%	0.09%	0.09%		0.33%
Gonyalax polygramma				0.11%				0.25%
Gonyalax spp.					0.23%		0.07%	
Prorocentrum spp.		0.12%		1.16%	1.85%	0.09%	0.63%	2.09%
Protoperidinium spp.		0.02%		0.21%	0.08%			0.25%
Pyrophacus horoligium								0.08%
Flagellates								
Ciliates		0.37%	0.07%	9.20%	0.45%	0.09%		0.42%
Choanoflagellates		0.20%	0.65%		0.24%	0.05%		0.67%
Unidentified	0.65%	1.82%	3.76%	11.42%	9.74%	4.47%	17.74%	20.15%

Appendix H. Total iron concentrations (TFe) in the bottles for the Fe enrichment incubation experiments.

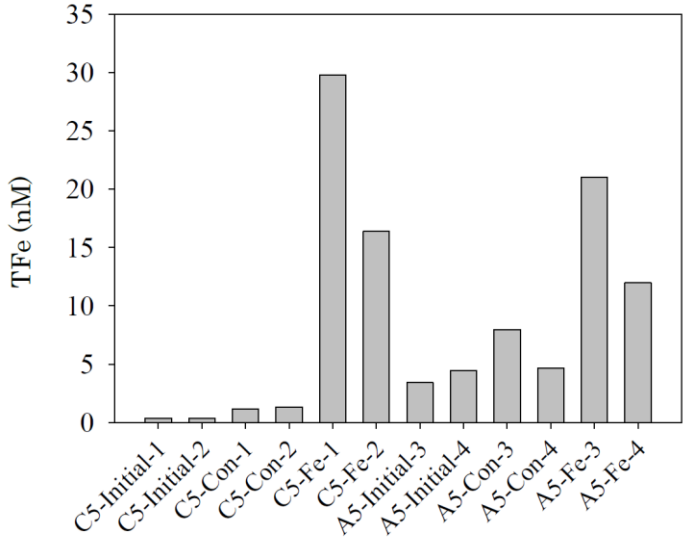

The results of +DFB bottles were excluded from the table because it was not possible to determine effective (i.e., bioavailable) Fe concentration in the bottle and/or released from DFB.

Appendix I. Functional absorption cross section of PSII (σPSII) of phytoplankton determined with FIRe fluorometry from the surface (open bars) and from 5% light depth (closed bars) at stations C5 (two left 4 bars) and A5 (two right bars).

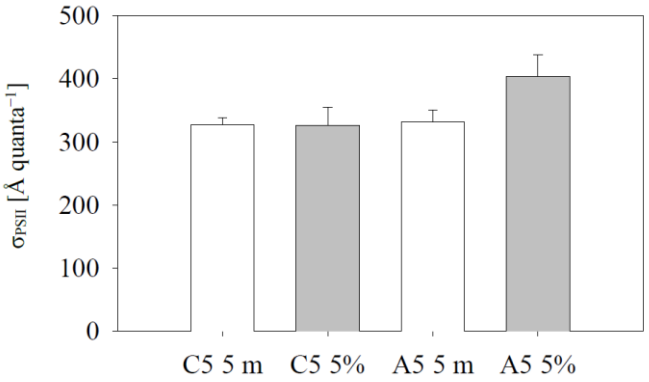

Appendix J. Primer sets and PCR conditions of qPCR and qRT PCR for the photosynthesis-related *psbA* and *rbcL* genes

psbA	
Forward primer	5'-AGAACCACCAAATACACCAGCAA-3'
Reverse primer	5'-TCCAAGCTGAGCACAACATCTT-3'
Amplicon size	71
PCR condition	94 °C for 60 s; 40 cycles under 98 °C for 10 s, 62 °C for 60 s, and 72 °C for 60s
Reference	Krell et al. (2007)
rbcL	
Forward primer	5′-GATGATGARAAYATTAACTCW-3′
Reverse primer	5′-TAWGAACCTTTWACTTCWCC-3′
Amplicon size	113
PCR condition	94 °C for 60 s; 40 cycles under 98 °C for 10 s, 55 °C for 60 s, and 72 °C for 60s
Reference	John et al. (2007); Endo et al. (2015)

Appendix K. Temporal variations in Fe concentrations in under-ice seawater during the LFe incubation experiments.

Treatment	Day	Fe (nM)			Fe' (pM)		
		Ave		SD	Ave		SD
LFe+HL	Ini	23	±	25	4.6	±	5.0
	D00	32	±	0	6.5	±	0.0
	D05	22	±	15	4.4	±	3.1
	D10	38	±	32	7.6	±	6.5
	D15	22	±	15	4.4	±	0.0
	D20	27	±	8	5.4	±	1.5
	Melt	27	±	8	5.4	±	1.5
LFe+LL	Ini	20	±	0	4.1	±	0.0
	D00	22	±	0	4.3	±	0.0
	D05	43	±	22	8.7	±	4.4
	D10	22	±	0	4.4	±	0.0
	D15	33	±	39	6.6	±	7.9
	D20	22	±	15	4.4	±	3.1
	Melt	25	±	0	5.1	±	0.0

LFe: low Fe; HL: high light; LL: low light; Fe': concentrations of inorganic Fe species calculated using the software the software Visual MINTEQ, ver. 3.1 (https://vminteq.lwr.kth.se) based on measure Fe concentration and the EDTA concentration (see section 5.2.1).

During the incubations, high Fe concentrations were opportunistically observed. Pankowski and McMinn (2008a) reported that photosynthetic performance (i.e. F_v/F_m and relative ETR_{max} ($rETR_{max}$) with PAM fluorometry) of *F. cylindrus* isolated from Antarctic pack ice, as this study, was suppressed if Fe' concentration were 5.5 pM. They also observed significant jumps of F_v/F_m and $rETR_{max}$ if Fe' concentration exceeded to 10 pM. Although average Fe' concentrations exceeded to 5.5 pM twice in both treatments, no significant variation was observed during both incubations (One-way ANOVA) due to their large errors. It was evident that the ferrozine method has a limitation due to the low absorbance, the method, however, seemed to be the most powerful way to determine Fe concentration complexed with a high concentration of EDTA because EDTA can interfere the well-established pre-concentration steps. Moreover, the ferrozine method seemed to be relatively sensitive compared with ICP-MS.

REFERENCES

Abe, Y., Yamaguchi, A., Matsuno, K., Kono, T., Imai, I., 2014. Short-term changes in the population structure of hydromedusa *Aglantha digitale* during the spring phytoplankton bloom in the Oyashio region. Bull. Fish. Scicence, Hokkaido Univ. 64, 71–81. https://doi.org/10.14943/bull.fish.64.3.71

Alderkamp, A.C., Kulk, G., Buma, A.G.J., Visser, R.J.W., van Dijken, G.L., Mills, M.M., Arrigo, K.R., 2012. The effect of iron limitation on the photophysiology of *Phaeocystis antarctica* (prymnesiophyceae) and *Fragilariopsis cylindrus* (bacillariophyceae) under dynamic irradiance. J. Phycol. 48, 45–59. https://doi.org/10.1111/j.1529-8817.2011.01098.x

Allen, J.F., Nilsson, A., 1997. Redox signalling and the structural basis of regulation of photosynthesis by protein phosphorylation. Physiol. Plant. 100, 863–868. https://doi.org/10.1034/j.1399-3054.1997.1000412.x

Alou-Font, E., Roy, S., Agustí, S., Gosselin, M., 2016. Cell viability, pigments and photosynthetic performance of Arctic phytoplankton in contrasting ice-covered and open-water conditions during the spring-summer transition. Mar. Ecol. Prog. Ser. 543, 89–106. https://doi.org/10.3354/meps11562

Ambrose, W.G., Von Quillfeldt, C., Clough, L.M., Tilney, P.V.R., Tucker, T., 2005. The sub-ice algal community in the Chukchi sea: Large- and small-scale patterns of abundance based on images from a remotely operated vehicle. Polar Biol. 28, 784–795. https://doi.org/10.1007/s00300-005-0002-8

Aro, E.M., Virgin, I., Andersson, B., 1993. Photoinhibition of Photosystem II. Inactivation, protein damage and turnover. Biochim. Biophys. Acta 1143, 113−114. https://doi.org/10.1016/0005-2728(93)90134-2

Arrigo, K.R., 2017. Sea ice as a habitat for primary producers. In: Thomas, D.N.(ed.), Sea Ice, 3rd edition. Wiley Blackwell. 352−369.

Arrigo, K.R., 2014. Sea Ice Ecosystems. Ann. Rev. Mar. Sci. 6, 439–467. https://doi.org/10.1146/annurev-marine-010213-135103

Arrigo, K.R., Mock, T., Lizotte, M.P., 2010. Primary producers and sea ice. In: Thomas, D.N., Dieckmann, G.S. (eds.), Sea Ice, 2nd edition. Wiley Blackwell. 283−326.

Arrigo, K.R., Sullivan, C.W., 1994. A high resolution bio-optical model of microalgal growth: Tests using sea-ice algal community time-series data. Limnol. Oceanogr. 39, 609–631.

Arrigo, K.R., van Dijken, G.L., 2015. Continued increases in Arctic Ocean primary production. Prog. Oceanogr. 136, 60–70. https://doi.org/10.1016/j.pocean.2015.05.002

Arrigo, K.R., van Dijken, G.L., 2003. Phytoplankton dynamics within 37 Antarctic coastal polynya systems. J. Geophys. Res. 108, 3271. https://doi.org/10.1029/2002JC001739

Arrigo, K.R., van Dijken, G.L., Bushinsky, S., 2008. Primary production in the Southern Ocean, 1997-2006. J. Geophys. Res. Ocean. 113, C08004. https://doi.org/10.1029/2007JC004551

Arrigo, K.R., van Dijken, G.L., Strong, A.L., 2015. Environmental controls of marine productivity hot spots around Antarctica. J. Geophys. Res. Ocean. 120, 5545–5565. https://doi.org/10.1002/2015JC010888.

Arrigo, K.R., Worthen, D.L., Lizotte, M.P., Dixon, P., Dieckmann, G.S., 1997. Primary Production in Antarctic Sea Ice. Science 276, 394–397. https://doi.org/10.1126/science.276.5311.394

Assmy, P., Ehn, J.K., Fernández-Méndez, M., Hop, H., Katlein, C., Sundfjord, A., Bluhm, K., Daase, M., Engel, A., Fransson, A., Granskog, M.A., Hudson, S.R., Kristiansen, S., Nicolaus, M., Peeken, I., Renner, A.H.H., Spreen, G., Tatarek, A., Wiktor, J., 2013. Floating ice-algal aggregates below melting arctic sea ice. PLoS One 8, e76599. https://doi.org/10.1371/journal.pone.0076599

Azam, F., 1998. Microbial Control of Oceanic Carbon Flux. Science 280, 694–696.

Babin, M., 2008. Phytoplankton fluorescence: theory, current literature and in situ measurement. In: Babin, M., Roesler, C., Cullen, J.J. (eds.), Real-time Coastal Observing Systems for Marine Ecosystem Dynamics and Harmful Algal Blooms: Theory, Instrumentation and Modelling. UNESCO, 237−280.

Babin, M., Stramski, D., 2002. Light absorption by aquatic particles in the near-infrared spectral region. Limnol. Oceanogr. 47, 911–915. https://doi.org/10.4319/lo.2002.47.3.0911

Bailleul, B., Berne, N., Murik, O., Petroutsos, D., Prihoda, J., Tanaka, A., Villanova, V., Bligny, R., Flori, S., Falconet, D., Krieger-Liszkay, A., Santabarbara, S., Rappaport, F., Joliot, P., Tirichine, L., Falkowski, P.G., Cardol, P., Bowler, C., Finazzi, G., 2015. Energetic coupling between plastids and mitochondria drives CO_2 assimilation in diatoms. Nature 524, 366–369. https://doi.org/10.1038/nature14599

Bailleul, B., Rogato, A., de Martino, A., Coesel, S., Cardol, P., Bowler, C., Falciatore, A., Finazzi, G., 2010. An atypical member of the light-harvesting complex stress-related protein family modulates diatom responses to light. Proc. Natl. Acad. Sci. 107, 18214–18219. https://doi.org/10.1073/pnas.1007703107/-/DCSupplemental.www.pnas.org/cgi/doi/10.1073/pnas.1007703107

Bannister, T.T., 1974. Production equations in terms of Chlorophyll concentration, quantum yield and upper limit to production. Limnol. Oceanogr. 19, 1–12. https://doi.org/10.4319/lo.1974.19.1.0001

Banse, K., 1995. Community response to IRONEX. Nature 375, 112. https://doi.org/10.1038/375112a0

Banse, K., 1990. Does iron really limit phytoplankton production in the offshore subarctic Pacific? Limnol. Oceanogr. 35, 772–775. https://doi.org/10.4319/lo.1990.35.3.0772

Behrenfeld, M.J., 2010. Abandoning Sverdrup's Critical Depth Hypothesis on phytoplankton blooms. Ecology 91, 977–989. https://doi.org/10.1890/09-1207.1

Behrenfeld, M.J., Falkowski, P.G., 1997. Photosynthetic rates derived from satellite-based Chlorophyll concentration. Limnol. Oceanogr. 42, 1–20. https://doi.org/10.4319/lo.1997.42.1.0001

Behrenfeld, M.J., Halsey, K.H., Milligan, A.J., 2008. Evolved physiological responses of phytoplankton to their integrated growth environment. Philos. Trans. R. Soc. B Biol. Sci. 363, 2687–2703. https://doi.org/10.1098/rstb.2008.0019

Behrenfeld, M.J., Hu, Y., O'Malley, R.T., Boss, E.S., Hostetler, C.A., Siegel, D.A., Sarmiento, J.L., Schulien, J., Hair, J.W., Lu, X., Rodier, S., Scarino, A.J., 2017. Annual boom-bust cycles of polar phytoplankton biomass revealed by space-based lidar. Nat. Geosci. 10, 118–122. https://doi.org/10.1038/ngeo2861

Behrenfeld, M.J., Milligan, A.J., 2013. Photophysiological expressions of iron stress in phytoplankton. Ann. Rev. Mar. Sci. 5, 217–246. https://doi.org/10.1146/annurev-marine-121211-172356

Behrenfeld, M.J., Prasil, O., Babin, M., Bruyant, F., 2004. In search of a physiological basis for covariations in light-limited and light-saturated photosynthesis. J. Phycol. 40, 4–25. https://doi.org/10.1046/j.1529-8817.2004.03083.x

Behrenfeld, M.J., Prasil, O., Kolber, Z.S., Babin, M., Falkowski, P.G., 1998. Compensatory changes in Photosystem II electron turnover rates protect photosynthesis from photoinhibition. Photosynth. Res. 58, 259–268. https://doi.org/10.1023/A:1006138630573

Behrenfeld, M.J., Randerson, J.T., McClain, C.R., Feldman, G.C., Los, S.O., Tucker, C.J., Falkowski, P.G., Field, C.B., Frouin, R., Esaias, W.E., Kolber, D.D., Pollack, N.H., 2001. Biospheric primary production during an ENSO transition. Science 291, 2594–2597. https://doi.org/10.1126/science.1055071

Bernard, K., Gunther, L., Mahaffey, S., Qualls, K., Sugla, M., Saenz, B., Cossio, A., Walsh, J., Reiss, C., 2018. The contribution of ice algae to the winter energy budget of juvenile Antarctic krill in years with contrasting sea ice conditions. ICES J. Mar. Sci. https://doi.org/10.1093/icesjms/fsy145

Berner, T., Dubinsky, Z., Wyman, K., Falkowski, P.G., 1989. Photoadaptation and the "package" effect in *Dunaliella tertiolecta* (Chlorophyceae). J. Phycol. 25, 70–78. https://doi.org/10.1111/j.0022-3646.1989.00070.x

Bidigare, R.R., Frank, T.J., Zastrow, C., Brooks, J.M., 1986. The distribution of algal Chlorophylls and their degradation products in the Southern Ocean. Deep Sea Res. Part A, Oceanogr. Res. Pap. 33, 923–937. https://doi.org/10.1016/0198-0149(86)90007-5

Bluhm, B.A., Gradinger, R.R., Schnack-Schiel, S.B., 2010. Sea ice meio- and macrofauna. In: Thomas, D.N. (eds.), Dieckmann, G.S., Sea Ice, 2nd edition. Wiley Blackwell. 357−394.

Boetius, A., Albrecht, S., Bakker, K., Bienhold, C., Felden, J., Fernandez-Mendez, M., Hendricks, S.,

Katlein, C., Lalande, C., Krumpen, T., Nicolaus, M., Peeken, I., Rabe, B., Rogacheva, A., Rybakova, E., Somavilla, R., Wenzhofer, F., 2013. Export of algal biomass from the melting Arctic sea ice. Science 339, 1430–1432. https://doi.org/10.1126/science.1231346

Boetius, A., Anesio, A.M., Deming, J.W., Mikucki, J., Rapp, J.Z., 2015. Microbial ecology of the cryosphere : sea ice and glacial habitats. Nat. Rev. Microbiol. 13, 1–14. https://doi.org/10.1038/nrmicro3522

Bowman, J.S., 2015. The relationship between sea ice bacterial community structure and biogeochemistry: A synthesis of current knowledge and known unknowns. Elem. Sci. Anthr. 3, 000072. https://doi.org/10.12952/journal.elementa.000072

Boyd, P.W., Jickells, T., Law, C.S., Blain, S., Boyle, E.A., Buesseler, K.O., Coale, K.H., Cullen, J.J., de Baar, H.J.W., Follows, M., Harvey, M., Lancelot, C., Levasseur, M., Owens, N.P.J., Pollard, R., Rivkin, R.B., Sarmiento, J., Schoemann, V., Smetacek, V., Takeda, S., Tsuda, A., Turner, S., Watson, A.J., 2007. Mesoscale iron enrichment experiments 1993-2005: synthesis and future directions. Science 315, 612–617. https://doi.org/10.1126/science.1131669

Boyd, P.W., Lennartz, S.T., Glover, D.M., Doney, S.C., 2015. Biological ramifications of climate-change-mediated oceanic multi-stressors. Nat. Clim. Chang. 5, 71–79. https://doi.org/10.1038/nclimate2441

Boyd, P.W., Strzepek, R., Fu, F., Hutchins, D.A., 2010. Environmental control of open-ocean phytoplankton groups: Now and in the future. Limnol. Oceanogr. 55, 1353–1376. https://doi.org/10.4319/lo.2010.55.3.1353

Boye, M., Nishioka, J., Croot, P., Laan, P., Timmermans, K.R., Strass, V.H., Takeda, S., de Baar, H.J.W., 2010. Significant portion of dissolved organic Fe complexes in fact is Fe colloids. Mar. Chem. 122, 20–27. https://doi.org/10.1016/j.marchem.2010.09.001

Boye, M., van den Berg, C.M.G., de Jong, J.T.M., Leach, H., Croot, P., de Baar, H.J.W., 2001. Organic complexation of iron in the Southern Ocean. Deep. Res. I 48, 1477–1497.

Breitbarth, E., Gelting, J., Walve, J., Hoffmann, L.J., Turner, D.R., Hassellov, M., Ingri, J., 2009. Dissolved iron (II) in the Baltic Sea surface water and implications for cyanobacterial bloom development. Biogeosciences 6, 2397–2420.

Bricaud, A., Babin, M., Morel, A., Claustre, H., 1995. Variability in the Chlorophyll-specific absorption coefficients of natural phytoplankton : Analysis and parameterization. J. Geophys. Res. 100, 13321–13332.

Bruyant, F., Babin, M., Genty, B., Prasil, O., Behrenfeld, M.J., Claustre, H., Bricaud, A., Garczarek, L., Holtzendorff, J., Koblizek, M., Dousova, H., Partensky, F., 2005. Diel variations in the photosynthetic parameters of *ProChlorococcus* strain PCC 9511:Combined effects of light and cell cycle. Limnol. Oceanogr. 50, 850–863. https://doi.org/10.4319/lo.2005.50.3.0850

Büchel, C., Wilhelm, C., 1993. In vivo analysis of slow Chlorophyll fluorescence induction kinetics in algae: progress, problems and perspectives. Photochem. Photobiol. 58, 137–148. https://doi.org/10.1111/j.1751-1097.1993.tb04915.x

Cardol, P., Forti, G., Finazzi, G., 2011. Regulation of electron transport in microalgae. Biochim. Biophys. Acta - Bioenerg. 1807, 912–918. https://doi.org/10.1016/j.bbabio.2010.12.004

Caron, L., Berkaloff, C., Duval, J.-C., Jupin, H., 1987. Chlorophyll fluorescence transients from the diatom *Phaeodactylum tricornutum*: relative rates of cyclic phosphorulation and Chlororespiration. Photosynth. Res. 11, 131–139. https://doi.org/10.1163/026805597125825717

Chiba, S., Ono, T., Tadokoro, K., Midorikawa, T., Saino, T., 2004. Increased stratification and decreased lower trophic level productivity in the Oyashio region of the North Pacific: A 30-year retrospective study. J. Oceanogr. 60, 149–162. https://doi.org/10.1023/B:JOCE.0000038324.14054.cf

Claustre, H., Babin, M., Merien, D., Ras, J., Prieur, L., Dallot, S., Prasil, O., Dousova, H., Moutin, T., 2005. Toward a taxon-specific parameterization of bio-optical models of primary production: A case study in the North Atlantic. J. Geophys. Res. C Ocean. 110, C07S12. https://doi.org/10.1029/2004JC002634

Cleveland, J.S., Weidemann, A.D., 1993. Quantifying absorption by aquatic particles: A multiple scattering correction for glass-fiber filters. Limnol. Oceanogr. 38, 1321–1327. https://doi.org/10.4319/lo.1993.38.6.1321

Cohen, N.R., Ellis, K.A., Lampe, R.H., McNair, H., Twining, B.S., Maldonado, M.T., Brzezinski,

M.A., Kuzminov, F.I., Thamatrakoln, K., Till, C.P., Bruland, K.W., Sunda, W.G., Bargu, S., Marchetti, A., 2017. Diatom transcriptional and physiological responses to changes in iron bioavailability across ocean provinces. Front. Mar. Sci. 4, 1–20. https://doi.org/10.3389/fmars.2017.00360

Constable, A.J., Melbourne-Thomas, J., Corney, S.P., Arrigo, K.R., Barbraud, C., Barnes, D.K.A., Bindoff, N.L., Boyd, P.W., Brandt, A., Costa, D.P., Davidson, A.T., Ducklow, H.W., Emmerson, L., Fukuchi, M., Gutt, J., Hindell, M.A., Hofmann, E.E., Hosie, G.W., Iida, T., Jacob, S., Johnston, N.M., Kawaguchi, S., Kokubun, N., Koubbi, P., Lea, M.A., Makhado, A., Massom, R.A., Meiners, K., Meredith, M.P., Murphy, E.J., Nicol, S., Reid, K., Richerson, K., Riddle, M.J., Rintoul, S.R., Smith, W.O., Southwell, C., Stark, J.S., Sumner, M., Swadling, K.M., Takahashi, K.T., Trathan, P.N., Welsford, D.C., Weimerskirch, H., Westwood, K.J., Wienecke, B.C., Wolf-Gladrow, D., Wright, S.W., Xavier, J.C., Ziegler, P., 2014. Climate change and Southern Ocean ecosystems I: How changes in physical habitats directly affect marine biota. Glob. Chang. Biol. 20, 3004–3025. https://doi.org/10.1111/gcb.12623

Cosgrove, J., Borowitszka, M., 2011. Chlorophyll fluorescence terminology: An introduction. In: Suggett, D.J. (eds.), Prášil, O., Borowitzka, M., Chlorophyll *a* Fluorescence in Aquatic Sciences: Methods and Applications. Springer. 1−19.

Cox, G.F.N., Weeks, W.F., 1983. Equations for determining the gas and brine volumes in sea-ice samples. J. Glaciol. 29, 306–316. https://doi.org/10.1017/S0022143000008364

Crafts-Brandner, S.J., Salvucci, M.E., 2000. Rubisco activase constrains the photosynthetic potential of leaves at high temperature and CO_2. Proc. Natl. Acad. Sci. U. S. A. 97, 13430–13435. https://doi.org/10.1073/pnas.230451497

Cutter, G., Andersson, P., Codispoti, L., Croot, P., Francois, R., Lohan, M., Obata, H., Rutgers van der Loeff, M., 2010. Sampling and sample handling protocol for GEOTRACES cruises. Available at: http://www.geotraces.org/library/geotraces-policies/170-sampling-and-sample-handling-protocols-for-geotraces-cruises

D'Haene, S.E., Sobotka, R., Bu, L., Dekker, J.P., Komenda, J., 2015. Interaction of the PsbH subunit with a Chlorophyll bound to histidine 114 of CP47 is responsible for the red 77 K fl uorescence of Photosystem II. Biochim. Biophys. Acta 1847, 1327–1334. https://doi.org/10.1016/j.bbabio.2015.07.003

de Baar, H.J.W., de Jong, J.T.M., Bakker, D.C.E., Löscher, B.M., Veth, C., Bathmann, U. V., Smetacek, V., 1995. Importance of iron for plankton blooms and carbon dioxide drawdown in the Southern Ocean. Nature 412−415. https://doi.org/10.1038/373412a0

de Salas, M.F., Eriksen, R., Davidson, A.T., Wright, S.W., 2011. Protistan communities in the Australian sector of the Sub-Antarctic Zone during SAZ-Sense. Deep. Res. Part II Top. Stud. Oceanogr. 58, 2135–2149. https://doi.org/10.1016/j.dsr2.2011.05.032

Deppeler, S.L., Davidson, A.T., 2017. Southern Ocean Phytoplankton in a Changing Climate. Front. Mar. Sci. 4, 40. https://doi.org/10.3389/fmars.2017.00040

Descolas-Gros, C., de Billy, G., 1987. Temperature adaptation of RuBP carboxylase: kinetic properties in marine Antarctic diatoms. J. Exp. Mar. Bio. Ecol. 108, 147–158. https://doi.org/10.1016/S0022-0981(87)80019-9

Devos, N., Ingouff, M., Loppes, R., Matagne, R.F., 1998. Rubisco adaptation to low temperatures: a comparative study in psychrophilic and mesophilic unicellular algae. J. Phycol. 34, 655–660. https://doi.org/10.1046/j.1529-8817.1998.340655.x

Domingues, N., Matos, A.R., da Silva, J.M., Cartaxana, P., 2012. Response of the Diatom Phaeodactylum tricornutum to photooxidative stress resulting from high light exposure. PLoS One 7, 1–6. https://doi.org/10.1371/journal.pone.0038162

Eckardt, N.A., 2005. Photorespiration Revisited. Plant Cell 17, 2139–2141. https://doi.org/10.1105/tpc.105.035873

Edelman, M., Mattoo, A.K., 2008. D1-protein dynamics in photosystem II: The lingering enigma. Photosynth. Res. https://doi.org/10.1007/s11120-008-9342-x

Eicken, H., 2009. Ice sampling and basic sea ice core analysis. In: Eicken, H., Gradinder, R., Salganek, M., Shirasawa, K., Perovich, D., Leppäranta, M. (eds.), Field Techniques for Sea Ice Research. University of Alaska Press. 117−140.

Ellis, R.J., 2010. Tackling unintelligent design. Nature 463, 164–165.

https://doi.org/10.1029/2008GL036500
Endo, H., Ogata, H., Suzuki, K., 2018. Contrasting biogeography and diversity patterns between diatoms and haptophytes in the central Pacific Ocean. Sci. Rep. 1–30. https://doi.org/10.1038/s41598-018-29039-9
Endo, H., Sugie, K., Yoshimura, T., Suzuki, K., 2016. Response of spring diatoms to CO_2 availability in the western North Pacific as determined by next-generation sequencing. PLoS One 11, e0154291. https://doi.org/10.1371/journal.pone.0154291
Endo, H., Sugie, K., Yoshimura, T., Suzuki, K., 2015. Effects of CO_2 and iron availability on *rbc* gene expression in Bering Sea diatoms. Biogeosciences 12, 2247–2259. https://doi.org/10.5194/bg-12-2247-2015
Endo, H., Yoshimura, T., Kataoka, T., Suzuki, K., 2013. Effects of CO_2 and iron availability on phytoplankton and eubacterial community compositions in the northwest subarctic Pacific. J. Exp. Mar. Bio. Ecol. 439, 160–175. https://doi.org/10.1016/j.jembe.2012.11.003
Ensminger, I., Busch, F., Huner, N.P.A., 2006. Photostasis and cold acclimation: Sensing low temperature through photosynthesis. Physiol. Plant. 126, 28–44. https://doi.org/10.1111/j.1399-3054.2006.00627.x
Eppley, R.W., 1972. Temperature and phytoplankton growth in the sea. Fish. Bull. 70, 1063–1085. https://doi.org/163346
Eriksen, R., Trull, T.W., Davies, D., Jansen, P., Davidson, A.T., Westwood, K., van den Enden, R., 2018. Seasonal succession of phytoplankton community structure from autonomous sampling at the Australian Southern Ocean Time Series site. Mar. Ecol. Prog. Ser. 589, 13–31. https://doi.org/10.3354/meps12420
Falkowski, P.G., 1994. The role of phytoplankton photosynthesis in global biogeochemical cycles. Photosynth. Res. 39, 235–258. https://doi.org/10.1007/BF00014586
Falkowski, P.G., Greene, R.M., Geider, R.J., 1992. Physiological limitations on phytoplankton productivity in the ocean. Oceanography 5, 84–91.
Falkowski, P.G., Laws, E.A., Barber, R., Murray, J., 2003. Phytoplankton and their role in primary, new, and export production. Ocean Biogeochem. 99–121. https://doi.org/10.1007/978-3-642-55844-3_5
Falkowski, P.G., Owens, T.G., 1980. Light-shade adaptation: Two Strategies in marine phytoplankton. Plant Physiol. 66, 592–595. https://doi.org/10.1104/pp.66.4.592
Falkowski, P.G., Raven, J.A., 2013. Aquatic photosynthesis. Princeton University Press.
Farid, H.T., Schulz, K.G., Rose, A.L., 2018. Measurering total Fe concentrations in phytoplankton cultures in the presence of synthetic and organic ligands using a modified ferrozine method. Mar. Chem. 203, 22−27.
Feikema, W.O., Marosvölgyi, M.A., Lavaud, J., van Gorkom, H.J., 2006. Cyclic electron transfer in photosystem II in the marine diatom Phaeodactylum tricornutum. Biochim. Biophys. Acta 1757, 829–834. https://doi.org/10.1016/j.bbabio.2006.06.003
Fernández-Méndez, M., Katlein, C., Rabe, B., Nicolaus, M., Peeken, I., Bakker, K., Flores, H., Boetius, A., 2015. Photosynthetic production in the central Arctic Ocean during the record sea-ice minimum in 2012. Biogeosciences 12, 3525–3549. https://doi.org/10.5194/bg-12-3525-2015
Fernández-Méndez, M., Wenzhöfer, F., Peeken, I., Sørensen, H.L., Glud, R.N., Boetius, A., 2014. Composition, buoyancy regulation and fate of ice algal aggregates in the Central Arctic Ocean. PLoS One 9, e107452. https://doi.org/10.1371/journal.pone.0107452
Field, C.B., Behrenfeld, M.J., Randerson, J.T., Falkowski, P., 1998. Primary production of the biosphere: Integrating terrestrial and oceanic components. Science 281, 237–240. https://doi.org/10.1126/science.281.5374.237
Forbes, J.R., Denman, K.L., Mackas, D.L., 1986. Determinations of photosynthetic capacity in coastal marine phytoplankton: Effects of assay irradiance and variability of photosynthetic parameters. Mar. Ecol. Prog. Ser. 32, 181–191. https://doi.org/10.3354/meps032181
Fujiki, T., Matsumoto, K., Mino, Y., Sasaoka, K., Wakita, M., Kawakami, H., Honda, M.C., Watanabe, S., Saino, T., 2014. Seasonal cycle of phytoplankton community structure and photophysiological state in the western subarctic gyre of the North Pacific. Limnol. Oceanogr. 59, 887–900. https://doi.org/10.4319/lo.2014.59.3.0887

Furuya, K., Hasegawa, O., Yoshikawa, T., Taguchi, S., 1998. Photosynthesis-irradiance relationship of phytoplankton and primary production in the vicinity of Kuroshio warm core ring in spring. J. Oceanogr. 54, 545–552. https://doi.org/10.1007/BF02742456

Galindo, V., Gosselin, M., Lavaud, J., Mundy, C.J., Else, B., Ehn, J., Babin, M., Rysgaard, S., 2017. Pigment composition and photoprotection of Arctic sea ice algae during spring. Mar. Ecol. Prog. Ser. 585, 49–69.

Garrison, D.L., 1991. Antarctic sea ice biota. Am. Zool. 31, 17–33. https://doi.org/10.1093/icb/31.1.17

Garrison, D.L., Buck, K.R., 1986. Organism losses during ice melting: a serious bias in sea ice community studies. Polar Biol. 6, 237–239.

Gasol, J. M., Kirchman, D.L., 2018. Microbial Ecology of the Oceans, 3rd Edition. Wiley Blackwell, 528 pp.

Geider, R.J., La Roche, J., 1994. The role of iron in phytoplankton photosynthesis, and the potential for iron-limitation of primary productivity in the sea. Photosynth. Res. 39, 275–301. https://doi.org/10.1007/BF00014588

Geider, R.J., MacIntyre, H.L., Kana, T.M., 1997. Dynamic model of phytoplankton growth and acclimation: Responses of the balanced growth rate and the Chlorophyll *a*:carbon ratio to light, nutrient-limitation and temperature. Mar. Ecol. Prog. Ser. 148, 187–200. https://doi.org/10.3354/meps148187

Geider, R.J., Moore, C.M., Suggett, D.J., 2014. Ecology of marine phytoplankton. In: Monson, R.K. (ed.), Ecology and Environment. Springer. 483−531.

Genty, B., Briantais, J.-M., Baker, N.R., 1989. The relationship between the quantum yield of photosynthetic electron transport and quenching of Chlorophyll fluorescence. Biochim. Biophys. Acta 990, 87–92. https://doi.org/10.1016/S0304-4165(89)80016-9

Georg, J., Kostova, G., Vuorijoki, L., Schön, V., Kadowaki, T., Huokko, T., Baumgartner, D., Müller, M., Klähn, S., Allahverdiyeva, Y., Hihara, Y., Futschik, M.E., Aro, E.M., Hess, W.R., 2017. Acclimation of oxygenic photosynthesis to iron starvation is controlled by the sRNA IsaR1. Curr. Biol. 27, 1425–1436.e7. https://doi.org/10.1016/j.cub.2017.04.010

Gibson, J.A.E., Trull, T.W., 1999. Annual cycle of fCO2 under sea-ice and in open water in Prydz Bay, East Antractica. Mar. Chem. 66, 187–200.

Gledhill, M., Buck, K., 2012. The organic complexation of iron in the marine environment: a review. Front. Microbiol. 3, 69. https://doi.org/10.3389/fmicb.2012.00069

Goss, R., Jakob, T., 2010. Regulation and function of xanthophyll cycle-dependent photoprotection in algae. Photosynth. Res. 106, 103–122. https://doi.org/10.1007/s11120-010-9536-x

Goss, R., Lepetit, B., 2015. Biodiversity of NPQ. J. Plant Physiol. 172, 13–32. https://doi.org/10.1016/j.jplph.2014.03.004

Gosselin, M., Levasseur, M., Wheeler, P.A., 1997. New measurements of phytoplankton and ice algal production in the Arctic Ocean. Deep Sea Res. II 44, 1623−1644.

Govindjee, 1995. Sixty-three years since Kautsky: Chlorophyll *a* fluorescence. Aust. J. Plant Physiol. 22, 131−160. https://doi.org/10.1071/PP9950131

Grant, B.R., 1967. Growth of *Cylindrotheca closterium* var. *california* (Mereschk.) Reinmann & Lewin on nitrate, ammonia, and urea. Mar. Freshw. Res. 18, 129–136.

Greene, R.M., Geider, R.J., Falkowski, P.G., 1991. Effect of iron limitation on photosynthesis in a marine diatom. Limnol. Oceanogr. 36, 1772–1782. https://doi.org/10.4319/lo.1991.36.8.1772

Greene, R.M., Geider, R.J., Kolber, Z., Falkowski, P.G., 1992. Iron-induced changes in light harvesting and photochemical energy conversion processes in eukaryotic marine algae. Plant Physiol. 100, 565–575. https://doi.org/10.1104/pp.100.2.565

Grose, M., McMinn, A., 2003. Algal biomass in east Antarctic Pack Ice: how much is in the east? In: Huiskes, A.H.L., Gieskes, W.W.C., Roema, J., Schorno, R.M.L., van der Vies, S.M., Wolff, W.J. (eds.), Antarctic Biology in a Global Context: VIIIth SCAR International Biology Symposium 2003, 21-25.

Grossart, H.-P., Czub, G., Simon, M., 2006. Algae-bacteria interactions and their effects on aggregation and organic matter flux in the sea. Environ. Microbiol. 8, 1074–1084. https://doi.org/10.1111/j.1462-2920.2006.00999.x

Grotti, M., Soggia, F., Ianni, C., Frache, R., 2005. Trace metals distributions in coastal sea ice of Terra Nova Bay, Ross Sea, Antarctica. Antarc. Sci. 17, 289–300. https://doi.org/10.1017/S0954102005002695

Gruber, N., Keeling, C.D., Bates, N.R., 2002. Interannual variability in the North Atlantic Ocean carbon sink. Science 298, 2374–2379.

Haecky, P., Jonsson, S., Andersson, A., 1998. Influence of sea ice on the composition of the spring phytoplankton bloom in the northern Baltic Sea. Polar Biol. 20, 1–8. https://doi.org/10.1007/s003000050270

Hama, T., Miyazaki, T., Ogawa, Y., Iwakuma, T., Takahashi, M., Otsuki, A., Ichimura, S., 1986. Measurement of photosynthetic production of a marine phytoplankton population using a stable ^{13}C isotope. Mar. Biol. 73, 31–36.

Harrison, W.G., Platt, T., 1986. Photosynthesis-irradiance relationships in polar and temperate phytoplankton populations. Polar Biol. 5, 153–164. https://doi.org/10.1007/BF00441695

Harvey, H.W., 1933. On the rate of diatom growth. J. Mar. Biol. Assoc. United Kingdom 19, 253–276.

Hasle, G.R., Syvertsen, E.E., 1997. Marine Diatoms. In: Tomas, C.R. (ed.), Identifying Maine Phytoplankton. Academic Press, 5−386.

Hassler, C.S., Schoemann, V., 2009. Bioavailability of organically bound Fe to model phytoplankton of the Southern Ocean. Biogeosciences 6, 2281–2296. https://doi.org/10.5194/bg-6-2281-2009

Hassler, C.S., Norman, L., Mancuso Nichols, C.A., Clementson, L.A., Robinson, C., Schoemann, V., Watson, R.J., Doblin, M.A., 2015. Iron associated with exopolymeric substances is highly bioavailable to oceanic phytoplankton. Mar. Chem. 173, 136–147. https://doi.org/10.1016/j.marchem.2014.10.002

Hassler, C.S., Schoemann, V., Nichols, C.M., Butler, E.C. V., Boyd, P.W., 2011. Saccharides enhance iron bioavailability to Southern Ocean phytoplankton. Proc. Natl. Acad. Sci. 108, 1076–1081. https://doi.org/10.1073/pnas.1010963108

Hassler, C.S., van den Berg, C.M.G., Boyd, P.W., 2017. Toward a regional classification to provide a more inclusive examination of the ocean biogeochemistry of iron-binding ligands. Front. Mar. Sci. 4, 1–19. https://doi.org/10.3389/fmars.2017.00019

Hattori-Saito, A., Nishioka, J., Ono, T., McKay, R.M.L., Suzuki, K., 2010. Iron deficiency in micro-sized diatoms in the Oyashio region of the Western subarctic Pacific during spring. J. Oceanogr. 66, 105–115. https://doi.org/10.1007/s10872-010-0009-9

Hegseth, E.N., 1992. Sub-ice algal assemblages of the Barents Sea: Species composition, chemical composition, and growth rates. Polar Biol. 12, 485–496. https://doi.org/10.1007/BF00238187

Hill, R., Larkum, A.W.D., Prášil, O., Kramer, D.M., Szabó, M., Kumar, V., Ralph, P.J., 2012. Light-induced dissociation of antenna complexes in the symbionts of scleractinian corals correlates with sensitivity to coral bleaching. Coral Reefs 31, 963–975. https://doi.org/10.1007/s00338-012-0914-z

Hirata, T., Hardman-Mountford, N.J., Brewin, R.J.W., Aiken, J., Barlow, R., Suzuki, K., Isada, T., Howell, E., Hashioka, T., Noguchi-Aita, M., Yamanaka, Y., 2011. Synoptic relationships between surface Chlorophyll-*a* and diagnostic pigments specific to phytoplankton functional types. Biogeosciences 8, 311−327. http://doi.org/10.5194/bg-8-311-2011.

Hirata, T., Suzuki, K., 2017. Seasonal effects of photophysiology and Chlorophyll *a* abundance on phytoplankton group-specific primary production in the Kuroshio region as revealed by SeaStar/SeaWiFS. Biogeosciences Discuss. 1–28. https://doi.org/10.5194/bg-2017-164

Hirawake, T., Shinmyo, K., Fujiwara, A., Saitoh, S.-I., 2012. Satellite remote sensing of primary productivity in the Bering and Chukchi Seas using an absorption-based approach. ICES J. Mar. Sci. 69, 1194–1204. https://doi.org/10.1093/icesjms/fss111

Hirawake, T., Takao, S., Horimoto, N., Ishimaru, T., Yamaguchi, Y., Fukuchi, M., 2011. A phytoplankton absorption-based primary productivity model for remote sensing in the Southern Ocean. Polar Biol. 34, 291–302. https://doi.org/10.1007/s00300-010-0949-y

Hoegh-Gludberg, O., Bruno, J.F., 2010. The impact of climate change on the world's marine ecosystems. Sceince 328, 1523–1529.

Honda, M.C., 2003. Biological pump in northwestern North Pacific. J. Oceanogr. 59, 671–684.

https://doi.org/10.1023/B:JOCE.0000009596.57705.0c
Honjo, S., Manganini, S.J., Wefer, G., 1988. Annual particle fulx and a winter outburst of sedimentation in the northern Norwegian Sea. Deep. Res. 35, 1223–1234.
Hooker, S.B., Morrow, J.H., Matsuoka, A., 2013. Apparent optical properties of the Canadian Beaufort Sea - Part 2: The 1% and 1 cm perspective in deriving and validating AOP data products. Biogeosciences 10, 4511–4527. https://doi.org/10.5194/bg-10-4511-2013
Hopkinson, B.M., Barbeau, K.A., 2008. Interactive influences of iron and light limitation on phytoplankton at subsurface Chlorophyll maxima in the eastern North Pacific. Limnol. Oceanogr. 53, 1303–1318. https://doi.org/10.4319/lo.2008.53.4.1303
Horner, R.A., Sea ice biota. CRC Press, 215pp.
Horner, R., Ackley, S.F., Dieckmann, G.S., Gulliksen, B., Hoshiai, T., Legendre, L., Melnikov, I.A., Reeburgh, W.S., Spindler, M., Sullivan, C.W., 1992. Ecology of sea ice biota 1.Habitat, terminology, and methodology. Polar Biol. 12, 4417–427. https://doi.org/10.1007/BF00243114
Hooker, S.B., 2014. Mobilization protocols for hybrid sensors for environmental AOP sampling (HySEAS) observations. In: NASA Tech. Pub. NASA Goddard Space Flight Center, Greenbelt, Maryland, pp. 105 2014−217518.
Huner, N.P.A., Öquist, G., Melis, A., 2003. Photostasis in plants, green algae and cyanobacteria: the role of light harvesting antenna complexes. In: Green, B.R., Parson, W.W., (eds.) Advances in Photosynthesis and Respiration Light Harvesting Antennas in Photosynthesis. Kluwer Academic Publishers, Dordrecht, 401–421.
Huner, N.P.A., Öquist, G., Sarhan, F., 1998. Energy balance and acclimation to light and cold. Trends Plant Sci. 3, 224–230. https://doi.org/10.1016/S1360-1385(98)01248-5
Huot, Y., Babin, M., 2011. Overview of fluorescence protocols: Theory, basic concepts, and practice. In: Suggett, D.J., Prášil, O., Borowitzka, M. (eds.), Chlorophyll *a* Fluorescence in Aquatic Sciences: Methods and Applications. Springer. 31−74.
Hutchins, D.A., DiTullio, G.R., Zhang, Y., Bruland, K.W., 1998. An iron limitation mosaic in the Californian upwelling regime. Limnol. Oceanogr. 43, 1037–1054.
Hutchins, D.A., Franck, V.M., Brzezinski, M.A., Bruland, K.W., 1999a. Inducing phytoplankton iron limitation in iron-replete coastal waters with a strong chelating ligand. Limnol. Oceanogr. 44, 1009–1018. https://doi.org/10.4319/lo.1999.44.4.1009
Hutchins, D.A., Witter, A.E., Butler, A., Luther, G.W., 1999b. Competition among marine phytoplankton for different chelated iron species. Nature 400, 858–861. https://doi.org/Doi 10.1038/23680
Ikeda, T., Shiga, N., Yamaguchi, A., 2008. Structure, biomass distribution and trophodynamics of the pelagic ecosystem in the Oyashio region, western subarctic Pacific. J. Oceanogr. 64, 339–354. https://doi.org/10.1007/s10872-008-0027-z
Isada, T., Hattori-Saito, A., Saito, H., Ikeda, T., Suzuki, K., 2010. Primary productivity and its bio-optical modeling in the Oyashio region, NW Pacific during the spring bloom 2007. Deep. Res. II 57, 1653–1664. https://doi.org/10.1016/j.dsr2.2010.03.009
Isada, T., Hattori-Saito, A., Saito, H., Kondo, Y., Nishioka, J., Kuma, K., Hattori, H., McKay, R.M.L., Suzuki, K., 2018. Responses of phytoplankton assemblages to iron availability and mixing water masses during the spring bloom in the Oyashio region, NW Pacific. Limnol. Oceanogr. 1–20. https://doi.org/10.1002/lno.11031
Isada, T., Iida, T., Liu, H., Saitoh, S.I., Nishioka, J., Nakatsuka, T., Suzuki, K., 2013. Influence of Amur River discharge on phytoplankton photophysiology in the Sea of Okhotsk during late summer. J. Geophys. Res. Ocean. 118, 1995–2013. https://doi.org/10.1002/jgrc.20159
Isada, T., Kuwata, A., Saito, H., Ono, T., Ishii, M., Yoshikawa-Inoue, H., Suzuki, K., 2009. Photosynthetic features and primary productivity of phytoplankton in the Oyashio and Kuroshio-Oyashio transition regions of the northwest Pacific. J. Plankton Res. 31, 1009–1025. https://doi.org/10.1093/plankt/fbp050
Isoda, Y., Kishi, M., 2003. A summary of “coastal Oyashio” symposium (in Japanese). Bull. Coast. Ocean. 41, 1–3.
Jassby, A.D., Platt, T., 1976. Mathematical formulation of the relationship between photosynthesis and light for phytoplankton. Limnol. Oceanogr. 21, 540–547.

https://doi.org/10.4319/lo.1976.21.4.0540
Jeffrey, S.W.& G.M.H., 1987. Chlorophyllase distribution in ten classes of phytoplankton: a problem for Chlorophyll analysis. Mar. Ecol. Prog. Ser. 35, 293–304. https://doi.org/10.3354/meps035293
Jeffrey, S.W., Mantoura, R.F., Wright, S.W., 1997. Phytoplankton pigments in oceanography: guidelines to modern methods. Unesco Publishing.
Jiao, N., Herndl, G.J., Hansell, D.A., Benner, R., Kattner, G., Wilhelm, S.W., Kirchman, D.L., Weinbauer, M.G., Luo, T., Chen, F., Azam, F., 2010. Microbial production of recalcitrant dissolved organic matter: long-term carbon storage in the global ocean. Nat. Rev. Microbiol. 8, 593–599. https://doi.org/10.1038/nrmicro2386
Jing, H., Cheung, S., Xia, X., Suzuki, K., Nishioka, J., Liu, H., 2017. Geographic distribution of ammonia-oxidizing archaea along the kuril Islands in the western subarctic Pacific. Front. Microbiol. 8, 1–12. https://doi.org/10.3389/fmicb.2017.01247
Jing, H., Liu, H., Suzuki, K., 2009. Phylogenetic diversity of marine *Synechococcus* spp. in the Sea of Okhotsk. Aquat. Microb. Ecol. 56, 55–63. https://doi.org/10.3354/ame01316
John, D.E., Patterson, S.S., Paul, J.H., 2007. Phytoplankton-group specific quantitative polymerase chain reaction assays for RuBisCO mRNA transcripts in seawater. Mar. Biotechnol. 9, 747–759. https://doi.org/10.1007/s10126-007-9027-z
Joliot, A., Joliot, P., 1964. Etude cinetique de la reaction photochemique liberant l'oxygene au cours de la photosynthese. Comptes rendus Hebd. des séances l' Académie des Sci. Série B 258, 4622–4625.
Joliot, P., Joliot, A., 2003. Excitation transfer between photosynthetic units: The 1964 experiment. Photosynth. Res. 76, 241–245. https://doi.org/10.1023/A:1024908829819
Jørgensen, E.G., 1968. The adaptation of plankton algae. II. Aspects of the temperature adaptation of *Skeletonema costatum*. Physiol. Plant. 21, 423–427. https://doi.org/10.1111/j.1399-3054.1968.tb07266.x
Kanna, N., Nishioka, J., 2016. Bio-availability of iron derived from subarctic first-year sea ice. Mar. Chem. 186, 189–197. https://doi.org/10.1016/j.marchem.2016.09.009
Kanna, N., Sibano, Y., Toyota, T., Nishioka, J., 2018. Winter iron supply processes fueling spring phytoplankton growth in a sub-polar marginal sea, the Sea of Okhotsk: Importance of sea ice and the East Sakhalin Current. Mar. Chem. 206, 109–120. https://doi.org/10.1016/j.marchem.2018.08.006
Kanna, N., Toyota, T., Nishioka, J., 2014. Iron and macro-nutrient concentrations in sea ice and their impact on the nutritional status of surface waters in the southern Okhotsk Sea. Prog. Oceanogr. 126, 44–57. https://doi.org/10.1016/j.pocean.2014.04.012
Kasai, H., Saito, H., Yoshimori, A., Taguchi, S., 1997. Variability in timing and magnitude of spring bloom in the Oyashio region, the western subarctic Pacific off Hokkaido, Japan. Fish. Oceanogr. 6, 118–129. https://doi.org/10.1046/j.1365-2419.1997.00034.x
Katayama, T., Makabe, R., Sampei, M., Hattori, H., Sasaki, H., Taguchi, S., 2017. Photoprotection and recovery of photosystem II in the Southern Ocean phytoplankton. Polar Sci. 12, 5–11. https://doi.org/10.1016/j.polar.2016.12.003
Katayama, T., Taguchi, S., 2013. Photoprotective responses of ice algal community in Saroma-Ko Lagoon, Hokkaido, Japan. Polar Biol. 36, 1431–1439.
Katlein, C., Fernández-Méndez, M., Wenzhöfer, F., Nicolaus, M., 2015. Distribution of algal aggregates under summer sea ice in the Central Arctic. Polar Biol. 38, 719–731. https://doi.org/10.1007/s00300-014-1634-3
Katsuki, K., Takahashi, K., 2005. Diatoms as paleoenvironmental proxies for seasonal productivity, sea-ice and surface circulation in the Bering Sea during the late Quaternary. Deep. Res. II 52, 2110–2130. https://doi.org/10.1016/j.dsr2.2005.07.001
Katsuki, K., Takahashi, K., Okada, M., 2003. Diatom assemblage and productivity changes during the last 340,000 years in the subarctic Pacific. J. Oceanogr. 59, 695–707. https://doi.org/10.1023/B:JOCE.0000009598.93075.78
Kautsky, H., Hilsch, A., 1931. Wechselwirkung zwischen angeregten Farbstoff-Moleküren und Sauerstoff. Berichte Der Dtsch Chem Gesellschaft 64, 2677–2683.

Kawakami, H., Honda, M.C., Matsumoto, K., Wakita, M., Kitamura, M., Fujiki, T., Watanabe, S., 2015. POC fluxes estimated from ^{234}Th in late spring-early summer in the western subarctic North Pacific. J. Oceanogr. 71, 311–324. https://doi.org/10.1007/s10872-015-0290-8

Kawakami, H., Yang, Y.L., Honda, M.C., Kusakabe, M., 2004. Particulate organic carbon fluxes estimated from ^{234}Th deficiency in winters and springs in the northwestern North Pacific. Geochem. J. 38, 581–592. https://doi.org/10.2343/geochemj.38.581

Kennedy, F., McMinn, A., Martin, A., 2012. Effect of temperature on the photosynthetic efficiency and morphotype of *Phaeocystis antarctica*. J. Exp. Mar. Bio. Ecol. 429, 7–14. https://doi.org/10.1016/j.jembe.2012.06.016

Kettunen, R., Pursiheimo, S., Rintamaki, E., van Wijk, K., Aro, E., 1997. Transcriptional and translational adjustments of *psbA* gene expression in mature Chloroplasts during photoinhibition and subsequent repair of photosystem II. Eur. J. Biochem. 247, 441–448.

Kiefer, D.A., Reynolds, R.A., 1992. Advances in understanding phytoplankton fluorescence and photosynthesis, in: Primary Productivity and Biogeochemical Cycles in the Sea. Springer, pp. 155–174.

Kirk, J.O., Light and Photosynthesis in Aquatic Ecosystems. 3rd edition. Cambridge Press, 649pp.

Kishino, M., Takahashi, M., Okami, N., Ichimura, S., 1985. Estimation of the spectral absorption coefficients of phytoplankton in a thermally stratified sea. Bull. Mar. Sci. 37, 634–642.

Klunder, M.B., Laan, P., Middag, R., De Baar, H.J.W., van Ooijen, J.C., 2011. Dissolved iron in the Southern Ocean (Atlantic sector). Deep. Res. II 58, 2678–2694. https://doi.org/10.1016/j.dsr2.2010.10.042

Koblížek, M., Kaftan, D., Nedbal, L., 2001. On the relationship between the non-photochemical quenching of the Chlorophyll fluorescence and the photosystem II light harvesting efficiency. A repetitive flash fluorescence induction study. Photosynth. Res. 68, 141–152. https://doi.org/10.1023/A:1011830015167

Kohlbach, D., Lange, B.A., Schaafsma, F.L., David, C., Vortkamp, M., Graeve, M., van Franeker, J.A., Krumpen, T., Flores, H., 2017. Ice algae-produced carbon is critical for overwintering of Antarctic krill *Euphausia superba*. Front. Mar. Sci. 4, 1–16. https://doi.org/10.3389/fmars.2017.00310

Kolber, Z., Falkowski, P.G., 1993. Use of active fluorescence to estimate phytoplankton photosynthesis in situ. Limnol. Oceanogr. 38, 1646–1665. https://doi.org/10.4319/lo.1993.38.8.1646

Kolber, Z.S., Barber, R.T., Coale, K.H., Fitzwater, S.E., Greene, R.M., Johnson, K.S., Lindley, S., Falkowski, P.G., 1994. Iron limitatiton of phytoplankton photosynthesis in the equatorial Pacific Ocean. Nature 371, 145–149. https://doi.org/10.1038/383508a0

Kolber, Z.S., Prášil, O., Falkowski, P.G., 1998. Measurements of variable Chlorophyll fluorescence using fast repetition rate techniques: Defining methodology and experimental protocols. Biochim. Biophys. Acta 1367, 88–106. https://doi.org/10.1016/S0005-2728(98)00135-2

Kondo, Y., Takeda, S., Nishioka, J., Sato, M., Saito, H., Suzuki, K., Furuya, K., 2013. Growth stimulation and inhibition of natural phytoplankton communities by model organic ligands in the western subarctic Pacific. J. Oceanogr. 69, 97–115. https://doi.org/10.1007/s10872-012-0160-6

Konno, S., Ohira, R., Harada, N., Jordan, R.W., 2007. Six new taxa of subarctic Parmales (Chrysophyceae). J. Nannoplankt. Res. 29, 108–128.

Kono, T., 1997. Modification of the Oyashio water in the Hokkaido and Tohoku areas. Deep. Res. I 44, 669–688. https://doi.org/10.1016/S0967-0637(96)00108-2

Kono, T., Foreman, M., Chandler, P., Kashiwai, M., 2004. Coastal Oyashio south of Hokkaido, Japan. J. Phys. Oceanogr. 34, 1477–1494.

Kono, T., Sato, M., 2010. A mixing analysis of surface water in the Oyashio region: Its implications and application to variations of the spring bloom. Deep. Res. II 57, 1595–1607. https://doi.org/10.1016/j.dsr2.2010.03.004

Kramer, D.M., Johnson, G., Kiirats, O., Edwards, G.E., 2004. New fluorescence parameters for the determination of Q_A redox state and excitation energy fluxes. Photosynth. Res. 79, 209–218. https://doi.org/10.1023/B:PRES.0000015391.99477.0d

Krause, G.H., Weis, E., 1984. Chlorophyll fluorescence as a tool in plant physiology - II.

Interpretation of fluorescence signals. Photosynth. Res. https://doi.org/10.1007/BF00028527

Krembs, C., Eicken, H., Deming, J.W., 2011. Exopolymer alteration of physical properties of sea ice and implications for ice habitability and biogeochemistry in a warmer Arctic. Proc. Natl. Acad. Sci. U. S. A. 108, 3653–3658. https://doi.org/10.1073/pnas.1100701108

Krieger-Liszkay, A., Feilke, K., 2016. The dual role of the Plastid Terminal Oxidase PTOX: Between a protective and a pro-oxidant Function. Front. Plant Sci. 6, 1147. https://doi.org/10.3389/fpls.2015.01147

Kromkamp, J.C., Forster, R.M., 2003. The use of variable fluorescence measurements in aquatic ecosystems: differences between multiple and single turnover measuring protocols and suggested terminology. Eur. J. Phycol. 38, 103–112. https://doi.org/10.1080/0967026031000094094

Kropuenske, L.R., Mills, M.M., van Dijken, G.L., Alderkamp, A., Berg, G.M., Robinson, D.H., Welschmeyer, N.A., Arrigo, K.R., 2010. Strategies and rates of photoacclimatiton in two major phytoplankton taxa: *Phaeocystis antactica* (haptophyta) and *Frafilariopsis cylindrus* (Bacillariophyceae). J. Phycol. 46, 1138–1151. https://doi.org/10.1111/j.1529-8817.2010.00922.x

Kropuenske, L.R., Mills, M.M., van Dijken, G.L., Bailey, S., Robinson, D.H., Welschmeyer, N.A., Arrigo, K.R., 2010b. Photophysiology in two major southern ocean phytoplankton taxa: Photoprotection in *Phaeocystis antarctica* and *Fragilariopsis cyliundrus*. Limnol. Ocean. 54. https://doi.org/10.1093/icb/icq021

Kuczynska, P., Jemiola-Rzeminska, M., Strzalka, K., 2015. Photosynthetic pigments in diatoms. Mar. Drugs 13, 5847–5881. https://doi.org/10.3390/md13095847

Kuma, K., Nishioka, J., Matsunaga, K., 1996. Controls on iron(III) hydroxide solubility in seawater: The influence of pH and natural organic chelators. Limnol. Oceanogr. 41, 396–407. https://doi.org/10.4319/lo.1996.41.3.0396

Kusaka, A., Azumaya, T., Kawasaki, Y., 2013. Monthly variations of hydrographic structures and water mass distribution off the Doto area, Japan. J. Oceanogr. 69, 295–312. https://doi.org/10.1007/s10872-013-0174-8

Kustka, A.B., Jones, B.M., Hatta, M., Field, M.P., Milligan, A.J., 2015. The influence of iron and siderophores on eukaryotic phytoplankton growth rates and community composition in the Ross Sea. Mar. Chem. 173, 195–207. https://doi.org/10.1016/j.marchem.2014.12.002

La Roche, J., Boyd, P.W., McKay, R.M.L., Geider, R.J., 1996. Flavodoxin as an *in situ* marker for iron stress in phytoplankton. Nature 382, 802−805. https://doi.org/10.1038/382802a0

Lacour, T., Larivière, J., Ferland, J., Bruyant, F., Lavaud, J., Babin, M., 2018. The role of sustained photoprotective non-photochemical quenching in low temperature and high light acclimation in the bloom-forming Arctic diatom *Thalassiosira gravida*. Front. Mar. Sci. 5, 1–16. https://doi.org/10.3389/fmars.2018.00354

Lalli, C.M., Parsons, T.R., 1993. Biological Oceanography. 2nd edition. Butterworth Heinemann, 314pp.

Lannuzel, D., Grotti, M., Abelmoschi, M.L., van der Merwe, P., 2015. Organic ligands control the concentrations of dissolved iron in Antarctic sea ice. Mar. Chem. 174, 120–130. https://doi.org/10.1016/j.marchem.2015.05.005

Lannuzel, D., Schoemann, V., de Jong, J., Chou, L., Delille, B., Becquevort, S., Tison, J.-L., 2008. Iron study during a time series in the western Weddell pack ice. Mar. Chem. 108, 85–95. https://doi.org/10.1016/j.marchem.2007.10.006

Lannuzel, D., Schoemann, V., de Jong, J., Tison, J.-L., Chou, L., 2007. Distribution and biogeochemical behaviour of iron in the East Antarctic sea ice. Mar. Chem. 106, 18–32. https://doi.org/10.1016/j.marchem.2006.06.010

Lannuzel, D., Vancoppenolle, M., van der Merwe, P., de Jong, J., Meiners, K.M., Grotti, M., Nishioka, J., Schoemann, V., 2016. Iron in sea ice: Review and new insights. Elem. Sci. Anthr. 4, 000130. https://doi.org/10.12952/journal.elementa.000130

Laudenbach, D.E., Reith, M.E., Straus, N.A., 1988. Isolation, sequence analysis, and transcriptional studies of the flavodoxin gene from Anacystis nidulans R2. J. Bacteriol. 170, 258–265. https://doi.org/10.1128/jb.170.1.258-265.1988

Lazár, D., Ilík, P., Kruk, J., Strzałka, K., Nauš, J., 2005. A theoretical study on effect of the initial

redox state of cytochrome b_{559} on maximal chlorophyll fluorescence level (F_M): implications for photoinhibition of photosystem II. J. Theor. Biol. 233, 287−300.

Lavaud, J., Rousseau, B., Etienne, A.-L., 2002. In diatoms, a transthylakoid proton gradient alone is not sufficient to induce a non-photochemical fluorescence quenching. FEBS Lett. 523, 163–166. https://doi.org/10.1016/S0014-5793(02)02979-4

Legendre, L., Ackley, S., Dieckmann, G., Gulliksen, B., Horner, R., Hoshiai, T., Melnikov, I., Reeburgh, W., Spindler, M., Sullivan, C., 1992. Ecology of sea ice biota. Polar Biol. 12, 429–444. https://doi.org/10.1007/BF00243114

Legendre, P., Gallagher, E.D., 2001. Ecologically meaningful transformations for ordination of species data. Oecologia 129, 271–280. https://doi.org/10.1007/s004420100716

LeGresley, M., McDermott, G., 2010. Counting chamber methods for quantitative phytoplankton analysis-haemocytometer, Palmer-Maloney cell and Sedwick-rafter cell. In: Karlson, B., Cusack, C., Bresnan, E. (eds.), Microscopic and Molecular Methods for Quantitative Phytoplankton Analysis. UNESCO. 25−30.

Li, W., Smith, J., Platt, T., 1984. Temperature response of photosynthetic capacity and carboxylase activity in Arctic marine phytoplankton. Ecology 17, 237–243. https://doi.org/10.3354/meps017237

Liu, H., Suzuki, K., Nishioka, J., Sohrin, R., Nakatsuka, T., 2009. Phytoplankton growth and microzooplankton grazing in the Sea of Okhotsk during late summer of 2006. Deep. Res. I 56, 561–570. https://doi.org/10.1016/j.dsr.2008.12.003

Lizotte, M.P., 2003. The microbiology of sea ice. In: Thomas, D.N., Dieckmann, G.S. (eds.), Sea Ice: An Introduction to Its Physics, Chemistry, Biology and Geology. Wiley Blackwell. 184−210.

Lizotte, M.P., 2001. The Contributions of sea ice algae to Antarctic marine primary production. Am. Zool. 41, 57–73. https://doi.org/10.1668/0003-1569

Lommer, M., Specht, M., Roy, A.S., Kraemer, L., Andreson, R., Gutowska, M.A., Wolf, J., Bergner, S. V., Schilhabel, M.B., Klostermeier, U.C., Beiko, R.G., Rosenstiel, P., Hippler, M., LaRoche, J., 2012. Genome and low-iron response of an oceanic diatom adapted to chronic iron limitation. Genome Biol. 13. https://doi.org/10.1186/gb-2012-13-7-r66

Loose, B., Miller, L.A., Elliott, S., Papakyriakou, T., 2011. Sea ice biogeochemistry and material transportacross the frozen interface. Oceanography 24, 202–218.

Lundmark, T., Bergh, J., Strand, M., Koppel, A., 1998. Seasonal variation of maximum photochemical efficiency in boreal Norway spruce stands. Trees - Struct. Funct. 13, 63–67. https://doi.org/10.1007/s004680050187

Lyon, B., Mock, T., 2014. Polar microalgae: New approaches towards understanding adaptations to an extreme and changing environment. Biology 3, 56–80.

Maccario, L., Sanguino, L., Vogel, T.M., Larose, C., 2015. Snow and ice ecosystems: Not so extreme. Res. Microbiol. 166, 782–795. https://doi.org/10.1016/j.resmic.2015.09.002

MacIntyre, H.L., Kana, T.M., Anning, T., Geider, R.J., 2002. Photoacclimation of photosynthesis irradiance response curves and photosynthetic pigments in microalgae and cyanobacteria. J. Phycol. https://doi.org/10.1046/j.1529-8817.2002.00094.x

Maldonado, M.T., Boyd, P.W., Harrison, P.J., Price, N.M., 1999. Co-limitation of phytoplankton growth by light and Fe during winter in the NE subarctic Pacific Ocean. Deep. Res. Part II Top. Stud. Oceanogr. 46, 2475–2485. https://doi.org/10.1016/S0967-0645(99)00072-7

Maldonado, M.T., Price, N.M., 1999. Utilization of Fe bound to strong organic ligands by phytoplankton communities in the subarctic Pacific Ocean. Deep. Res. II 46, 2447–2473. https://doi.org/10.1016/S0967-0645(99)00071-5

Mangoni, O., Saggiomo, M., Modigh, M., Catalano, G., Zingone, A., Saggiomo, V., 2009. The role of platelet ice microalgae in seeding phytoplankton blooms in Terra Nova Bay (Ross Sea, Antarctica): A mesocosm experiment. Polar Biol. 32, 311–323. https://doi.org/10.1007/s00300-008-0507-z

Marchetti, A., Sherry, N.D., Kiyosawa, H., Tsuda, A., Harrison, P.J., 2006. Phytoplankton processes during a mesoscale iron enrichment in the NE subarctic Pacific: Part I—Biomass and assemblage. Deep Sea Res. Part II Top. Stud. Oceanogr. 53, 2095–2113. https://doi.org/10.1016/j.dsr2.2006.05.038

Marra, J., Trees, C.C., O'Reilly, J.E., 2007. Phytoplankton pigment absorption: A strong predictor of primary productivity in the surface ocean. Deep. Res. Part I Oceanogr. Res. Pap. 54, 155–163. https://doi.org/10.1016/j.dsr.2006.12.001

Martin, A., Anderson, M.J., Thorn, C., Davy, S.K., Ryan, K.G., 2011. Response of sea-ice microbial communities to environmental disturbance: An in situ transplant experiment in the Antarctic. Mar. Ecol. Prog. Ser. 424, 25–37. https://doi.org/10.3354/meps08977

Martin, A., McMinn, A., Davy, S.K., Anderson, M.J., Miller, H.C., Hall, J. a., Ryan, K.G., 2012a. Preliminary evidence for the microbial loop in Antarctic sea ice using microcosm simulations. Antarct. Sci. 24, 547–553. https://doi.org/10.1017/S0954102012000491

Martin, A., McMinn, A., Heath, M., Hegseth, E.N., Ryan, K.G., 2012b. The physiological response to increased temperature in over-wintering sea ice algae and phytoplankton in McMurdo Sound, Antarctica and Tromsø Sound, Norway. J. Exp. Mar. Bio. Ecol. 428, 57–66. https://doi.org/10.1016/j.jembe.2012.06.006

Martin, J.H., Coale, K.H., Johnson, K.S., Fitzwater, S.E., Gordon, R.M., Tanner, S.J., Hunter, C.N., Elrod, V.A., Nowicki, J.L., Coley, T.L., Barber, R.T., Lindley, S., Watson, A.J., Van Scoy, K., Law, C.S., Liddicoat, M.I., Ling, R., Stanton, T., Stockel, J., Collins, C., Anderson, A., Bidigare, R., Ondrusek, M., Latasa, M., Millero, F.J., Lee, K., Yao, W., Zhang, J.Z., Friederich, G., Sakamoto, C., Chavez, F., Buck, K., Kolber, Z., Greene, R., Falkowski, P., Chisholm, S.W., Hoge, F., Swift, R., Yungel, J., Turner, S., Nightingale, P., Hatton, A., Liss, P., Tindale, N.W., 1994. Testing the iron hypothesis in ecosystems of the equatorial Pacific Ocean. Nature 371, 123–129. https://doi.org/10.1038/371123a0

Martin, J.H., Fitzwater, S.E., 1988. Iron deficiency limits phytoplankton growth in the north-east Pacific subarctic. Nature 331, 341–343. https://doi.org/10.1038/331341a0

Martin, J.H., Gordon, R.M., Fitzwater, S.E., 1990. Iron in Antartic waters. Nature 345, 156–158. https://doi.org/10.1016/0021-9797(80)90501-9

Matson, P.G., Washburn, L., Martz, T.R., Hofmann, G.E., 2014. Abiotic versus biotic drivers of ocean pH variation under fast sea ice in McMurdo Sound, Antarctica. PLoS One 9, e107239. https://doi.org/10.1371/journal.pone.0107239

Maxwell, D.P., Laudenbach, D.E., Huner, N., 1995. Redox regulation of light-harvesting complex II and *cab* mRNA abundance in *Dunaliella salina*. Plant Physiol. 109, 787–795. https://doi.org/10.1104/pp.109.3.787

McDonald, A.E., Ivanov, A.G., Bode, R., Maxwell, D.P., Rodermel, S.R., Hüner, N.P.A., 2011. Flexibility in photosynthetic electron transport: The physiological role of plastoquinol terminal oxidase (PTOX). Biochim. Biophys. Acta 1807, 954–967. https://doi.org/10.1016/j.bbabio.2010.10.024

McKay, R.M.L., Geider, R.J., LaRoche, J., 1997. Physiological and biochemical response of the photosynthetic apparatus of two marine diatoms to Fe stress. Plant Physiol. 114, 615–622. https://doi.org/10.1104/pp.114.2.615

McKew, B.A., Davey, P., Finch, S.J., Hopkins, J., Lefebvre, S.C., Metodiev, M. V., Oxborough, K., Raines, C.A., Lawson, T., Geider, R.J., 2013. The trade-off between the light-harvesting and photoprotective functions of fucoxanthin-Chlorophyll proteins dominates light acclimation in *Emiliania huxleyi* (clone CCMP 1516). New Phytol. 200, 74–85. https://doi.org/10.1111/nph.12373

McMinn, A., 2017. Ice Acidification: A review of the effects of ocean acidification on sea ice microbial communities. Biogeosciences 14, 3917–3935. https://doi.org/10.5194/bg-2017-111

McMinn, A., Ashworth, C., Bhagooli, R., Martin, A., Salleh, S., Ralph, P., Ryan, K., 2012. Antarctic coastal microalgal primary production and photosynthesis. Mar. Biol. 159, 2827–2837. https://doi.org/10.1007/s00227-012-2044-0

McMinn, A., Hattori, H., Hirawake, T., Iwamoto, A., 2008. Preliminary investigation of Okhotsk Sea ice algae; taxonomic composition and photosynthetic activity. Polar Biol. 31, 1011–1015. https://doi.org/10.1007/s00300-008-0433-0

McMinn, A., Hegseth, E.N., 2004. Quantum yield and photosynthetic parameters of marine microalgae from the southern Arctic Ocean, Svalbard. J. Mar. Biol. Assoc. United Kingdom 84, 865–871. https://doi.org/10.1017/S0025315404010112h

McMinn, A., Muller, M.N., Martin, A., Ryan, K.G., 2014. The response of Antarctic sea ice algae to

changes in pH and CO_2. PLoS One 9, e86984. https://doi.org/10.1371/journal.pone.0044459

McMinn, A., Pankowski, A., Ashworth, C., Bhagooli, R., Ralph, P., Ryan, K., 2010. In situ net primary productivity and photosynthesis of Antarctic sea ice algal, phytoplankton and benthic algal communities. Mar. Biol. 157, 1345–1356. https://doi.org/10.1007/s00227-010-1414-8

McMinn, A., Ryan, K., Gademann, R., 2003. Diurnal changes in photosynthesis of Antarctic fast ice algal communities determined by pulse amplitude modulation fluorometry. Mar. Biol. 143, 359–367. https://doi.org/10.1007/s00227-003-1052-5

McNeil, B.I., Tagliabue, A., Sweeney, C., 2015. A multi-decadal delay in the onset of corrosive 'acidified' waters in the Ross Sea of Antarctica due to strong air-sea CO_2 disequilibrium. Geophys. Res. Lett. 37, 1–5. https://doi.org/10.1029/2010GL044597

McQuoid, M.R., Godhe, A., 2004. Recruitment of coastal planktonic diatoms from benthic versus pelagic cells: Variations in bloom development and species composition. Limnol. Oceanogr. 49, 1123–1133. https://doi.org/10.4319/lo.2004.49.4.1123

Medina, M., Gómez-Moreno, C., 2004. Interaction of ferredoxin-$NADP^+$ reductase with its substrates: Optimal interaction for efficient electron transfer. Photosynth. Res. 79, 113−131. https://doi.org/10.1023/B:PRES.0000015386.67746.2c

Medvedeva, L.A., Nikulina, T. V., 2014. Catalogue of freshwater algae of the southern part of the Russian Far East, Catalogue of freshwater algae of the southern part of the Russian Far East. 279 pp.

Meier, W.N., 2017. Losing Arctic sea ice: observations of the recent decline and the long-term context. In: Thomas, D.N. (ed.), Sea Ice, 3rd edition. Wiley Blackwell. 290−303.

Meiners, K.M., Vancoppenolle, M., Carnat, G., Castellani, G., Dellile, B., Dellile, D., Dieckman, G.S., Flores, H., Fripiat, F., Grotti, M., Lange, B.A., Lannuzel, D., Martin, A., McMinn, A., Nomura, D., Peeken, I., Rivaro, P., Ryan, K.G., Stefel, J., Swardling, K.M., Thomas, D.N., Tison, J.-L., van der Merwe, P., van Leeuwe, M.A., Weldrick, C., Yang, E.J., 2018. Chlorophyll-*a* in Antarctic landfast sea ice: a first synthesis of historical ice-core data. Journal of Geophysical Research: Ocean, in press.

Melis, A., 1999. Photosystem-II damage and repair cycle in Chloroplasts: what modulates the rate of photodamage in vivo? Trends Plant Sci. 4, 130–135. https://doi.org/10.1016/S1360-1385(99)01387-4

Melnikov, I.A., Bondarchuk, L.L., 1987. Ecology of mass accumulations of colonial diatom algae under drifting Arctic ice. Oceanology 27, 233–236.

Michel, C., Ingram, R.G., Harris, L.R., 2006. Variability in oceanographic and ecological processes in the Canadian Arctic Archipelago. Prog. Oceanogr. 71, 379–401. https://doi.org/10.1016/j.pocean.2006.09.006

Miller, L.A., Fripiat, F., Else, B.G.T., Bowman, J.S., Brown, K.A., Collins, R.E., Ewert, M., Fransson, A., Gosselin, M., Lannuzel, D., Meiners, K.M., Michel, C., Nishioka, J., Nomura, D., Papadimitriou, S., Russell, L.M., Sørensen, L.L., Thomas, D.N., Tison, J.-L., van Leeuwe, M.A., Vancoppenolle, M., Wolff, E.W., Zhou, J., 2015. Methods for biogeochemical studies of sea ice: The state of the art, caveats, and recommendations. Elem. Sci. Anthr. 3, 000038. https://doi.org/10.12952/journal.elementa.000038

Millero, F., Woosley, R., DiTrolio, B., Waters, J., 2009. Effect of ocean acidification on the speciation of metals in seawater. Oceanography 22, 72–85. https://doi.org/10.5670/oceanog.2009.98

Millero, F.J., Sotolongo, S., Izaguirre, M., 1987. The oxidation kinetics of Fe (II) in seawater. Geochim. Cosmochim. Acta 51, 793–801.

Misumi, K., Lindsay, K., Moore, J.K., Doney, S.C., Bryan, F.O., Tsumune, D., Yoshida, Y., 2014. The iron budget in ocean surface waters in the 20th and 21st centuries: Projections by the Community Earth System Model version 1. Biogeosciences 11, 33–55. https://doi.org/10.5194/bg-11-33-2014

Mochizuki, M., Shiga, N., Saito, M., Imai, K., Nojiri, Y., 2002. Seasonal changes in nutrients, Chlorophyll a and the phytoplankton assemblage of the western subarctic gyre in the Pacific Ocean. Deep. Res. II 49, 5421–5439. https://doi.org/10.1016/S0967-0645(02)00209-6

Mock, T., Hoch, N., 2005. Long-term temperature acclimation of photosynthesis in steady-state cultures of the polar diatom *Fragilariopsis cylindrus*. Photosynth. Res. 85, 307–317.

https://doi.org/10.1007/s11120-005-5668-9

Mock, T., Otillar, R.P., Strauss, J., McMullan, M., Paajanen, P., Schmutz, J., Salamov, A., Sanges, R., Toseland, A., Ward, B.J., Allen, A.E., Dupont, C.L., Frickenhaus, S., Maumus, F., Veluchamy, A., Wu, T., Barry, K.W., Falciatore, A., Ferrante, M.I., Fortunato, A.E., Glöckner, G., Gruber, A., Hipkin, R., Janech, M.G., Kroth, P.G., Leese, F., Lindquist, E.A., Lyon, B.R., Martin, J., Mayer, C., Parker, M., Quesneville, H., Raymond, J.A., Uhlig, C., Valas, R.E., Valentin, K.U., Worden, A.Z., Armbrust, E.V., Clark, M.D., Bowler, C., Green, B.R., Moulton, V., van Oosterhout, C., Grigoriev, I. V., 2017. Evolutionary genomics of the cold-adapted diatom *Fragilariopsis cylindrus*. Nature 541, 536–540. https://doi.org/10.1038/nature20803

Monterey, G., Levitus, S., 1997. Seasonal Variability of Mixed Layer Depth for the World Ocean, NOAA Atlas NESDIS.

Moore, C.M., Seeyave, S., Hickman, A.E., Allen, J.T., Lucas, M.I., Planquette, H., Pollard, R.T., Poulton, A.J., 2007. Iron–light interactions during the CROZet natural iron bloom and EXport experiment (CROZEX) I: Phytoplankton growth and photophysiology. Deep. Res. II 54, 2045–2065. https://doi.org/10.1016/j.dsr2.2007.06.011

Moore, J.K., Braucher, O., 2008. Sedimentary and mineral dust sources of dissolved iron to the world ocean To cite this version : Biogeosciences Sedimentary and mineral dust sources of dissolved iron to the world ocean. Biogeosciences 631–656.

Morán, X.A.G., 2007. Annual cycle of picophytoplankton photosynthesis and growth rates in a temperate coastal ecosystem: A major contribution to carbon fluxes. Aquat. Microb. Ecol. 49, 267–279. https://doi.org/10.3354/ame01151

Morán, X.A.G., Scharek, R., 2015. Photosynthetic parameters and primary production, with focus on large phytoplankton, in a temperate mid-shelf ecosystem. Estuar. Coast. Shelf Sci. 154, 145–156. https://doi.org/10.1016/j.ecss.2014.12.047

Morel, A., 1988. Optical modeling of the upper ocean in relation to its biogenous matter content (case I waters). J. Geophys. Res. 93, 10749. https://doi.org/10.1029/JC093iC09p10749

Morel, A., Bricaud, A., 1981. Theoretical results concerning light absorption in a discrete medium, and application to specific absorption of phytoplankton. Deep. Res. 28, 1375–1393. https://doi.org/10.1016/0198-0149(81)90039-X

Morel, A., Gentili, B., Claustre, H., Babin, M., Bricaud, A., Ras, J., Tièche, F., 2007. Optical properties of the '"clearest"' natural waters. Limnol. Oceanogr. 52, 217–229. https://doi.org/10.4319/lo.2007.52.1.0217

Morel, F.M.M., Price, N.M., 2007. The biogeochemical cycles of trace metals. Science 944, 944–948. https://doi.org/10.1126/science.1083545

Morgan-Kiss, R.M., Priscu, J.C., Pocock, T., Gudynaite-Savitch, L., Huner, N.P.A., 2006. Adaptation and acclimation of photosynthetic microorganisms to permanently cold environments. Microbiol. Mol. Biol. Rev. 70, 222–252. https://doi.org/10.1128/MMBR.70.1.222-252.2006

Moteki, M., Odate, T., Hosie, G.W., Takahashi, K.T., Swadling, K.M., Tanimura, A., 2017. Ecosystem studies in the Indian Ocean sector of the Southern Ocean undertaken by the training vessel Umitaka-maru. Polar Sci. 12, 1–4. https://doi.org/10.1016/j.polar.2017.04.002

Nakatsuka, T., 2002. An extremely turbid intermediate water in the Sea of Okhotsk: Implication for the transport of particulate organic matter in a seasonally ice-bound sea. Geophys. Res. Lett. 29, 29–32. https://doi.org/10.1029/2001GL014029

Nichols, C.A.M., Guezennec, J., Bowman, J.P., 2005. Bacterial exopolysaccharides from extreme marine environments with special consideration of the Southern Ocean, sea ice, and deep-sea hydrothermal vents: A review. Mar. Biotechnol. 7, 253–271. https://doi.org/10.1007/s10126-004-5118-2

Nishimura, A., Hamatsu, T., Yabuki, K., 2002. Recruitment fluctuations and biological responses of walleye pollock in the Pacific coast of Hokkaido. Fish. Sci. 68, 206–209.

Nishioka, J., Mitsudera, H., Yasuda, I., Liu, H., Nakatsuka, T., Volkov, Y.N., 2014a. Biogeochemical and physical processes in the Sea of Okhotsk and the linkage to the Pacific Ocean. Prog. Oceanogr. 126, 1–7. https://doi.org/10.1016/j.pocean.2014.04.027

Nishioka, J., Nakatsuka, T., Ono, K., Volkov, Y.N., Scherbinin, A., Shiraiwa, T., 2014b. Quantitative evaluation of iron transport processes in the Sea of Okhotsk. Prog. Oceanogr. 126, 180–193. https://doi.org/10.1016/j.pocean.2014.04.011

Nishioka, J., Nakatsuka, T., Watanabe, Y.W., Yasuda, I., Kuma, K., Ogawa, H., Ebuchi, N., Scherbinin, A., Volkov, Y.N., Shiraiwa, T., Wakatsuchi, M., 2013. Intensive mixing along an island chain controls oceanic biogeochemical cycles. Global Biogeochem. Cycles 27, 920–929. https://doi.org/10.1002/gbc.20088

Nishioka, J., Obata, H., 2017. Dissolved iron distribution in the western and central subarctic Pacific : HNLC water formation and biogeochemical processes. Limnol. Ocean. 2004–2022. https://doi.org/10.1002/lno.10548

Nishioka, J., Ono, T., Saito, H., Nakatsuka, T., Takeda, S., Yoshimura, T., Suzuki, K., Kuma, K., Nakabayashi, S., Tsumune, D., Mitsudera, H., Johnson, W.K., Tsuda, A., 2007. Iron supply to the western subarctic Pacific: Importance of iron export from the Sea of Okhotsk. J. Geophys. Res. Ocean. 112. https://doi.org/10.1029/2006JC004055

Nishioka, J., Ono, T., Saito, H., Sakaoka, K., Yoshimura, T., 2011. Oceanic iron supply mechanisms which support the spring diatom bloom in the Oyashio region, western subarctic Pacific. J. Geophys. Res. 116, C02021. https://doi.org/10.1029/2010JC006321

Nishioka, J., Takeda, S., Wong, C.S., Johnson, W.K., 2001. Size-fractionated iron concentrations in the northeast Pacific Ocean: Distribution of soluble and small colloidal iron. Mar. Chem. 74, 157–179. https://doi.org/10.1016/S0304-4203(01)00013-5

Norman, L., Worms, I.A.M., Angles, E., Bowie, A.R., Nichols, C.M., Ninh Pham, A., Slaveykova, V.I., Townsend, A.T., David Waite, T., Hassler, C.S., 2015. The role of bacterial and algal exopolymeric substances in iron chemistry. Mar. Chem. 173, 148–161. https://doi.org/10.1016/j.marchem.2015.03.015

Nosaka, Y., Isada, T., Kudo, I., Saito, H., Hattori, H., Tsuda, A., Suzuki, K., 2014. Light utilization efficiency of phytoplankton in the Western Subarctic Gyre of the North Pacific during summer. J. Oceanogr. 70, 91–103. https://doi.org/10.1007/s10872-013-0217-1

Nosaka, Y., Yamashita, Y., Suzuki, K., 2017. Dynamics and origin of transparent exopolymer particles in the Oyashio region of the western subarctic Pacific during the spring diatom bloom. Front. Mar. Sci. 4, 1–16. https://doi.org/10.3389/fmars.2017.00079

Nymark, M., Valle, K.C., Hancke, K., Winge, P., Andresen, K., Johnsen, G., Bones, A.M., Brembu, T., 2013. Molecular and photosynthetic responses to prolonged darkness and subsequent acclimation to re-Illumination in the diatom *Phaeodactylum tricornutum*. PLoS One 8, e58722.

Obata, H., Karatani, H., Matsui, M., Nakayama, E., 1997. Fundamental studies for chemical speciation of iron in seawater with an improved analytical method. Mar. Chem. 56, 97–106.

Obata, H., Karatani, H., Nakayama, E., 1993. Automated determination of iron in seawater by chelating resin concentration and chemiluminescence detection. Anal. Chem. 65, 1524–1528. https://doi.org/10.1021/ac00059a007

Obayashi, Y., Tanoue, E., Suzuki, K., Handa, N., Nojiri, Y., Wong, C.S., 2001. Spatial and temporal variabilities of phytoplankton community structure in the northern North Pacific as determined by phytoplankton pigments. Deep. Res. I 48, 439–469. https://doi.org/Doi 10.1016/S0967-0637(00)00036-4

Ogasawara, J., 1990. Physics on the east and south coasts of Hokkaido (in Japanese), In: Kunishi, H. (ed.), Coastal Oceanography of Japanese Islands. p. 839.

Ogawa, H., Amagai, Y., Koike, I., Kaiser, K., Benner, R., 2001. Production of refractory dissolved organic matter by bacteria. Science 292, 917–920. https://doi.org/10.1126/science.1057627

Oguma, S., Ono, T., Kusaka, A., Kasai, H., Kawasaki, Y., Azumaya, T., 2008. Isotopic tracers for water masses in the coastal region of Eastern Hokkaido. J. Oceanogr. 64, 525–539. https://doi.org/10.1007/s10872-008-0044-y

Ohshima, K.I., Nihashi, S., 2005. A simplified ice-ocean coupled model for the Antarctic ice melt season. J. Phys. Oceanogr. 35, 188. https://doi.org/10.1175/JPO-2675.1

Ohshima, K.I., Wakatsuchi, M., Fukamachi, Y., 2002. Near-surface circulation and tidal currents of the Okhotsk Sea observed with satellite-tracked drifters. J. Geophys. Res. 107, 3195. https://doi.org/10.1029/2001JC001005

Ohtani, K., 1971. Studies on the change of the hydrographic conditions in the Funka Bay PartII: Characteristics of the waters occupying the Funka Bay (in Japanese with English abstract). Bull. Fac. Fish. Hokkaido Univ. 22, 58–61.

Okamoto, S., Hirawake, T., Saitoh, S.I., 2010. Interannual variability in the magnitude and timing of

the spring bloom in the Oyashio region. Deep. Res. II 57, 1608–1617. https://doi.org/10.1016/j.dsr2.2010.03.005

Ono, T., Tadokoro, K., Midorikawa, T., Nishioka, J., Saino, T., 2002. Multi-decadal decrease of net community production in western subarctic North Pacific. Geophys. Res. Lett. 29, 3–6. https://doi.org/10.1029/2001GL014332

Onodera, J., Takahashi, K., Honda, M.C., 2005. Pelagic and coastal diatom fluxes and the environmental changes in the northwestern North Pacific during December 1997-May 2000. Deep. Res. Part II Top. Stud. Oceanogr. 52, 2218–2239. https://doi.org/10.1016/j.dsr2.2005.07.005

Öquist, G., Huner, N.P.A., 2003. Photosynthesis of overwintering evergreen plants. Annu. Rev. Plant Biol. 54, 329–355. https://doi.org/10.1146/annurev.arplant.54.072402.115741

Orr, J.C., Fabry, V.J., Aumont, O., Bopp, L., Doney, S.C., Feely, R.A., Gnanadesikan, A., Gruber, N., Ishida, A., Joos, F., Key, R.M., Lindsay, K., Maier-reimer, E., Matear, R., Monfray, P., Mouchet, A., Najjar, R.G., Slater, R.D., Totterdell, I.J., Weirig, M., Yamanaka, Y., Yool, A., 2005. Anthropogenic ocean acidification over the twenty-first century and its impact on calcifying organisms. Nature 437, 681–686. https://doi.org/10.1038/nature04095

Oxborough, K., Baker, N.R., 1997. Resolving Chlorophyll *a* fluorescence images of photosynthetic efficiency into photochemical and non-photochemical components - Calculation of *qP* and *Fv'/Fm'* without measuring *Fo'*. Photosynth. Res. 54, 135–142. https://doi.org/10.1023/A:1005936823310

Oxborough, K., Moore, C.M., Suggett, D.J., Lawson, T., Chan, H.G., Geider, R.J., 2012. Direct estimation of functional PSII reaction center concentration and PSII electron flux on a volume basis: a new approach to the analysis of Fast Repetition Rate fluorometry (FRRf) data. Limnol. Oceanogr. Methods 10, 142–154. https://doi.org/10.4319/lom.2012.10.142

Palmisano, A.C., SooHoo, J.B., Sullivan, C.W., 1987. Effects of four environmental variables on photosynthesis-irradiance relationships in Antarctic sea-ice microalgae. Mar. Biol. 94, 299–306. https://doi.org/10.1007/BF00392944

Pankowski, A., McMinn, A., 2008a. Iron availability regulates growth, photosynthesis, and production of ferredoxin and flavodoxin in Antarctic sea ice diatoms. Aquat. Biol. 4, 273–288. https://doi.org/10.3354/ab00116

Pankowski, A., McMinn, A., 2008b. Ferredoxin and flavodoxin in eastern Antarctica pack ice. Polar Biol. 31, 1153–1165. https://doi.org/10.1007/s00300-008-0451-y

Pankowski, A., McMinn, A., 2009. Development of immunoassays for the iron-regulated proteins ferredoxin and flavodoxin in polar microalgae. J. Phycol. 45, 771–783. https://doi.org/10.1111/j.1529-8817.2009.00687.x

Parkinson, C.L., Gloersen, P., 1993. Global sea ice coverage. Atlas Satell. Obs. Relat. to Glob. Chang. 371–383.

Paul, C., Barofsky, A., Vidoudez, C., Pohnert, G., 2009. Diatom exudates influence metabolism and cell growth of co-cultured diatom species. Mar. Ecol. Prog. Ser. 389, 61–70. https://doi.org/10.3354/meps08162

Petrich, C., Eicken, H., Overview of sea ice growth and properties. In: Thomas, D.N. (ed.) Sea Ice, 3rd edition. Wiley Blackwell. 1−41.

Petrou, K., Hill, R., Brown, C.M., Campbell, D.A., Doblin, M.A., Ralph, P.J., 2010. Rapid photoprotection in sea-ice diatoms from the East Antarctic pack ice. Limnol. Oceanogr. 55, 1400–1407. https://doi.org/10.4319/lo.2010.55.3.1400

Petrou, K., Hill, R., Doblin, M.A., McMinn, A., Johnson, R., Wright, S.W., Ralph, P.J., 2011. Photoprotection of sea-ice microalgal communities from the east Antarctic pack ice. J. Phycol. 47, 77–86. https://doi.org/10.1111/j.1529-8817.2010.00944.x

Petrou, K., Kranz, S.A., Trimborn, S., Hassler, C.S., Ameijeiras, S.B., Sackett, O., Ralph, P.J., Davidson, A.T., 2016. Southern Ocean phytoplankton physiology in a changing climate. J. Plant Physiol. 203, 135–150. https://doi.org/10.1016/j.jplph.2016.05.004

Petrou, K., Ralph, P.J., 2011. Photosynthesis and net primary productivity in three Antarctic diatoms: Possible significance for their distribution in the Antarctic marine ecosystem. Mar. Ecol. Prog. Ser. 437, 27–40. https://doi.org/10.3354/meps09291

Pfannschmidt, T., 2003. Chloroplast redox signals: How photosynthesis controls its own genes.

Trends Plant Sci. 8, 33–41. https://doi.org/10.1016/S1360-1385(02)00005-5

Platt, T., Gallegos, C.L., Harrison, W.G., 1980. Photoinibition of photosynthesis in natural assemblages of marine phytoplankton. J. Mar. Res. 38, 687−701. https://doi.org/citeulike-article-id:3354339

Platt, T., Jassby, A.D., 1976. The relationship between photosynthesis and light for natural assemblages of coastal marine phytoplankton. J. Phycol. 12, 421–430. https://doi.org/10.1111/j.1529-8817.1976.tb02866.x

Platt, T., Sathyendranath, S., Ullloa, O., Harrison, W.G., Hoepffner, N., Goes, J., 1992. Nutrient control of phytoplankton photosynthesis in the Western North Atlantic. Nature 356, 229–231. https://doi.org/10.1038/356229a0

Prášil, O., Adir, N., Ohad, I., 1992. Dynamics of photosystem II: mechanism of photoinhibition and recovery processes. In: Barber, J. (ed.), Topics in Photosynthesis, Vol 11. Elsevier. 293−348.

Prášil, O., Bína, D., Medová, H., Řeháková, K., Zapomelová, E., Veselá, J., Oren, A., 2009. Emission spectroscopy and kinetic fluorometry studies of phototrophic microbial communities along a salinity gradient in solar saltern evaporation ponds of Eilat, Israel. Aquat. Microb. Ecol. 56, 285–296. https://doi.org/10.3354/ame01311

Prášil, O., Kolber, Z., Berry, J.A., Falkowski, P.G., 1996. Cyclic electron flow around Photosystem II in vivo. Photosynth. Res. 48, 395–410.

Prezelin, B.B., 1992. Diel periodicity in phytoplankton productivity. Hydrobiologia 238, 1–35. https://doi.org/10.1117/12.2234235

Price, N.M., Harrison, G.I., Hering, J.G., Hudson, R.J., Nirel, P.M. V., Palenik, B., Morel, F.M.M., 1989. Preparation and chemistry of the artificial algal culture medium Aquil. Biol. Oceanogr. 6, 443–461. https://doi.org/10.1080/01965581.1988.10749544

Ralph, P.J., McMinn, A., Ryan, K.G., Ashworth, C., 2005. Short-term effect of temperature on the photokinetics of microalgae from the surface layers of Antarctic pack ice. J. Phycol. 41, 763–769. https://doi.org/10.1111/j.1529-8817.2005.00106.x

Ralph, P.J., Ryan, K.G., Martin, A., Fenton, G., 2007. Melting out of sea ice causes greater photosynthetic stress in algae than freezing in. J. Phycol. 43, 948–956. https://doi.org/10.1111/j.1529-8817.2007.00382.x

Ratkova, T.N., Wassmann, P., 2005. Sea ice algae in the White and Barents seas: Composition and origin. Polar Res. 24, 95–110. https://doi.org/DOI 10.1111/j.1751-8369.2005.tb00143.x

Raven, J.A., Geider, R.J., 1988. Temperature and algal growth. New Phytol. 110, 441–461. https://doi.org/10.1111/j.1469-8137.1988.tb00282.x

Riebesell, U., SChloss, I., Smetacek, V., 1991. Aggregation of algae released from melting sea ice: implications for seeding and sedimentation. Polar Biol. 11, 239–248. https://doi.org/10.1007/BF00238457

Riebesell, U., Wolf-Gladrow, D.A., Smetacek, V., 1993. Carbon dioxide limitation of marine phytoplankton growth rates. Nature 361, 249–251. https://doi.org/10.1038/361249a0

Riley, G.A., 1946. Factors controlling phytoplankton populations on George Bank. J. Mar. Res. 6, 54–72.

Rintala, J.M., Piiparinen, J., Blomster, J., Majaneva, M., Müller, S., Uusikivi, J., Autio, R., 2014. Fast direct melting of brackish sea-ice samples results in biologically more accurate results than slow buffered melting. Polar Biol. 37, 1811–1822. https://doi.org/10.1007/s00300-014-1563-1

Rost, B., Riebesell, U., Sültemeyer, D., 2006. Carbon acquisition of marine phytoplankton. Limnol. Oceanogr. https://doi.org/10.4319/lo.2006.51.1.0012

Round, F.E., Crawford, R.M., Mann, D.G., 2007. The Diatoms: Biology morphology of the genera. Cambridge Univ. Press.

Roukaerts, A., Nomura, D., Deman, F., Hattori, H, Dehairs, F., Fripiat, F., 2018. The effect of melting treatments on the assessment of biomass and nutrients ice sea ice (Saroma-ko lagoon, Hokkaido, Japan). Polar Biology, in press.

Rue, E.L., Bruland, K.W., 1995. Complexation of iron(III) by natural organic ligands in the Central North Pacific as determined by a new competitive ligand equilibration/adsorptive cathodic stripping voltammetric method. Mar. Chem. 50, 117–138. https://doi.org/10.1016/0304-4203(95)00031-L

Ryan-Keogh, T.J., Thomalla, S.J., Mtshali, T.N., Little, H., 2017. Modelled estimates of spatial variability of iron stress in the Atlantic sector of the Southern Ocean. Biogeosciences 14, 3883–3897. https://doi.org/10.5194/bg-14-3883-2017

Ryan, K.G., Tay, M.L., Martin, A., Mcminn, A., Davy, S.K., 2011. Chlorophyll fluorescence imaging analysis of the responses of Antarctic bottom-ice algae to light and salinity during melting. J. Exp. Mar. Bio. Ecol. 399, 156–161. https://doi.org/10.1016/j.jembe.2011.01.006

Sabine, C.L., Feely, R.A., Gruber, N., Key, R.M., Lee, K., Bullister, J.L., Wanninkhof, R., Wong, C.S., Wallace, D.W.R., Tilbrook, B., Millero, F.J., Peng, T., Kozyr, A., Ono, T., Rios, A.F., 2004. The oceanic sink for anthropogenic CO2. Science 305, 367–71. https://doi.org/10.1126/science.1097403

Saito, H., Tsuda, A., 2003. Influence of light intensity on diatom physiology and nutrient dynamics in the Oyashio region. Prog. Oceanogr. 57, 251–263. https://doi.org/10.1016/S0079-6611(03)00100-9

Saito, H., Tsuda, A., Kasai, H., 2002. Nutrient and plankton dynamics in the Oyashio region of the western subarctic Pacific Ocean. Deep. Res. II 49, 5463–5486. https://doi.org/10.1016/S0967-0645(02)00204-7

Sakshaug, E., 2004. Primary and secondary production in the Arctic seas. In: Stein, R., MacDonald, R.W. (eds.), The Organic Carbon Cycle in the Arctic Ocean. Springer, 57−81.

Sakshaug, E., Bricaud, A., Dandonneau, Y., Falkowski, P.G., Kiefer, D.A., Legendre, L., Morel, A., Parslow, J., Takahashi, M., 1997. Parameters of photosynthesis: definitions, theory and interpretation of results. J. Plankton Res. 19, 1637–1670. https://doi.org/10.1093/plankt/19.11.1637

Sakurai, Y., 2007. An overview of the Oyashio ecosystem. Deep. Res. II 54, 2526–2542. https://doi.org/10.1016/j.dsr2.2007.02.007

Sarmiento, J.L., Gruber, N., 2006. Ocean Biogeochemical Dynamics. Princeton University Press. 503 pp.

Sarmiento, J.L., Hughes, T.M.C., Stouffer, R.J., Manabe, S., 1998. Simulated response of the ocean carbon cycle to anthropogenic climate warming. Nature 393, 245–249. https://doi.org/10.1038/30455

Sarmiento, J.L., Siegenthaler, U., 1992. New production and the global carbon cycle. In: Falkowski, P.G., Woodhead, A.D., Primary Productivity and Biogeochemical Cycles in the Sea. pp. 317–332.

Sarthou, G., Timmermans, K.R., Blain, S., Tréguer, P., 2005. Growth physiology and fate of diatoms in the ocean: A review. J. Sea Res. https://doi.org/10.1016/j.seares.2004.01.007

Sathyendranath, S., Platt, T., Forget, M.-H., 2007. Ocean primary production: Comparison of models, in: OCEANS 2007 - Europe. pp. 1–3. https://doi.org/10.1109/OCEANSE.2007.4302468

Satoh, H., Yamaguchi, Y., Watanabe, K., Tanimura, A., Fukuchi, M., Aruga, Y., 1989. Photosynthetic nature of ice algae and their contribution to the primary production in Lagoon Saroma Ko, Hokkaido, Japan. Proc. NIPR Symp. Polar Biol. 2, 1–8.

Schauer, U., 1995. The release of brine-enriched shelf water from Storfjord into the Norwegian Sea. J. Geophys. Res. 100, 16015. https://doi.org/10.1029/95JC01184

SChloss, P.D., Westcott, S.L., Ryabin, T., Hall, J.R., Hartmann, M., Hollister, E.B., Lesniewski, R.A., Oakley, B.B., Parks, D.H., Robinson, C.J., Sahl, J.W., Stres, B., Thallinger, G.G., van Horn, D.J., Weber, C.F., 2009. Introducing mothur: Open-source, platform-independent, community-supported software for describing and comparing microbial communities. Appl. Environ. Microbiol. 75, 7537–7541. https://doi.org/10.1128/AEM.01541-09

Schreiber, U., 1998. Chlorophyll fluorescence: New instruments for special applications. Photosynth. Mech. Eff. V, 4253–4258. https://doi.org/10.1007/978-94-011-3953-3_984

Schuback, N., Flecken, M., Maldonado, M.T., Tortell, P.D., 2016. Diurnal variation in the coupling of photosynthetic electron transport and carbon fixation in iron-limited phytoplankton in the NE subarctic Pacific. Biogeosciences 13, 1019–1035. https://doi.org/10.5194/bg-13-1019-2016

Schuback, N., Schallenberg, C., Duckham, C., Maldonado, M.T., Tortell, P.D., 2015. Interacting effects of light and iron availability on the coupling of photosynthetic electron transport and CO_2-assimilation in marine phytoplankton. PLoS One 10, 1–30. https://doi.org/10.1371/journal.pone.0133235

Schwarz, V., Andosch, A., GeretsChläger, A., Affenzeller, M., Lütz-Meindl, U., 2017. Carbon starvation induces lipid degradation via autophagy in the model alga *Micrasterias*. J. Plant Physiol. 208, 115–127. https://doi.org/10.1016/j.jplph.2016.11.008

Shaked, Y., Lis, H., 2012. Disassembling iron availability to phytoplankton. Front. Microbiol. 3, 1–26. https://doi.org/10.3389/fmicb.2012.00123

Shi, D., Xu, Y., Hopkinson, B.M., Morel, F.M.M., 2010. Effect of ocean acidification on iron availability to marine phytoplankton. Science 1183517, 1–4.

Shi, X., Gao, W., Chao, S., Zhang, W., Meldrum, D.R., 2013. Monitoring the single-cell stress response of the diatom *Thalassiosira pseudonana* by quantitative real-time reverse transcription-PCR. Appl. Environ. Microbiol. 79, 1850–1858. https://doi.org/10.1128/AEM.03399-12

Shinada, A., Shiga, N., Ban, S., 1999. Structure and magnitude of diatom spring bloom in Funka Bay, southwestern Hokkaido, Japan, as influenced by the intrusion of Coastal Oyashio Water. Plankt. Biol. Ecol. 46, 24–29.

Siegel, D.A., Buesseler, K.O., Behrenfeld, M.J., Benitez-Nelson, C.R., Boss, E., Brzezinski, M.A., Burd, A., Carlson, C.A., D'Asaro, E.A., Doney, S.C., Perry, M.J., Stanley, R.H.., Steinberg, D.K., 2016. Prediction of the export and fate of global ocean net primary production: The EXPORTS science plan. Front. Mar. Sci. 3, 1–10. https://doi.org/10.3389/fmars.2016.00022

Smetacek, V., 1999. Diatoms and the ocean carbon cycle. Protist News 150, 25–32. https://doi.org/10.1016/S1434-4610(99)70006-4

Smetacek, V.S., 1985. Role of sinking in diatom life-hystory: ecological, evolutionary and geological significance. Mar. Biol. 84, 239–251. https://doi.org/10.1007/BF00392493

Smillie, R.M., 1965. Isolation of phytoflavin, a flavoprotein with Chloroplast ferredoxin activity. Plant Physiol. 40, 1124–1128.

Smith, W.O., Nelson, D.M., 1986. Importance of ice edge phytoplankton production in the Southern Ocean. Bioscience 36, 251–257. https://doi.org/10.2307/1310215

Sournia, A., Chretiennotdinet, M.J., Ricard, M., 1991. Marine phytoplankton - How many species in the world ocean. J.Plankton.Res. 13, 1093–1099.

Stammerjohn, S., Maksym, T., 2017. Gaining (and losing) Antarctic sea ice: variability, trends and mechanisms. In: Thomas, D.N. (ed.), Sea Ice, 3rd edition. Wiley Blackwell. 261−289.

Steenman-Nielsen, E., 1952. The use of radio-active carbon (C^{14}) for measuring organic production in the sea. J. Cons. Int. Explor. Mer. 18, 117–140.

Steenman-Nielsen, E., Jørgensen, E.G., 1968. The adaptation of plankton algae I. Genaral part. Physiol. Plant. 21, 401–413.

Stefels, J., Carnat, G., Dacey, J.W.H., Goossens, T., Elzenga, J.T.M., Tison, J.-L., 2012. The analysis of dimethylsulfide and dimethylsulfoniopropionate in sea ice: Dry-crushing and melting using stable isotope additions. Mar. Chem. 128–129, 34–43. https://doi.org/10.1016/j.marchem.2011.09.007

Steiner, N., Deal, C., Lannuzel, D., Lavoie, D., Massonnet, F., Miller, L.A., Moreau, S., Popova, E., Stefels, J., Tedesco, L., 2016. What sea-ice biogeochemical modellers need from observers. Elem. Sci. Anthr. 4, 000084. https://doi.org/10.12952/journal.elementa.000084

Stoecker, D.K., 1999. Mixotrophy among Dinoflagellates. J. Eukaryot. Microbiol. 46, 397–401. https://doi.org/10.1111/j.1550-7408.1999.tb04619.x

Stroeve, J., Holland, M.M., Meier, W., Scambos, T., Serreze, M., 2007. Arctic sea ice decline: Faster than forecast. Geophys. Res. Lett. 34, 1–5. https://doi.org/10.1029/2007GL029703

Stookey, L.L., 1970. Ferrozine - A new spectrophotometric reagent for iron. Anal. Chem. 42, 779−781.

Strzepek, R.F., Hunter, K.A., Frew, R.D., Harrison, P.J., Boyd, P.W., 2012. Iron-light interactions differ in Southern Ocean phytoplankton. Limnol. Oceanogr. 57, 1182–1200. https://doi.org/10.4319/lo.2012.57.4.1182

Stumm, M., Massom, R.A., 2010. Snow and sea ice. In: Thomas, D.N., Dieckmann, G.S. (eds.), Sea Ice, 2nd edition. Wiley Blackwell. 153−204.

Stumm, W., Morgan, J.J., 1996. Aquatic Chemistry, 3rd edition. Wiley-Interscience.

Suggett, D.J., Prášil, O., Borowitzka, M.A., 2011. Chlorophyll *a* Fluorescence in Aquatic Sciences: Methods and Applications. Springer. 323pp.

Suggett, D., Stambler, N., O, P., Kolber, Z., Quigg, A., Vázquez-Dominguez, E., Zohary, T., Berman, T., Iluz, D., Levitan, O., Lawson, T., Meeder, E., Lazar, B., Bar-Zeev, E., Medova, H., Berman-Frank, I., 2009a. Nitrogen and phosphorus limitation of oceanic microbial growth during spring in the Gulf of Aqaba. Aquat. Microb. Ecol. 56, 227–239. https://doi.org/10.3354/ame01357

Suggett, D.J., Moore, C.M., Hickman, A.E., Geider, R.J., 2009b. Interpretation of fast repetition rate (FRR) fluorescence: Signatures of phytoplankton community structure versus physiological state. Mar. Ecol. Prog. Ser. 376, 1–19. https://doi.org/10.3354/meps07830

Sugie, K., Kuma, K., 2008. Resting spore formation in the marine diatom *Thalassiosira nordenskioeldii* under iron- and nitrogen-limited conditions. J. Plankton Res. 30, 1245–1255. https://doi.org/10.1093/plankt/fbn080

Sugie, K., Nishioka, J., Kuma, K., Volkov, Y.N., Nakatsuka, T., 2013. Availability of particulate Fe to phytoplankton in the Sea of Okhotsk. Mar. Chem. 152, 20–31. https://doi.org/10.1016/j.marchem.2013.03.005

Sugie, K., Suzuki, K., 2017. Characterization of the synoptic-scale diversity, biogeography, and size distribution of diatoms in the North Pacific. Limnol. Oceanogr. 62, 884–897. https://doi.org/10.1002/lno.10473

Sugiura, J., 1956. A note on current branches in the Oyashio area (Japanese). J. Oceanogr. Soc. Jpn. 12, 1–3.

Sunda, W., Huntsman, S., 2003. Effect of pH, light, and temperature on Fe-EDTA chelation and Fe hydrolysis in seawater. Mar. Chem. 84, 35–47. https://doi.org/10.1016/S0304-4203(03)00101-4

Sunda, W.G., Huntsman, S.A., 1997. Interrelated influence of iron, light and cell size on marine phytoplankton growth. Nature 390, 389–392. https://doi.org/10.1038/37093

Sunda, W.G., Huntsman, S.A., 1995. Iron uptake and growth limitation in oceanic and coastal phytoplankton. Mar. Chem. 50, 189–206.

Suzuki, K., Handa, N., Nishida, T., Wong, C.S., 1997. Estimation of phytoplankton succession in a fertilized mesocosm during summer using high-performance liquid chromatographic analysis of pigments. J. Exp. Mar. Bio. Ecol. 214, 1–17. https://doi.org/10.1016/S0022-0981(97)00003-8

Suzuki, K., Hattori-Saito, A., Sekiguchi, Y., Nishioka, J., Shigemitsu, M., Isada, T., Liu, H., McKay, R.M.L., 2014. Spatial variability in iron nutritional status of large diatoms in the Sea of Okhotsk with special reference to the Amur River discharge. Biogeosciences 11, 2503–2517. https://doi.org/10.5194/bg-11-2503-2014

Suzuki, K., Kamimura, A., Hooker, S.B., 2015. Rapid and highly sensitive analysis of Chlorophylls and carotenoids from marine phytoplankton using ultra-high performance liquid chromatography (UHPLC) with the first derivative spectrum chromatogram (FDSC) technique. Mar. Chem. 176, 96–109. https://doi.org/10.1016/j.marchem.2015.07.010

Suzuki, K., Kuwata, A., Yoshie, N., Shibata, A., Kawanobe, K., Saito, H., 2011. Population dynamics of phytoplankton, heterotrophic bacteria, and viruses during the spring bloom in the western subarctic Pacific. Deep. Res. I 58, 575–589. https://doi.org/Doi 10.1016/J.Dsr.2011.03.003

Suzuki, K., Liu, H., Saino, T., Obata, H., Takano, M., Okamura, K., Sohrin, Y., Fujishima, Y., 2002a. East-west gradients in the photosynthetic potential of phytoplankton and iron concentration in the subarctic Pacific Ocean during early summer. Limnol. Oceanogr. 47, 1581–1594. https://doi.org/10.4319/lo.2002.47.6.1581

Suzuki, K., Minami, C., Liu, H., Saino, T., 2002b. Temporal and spatial patterns of chemotaxonomic algal pigments in the subarctic Pacific and the Bering Sea during the early summer of 1999. Deep. Res. II 49, 5685–5704. https://doi.org/10.1016/S0967-0645(02)00218-7

Suzuki, K., Saito, H., Isada, T., Hattori-Saito, A., Kiyosawa, H., Nishioka, J., McKay, R.M.L., Kuwata, A., Tsuda, A., 2009. Community structure and photosynthetic physiology of phytoplankton in the northwest subarctic Pacific during an in situ iron fertilization experiment (SEEDS-II). Deep. Res. II 56, 2733–2744. https://doi.org/10.1016/j.dsr2.2009.06.001

Suzuki, R., Ishimaru, T., 1990. An improved method for the determination of phytoplankton Chlorophyll using N, N-dimethylformamide. J. Oceanogr. Soc. Japan 46, 190–194. https://doi.org/10.1007/BF02125580

Sverdrup, H.U., 1953. On conditions for the vernal blooming of phytoplankton. J. du Cons. Int. pour l'Exploration la Mer 18, 287–295.

Syvertsen, E.E., 1991. Ice algae in the Barents Sea: types of assemblages, origin, fate and role in the

ice-edge phytoplankton bloom. Polar Res. 10, 277–288. https://doi.org/10.1111/j.1751-8369.1991.tb00653.x

Szechynska-Hebda, M., Kruk, J., Gorecka, M., Karpinska, B., Karpinski, S., 2010. Evidence for Light Wavelength-Specific Photoelectrophysiological Signaling and Memory of Excess Light Episodes in Arabidopsis. Plant Cell Online 22, 2201–2218. https://doi.org/10.1105/tpc.109.069302

Tada, Y., Nakaya, R., Goto, S., Yamashita, Y., Suzuki, K., 2017. Distinct bacterial community and diversity shifts after phytoplankton-derived dissolved organic matter addition in a coastal environment. J. Exp. Mar. Bio. Ecol. 495, 119–128. https://doi.org/10.1016/j.jembe.2017.06.006

Tada, Y., Taniguchi, A., Nagao, I., Miki, T., Uematsu, M., Tsuda, A., Hamasaki, K., 2011. Differing growth responses of major phylogenetic groups of marine bacteria to natural phytoplankton blooms in the Western North Pacific Ocean. Appl. Environ. Microbiol. 77, 4055–4065. https://doi.org/10.1128/AEM.02952-10

Taguchi, S., 1976. Relationship between photosynthesis and cell size of marine diatoms. J. Phycol. 12, 185–189.

Taguchi, S., Saito, H., Shirasawa, K., Hattori, H., 1997. Vertical flux of ice algal cells during the ice melting and breaking periods in Saroma Ko Lagoon, Hokkaido, Japan. Proc. NIPR Symp. Polar Biol. 10, 56–65.

Takahashi, T., Sutherland, S.C., Sweeney, C., Poisson, A., Metzl, N., Tilbrook, B., Bates, N., Wanninkhof, R., Feely, R.A., Sabine, C., Olafsson, J., Nojiri, Y., 2002. Global sea-air CO_2 flux based on climatological surface ocean pCO_2, and seasonal biological and temperature effects. Deep. Res. II 49, 1601–1622. https://doi.org/10.1016/S0967-0645(02)00003-6

Takeda, S., Obata, H., 1995. Response of equatorial Pacific phytoplankton to subnanomolar Fe enrichment. Mar. Chem. 50, 219–227. https://doi.org/10.1016/0304-4203(95)00037-R

Tang, K.W., Elliott, D.T., 2014. Copepod carcasses: Occurrence, fate and ecological importance. In: Seuront, L. (ed.), Copepods: Diversity, Habitat and Behavior. Nova Science Publishers. pp. 255−278.

Taniguchi, A., 1999. Differences in the structure of the lower trophic levels of pelagic ecosystems in the eastern and western subarctic Pacific. Prog. Oceanogr. 43, 289–315. https://doi.org/10.1016/S0079-6611(99)00011-7

Thornton, D., 2002. Diatom aggregation in the sea: mechanisms and ecological implications. Eur. J. Phycol. 37, 149–161. https://doi.org/10.1017/S0967026202003657

Timmermans, K.R., Davey, M.S., van der Wagt, B., Snoek, J., Geider, R.J., Veldhuis, M.J.W., Gerringa, L.J.A., De Baar, H.J.W., 2001. Co-limitation by iron and light of *Chaetoceros brevis*, *C. dichaeta* and *C. calcitrans* (Bacillariophyceae). Mar. Ecol. Prog. Ser. 217, 287–297. https://doi.org/10.3354/meps217287

Timmermans, K.R., van der Wagt, B., de Baar, H.J.W., 2004. Growth rates, half-saturation constants, and silicate, nitrate, and phosphate depletion in relation to iron availability of four large, open-ocean diatoms from the Southern Ocean. Limnol. Oceanogr. 49, 2141–2151. https://doi.org/10.4319/lo.2004.49.6.2141

Ting, C.S., Owens, T.G., 1993. Photochemical and nonphotochemical fluorescence quenching processes in the diatom *Phaeodactylum tricornutum*. Plant Physiol. 101, 1323–1330. https://doi.org/http://dx.doi.org/

Tomas, C.R., Identifying Maine Phytoplankton. Academic Press, 858pp.

Tovar-Sánchez, A, Duarte, C.M., Alonso, J.C., Lacorte, S., Tauler, R., Malagón, C.G., 2010. Impacts of metals and nutrients released from melting multiyear Arctic sea ice 115, 1–7. https://doi.org/10.1029/2009JC005685

Tranter, D.J., 1982. Interlinking of physical and biological processes in the Antarctic Ocean. In: Barnes, H (ed.)., Oceanography and Marine Biology: An Annual Review volume 20. Aberdeen University Press. 1−37.

Tréguer, P., Bowler, C., Moriceau, B., Dutkiewicz, S., Gehlen, M., Aumont, O., Bittner, L., Dugdale, R., Finkel, Z., Iudicone, D., Jahn, O., Guidi, L., Lasbleiz, M., Leblanc, K., Levy, M., Pondaven, P., 2018. Influence of diatom diversity on the ocean biological carbon pump. Nat. Geosci. 11, 27–37. https://doi.org/10.1038/s41561-017-0028-x

Triantaphylides, C., Krischke, M., Hoeberichts, F.A., Ksas, B., Gresser, G., Havaux, M., Van

Breusegem, F., Mueller, M.J., 2008. Singlet oxygen is the major reactive oxygen species involved in photooxidative damage to plants. Plant Physiol. 148, 960–968. https://doi.org/10.1104/pp.108.125690

Tsuda, A., Takeda, S., Saito, H., Nishioka, J., Kudo, I., Nojiri, Y., Suzuki, K., Uematsu, M., Wells, M.L., Tsumune, D., Yoshimura, T., Aono, T., Aramaki, T., CoChlan, W.P., Hayakawa, M., Imai, K., Isada, T., Iwamoto, Y., Johnson, W.K., Kameyama, S., Kato, S., Kiyosawa, H., Kondo, Y., Levasseur, M., Machida, R.J., Nagao, I., Nakagawa, F., Nakanishi, T., Nakatsuka, S., Narita, A., Noiri, Y., Obata, H., Ogawa, H., Oguma, K., Ono, T., Sakuragi, T., Sasakawa, M., Sato, M., Shimamoto, A., Takata, H., Trick, C.G., Watanabe, Y.W., Wong, C.S., Yoshie, N., 2007. Evidence for the grazing hypothesis: Grazing reduces phytoplankton responses of the HNLC ecosystem to iron enrichment in the western subarctic pacific (SEEDS II). J. Oceanogr. 63, 983–994. https://doi.org/10.1007/s10872-007-0082-x

Tsuda, A., Takeda, S., Saito, H., Nishioka, J., Nojiri, Y., Kudo, I., Kiyosawa, H., Shiomoto, A., Imai, K., Ono, T., Shimamoto, A., Tsumune, D., Yoshimura, T., Aono, T., Hinuma, A., Kinugasa, M., Suzuki, K., Sohrin, Y., Noiri, Y., Tani, H., Deguchi, Y., Tsurushima, N., Ogawa, H., Fukami, K., Kuma, K., Saino, T., 2003. A mesoscale iron enrichment in the western subarctic Pacific induces a large centric diatom bloom. Science 300, 958–961. https://doi.org/10.1126/science.1082000

Tsunogai, S., Watanabe, S., Sato, T., 1999. Is there a “continental shelf pump” for the absorption of atmospheric CO_2? Tellus, Ser. B Chem. Phys. Meteorol. 51, 701–712. https://doi.org/10.3402/tellusb.v51i3.16468

Twining, B.S., Baines, S.B., 2013. The trace metal composition of marine phytoplankton. Ann Rev Mar Sci 5, 191–215. https://doi.org/10.1146/annurev-marine-121211-172322

Ugalde, S.C., Martin, A., Meiners, K.M., McMinn, A., Ryan, K.G., 2014. Extracellular organic carbon dynamics during a bottom-ice algal bloom (Antarctica). Aquat. Microb. Ecol. 73, 195–210. https://doi.org/10.3354/ame01717

Underwood, G., Fietz, S., Papadimitriou, S., Thomas, D., Dieckmann, G., 2010. Distribution and composition of dissolved extracellular polymeric substances (EPS) in Antarctic sea ice. Mar. Ecol. Prog. Ser. 404, 1–19. https://doi.org/10.3354/meps08557

Underwood, G., Provot, L., 2000. Determining the environmental preferences of four estuarine epipelic diatom taxa: Growth across a range of salinity, nitrate and ammonium conditions. Eur. J. Phycol. 35, 173–182. https://doi.org/10.1080/09670260010001735761

Urao, T., Yamaguchi-Shinozaki, K., Shinozaki, K., 2000. Two-component systems in plant signal transduction. Trends Plant Sci. 5, 67–79. https://doi.org/10.1016/S1360-1385(99)01542-3

van de Poll, W.H., Lagunas, M., De Vries, T., Visser, R.J.W., Buma, A.G.J., 2011. Non-photochemical quenching of Chlorophyll fluorescence and xanthophyll cycle responses after excess PAR and UVR in *Chaetoceros brevis*, *Phaeocystis antarctica* and coastal Antarctic phytoplankton. Mar. Ecol. Prog. Ser. 426, 119–131. https://doi.org/10.3354/meps09000

van den Berg, C.M.G., 1995. Evidence for organic complexation of iron in seawater. Mar. Chem. 50, 139–157. https://doi.org/10.1016/0304-4203(95)00032-M

van der Merwe, P., Lannuzel, D., Bowie, A.R., Meiners, K.M., 2011. High temporal resolution observations of spring fast ice melt and seawater iron enrichment in East Antarctica. J. Geophys. Res. Biogeosciences 116, 1–18. https://doi.org/10.1029/2010JG001628

van Heukelem, L., Thomas, C.S., 2001. Computer-assisted high-performance liquid chromatography method development with applications to the isolation and analysis of phytoplankton pigments. J. Chromatogr. A 910, 31–49. https://doi.org/10.1016/S0378-4347(00)00603-4

van Leeuwe, M.A., Tedesco, L., Arrigo, K.R., Assmy, P., Campbell, K., Meiners, K.M., Rintala, J.-M., Selz, V., Thomas, D.N., Stefels, J., Deming, J.W., 2018. Microalgal community structure and primary production in Arctic and Antarctic sea ice: A synthesis. Elem Sci Anth 6. https://doi.org/10.1525/elementa.267

van Oijen, T., van Leeuwe, M.A., Gieskes, W.W.C., de Baar, H.J.W., 2004. Effects of iron limitation on photosynthesis and carbohydrate metabolism in the Antarctic diatom Chaetoceros brevis (Bacillariophyceae). Eur. J. Phycol. 39, 161–171. https://doi.org/10.1080/0967026042000202127

Vancoppenolle, M., Meiners, K.M., Michel, C., Bopp, L., Brabant, F., Carnat, G., Delille, B.,

Lannuzel, D., Madec, G., Moreau, S., Tison, J.L., van der Merwe, P., 2013. Role of sea ice in global biogeochemical cycles: Emerging views and challenges. Quat. Sci. Rev. 79, 207–230. https://doi.org/10.1016/j.quascirev.2013.04.011

Vaughan, D.G., Marshall, G., Connoley, W.M., Parkinson, J.C., Mulvaney, R., Hodgson, D., King, J.C., Pudsey, C.J., Turner, J., 2003. Recent rapid regional climate warming on the Antarctic Peninsula. Clim. Chnage 60, 243–274. https://doi.org/10.1126/science.1189930

Verity, P.G., 1981. Effects of temperature, irradiance, and daylength on the marine diatom *Leptocylindrus danicus* Cleve. II. Excretion. J. Exp. Mar. Bio. Ecol. 55, 159–169. https://doi.org/10.1016/0022-0981(81)90109-X

Wakatsuchi, M., Martin, S., 1991. Water circulation in the kuril basin of the Okhotsk Sea and its relation to eddy formation. J. Oceanogr. Soc. Japan 47, 152–168. https://doi.org/10.1007/BF02301064

Wang, S., Bailey, D., Lindsay, K., Moore, J.K., Holland, M., 2014. Impact of sea ice on the marine iron cycle and phytoplankton productivity. Biogeosciences 11, 4713–4731. https://doi.org/10.5194/bg-11-4713-2014

Wassmann, P., Ratkova, T., Andreassen, I., Vernet, M., Pedersen, G., Rey, F., 1999. Spring bloom development in the marginal ice zone and the central Barents Sea. Mar. Ecol. 20, 321–346. https://doi.org/10.1046/j.1439-0485.1999.2034081.x

Webb, W.L., Newton, M., Starr, D., 1974. Carbon dioxide exchange of *Alnus rubra*. Oecologia 17, 281–291. https://doi.org/10.1007/BF00345747

Wells, M.L., 1999. Manipulating iron availability in neashore waters. Limnol. Oceanogr. 44, 1002–1008.

Welschmeyer, N.A., 1994. Fluorometric analysis of Chlorophyll *a* in the presence of Chlorophyll *b* and pheopigments. Limnol. Oceanogr. 39, 1985–1992. https://doi.org/10.4319/lo.1994.39.8.1985

Werner, I., 1997. Grazing of Arctic under-ice amphipods on sea-ice algae. Mar. Ecol. Prog. Ser. 160, 93–99. https://doi.org/10.3354/meps160093

Wood, A.M., Everroad, R.C., Wingard, L.M., 2005. Measuring growth rates in microalgal culture. In: Andersen, R.A. (ed.), Algal Culturing Techniques. Elsevier. 269−285.

Wright, S.W., van den Enden, R.L., Pearce, I., Davidson, A.T., Scott, F.J., Westwood, K.J., 2010. Phytoplankton community structure and stocks in the Southern Ocean (30-80°E) determined by CHEMTAX analysis of HPLC pigment signatures. Deep. Res. Part II Top. Stud. Oceanogr. 57, 758–778. https://doi.org/10.1016/j.dsr2.2009.06.015

Yagi, M., Yasuda, I., 2012. Deep intense vertical mixing in the Bussol' Strait. Geophys. Res. Lett. 39, 1–5. https://doi.org/10.1029/2011GL050349

Yamaguchi, A., Miwa, Y., Inoue, K., Matsumoto, T., 2003. Characteristics of zooplankton community in the coastal Oyahsio water (in Japanese with English abstract). Bull. Coast. Oceanogr. 41, 23–31.

Yamamoto-Kawai, M., McLaughlin, F.A., Carmack, E.C., Nishino, S., Shimada, K., 2009. Aragonite undersaturation in the Arctic. Science 326, 1098–1100. https://doi.org/10.1126/science.1174190

Yamamoto, S., Michel, C., Gosselin, M., Demers, S., Fukuchi, M., Taguchi, S., 2014. Photosynthetic characteristics of sinking microalgae under the sea ice. Polar Sci. 8, 385–396. https://doi.org/10.1016/j.polar.2014.07.007

Yan, D., Beardall, J., Gao, K., 2018. Variation in cell size of the diatom Coscinodiscus granii influences photosynthetic performance and growth. Photosynth. Res. 137, 4152. https://doi.org/10.1007/s11120-017-0476-6

Yasuda, I., 2003. Hydrographic structure and variability in the Kuroshio-Oyashio transition area. J. Oceanogr. 59, 389–402.

Yoshida, K., Endo, H., Lawrenz, E., Isada, T., Hooker, S.B., Prášil, O., Suzuki, K., 2018. Community composition and photophysiology of phytoplankton assemblages in coastal Oyashio waters of the western North Pacific during early spring. Estuar. Coast. Shelf Sci. 212, 80–94. https://doi.org/10.1016/j.ecss.2018.06.018

Yoshie, N., Suzuki, K., Kuwata, A., Nishioka, J., Saito, H., 2010. Temporal and spatial variations in photosynthetic physiology of diatoms during the spring bloom in the western subarctic Pacific.

Mar. Ecol. Prog. Ser. 399, 39–52. https://doi.org/10.3354/meps08329

Yoshie, N., Yamanaka, Y., Kishi, M.J., Saito, H., 2003. One dimensional ecosystem model simulation of the effects of vertical dilution by the winter mixing on the spring diatom bloom. J. Oceanogr. 59, 563–571. https://doi.org/10.1023/B:JOCE.0000009586.02554.d3

Yoshimori, A., Ishizaka, J., Kono, T., Kasai, H., Saito, H., Kishi, M.J., Taguchi, S., 1995. Modeling of spring bloom in the western subarctic Pacific (off Japan) with observed vertical density structure. J. Oceanogr. 51, 471–488. https://doi.org/10.1007/BF02286393

Yoshimura, T., Nishioka, J., Nakatsuka, T., 2010. Iron nutritional status of the phytoplankton assemblage in the Okhotsk Sea during summer. Deep. Res. I 57, 1454–1464. https://doi.org/10.1016/j.dsr.2010.08.003

Young, J.N., Goldman, J.A.L., Kranz, S.A., Tortell, P.D., Morel, F.M.M., 2015. Slow carboxylation of Rubisco constrains the rate of carbon fixation during Antarctic phytoplankton blooms. New Phytol. 205, 172–181. https://doi.org/10.1111/nph.13021